Synthesis and Photophysical Investigation of Axially and Peripherally Modified Phthalocyanines for Improved Light-Harvesting and Photoreactivity

Kumulative Dissertation

zur

Erlangung des Doktogrades der Naturwissenschaften

(Dr. rer. nat.)

dem Fachbereich Chemie

der Philipps-Universitat Marburg

vorgelegt von

Malcolm Alan Bartlett

(M.Sc. Chemie)

aus

Durban, Südafrika

Marburg (Lahn) 2018

Die vorliegende Arbeit wurde in der Zeit von Oktober 2013 bis September 2017 unter Leitung von Herrn Prof. Dr. Jörg Sundermeyer am Fachbereich Chemie der Philipps-Universität Marburg angefertigt.

Vom Fachbereich Chemie der Philipps-Universität Marburg (Hochschulkennziffer: 1180) als Dissertation angenommen am:
Erstgutachter: Prof. Dr. Jörg Sundermeyer
Zweitgutachterin: Prof. Dr. Olalla Vázquez
Tag der mündlichen Prüfung:

Erklärung

Ich erkäre, dass eine Promotion noch an keiner anderen Hochschule als der Philipps-Universität Marburg, Fachbereich Chemie, versucht wurde.

Ich versichere, dass ich meine vorgelegte Dissertation mit dem Titel

Synthesis and Photophysical Investigation of
Axially and Peripherally Modified Phthalocyanines for
Improved Light-Harvesting and Photoreactivity

selbst und ohne fremde Hilfe verfasst, nicht andere als die in ihr angegebenen Quellen oder Hilfsmittel benutzt, alle vollständig oder sinngemäß übernommenen Zitate als solche gekennzeichnet habe sowie die Dissertation in der vorliegenden oder einer ähnlichen Form noch bei keiner anderen in- oder ausländischen Hochschule anlässlich eines Promotionsgesuches oder zu anderen Prüfungszwecken eingereicht habe.

Marburg, den ___.___._____. Unterschrift: _____.

To my Family

"The more the words, the less the meaning, and how does that profit anyone?"

Ecclesiastes 6:11 (NIV)

Published parts of this work

Articles in Journals

M. A. Bartlett and J. Sundermeyer, Group 10 Metal-Thiocatecholate Capped Magnesium Phthalocyanines – Coupling Chromophore and Electron Donor/Acceptor Entities and its Impact on Sulfur Induced Red-Shifts*, Dalton Transactions*, **2018**, doi:10.1039/C8DT03681K

M. A. Bartlett, K. Mark and J. Sundermeyer, Synthesis, spectroscopy and singlet oxygen quantum yield of a non-aggregating hexadecamethyl-substituted phthalocyanine silicon(IV) derivative, *Inorg. Chem. Comm.*, **2018**, *98*, 41–43.

Presentations

M. A. Bartlett, M. Liebold and J. Sundermeyer, *Phthalocyanines in Photodynamic Therapy*, Loewe SynChemBio Kick-Off Meeting, Marburg, 2014.

Posters (Selection)

M. Liebold, M. A. Bartlett, A. Ibrahim and J. Sundermeyer, *Interfacial Bonding of Phthalocyanines and Pyrazinoporphyrazines with Axial and Equatorial Anchors,* Materialforschungstag Gießen, Juni 2014.

M. Kothe, M. A. Bartlett, G. Witte and J. Sundermeyer, *Low temperature deposition of oriented zinc phthalocyanine thin films and their optical characterization*, International Conference on Internal Interfaces, Marburg, 31 May – 3 June, 2016.

M. A. Bartlett, M. Kothe, G. Witte and J. Sundermeyer, *Equitorial Thioester Anchor – Towards Ordered Phthalocyanine Monolayers on Au(111)*, Ninth International Conference on Porphyrins and Phthalocyanines, Nanjing, PRC, 3-8 July, 2016.

M. A. Bartlett and J. Sundermeyer, *Metal-Capped Phthalocyanines, a New Class of High-Triplet Yielding Sensitisers*, Materialforschungstag Mitel Hessen, Gieβen, 28 June, 2017.

Acknowledgements

My special thanks go to Prof. Dr. Jörg Sundermeyer for taking the risk with an unknown student and allowing me to perform my doctoral work in his laboratory. I would also like to thank him for his support helping me apply for a DAAD scholarship, the many ensuing supervisor reports he wrote and his guidance and support during my time in Marburg.

I would like to thank Prof. Dr. Olalla Vázquez for taking on the responsibility of second examiner, as well as Prof. Dr. Norbert Hampp for participating in the examination process.

I would like to thank the *Deutsche Akademische Austausch Dienst* (DAAD) for the grant of a doctoral scholarship.

Thank you, as well, to the service departments of the chemistry faculty, particularly the mass spectrometry service, and their help in analysing often "troublesome" samples.

Collaborative projects would not have been possible without the effort and dedication of the doctoral candidates and their project supervisors. Many thanks to Michael Kothe, Prof. Dr. Gregor Witte, Laura Thomas, Prof. Dr. Roland Hartmann, Felix Zellmann and Prof. Dr. Michael Göbel.

Thank you to all members of the Sundermeyer research group who contributed to a conducive and pleasant work environment. Special thanks to our laboratory technicians Lisa Hamel and Irene Barth for their diligent and friendly support.

To all master's students who worked with me during their internships in the group: Refika Fidan, Ying Chen, Andreas Nguyen, Bernhard Leuber, Kerstin Mark, Shuai Zhou and Xingwen Zheng, thank you.

Thank you also to the friends that I have made while living in Germany, who have become like a second family. Your friendship, support and encouragement has been greatly appreciated.

To my parents, Alan and Gail, thank you so much for the many sacrifices you made in time and effort and the financial sacrifices that you made to enable me to study, as well as your encouragement over the years. Thank you also to my sister, Cara-Lesley, for her support and good advice. To my daughter, Enid, thank you for the many hours of company and smiles at the desk while writing this dissertation. Lastly, thank you to my dear wife, Erica, who left home and country to support me in my ambitions, and often believed in me more than I did.

Contents

Page

1 Introduction

1.1 Pigments and Dyes 1

1.1.1 A brief history of dyes and pigments 1

1.1.2 The discovery of phthalocyanines 2

1.2 Phthalocyanine 3

1.2.1 Synthesis of phthalocyanines 3

1.2.1.1 Methods and Mechanisms of Formation 3

1.2.1.2 Synthesis of asymmetric phthalocyanines 5

1.2.2 Properties of phthalocyanines 9

1.2.2.1 Properties in solution 10

1.3 Applications of phthalocyanines 14

1.3.1 Photosensitisers for energy conversion 14

1.3.1.1 Photovoltaic devices using phthalocyanines 15

1.3.1.2 Photoredox catalysts for H^+ reduction 20

1.3.2 Medicinally active compounds 24

1.3.2.1 Photosensitisers for photodynamic therapy 25

1.3.2.2 Photosensitisers in photothermal and photoacoustic therapy 26

1.3.2.3 Binders of G-quadruplex DNA 28

1.3.3 Phthalocyanines in self-assembled monolayers 29

1.3.4 Metal-imido phthalocyanine complexes 31

2 Purpose of the Work 34

3 Cumulative Section 37

3.1 Group 10 Metal-Thiocatecholate Capped Magnesium Phthalocyanines – Coupling Chromophore and Electron Donor/Acceptor Entities and its Impact on Sulfur Induced Red-Shifts 37

3.2 Peripheral Metallation of Phthalocyanine – Inducing New Effects in an Old Chromophore 40

3.3 Synthesis, Spectroscopy and Singlet Oxygen Quantum Yield of a Non-Aggregating Pc*Si Derivative 42

3.4 Zinc(II)Phthalocyanine-Thiol Monolayers on Gold: On the Oxidative Stability of the S-Au Bond 44
3.5 Imido Vanadium(IV) and Imido Chromium(IV) Phthalocyanine Complexes: Synthesis, Spectroscopy and Theoretical Investigations 46
3.6 Control of Intramolecular Electron Transfer in Perylene Dihydrazides and Perylene Diimides: A Comparative Study by Time-Resolved Spectroscopy 48

4 Summary 50

5 Zusammenfassung 59

6 Full Texts of the Discussed Manuscripts 69
6.1 Group 10 Metal-Thiocatecholate Capped Magnesium Phthalocyanines – Coupling Chromophore and Electron Donor/Acceptor Entities and its Impact on Sulfur Induced Red-Shifts 70
6.2 Peripheral Metallation of Phthalocyanine – Inducing New Effects in an Old Chromophore 83
6.3 Synthesis, Spectroscopy and Singlet Oxygen Quantum Yield of a Non-Aggregating Pc*Si Derivative 91
6.4 Zinc(II)Phthalocyanine-Thiol Monolayers on Gold: On the Oxidative Stability of the S-Au Bond 98
6.5 Imido Vanadium(IV) and Imido Chromium(IV) Phthalocyanine Complexes: Synthesis, Spectroscopy and Theoretical Investigations 107
6.6 Control of Intramolecular Electron Transfer in Perylene Dihydrazides and Perylene Diimides: A Comparative Study by Time-Resolved Spectroscopy 121

7 Summary of Non-Published Projects 134
7.1 Dithiolate and catecholate complexes 134
7.2 Work done within the Loewe SynChemBio network 136
7.2.1 Pc-oligonucleotide conjugate 137
7.2.2 Cationic Pc complexes for G-quadruplex binding 138
7.3 Work done within the SFB1083 141
7.4 Coordination chemistry of Pc bound niobium and tantalum 142
7.4.1 Imido Nb and imido Ta Pc complexes 142

7.4.2 Axial coordination of a tripyrrolic ligand to [$PcNbCl_3$] and [$PcTaCl_3$] 144
7.5 Experimental section 145
7.5.1 Synthesis of thiocatecholate and catecholate systems 145
7.5.2 Synthesis of [(^{PegS8}Pc)Zn] and [($^{PegS6/HOOC\text{^}S}$Pc)Zn] 147
7.5.3 Syntheses for [(^{Me2}TIPc)Mg]I_8 and [(^{Me}TIPc)Mg] 153
7.5.4 Notable syntheses involving niobium and tantalum 155

8 References 158

CHAPTER 1 | INTRODUCTION

1.1 Pigments, Dyes and Phthalocyanine

1.1.1 A Brief History of Dyes and Pigments

Since antiquity, man has been making use of pigments for dyeing fabrics, creating art and writing. Even then, the trade of dyes was a dynamic and multinational undertaking, probably the most famous of which is the trade of tyrian purple, a purple pigment obtained from the shell of molluscs, *Bolinus brandaris*; the dye was worth its own weight in silver owing to the difficulty of obtaining it.[1] Today, tyrian purple is known to be 6,6'-dibromoindigo, an organic compound with a conjugated π-system. This is common to many of the naturally occurring dyes, many of which share common structural features. For instance, both Lawsone from henna (*Lawsonia inermis*) and juglone from black walnut (*Juglans nigra*) are yellow coloured derivatives of naphthaquinone that are used cosmetically.

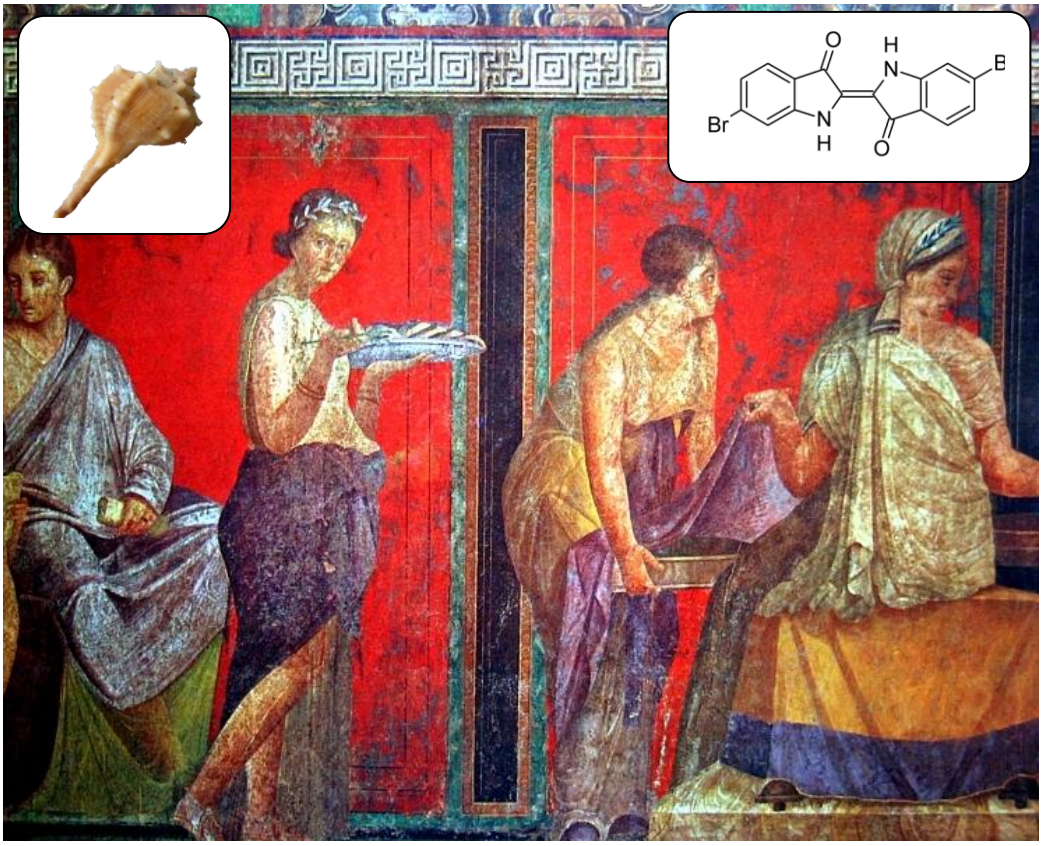

Figure 1.1: Fresco from Pompei*. Purple clothing was dyed using tyrian purple. Inset: (top left) shell of *Bolinus brandaris** (top right) the structure of this tyrian purple. *Photo credit: wikimedia

The terms "pigment" and "dye" refer to colorants that are either soluble or insoluble; a soluble pigment fixed to fabric, for instance, is then considered a dye. Because of the large demand for dyes, efforts have been made to synthesise either naturally occurring pigments or new compounds that have similar or better properties. The first synthetic pigment, the blue coloured aniline derivative mauveine, was made serendipitously by Sir WILLIAM HENRY PERKIN[2], while indigo, the scaffold of tyrian purple, was synthesised by ADOLF VON BAEYER[3], from indicane.

1.1.2 The Discovery of Phthalocyanine

Phthalocyanine (Pc) was first synthesised accidentally in 1907 as a side-product in the synthesis of 2-cyanobenzamide[4]. Its structure, however, was only elucidated in 1934 by LINSTEAD and ROBERTSON[5], who determined that it was a macrocyclic compound. The name phthalocyanine was derived from the use of phthalic acid derivatives for their synthesis and the Greek work *cyanos*, (κυανός) meaning "blue".[5] Pc is an 18-π electron aromatic macrocycle that is structurally related to the naturally occurring porphyrins (Por). Like Por, Pc is a divalent ligand that has a binding cavity with N-donor atoms. Pc differs from Por in that it has four [–N=] units instead of [–CH=] units in the meso-positions, and is annulated with four benzene units. When only the [–CH=] units are substituted for [–N=] units, the compounds are called porphyrazines (Pz); when a porphyrin is only annulated with benzene, the compound is called a benzoporphyrin (BPor). Additionally, there is a common nomenclature for discussing the different positions on a Pc where substitution/derivatisation can occur, namely, the non-peripheral and peripheral benzene [–CH=] units, which are termed the α- and β-position, respectively. Figure **1.2** shows the structures for these four macrocycles, as well as the common naming scheme for Pc.

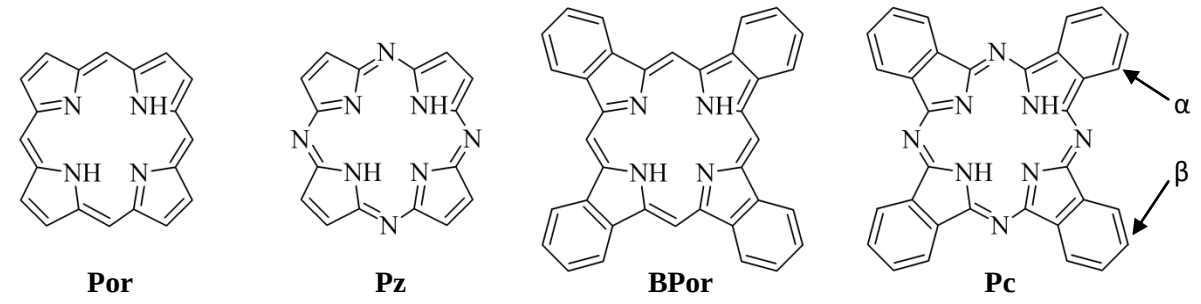

Figure 1.2: The structure of porphyrins (Por), porphyrazine (Pz), benzoporphyrin (BPor) and phthalocyanine (Pc), and the positional labelling scheme for Pc.

1.2 Phthalocyanine

1.2.1 Synthesis of Phthalocyanines

1.2.1.1 Methods and Mechanism of Formation

There are many different methods described in the literature for the synthesis of Pc and metallophthalocyanine (MPc) that make use of a variety of phthalic acid derivatives or, in the case of MPc, use preformed Pc ligand. Typically though, a cyclotetramerisation reaction using either a phthalonitrile or 1,3-diiminoisoindoline derivative is performed in the presence or absence of a metal salt depending on whether or not MPc or Pc is desired, respectively. The mechanism for the formation of MPc from phthalonitrile and a metal salt was principally studied by CHRISTIE *et al*.[6] Here, it is assumed that a nitrile group of phthalonitrile coordinates to the metal ion and is at the same time attacked by a nucleophile, "X", at the nitrile C atom. This catalyses an intramolecular reaction where the newly formed imino $=N^-$ unit attacks the neighbouring nitrile group to form an isoindoline. An anion is formed from isoindoline that can go on to attack other nitrile groups of a nearby phthalonitrile. In this way, four isoindoline groups form around the metal ion, which acts as a template for MPc formation. Upon ring closure, X is cleaved off and a two electron reduction of the macrocycle occurs to form the Pc ligand. In the above mechanism, X can either be the counter ion of a metal salt, such as chloride, Cl^-, or, if the reaction is carried out in an alcoholic solvent, then X could be an alcoholate, RO^-. The electrons required for the reduction could be supplied by oxidation of the the metal ion used (e.g. Cu(I) → Cu(II) for the synthesis of Cu(Pc)), by oxidation of halogen counter ions, (e.g. $2Cl^- \rightarrow Cl_2$) or by oxidation of the solvent itself (e.g. ROH → R(O)CH). The mechanism for the formation of MPc from a metal salt and phthalonitrile is shown in Scheme **1.1**.

The other commonly used precursors, 1,3-diiminoisoindoline derivatives, are known to be more reactive precursors for the synthesis of MPc/Pc. They are generally formed by the reaction of phthalonitrile with ammonia under basic conditions.[7] The mechanism for MPc formation is similar for both 1,3-diiminoisoindoline and phthalonitrile, but differs in the initial steps. Here, the isoindoline derivative binds the metal ion, but can be directly attacked

at the C 1/3-position by the imino group of another nearby 1,3-diiminoisoindoline to form a dimer. It is this dimer that then undergoes nucleophilic attack by X to promote ring closure.[8] The mechanism for MPc formation from 1,3-diiminoisoindoline is shown in Scheme **1.2**.

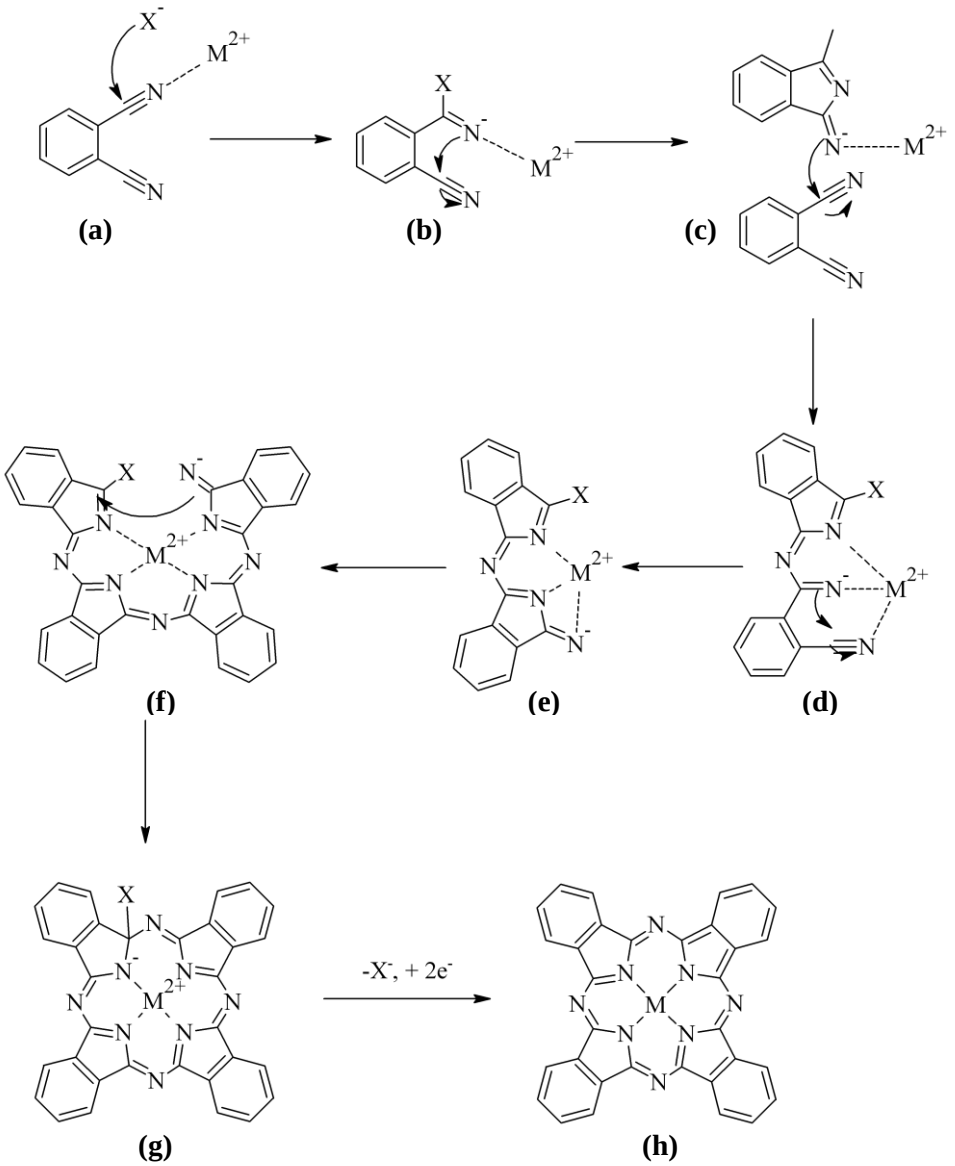

Scheme 1.1: Mechanism of metallophthalocyanine formation from phthalonitrile: **(a)** nucleophilic attack at nitrile carbon, **(b)** intramolecular ring closure to form isoindoline derivative, **(c)** nucleophilic attack of nearby nitrile group, **(d)** second intramolecular ring closure, **(e)** anionic dimer formed – repetition of **(c)** and **(d)** until four isoindoline moieties have been added, **(f)** ring closure around a template metal ion to give **(g)** an anti-aromatic macrocycle that then loses the initial attacking nucleophile with concomitant reduction of the macrocyclic ring **(h)**.

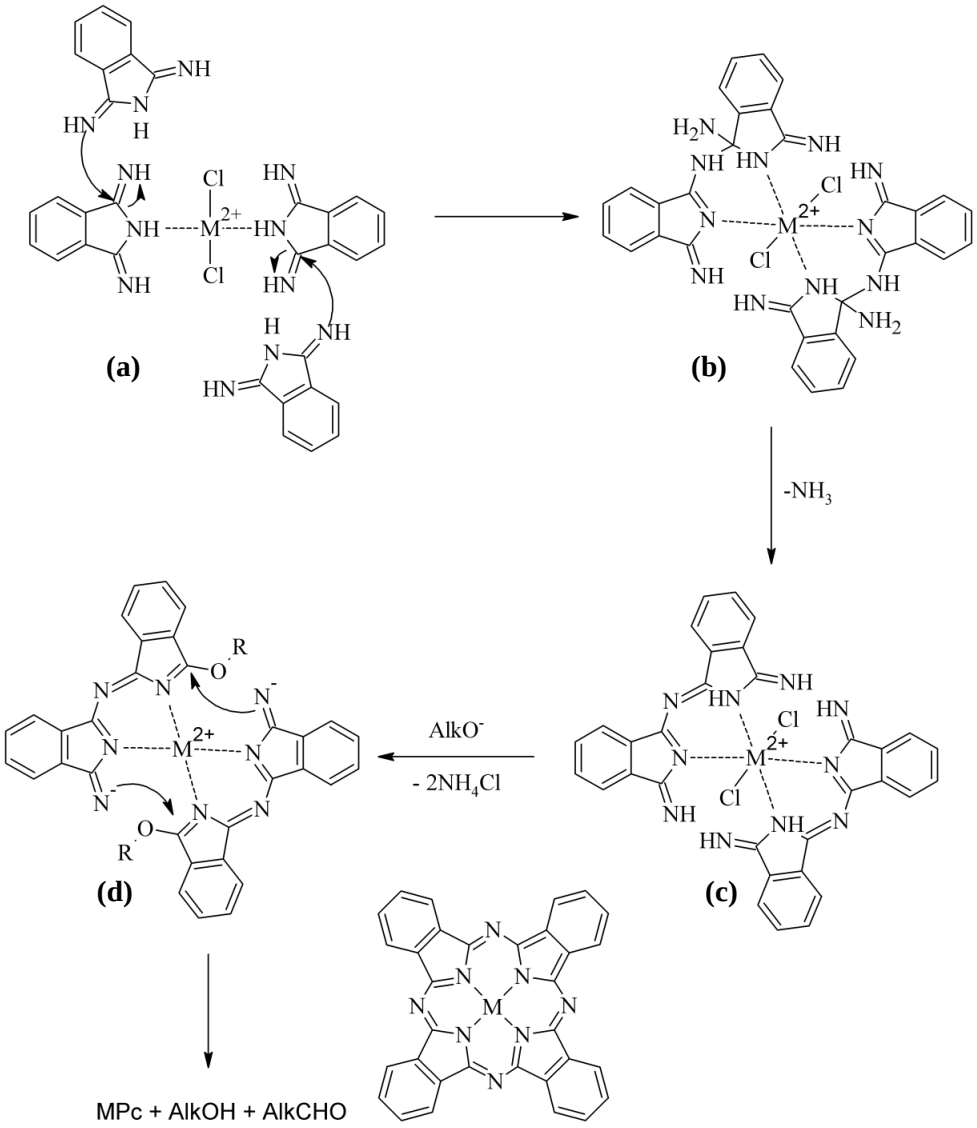

Scheme 1.2: Mechanism of metallophthalocyanine formation from 1,3-diiminoisoindoline: **(a)** Initial coordination of two 1,3-diiminoisoindolines to a metal ion, and nucleophilic attack by nearby 1,3-diiminoisoindolines, **(b)** dimer formation around a template metal ion, **(c)** loss of amino to form stable intermediate, **(d)**, nucleophilic attack by alkoxide and subsequent macrocyclic ring closure.

1.2.1.2 Synthesis of Asymmetric Phthalocyanines

The Pc compounds discussed so far are all symmetric molecules, that is, they are formed by the cyclisation of only one type of precursor. However, it is often advantageous or even necessary, to synthesise Pc compounds that have different functional groups. To do this, different precursors that together give the desired combination of functional groups are used together in a Pc synthesis. Because a Pc is composed of four precursors, up to six products

can be formed. To differentiate amongst the various products formed, each different precursor is assigned a letter, e.g. A and B, and the Pc isomer is named according using these letters. The six products formed from a mixture of two precursors are therefore referred to as the A_4, A_3B, *cis*-A_2B_2, *trans*-A_2B_2, AB_3 and B_4 products. The structures for these products as well as the common naming scheme for them are shown in Figure **1.3**. Various methods have been developed for the synthesis of asymmetric Pcs; these will described in the remainder of this section on Pc synthesis.

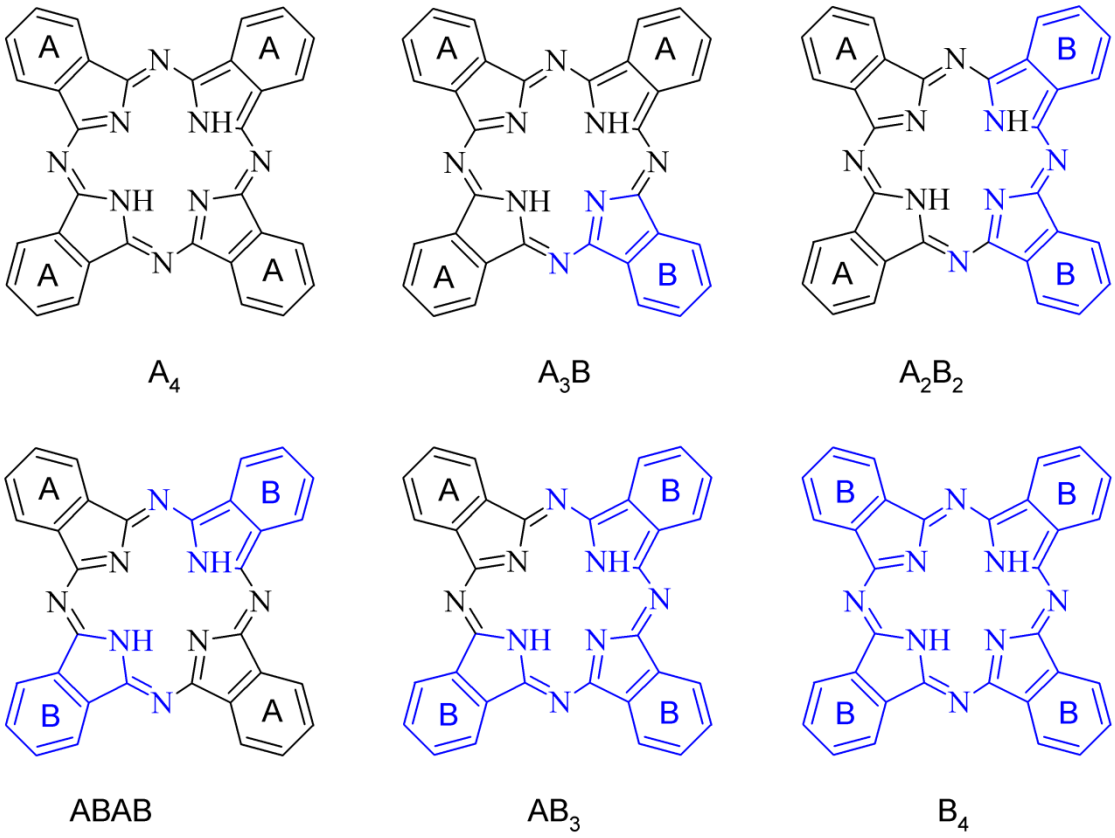

Figure 1.3: The six possible Pc products that can be formed by a mixed cyclisation of two different precursors A and B and the naming scheme for each one. The possible groups that differentiate A from B are not shown for simplicity.

Cocyclisation: This is conceptually the simplest method for producing asymmetric Pcs. In this procedure, two different Pc precursors are mixed together and reacted as usual to form a mixture of Pc products.[9] The exact amount of each product produced depends on both the ratio of the precursors to each other and their respective reactivities; this makes exact control

of product distribution problematic. Additionally, not every product that is obtained is necessarily desired. Because of this problem, various methods have been developed to produce certain products either selectively, or in higher ratios. However, cocylcisation continues to be a useful method for synthesising a complete series of products and is still used for fundamental Pc research.

Crossed condensation: Here, the formation of certain Pc products is favoured by the relative reactivity of different precursors to each other[10,11]. For instance, electron poor precursors, such as 1,3,3-trichloroisoindoline (Figure **1.4**), are combined with more nucleophilic precursors, such as 1,3-diiminoisoindoline derivatives. These precursors then react initially to form dimers, which can then go on to form tetrameric Pc compounds. This reaction pathway therefore favours the formation of A_2B_2 Pcs. The obvious disadvantage of this method is of course the need to synthesise precursors with compatible reactivity. While some precursors, such as 1,3-diiminoisoindoline, are commercially available, others can only be obtained in low yield after extensive synthetic procedures. Yields are also relatively low owing to the labile nature of the starting 1,3,3-trichloroisoindoline precursor. The more stable dithioimide (Figure **1.4**) has also been used with 1,3-diiminoisoindoline in an attempt to selectively synthesis A_2B_2 type Pcs.[12] Dithioimde is known to be susceptible to amine substitution at positions 1 and 3,[13] and phthalocyanine formation using these precursors occurs readily at low temperatures. However, selective formation of asymmetric phthalocyanines was only partially achieved, with mixtures of all products being formed.

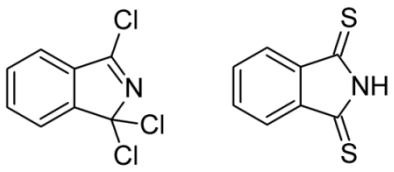

Figure 1.4: 1,3,3-trichloroisoindoline and 1,3-dithioimide – two Pc precursors particularly labile with regard to nucleophilic substitution examined for improving the selectivity of *trans*-A_2B_2 Pc products.

Alternatively, the proximity of certain precursor to each other can influence the final Pc product distribution. Either some precursors can include a large amount of steric bulk to prevent them from readily reacting with each other, but rather with less bulky precursors present, of two precursors can be tethered to each other to ensure that they react with each

other before reacting with other available precursors. An example of the first method is the reaction of 3,6-didecyloxyphthalonitriles with phthalonitrile,[14] which forms the *trans*-A_2B_2 isomer with good selectivity. An extreme example of the latter method was demonstrated by CHOW and NG, who linked four different precursors together and then reacted them in an intramolecular cyclisation to obtain an ABCD-type Pc in a yield of 7.2 %.[15] Figure **1.5** illustrates these two methods of controlling the product distribution by controlling the proximity of the Pc precursor molecules to one another.

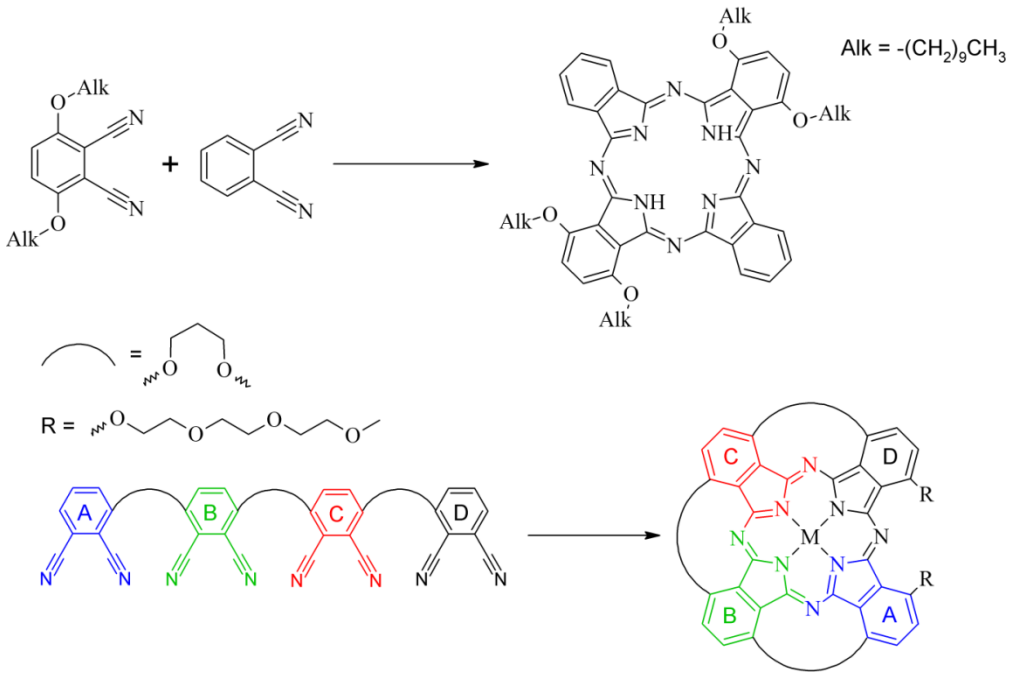

Figure 1.5: Using bulky groups prevents dinitriles from readily reacting with each (top),[14] while joining them together promotes intramolecular reactions (bottom).[15]

Polymer Support: Originally developed by LEZNOFF[16,17], the method of asymmetric phthalocyanine synthesis by polymer support relies on tethering a 1,3-diiminoisoindoline *via* a linking group onto a polymer. A second precursor is then added, and the cyclisation reaction is carried out. The excess precursor or undesired products can then be simply removed by washing before detaching the desired A_3B product with acid treatment. In this method, the ease of isolation of the desired product is counteracted by several drawbacks, including available polymer supports, linkers that can tolerate cyclisation conditions and yet be easily removed and compatible additional precursors. The biggest drawback to this

method, however, is the generally low yield of product obtained; 20 % being the maximum reported yield to date.

Ring expansion: This method can be thought of as an extension of the cross condensation method mentioned above. Here, instead of a dimer forming first, a trimer complex, known as a subphthalocyanine (SPc), is first synthesised. KOBAYASHI first reported that subphthalocyanines could be reacted with a 1,3-diiminoisoindoline in a high boiling solvent to form an A_3B Pc, with very high yields of 90 %[18] (Scheme **1.3**). Interestingly though, Pc compounds other than the desired A_3B-type product could be detected, which had lead to considerable discussion of the mechanism of the ring expansion[19]. Additionally, although a yield of 90 % was initially reported, most authors report significantly lower yields,[20] and the need to purify the Pc by column chromatography still exists. Considering the moderate yields of the subphthalocyanine starting material generally obtained,[21] this method does not significantly improve the yield of the A_3B product over all reaction steps.

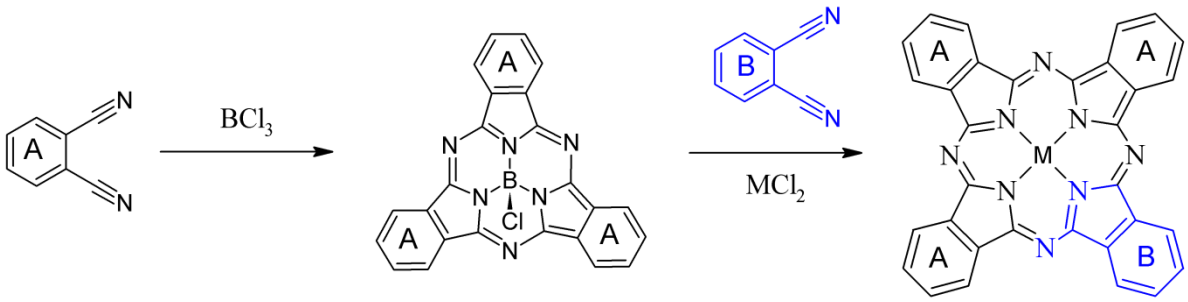

Scheme 1.3: Synthesis of an A_3B Pc by the KOBAYASHI ring expansion method.[18]

1.2.2 Properties of Phthalocyanines

Pcs have found wide-ranging applications because of the combination of their thermal and chemical stability combined with their unique optical properties.[5] Thermally, they are stable well above 500 ºC, a property that allows them to be purified by sublimation. They are also very chemically resistant, being stable towards strong bases and acids; for instance, dissolution and precipitation from sulfuric acid (98 %) is a common laboratory method for Pc purification.[22] This general robustness, therefore, is what enables them to be used so broadly. It is their optical properties, however, that provide the basis for them being used at all, and these shall be discussed in greater detail in the remainder of this section.

1.2.2.1 Properties in Solution

Analysis of the typical optical absorption spectrum of Pc shows two regions of intense absorption at ~350 nm and between 600-700 nm, termed the B- and Q-bands, respectively. The high energy absorptions of the B-band arise from transitions of the π electron system of the inner Pc ring, and are therefore not as strongly affected by the addition of derivates on the Pc periphery. Conversely, the low energy Q-band absorptions arise from $\pi \rightarrow \pi^*$ transitions of the HOMO to LUMO/LUMO+1, which are located primarily over the fused benzene rings. Depending on the symmetry of the Pc, there may either be one or two Q-band absorptions present for a Pc with D_{4h} or lower symmetry, respectively. This is because, for D_{4h} symmetric Pc, the LUMO and LUMO+1 are degenerate; breaking the symmetry therefore lifts the degeneracy of these two orbitals, resulting in a split of the Q-band absorption. This interpretation for the Pc absorption was first proposed by GOUTERMANN, and is known as the Goutermann four orbital model.[23] A schematic illustration of the B- and Q-band transitions and a molecular orbital diagram for these transitions is shown in Figure **1.6**.

As is typical for most organic dyes, upon photo-excitation the excited electron is in the singlet (S_1) state. From this state, it can either relax *via* radiative (fluorescence) or non-radiative decay (Internal Conversion or IC) or it can relax through inter-system crossing (ISC) to the triplet (T_1) state. From the T_1 state, it can again relax radiatively (phosphorescence) or non-radiatively (IC), or it can transfer its energy to a suitable quencher. (Scheme **1.4** shows the JABLONSKI diagram for these processes.)

The extent to which the various processes occur depends strongly on the symmetry of the Pc ligand, the metal, if any, coordinated and the extent and nature of substitution on the Pc ligand. For D_{4h} symmetric Pc, there is little difference in energy between the S_1 and T_1 states.[24] This favours a fast radiative decay process, i.e. fluorescence. Because there is little distortion of the rigid Pc structure upon photoexcitation, there is typically only a small Stokes shift of the emission relative to the absorption. When the degeneracy is lifted because the symmetry is broken, the energy difference between the S_1 and T_1 states is increased, which favours ISC. Consequently, either phosphorescence or energy transfer is more likely to occur as a result of this. ISC is also promoted by the coordination of d-block metals in the Pc central cavity.[25] d-block metals, of course, possess d-orbitals, which have the suitable geometry to promote spin-orbit coupling. The heavier the d-block metal, the stronger the

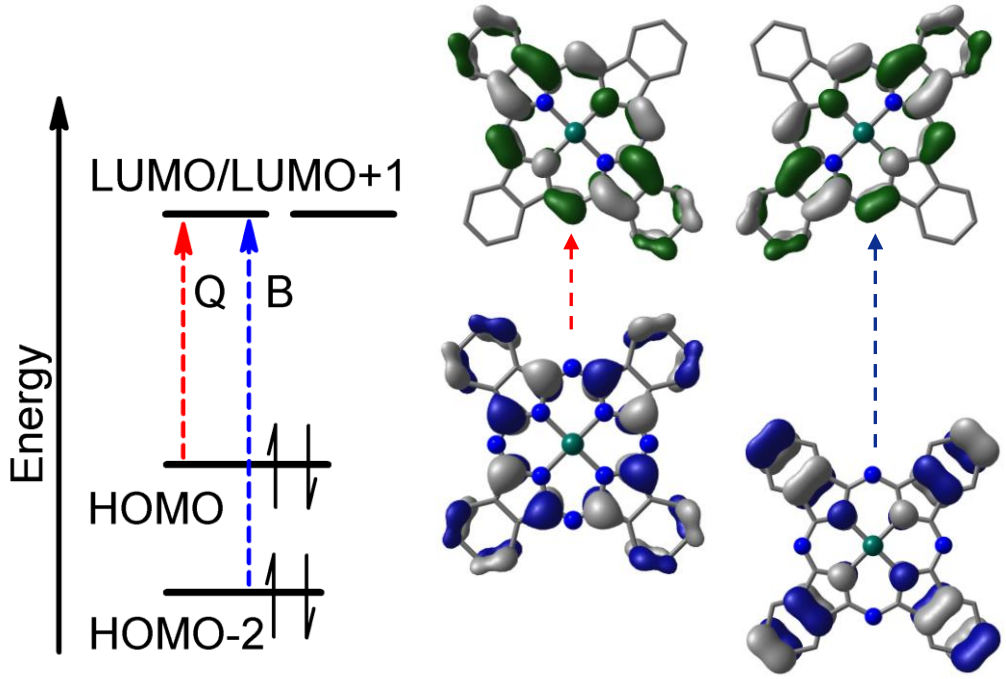

Figure 1.6: Energy level diagram for the B-band and Q-band transitions for a D_{4h} symmetric Pc. (Right) The molecular orbitals involved in the Q-band (red arrow) and B-band (blue arrow) transitions. The LUMO and LUMO+1 are energetically degenerate.[23]

spin-orbit coupling. Spin-orbit coupling is also promoted by the incorporation of heavier atoms, such as iodine, on the Pc ligand.[26] Spin-orbit coupling increases the rate of ISC, and therefore promotes the population of the T_1 state after photo-excitation.[27] Furthermore, the promotion of ISC is directly related to the molecular weight of the metal ion coordinated; this is known as the heavy atom effect.[28]

The energy of the Q-band absorption can also be strongly affected by substitution at the α- or β-position. It has been known for many years that substitution at the β-positions with an organochalcogenide substituent, for instance, induces a bathochromic shift of the Q-band to $\geq$ 700 nm, causing the Pc colour to change from blue to green.[29] More recently, KOBAYASHI demonstrated that a bathochromic shift to over 800 nm can be achieved by substitution at the α-positions instead, so that the Q-band absorption is in the NIR, and the Pc derivatives have a brown colour.[30] In both instances, a bathochromic shift is induced because the organochalcogenides push electron density onto the Pc, thus decreasing the HOMO-LUMO gap. The stronger shift caused by substitution at the α-position is because the HOMO is

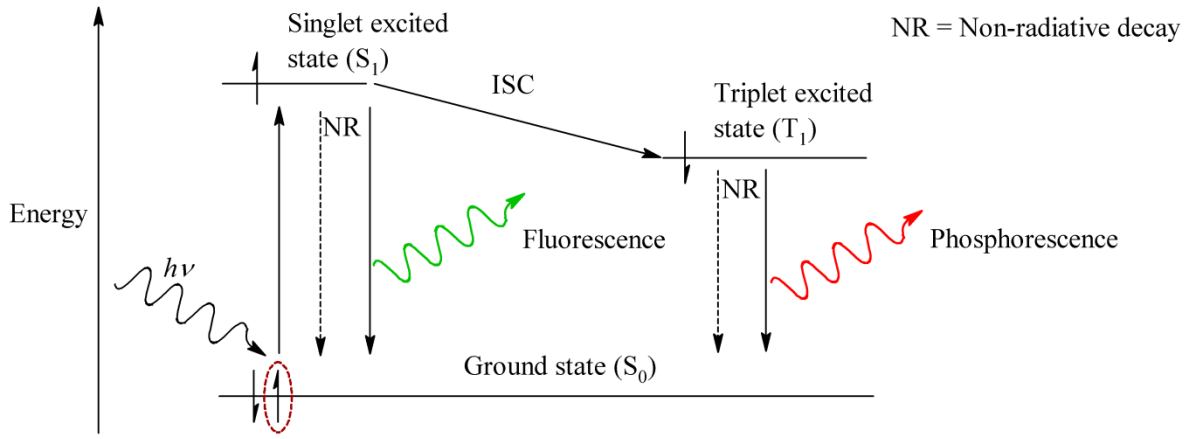

Scheme 1.4: JABLONSKI diagram illustrating the excited state dynamics of phthalocyanine.

located over this position while the LUMO is not, so that only the former orbital is significantly destabilised resulting in a larger decrease of the band-gap.

In addition to substitution on the fused benzene ring of Pc, it is also possible to change the energy of the HOMO-LUMO energy gap, and consequently the Q-band absorption energy, by substituting the benzo groups for other aromatic ring systems. The two most common groups used being pyrazine and naphthalene, and the two resulting macrocycles made using these groups are termed pyrazinoporphyrazine and naphthalocyanine, respectively. The addition of a pyrazine ring has the effect of increasing the HOMO-LUMO energy gap to cause a hyposchromic (blue) shift of the Q-band,[31] whereas a naphthalene ring has the opposite effect, causing a bathochromic (red) shift of the Q-band by extending the π-conjugation.[32] It is important to note that the chemical and thermal stability of both pyrazinoporphyrazines and naphthalocyanines is lowered compared to the parent Pc ligand.[33] Figure **1.7** illustrates the effect that substitution on or of the Pc-benzo ring has on the macrocycles optical properties. The optical absorption spectrum typically shown for a Pc ligand of complexes with the sharp Q-band peak is the spectrum for a monomeric species. However, owing to the flat structure of the ligand and the large π-system, there is a strong tendency for Pc compounds to aggregate in solution *via* π-stacking.[34] This stacking can be either head-to-head or side-on, in which case the species in solution are termed H- or J-

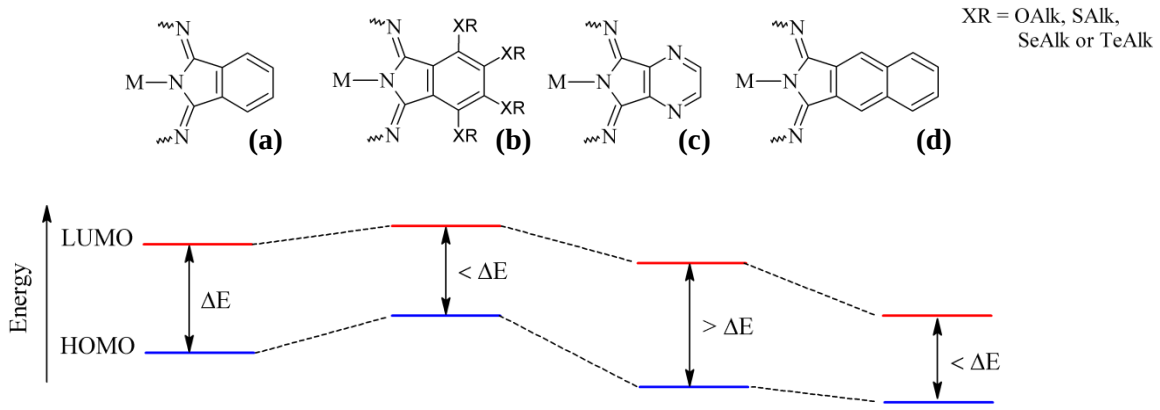

Figure 1.7: Modifications at or of the fused benzene rings of phthalocyanine (**a**), by substitution with group 16 elements (**b**), of benzene with 1,4-pyrazine (**c**) or of benzene for naphthalene (**d**) (top) to change Q-band absorption maximum by changing the HOMO-LUMO energy gap (bottom).

aggregates, respectively (Figure **1.8**).[35] Aggregation in solution is an important aspect of phthalocyanine photophysics and photochemistry, as it significantly alters the absorption and emission spectra of the compounds[36] as well as their photoreactivity;[37] this is incidentally also the reason for the generally poor solubility of unsubstituted Pc compounds. Therefore, Pc compounds are often modified with bulky groups on the Pc ligand to improve solubility and prevent the macrocycles from stacking together, such as the 1,1,4,4-tetramethyl-tetraline group first used by MIKHAELENKO.[38]

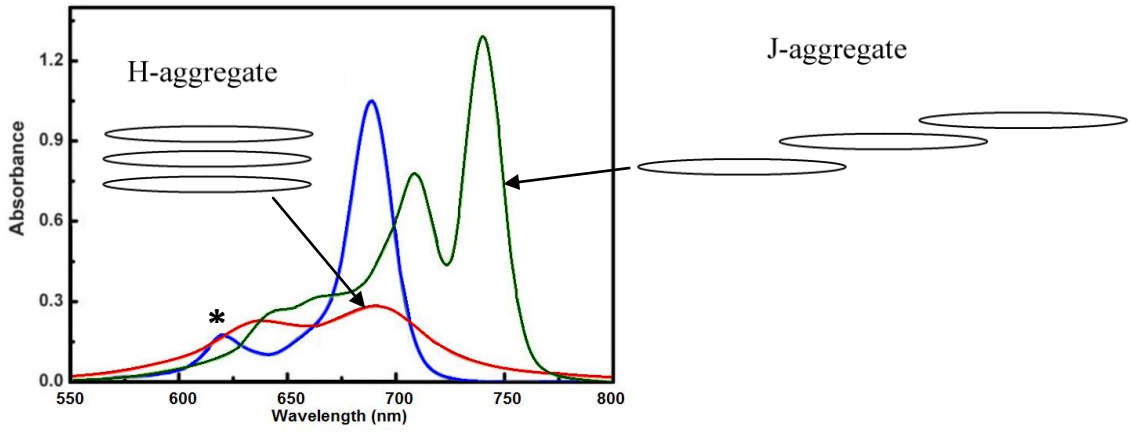

Figure 1.8: phthalocyanine H- (left) and J-aggregates (right) and the UV-Vis absorption spectra typically associated with such solution species (modified from reference 35).

As can be seen in Figure **1.8**, there is not a single transition associated with the Q-band, but rather, several other smaller bands can be seen at higher energies (these have been labelled with an asterisks, *, for the monomeric Pc spectrum). These addition bands arise because of coupling between vibronic states of the ground- and excited-state species, and are described by the Frank-Condon principle.[39]

1.3 Applications of phthalocyanines

Because of their robustness and optical properties, it is not surprising that Pcs have been used in a wide array of applications. The earliest and still most common use of Pc was, naturally, as a dye, and today can be found in paints, fabrics, lacquers[40,41] and plastics[5] and catalysts.[42] More recent and optoelectronic uses for them include their use in writeable compact discs,[43] as light filters in active matrix liquid crystal displays,[44] as photoconductors in laser printers[45] and as sensitisers in dye-sensitised solar cells (DSSCs).[46] Other optoelectronic applications where the use of Pcs is being researched are as optical limiters because of their non-linear optical properties,[47] as components in organic field effect transistors (OFETs),[46] organic light emitting diodes (OLEDs)[48] and as gas sensors.[49] In addition to the above mentioned applications, Pcs have been also been extensively investigated for medicinal applications as photosensititsers for the photodynamic therapy (PDT) of cancer cells,[50] the photodynamic inhibition (PDI) of bacterial cells[51] and the binding of G-quadruplex DNA.[52] Because of the large variety of applications of Pcs, the discussion of their application will be limited to those relevant to this work, *viz.* chromophores for energy applications, medicinal agents and electronic devices.

1.3.1 Phthalocyanines for energy conversion

Since the establishment of the *Erneubare-Energien-Gesetz* (Renewable Energy Law) in 2000, Germany has sought to transform its electricity supply based on fossil and nuclear fuel to completely renewable forms of electricity production.[53] As of 2016, renewable energy accounted for 33.9 % of the total electricity production in Germany, with photovoltaic systems producing a total of 38.2 TWh[54] in this same year. This increased reliance on renewable energy is not only located in Germany, but rather reflects a global trend.[55]

There is therefore pressure to develop ways of generating and storing renewable energy in a cost effective way. Like other chromophores, it is possible to use phthalocyanines for

renewable energy production in two different ways. The first is as a photosensitiser in photovoltaic devices. The second is as a photocatalyst for the production of so-called solar fuels, such as H_2. Each of these technologies will be reviewed in the following two sections, with a focus on the use and challenges of phthalocyanines in each of them.

1.3.1.1 Photovoltaic devices using phthalocyanines

Photovoltaic devices are a type of opto-electronic device where a photon is injected and an electron and hole are ejected. The separation of the electron-hole pair occurs at the interface of a semiconductor heterojunction. The basic principle underlying all solar cells is that absorption of a photon in the semiconductor results in the generation of an electron-hole pair. The excess electrons in the conduction band holes in the valence band are then separated by the internal junction field before recombination can occur. This separation of charges produces an open-circuit voltage, V_{OC}, or a short-circuit current density, J_{SC}.[56]

Solid state silicon based solar cells based on either single crystal, multi-crystalline or amorphous silicon have traditionally dominated the photovoltaic field, owing to their early discovery[57] and the availability of materials from the semiconductor industry.[58] Crystalline silicon devices offer the greatest efficiency of 24 % while amorphous silicon devices can only achieve a maximum efficiency of 18 %.[59] Crystalline silicon is an attractive material to use because of the high abundance of this element in the earth's crust. However, the expense of its purification has prevented its wide-spread terrestrial use. Other solid state heterojunction systems have been developed since then that have shown improved efficiency compared Si based devices, such as GaAs, which is the most efficient single junction device, with an efficiency of over 28 %.[60] The incorporation of toxic chemicals into these devices does of course pose health and environmental concerns. These problems lead chemists towards the development of solar cells that did not rely on expensive or toxic materials for their construction. Hence, solar cells have been developed using organic dyes, which provide the driving force of electron-hole production.

Dye-Sensitised-Solar-Cells (DSSCs): DSSCs are unique compared to other solar cell materials, in that the various processes of light harvesting and electron and hole transport are performed by different materials in the cell.[61,62] Figure **1.9** shows a schematic representation of a typical DSSC. Here, the dye or photosensitiser (PS) is adsorbed or anchored onto a wide-band-gap mesoporous metal-oxide semiconductor, which has been sintered together so that

electronic conduction can occur. The metal-oxide semiconductor is typically TiO_2, but ZnO, SnO_2 and Nb_2O_5 have also been used.[63] This dye/semiconductor junction forms the core of the device, where light is absorbed by the dye and the photoexcited electron transfers to the metal-oxide semiconductor's conduction band, which then carries the electron to one of the electrodes.[64] A redox couple, usually iodide/triiodide (I^-/I_3^-), then reduces the oxidised dye radical ($PS^{\bullet+}$), which formed after electron injection, and transports the positive charge (electron hole) to a counter electrode.[65] The voltage generated under illumination is dependent on the Fermi level of the electron in the solid and the redox potential of the redox mediator.[58]

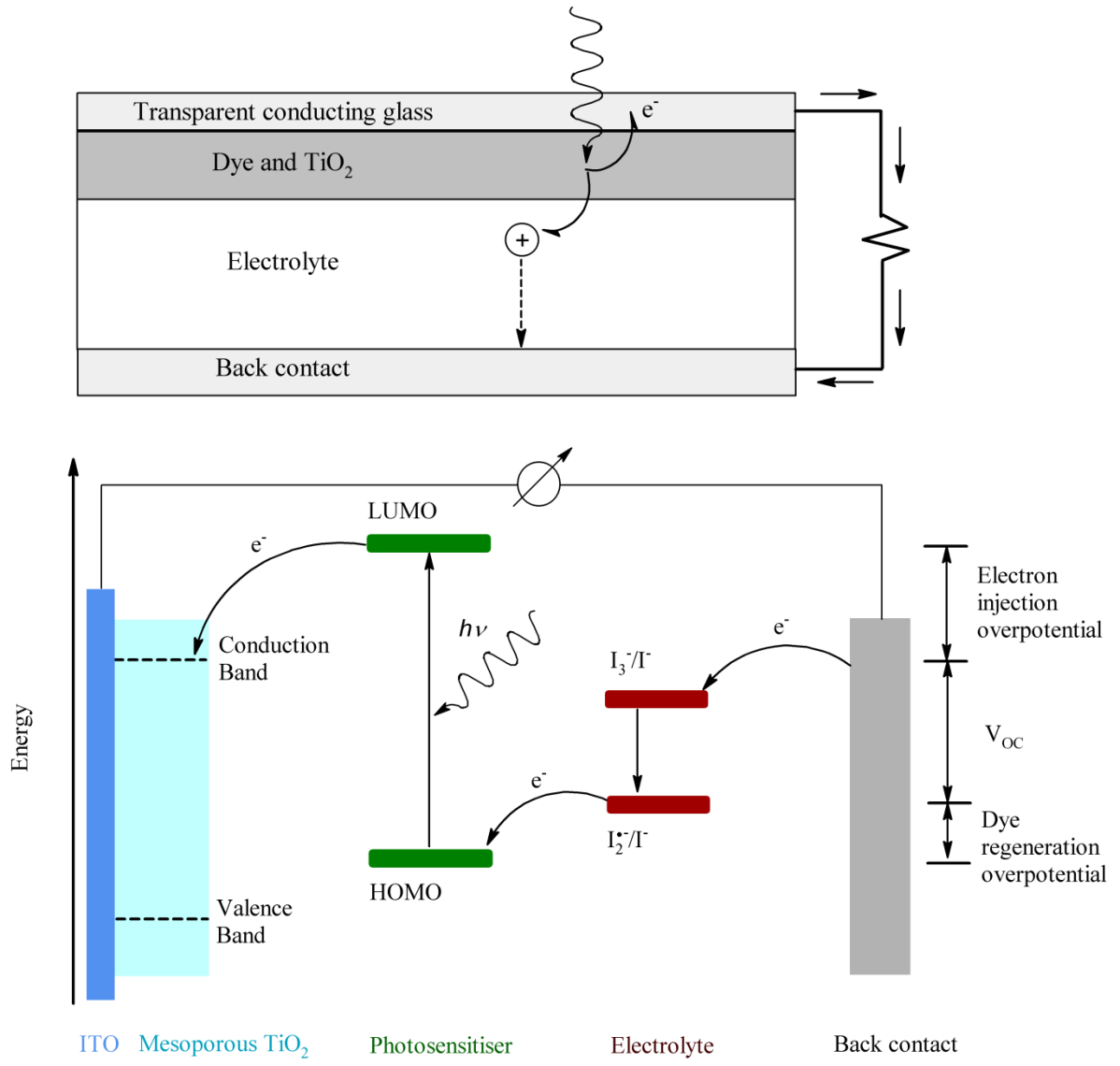

Figure 1.9: Schematic assembly of a DSSC (top) and an energy level diagram showing the principle of operation of a DSSC (bottom).

As can be seen from the construction and operational principle of a DSSC, the dye used plays a crucial role in the initial charge formation and electron donation. Much effort has therefore been devoted to the synthesis and study of various types of dyes that can function as effective PSs. Many different dye classes have been synthesised and investigated; the earliest of which were bpy-ruthenium based complexes in so-called Grätzel cells.[66] These dyes have broad absorption spectra but low molar attenuation coefficients and weak absorption towards the NIR region. Although DSSC devices based on these dyes do work, the expense and limited availability of Ru, as well as the desire for improved light harvesting, have driven the research into new dye classes, including cyclopentadithiophenes,[67] porphyrins and phthalocyanines. In general, the dye should meet certain criteria, namely:

- Have a strong absorbance in as much of the visible and NIR regions as possible,
- The HOMO and LUMO of the dye must match the valence and conduction band of the semiconductor, respectively,
- The HOMO of the dye must be energetically lower than the HOMO of the redox mediator,
- Charge transfer (CT) between the dye and semiconductor substrate should be efficient, being realised by adsorption, chemisorption or covalent binding of the dye to the semiconductor,
- The adsorbed or chemisorbed dye should be stable for long periods of time,
- The individual dye molecules should pack tightly onto the metal-oxide surface for maximum light absorption, but…
- not so tightly that they aggregate and quench one another's excited states..

Because greater amounts of red and infrared light reach the earth's surface, improving Pc light absorption in the near-IR (NIR) area continues to be a major research focus. How changes to the Pc ligand cause a shift of the Q-band absorption was already discussed in section **1.2.2.1**. More recently, it has been found that chelation of P(V) in the central Pc cavity induces a further red-shift of the Q-band. When combined with an organochalcogenide substituted Pc ligand, a red-shift of the Q-band absorption maximum to over 1000 nm can be obtained.[30]

A disadvantage of Pc dyes is their low absorbance between the B- and Q-band. This is a region of at least 300 nm (more if the Q-band has been red-shifted) that is entirely unutilised by Pc photosensitisers. Understandably then, there has been much effort in synthesising a chromophore that possess absorption in the entire visible to near-IR region; such a chromophore is termed to have panchromatic absorbance.[68] Although there have been several notable reports of sensitisers having panchromatic absorbance recently,[69] these are in fact conjugates or supramolecular assemblies of two or more different chromophores. Often, a very complicated and low yielding synthesis is required to make them, and their energy conversion efficiency has still not greatly improved compared to simple systems. Despite this, they continue to gain much attention because of the potential usefulness of these systems for solar energy conversion. An example of one such system using a subPc and three Zn(Pc) complexes in shown in Figure **1.11**.

An additional strategy that is used to improve dye performance is to couple the dye with a suitable electron donor and acceptor group to facilitate separation of the exciton pair and injection into the semiconductor substrate. The best energy conversion efficiency for

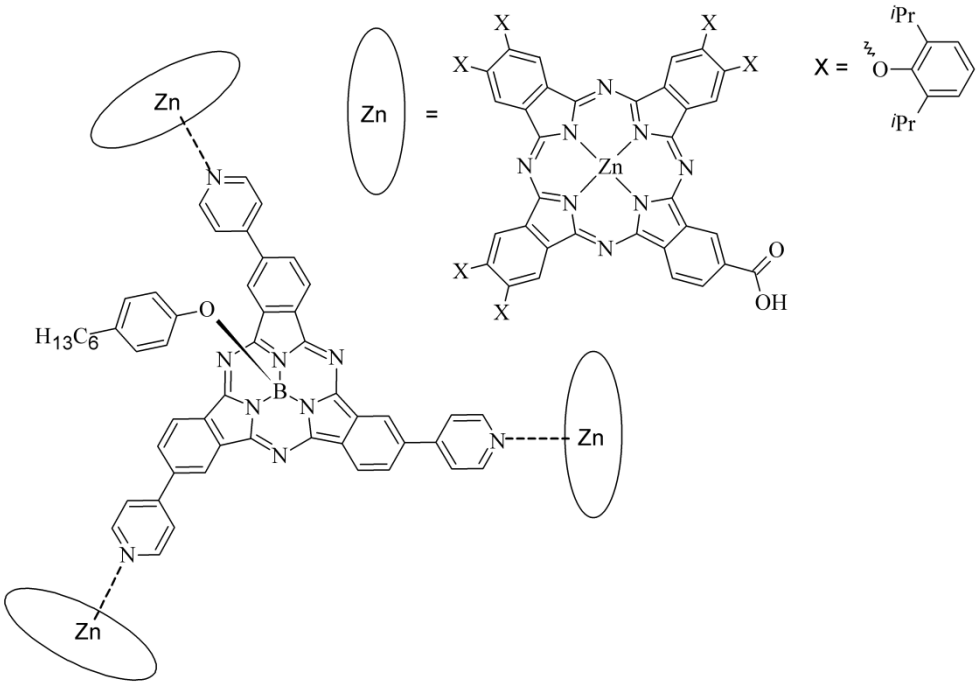

Figure 1.11: Conjugation of multiple chromophores is a common strategy for improving light harvesting. Depicted is an example of a four component system employing two different chromophores.[69,e)]

phthalocyanine dyes reported to date is just over 6 % for **TT40**[70] and **PcS20**.[71] Both Pcs have the donor-dye-acceptor structure (Figure **1.12**). This is however still only half as high as the best reported energy conversion efficiency for a DSSCs using Ru-based or porphyrin dyes (> 12 %).[72]

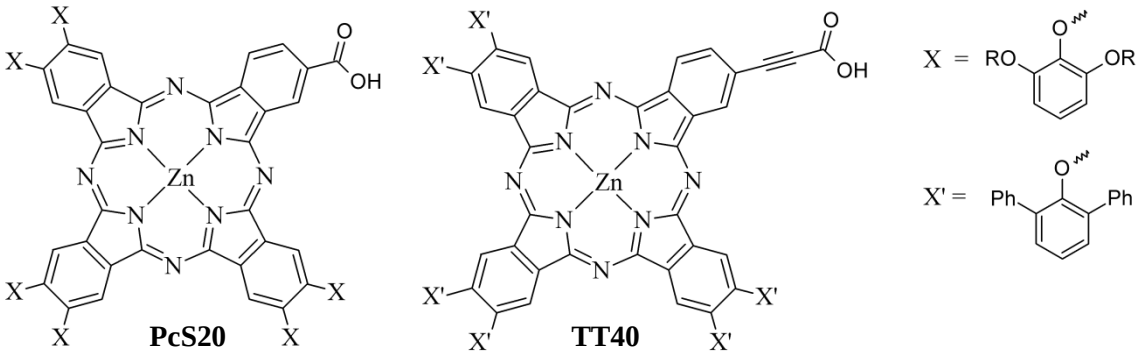

Figure 1.12: Structures of the best performing phthalocyanine-based dyes **TT40** and **PcS20** used in a dye-sensitised solar cell (DSSC) containing TiO_2.

A largely overlooked aspect of photosensitiser design is the spin state of the excited electron, *i.e.* if the PS is in the singlet (S_1) or triplet (T_1) excited state. For Ru based PSs, photoexcitation leads to population of the T_1 state, from which electron injection into the semiconductor occurs.[73] Population of and injection from the T_1 state is indeed advantageous. The T_1 state is energetically lower than the S_1 state, and therefore the interfacial energy difference and driving force for electron injection is less favourable. However, the lifetime of the T_1 state is significantly longer than that of the S_1 state, in the range of 5 orders of magnitude.[73] This enables a high quantum efficiency of electron injection from this state, as opposed to the S1 state, where many of the excited electrons relax to the ground state before they can be transferred to the semiconductor. Considering that Ru-based dyes have much lower absorbance than phthalocyanine and yet still manage to outperform them in terms of energy conversion efficiency, an investigation of the strongly absorbing chromophores with a well-populated triplet state is warranted.

Organic photovoltaic cells: In addition to being used as sensitisers in DSSCs, phthalocyanines have also been investigated for use in organic photovoltaic (OPV) cells. These cells are based on optically and electrically active polymers and small molecules with overlapping band-gaps, and, like DSSCs, are attractive as low-cost alternatives to traditional

inorganic solar cells.[74] In OPVs, the cathode is typically a transparent conductor, such as ITO glass and the anode is a metallic conductor, such as aluminium. They offer the additional advantages of being thin, lightweight and flexible.[75] In an OPV, a photon excites an electron in the photosensitiser HOMO to the LUMO, where it then moves to the LUMO of an acceptor molecule. In this way, the electron-hole pair is separated so that the electron and hole can diffuse to the respective electrodes. OPVs can be further differentiated by their architectures. When the donor and acceptor are deposited in layers, the cells are termed planar heterojunction (PHJ) cells, and when the donor and acceptor are deposited together in a blended film, the cell is termed a bulk heterojunction (BHJ) cell.

The first OPV reported was in 1986 by TANG *et al*, who used p-type copper phthalocyanine as the donor material mixed with an n-type tetracarboxylic perylene derivative as the acceptor material with a PHJ architecture; the cell achieved an efficiency of 1 %. Since then, phthalocyanines are often used with fullerenes or carbon nanotubes as electron acceptors.[76] There are numerous examples where fullerenes, in particular, are modified with a binding group, typically a pyridyl group, to covalently interact with the donor, typically a zinc(II)phthalocyanine derivative, to improve the efficiency of charge transfer between donor and acceptor.[77] In these charge-transfer complexes, the fullerene derivative is coordinated at the pyridyl N-atom to the central zinc(II) ion of the phthalocyanine. Phthalocyanines have also been used as additives in other BHJ cells where a polymer donor is used. Here, the phthalocyanine ligand is often modified to form a covalent attachment with the donor polymer (see Fig. **1.13**). Alternatively, the phthalocyanine derivative acts as an additive to improve the blend morphology and charge separation (CS) between acceptor and donor entities; an example of which is the axially modified bis(trihexylsiloxy)-silicon(IV) phthalocyanine, which was used in a BHJ device to significantly improve the cell efficiency from 2.2 % to 2.7 %.[78] Figure **1.13** shows representative examples of a Pc-fullerene and Pc-polymer conjugate and a PcSi BHJ additive.

1.3.1.2 Photoredox catalysts for H^+ reduction

As mentioned in section **1.3.1**, a second possibility for producing renewable energy is by the synthesis of solar fuels. These constitute any fuel produced directly or indirectly by solar energy, but often the target fuels are hydrogen from H_2O due to the massive abundance of water or carbon-based compounds from atmospheric CO_2.[79] Photocatalytic water splitting over the semiconductor TiO_2 was demonstrated already in 1972.[80] Since then, various

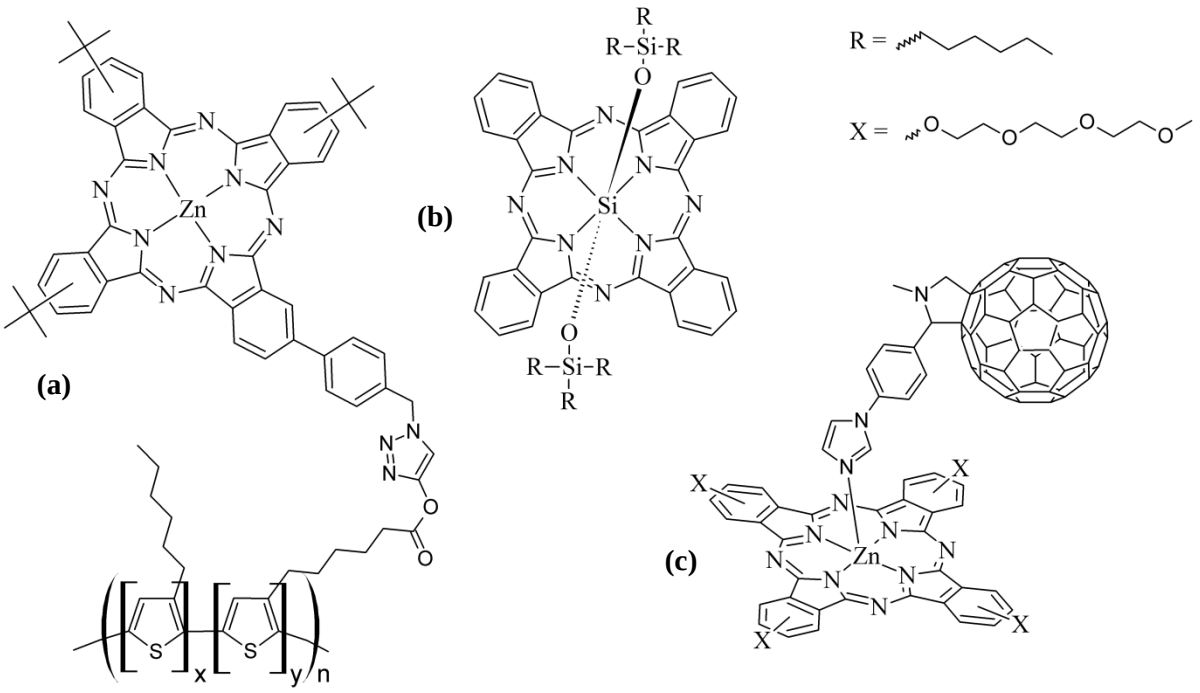

Figure 1.13: Metallo phthalocyanines used in the construction of organic solar cells: **(a)** Zn(Pc)-polymer,[77:c)] **(b)** PcSi[78] and **(c)** Zn(Pc)-fullerene.[77:b)]

semiconductor combinations, both organic and inorganic, have been tested in the hopes of developing a viable system.[81] Molecular chromophores can also be used for water splitting, because the photoexcited species has both an unpaired electron and an electron hole, making it simultaneously a powerful reductant and oxidant, respectively.[82]

Other molecular species can be used for catalytic water splitting when they are activated electrochemically, that is, when a radical anion or cation is generated. Owing to the huge variety of photocatalytic water splitting systems being investigated, only molecular photocatalysts will be considered in the remainder of this section. The mechanism of H^+ reduction by molecular catalysts is believed to occur *via* an initial one-electron reduction and proton binding at the metal-donor ligand, followed by a second one-electron reduction and proton binding at the metal centre. The individual hydride ligands then bind to each other and are released as molecular hydrogen.[83] It has been suggested, however, that initial binding of both protons occurs exclusively at the metal centre[84] or at the donor ligands, followed by migration to the metal centre.[85] Scheme **1.5** shows the initially described mechanism for H^+ reduction by a molecular catalyst.

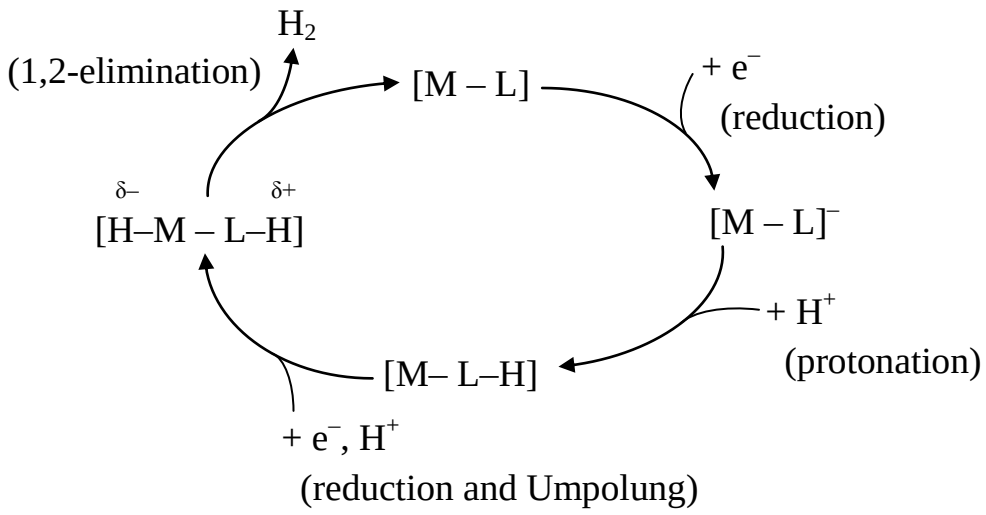

Scheme 1.5: The postulated mechanism of H^+ reduction to H_2.[83]

Light-driven generation of H_2 requires a photosensitiser for electron-hole formation, a means of separating the electron-hole pair, a catalyst for collecting protons and electrons and a proton source.[86] While molecular catalysts have been developed using 3-, 4-, and 5d transition metals, there is particular interest in using inexpensive 3d metals. Most molecular catalyst investigated[87] have used Co, Ni and Fe complexed by four N-atoms, such as in [14]tetraene-N_4 macrocycles[88] and dimethyl glyoxime derivaties (Figure **PR1**).[89] Notable exceptions are complexes based on the [FeFe]- and [NiFe]-hydrogenase enzymes',[90] active sites, a dinuclear M-Fe complex with mostly thiolate land carbonyl ligands. Photocatalytic activity is achieved by coupling a chromophore, such as a Ru(bpy) derivative, to the 3d metal catalyst. In these systems, the electrons required for H^+ reduction are supplied to the catalyst by the excited chromophore (PS*), which is regenerated using a sacrificial electron donor, such as triethanolamine. The highest turn-over number (TON) for a non-noble metal based photocatalytic system reported is 2 700, using the bio-inspired $[Ni(P_2^{Ar}N_2^{Ar})_2](BF_4)_2$ catalyst (Figure **1.14**) of DuBois *et al.* in the presence of Eosin Y as sensitisers and ascorbic acid as sacrificial reductant.[91] This is considerably less than many noble metal photocatalysts, such as a BODIPY sensitised platinum diimine dithiolate (PtN_2S_2) system (Figure **1.14**), which shows a TON of *ca.* 40 000.[86]

For catalytic activity to exist, the ligand used must be able to stabilise different metal oxidation states and geometries. Non-innocent dithiolene and thiocatecholate ligands have been of special interest for over five decades[92] because of their rich redox chemistry.[93]

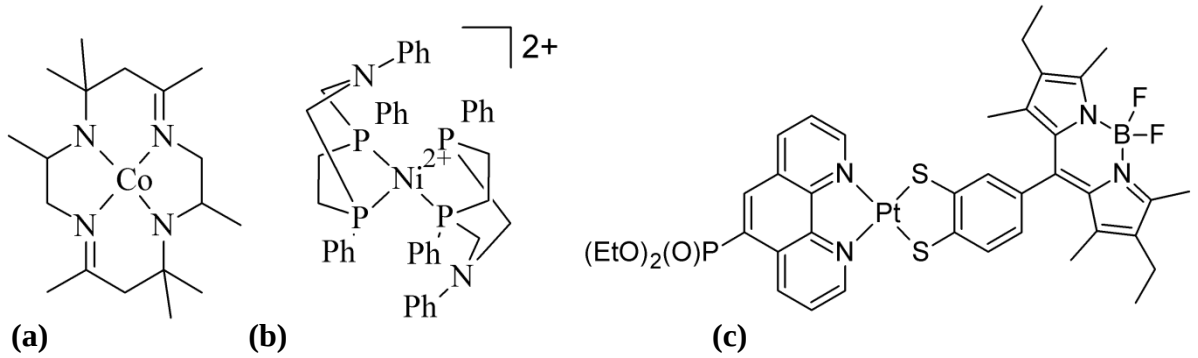

Figure 1.14: Molecular catalytic systems using: (**a**) a tetraaza-macrocyclic ligand, (**b**) biomimetic principles and (**c**) a conjugated photosensitiser.

Because of their ability to be reversibly oxidised and reduced, it is possible to use them as electron donor ligands in heteroleptic complexes of the type [S_2-M-L_2], where L_2 is typically a neutral, bidentate aza-ligand. Strong ligand-to-ligand charge transfer (LLCT) bands are observed in such complexes, the energy of which is readily tuned by changing the donor or acceptor ligand.[94] Owing to the strong LLCT and stable and reversible redox properties of these complexes, their use in mediating photocatalytic reactions, such as H^+ reduction to H_2, was already proposed twenty years ago.[95] Although this was proposed two decades ago, very little effort has been made in synthesising such systems. One noteworthy exception is the good performing BODIPY-PtN_2S_2 system described above. A synthetic method does, however, exist to combine up to four dithiolate ligand groups with tetraazaporphyrazine (tap) macrocycles (see Scheme **1.6**).[96]

The synthesis of tap macrocycles, as for phthalocyanines, almost always involves high temperatures and basic conditions, which are not compatible with common thiol(ate)

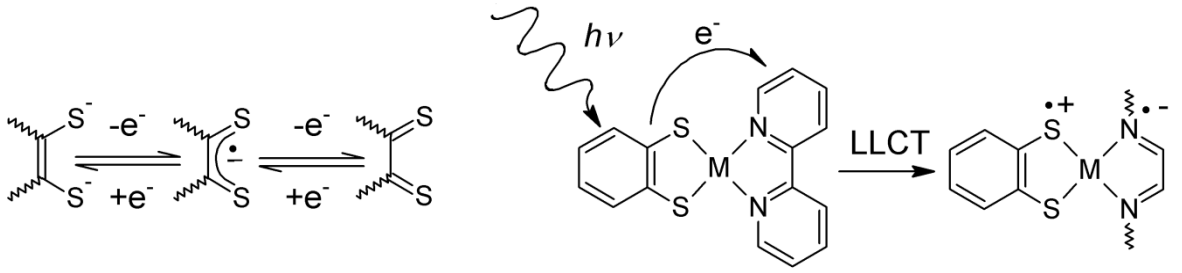

Figure 1.15: (left) The redox-active nature of 1,2-dithiolene groups, and (right) the process of ligand-to-ligand charge transfer (LLCT) between a 1,2-thiocatecholate donor and diimine acceptor.

protecting groups. A method was demonstrated by the groups of Barrett and Holm, who masked the thiolate as an S-benzyl group.[96] This group could then be cleaved under Birch-type conditions by reduction with Na in NH_3 (l). Di-, tri-, tetra- and penta-nuclear complexes were synthesised by coordinating metals through the peripheral dithiolate groups. Only basic structural and spectroscopic properties of these complexes were however studied. Any potential they have as photocatalysts is therefore unknown. The same strategy was applied to synthesise a pentanuclear Pc complex with four peripheral S_2SnBu_2 groups, for which only minimal characterisation was conducted.[97] The effect that dithiolate formation and metal coordination has on the electronic and spectral properties of Pc, as well as the potential of this chromophore to promote light-driven catalytic reactions, remains to be seen. Scheme **1.6** shows the synthesis of a pentanuclear tap complex.

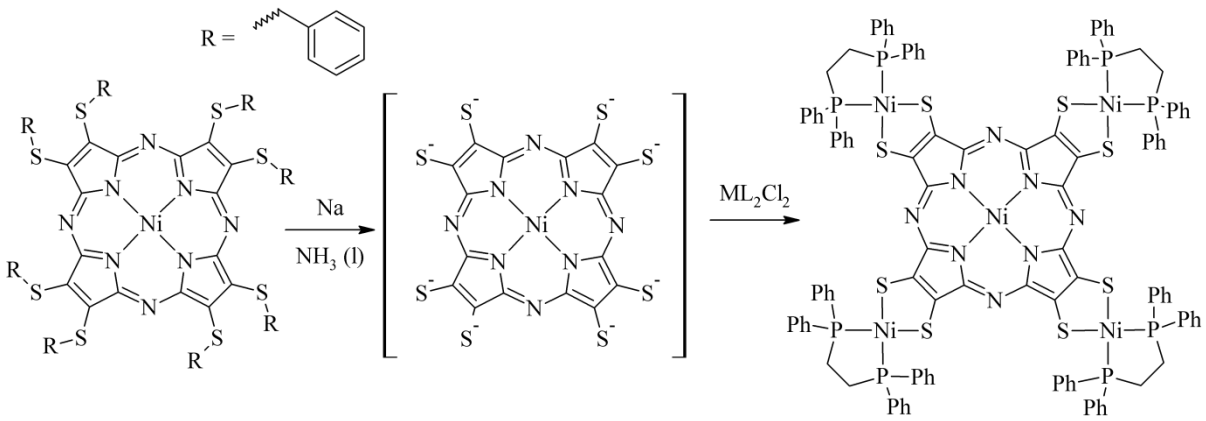

Scheme 1.6: Synthesis of the pentanuclear tetradithiolene-tsp complex $[Ni(dppe)]_4[Ni(pzot)]$ from the starting S-benzyl Ni(tap) complex.[96;b)]

1.3.2 Medicinally active compounds

As mentioned previously, phthalocyanines have also been investigated for their medicinal properties. They have been investigated mainly as cancer therapeutics and as bacteriocidal agents. These therapeutic properties are determined either by their ability to generate singlet oxygen or by their ability to bind specific biological targets. How these two properties work together with their desired functions will be discussed in the following two sections on medicinally active phthalocyanines.

1.3.2.1 Photosensitisers for photodynamic therapy

Photodynamic therapy (PDT) refers to the treatment of cancer using a light-absorbing drug, or photosensitiser (PS).[98] The PS is non-toxic until it is irradiated with light of a suitable wavelength, when it then transfers energy to triplet oxygen already dissolved in the tissue to generate singlet oxygen, known as a Type II reaction. Singlet oxygen is a reactive oxygen species (ROS) that causes cell damage and eventually cell death through apoptosis, necrosis or autophagy when produced in sufficient quantity. Alternatively, the PS can transfer energy directly to biomolecules, which leads to necrosis. This latter pathway is termed a type I reaction; in PDT, type I reactions occur far less frequently than type II reactions, and are therefore of lesser significance. The advantage of PDT is the selective nature of the treatment; the PS is only toxic where the tissue is irradiated. This greatly reduces the risk of damaging healthy tissue, even tissue that is close to the infected region.[50, 99] The process of PDT is illustrated in the JABLONSKI diagram below (Scheme **1.7**).

Photosensitisers can be broadly divided into three groups, namely first, second and third generation compounds.[100] Research into first generation compounds started in the early 1950's, where it was found that haematoporphyrin compounds localised in tumour tissues.

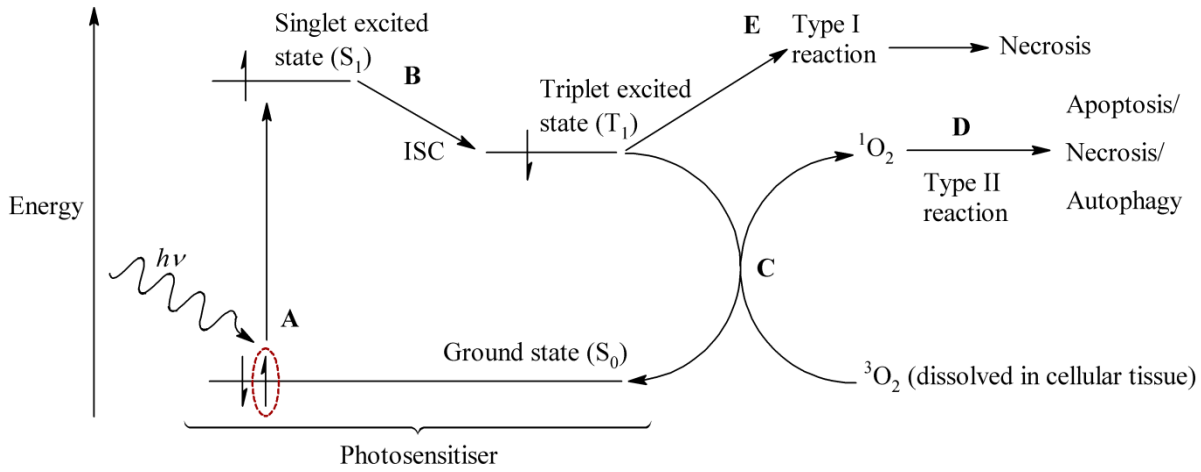

Scheme 1.7: Schematic JABLONSKI energy level diagram for the process of photodynamic therapy (PDT). A – light absorption by the photosensitiser, B – inter system crossing from the singlet (S_1) to the triplet (T_1) state, C – energy transfer from the T_1 state to triplet oxygen ($^3O_2$) forming singlet oxygen ($^1O_2$), D – type II reaction of $^1O_2$ with biomolecules leading to apoptosis, necrosis or autophagy, E – type I reaction between the excited PS* and biomolecules leading to necrosis.

Photofrin® (Figure **1.15)** is an example of a first generation drug, used for the treatment of lung, bladder, esophageal and cervical cancer.[101] It is an undefined haematoporphyrin mixture, rather than a discrete compound, that has good absorption only in the visible region, limiting its use to superficial tumours. In addition to this, it is insoluble in water, which further limits its usefulness. Second generation compounds sought to address the early problems of Photofrin® and other first generation compounds. A number of different macrocyclic systems related to haematoporphyrin were explored, including porphyrins, phthalocyanines, chlorins and corroles, as well as alternative systems, such as fullerenes.[102] Phthalocyanines have a significant advantage over the other tetrapyrrolic systems, as their absorption maximum is typically between 600 and 850 nm, which would allow for the treatment of non-superficial cancers. The major drawback of Pcs is their generally poor solubility in water, which was overcome by introducing either anionic groups, such as sulfontates[103] or carboxylates, onto the Pc ligand periphery, or by using charged groups coordinated axially *via* the central metal/atom.[104] Examples of compounds that use these strategies are Photosense®, which is a mixture of mono- to tetra-sulfonated aluminium Pc,[105] and the so-called Pc4, a silicon Pc with one axial aminosiloxyl group,[106] which has has undergone promising Phase I clinical trials (Figure **1.15**).[107] Second generation photosensitisers, therefore, showed good phototoxicity, but still lacked good selectivity for cancer cells. Third generation photosensitisers are being designed with improved selectivity in mind. Typically, they are conjugated to biomolecules, such as sugar molecules or peptides. Sugar molecules are taken-up at an increased rate by cancerous cells compared to healthy ones, which improves the localisation of PS in cancer cells. Additionally, because cancer cells over express certain receptors, conjugation of the corresponding peptide with a PS can further improve the specificity towards cancer cells. An example of a third generation phthalocyanine based PS investigated is galactose or glucose substituted SiPc[108] (Figure **1.15**).

1.3.2.2 Photosensitisers in photothermal and photoacoustic therapy

Photothermal therapy (PTT) is a related tumour treatment modality to photodynamic therapy, where a photothermal agent absorbs optical energy and converts it into thermal energy.[109] Thermal stress then causes cancer cells within the irradiated region to die. When the same photothermal agents are irradiated with pulsed light, the thermal energy is converted into an acoustic shockwave, which causes further cell death by mechanical destruction; this is known as photoacoustic therapy (PAT).[110]

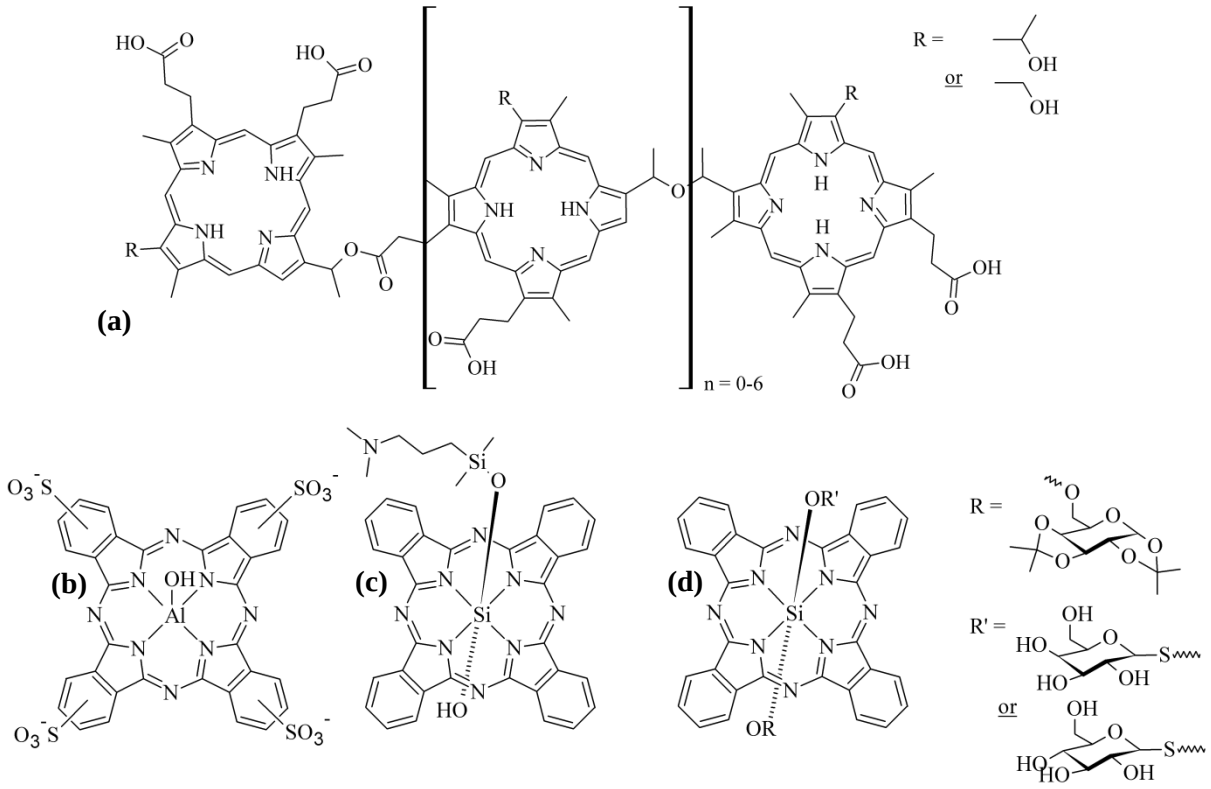

Figure 1.15: Representative first (**(a)** Photofrin®), second (**(b)** Photosense and **(c)** Pc4) and third (**(d)** Si(Gal)(Pc)) generation photosensitisers.[101]

Very recently, phthalocyanines have been shown to function as photothermal agents when their radiative emission (fluorescence) and intersystem crossing (ISC) processes are suppressed. This has generally been accomplished by inducing aggregation of the Pc complexes, typically by inclusion within a capsule.[110,111] It is also possible to promote the non-radiative, thermal relaxation pathways by incorporating groups onto the Pc ligand that quench the emission *via* the process of photoinduced electron transfer (PET) or by incorporating a paramagnetic metal into the structure.[112]

Photoinduced electron transfer is a well-known effect that occurs when an electron from a nearby donor group fills an electron hole left by photoexcitation of a chromophore. This effectively blocks the pathway for fluorescence, and promotes relaxation by non-radiative channels. Amino groups in particular are known to promote this effect. Zinc and silicon Pc complexes with amino groups substituted at the Pc ligand α-position and coordinated axially on silicon, respectively, were synthesised as PTT agents to demonstrate the added cytotoxic effect that heating has during irradiation.[112] In the same study, it was demonstrated how

copper Pc complexes had a significantly higher cytotoxicity than their corresponding zinc Pc complexes, showing the potential advantages of PTT over PDT modalities. Examples of these complexes are shown in Figure **1.16**.

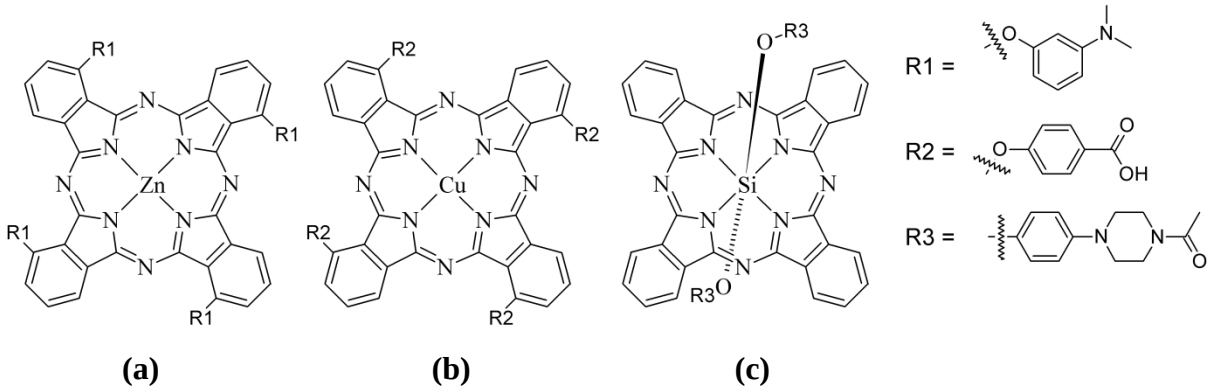

Figure 1.16: Examples of phthalocyanine complexes examined for use in photothermal therapy, relying on photoinduced electron transfer from amines on the Pc ligand **(a)** or central metal ion **(c)**, or paramagnetic metal induced decay processes **(b)**.[112]

1.3.2.2 Binders of G-quadruplex DNA

G-quadruplex DNA, or simply G4 DNA, is a non-canonical nucleic acid structure; that is, it is DNA that does not adopt the simple Watson-Crick duplex, but rather a complex four-stranded structure with stacked guanine tetrads, or G-quartets.[113] G4 DNA is a target for cancer therapy because of its location in telomeric DNA. During cell division in normal healthy somatic cells, telomere length decreases, thus limiting the potential proliferation of the cell. Conversely in 80-85 % of human tumour cells, telomeres are lengthened by telomerase. However, the presence of a G-quadruplex prevents telomerase activity, and therefore stabilisation of the G-quadruplex by ligand binding inhibits telomerase activity and prevents cell proliferation.

The two main requirements of a G4 ligand is that possess a large planar aromatic system to promote π-π stacking with the DNA nucleobases as well as cationic groups to improve interactions with the anionic charge of phosphates inherent to DNA. Both porphyrins and phthalocyanines, when modified with cationic groups, fulfil these requirements very well owing to their large π-systems. The tetracationic porphyrin derivative TMPyP4[114] was one of the earliest compounds explored as a G4 binder, and as such is often used as a standard in

G4 binding assays. However, the π-system of phthalocyanines overlaps better with the G-quartets than that of porphyrins. To date, the strongest G4 binder reported is the tetraguanidinium modified Pc, Zn-DIGP.[115] The structures of both TMPyP4 and Zn-DIGP are shown in Figure **1.17**.

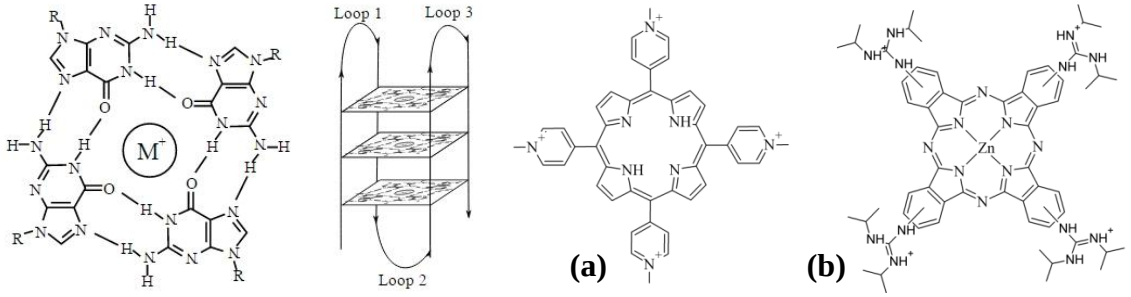

Figure 1.17: (Left) Two views of the structure of G-quadruplex DNA*. Two tetracationic binders of the G-quadruplex motif: porphyrin derivative TMPyP4 **(a)** and phthalocyanine derivative Zn-DIGP **(b)**. *G4 DNA graphic: Wikimedia.

1.3.3 Phthalocyanines in self-assembled monolayers

Many different properties and uses of phthalocyanines have been reviewed in the preceding sections of this chapter. When Pcs are used in optoelectronic applications, very often a film coating a substrate is required,[116] such as when sensitising metal oxide semiconductors in solar cells. Because the order (or lack thereof) of the initial layer deposited has consequences for any further deposited layers and/or proper functioning of a potential device, understanding and controlling the first layer deposited has become an important topic in utilising Pcs for device fabrication. The first molecular layer that deposits, regardless of the order of the molecules on the surface, is termed a monolayer. When molecules order themselves in some way, a self-assembled monolayer (SAM) is formed. SAMs, therefore, spontaneously adsorb on a solid surface, which is located either in solution or in the gas phase.[117] SAM formation on a substrate is typically achieved by including a functional group on a Pc that will preferentially bind to the substrate. There are numerous examples of Pc derivatives with a carboxylate group, for instance, which is intended to bind selectively with metal oxide semiconductors, such as TiO_2. In the study of SAMs, though, the best characterised systems are of gold–thiol SAMs. [117] Gold is ubiquitous in electronic devices,

and interfacing gold with organic, metal-organic and biomolecular systems through a SAM provides an interface between these two worlds.[117]

The incorporation of a thiol group on a Pc should therefore make a compound capable of forming a Pc-thiol-gold SAM. Pioneering work in this field was performed by COOK *et al.*,[118] who appended singlet thiolalcohol groups at the Pc α-position using alkyl chains of varying length. The stability of these SAMs increased with the length of the alkyl chain. Since then, various other authors have reported the synthesis of Pc derivatives with thioethers, thioalcohols and amines, and their adsorption onto gold.[118,119,120,121] Apart from fundamental studies on the ordering of the Pc complexes on the various substrates, they have also been used as photoelectronic switching devices,[119] as electrocatalysts for oxidation[120] and as singlet oxygen generators in nanoparticle mediated photodynamic therapeutic.[122] A review of this literature, however, reveals a surprising lack of attention as to the integrity of the SAM formed. In the majority of cases, Pcs are modified with multiple anchoring groups so that no particular molecular orientation is preferred; this is almost always not evaluated. Additionally, the surface bound species are also not examined, instead it is just assumed that the desired binding has formed. Figure **1.18** shows the structures of Pc-thiol derivatives investigated by COOK *et al.*, as well as those typically used in studies of Pc-Au SAMs. Fundamental studies on the formation of Pc-thiol-gold SAMs need to be performed before this interesting and useful class of materials can be successfully used with gold substrates.

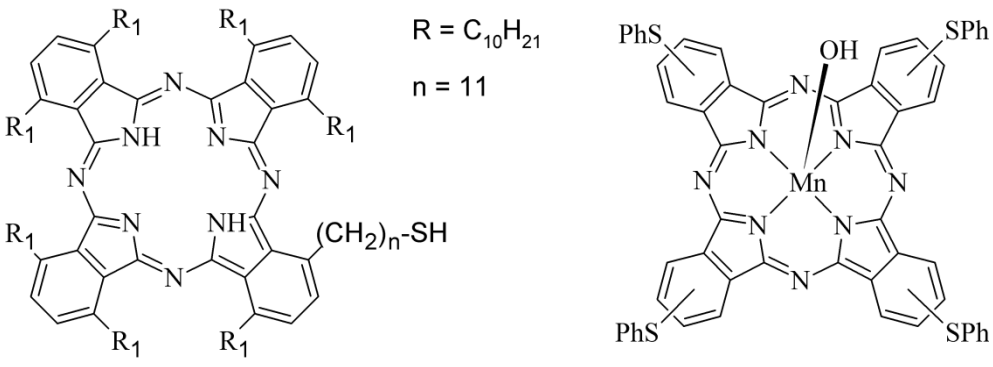

Figure 1.18: Structures of thiolalcohol- and thioether-Pc complexes used for SAM formation on gold substrates. While some effort has been made to synthesised isomerically pure compounds (left)[118], most are not designed with any specific binding orientation in mind (right).[119-d)]

1.3.4 Metal-imido phthalocyanine complexes

As seen for most the Pc complexes described above, modification of the complex is generally restricted to the Pc ligand itself. However, the Pc ligand is capable of coordinating almost all transition metals, which opens the possibility for the coordination of additional ligands at the coordinatively unsaturated metal centre. This property has been exploited to use phthalocyanines in molecular wires,[123] photoactive medicines,[124] photosensitisers in renewable energy production, [125] and as catalysts.[126] Even complexes with very simple axial ligands, such as PcTiO,[127] PcVO[128] and PcAlCl,[129] have shown an affinity for forming homogenous, highly ordered mono- and bilayers. This is because the induced dipole, absent in planar Pc complexes, favours certain arrangements over others, and thus alters the conductivity and optical properties of Pc films. Despite this, there has been comparatively little work done to explore the synthesis and properties of metallo Pc complexes with novel axial ligands. In the remainder of this section, the synthesis and properties of metal-imido phthalocyanine complexes will be briefly reviewed.

Metal-imido (M=NR) complexes are known to catalyse a variety of reactions, including: olefin polymerisation reactions,[130] ring opening of epoxides,[131] aziridines[132] and cyclopropanation of olefins.[133] The M=N bond is typically synthesised by combined two equivalents of LiNHR with a metal chloride; LiCl and H_2NR are by-products of this reaction. Pc related (Porphyrin)M(NR) derivatives have been synthesised in this way with group 4 (Zr, Hf)[134], 6 (Cr, Mo)[135], 7(Mn)[136], 8 (Ru)[137] and 9 (Co)[138] metals starting from the (Por)MCl_2 complexes. An exception is the (Por)Cr(NR) complex, that is synthesised by oxidative addition of an organic azide to a Cr(II) centre to form the Cr(IV)(NR) species and N_2 gas.[135] Additionally, it was demonstrated that Ru and Mn complexes catalysed N-atom transfer as aziridination of aromatic alkenes and amidation of benzylic hydrocarbons with PhI=NTs as nitrogen source.[136] Similarly, PcM(NR) complexes have been synthesised, where M is Ti,[139] Mo, W and Re.[140] Catalytic activity was again demonstrated for the Ti complex, where addition of RNCO to the titanyl (Ti=O) complex produced carbodiimides (R–N=C=N–R) for both aromatic and alkyl "R" groups (Scheme **1.8**). The catalytic cycle proceeds *via* a PcTi(NR) intermediate.

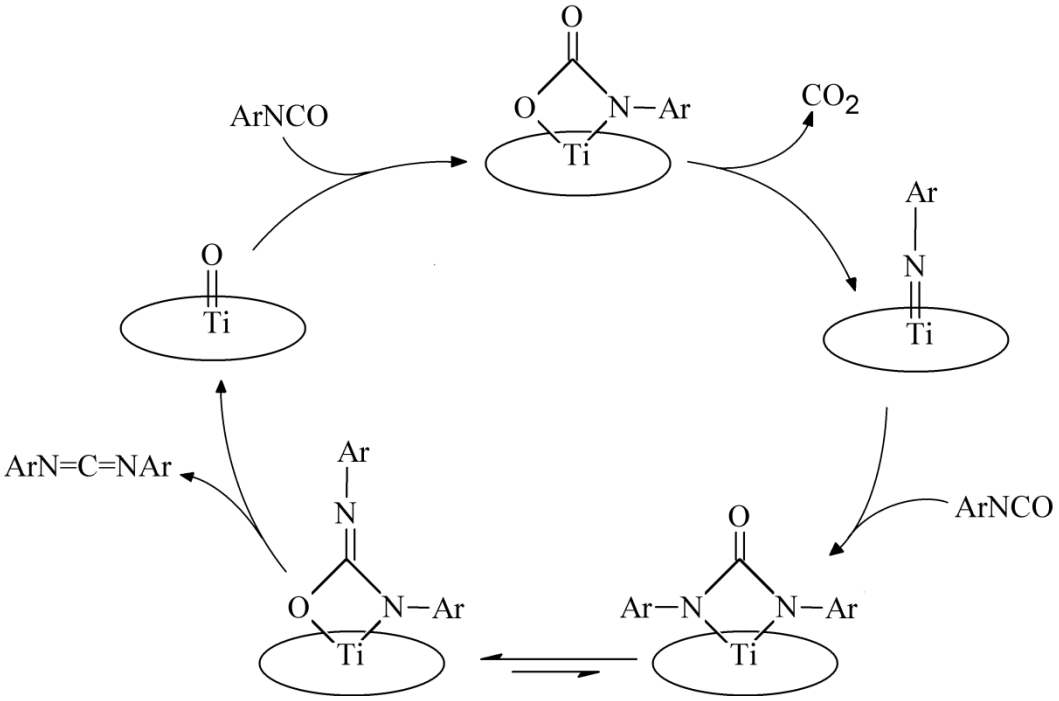

Scheme 1.8: Catalytic metathetic carbodiimide synthesis by PcTiO using RNCO as feedstock.[139]

In contrast to the synthesis of (Por)M(NR), which typically start from the metal-chloro complex, it is possible to synthesis PcM(NR) complexes directly using $M(NR)_xCl_y$ starting complexes as templates for the Pc formation. For Mo, Re and W complexes synthesised this way, an additional chloro ligand is also still coordinated to the metal to give complexes of the type PcM(NR)Cl. Although not expected to have a strong influence on the Pc complexes optical properties, imido ligand coordination does induce small red-shifts in the Pc ligand's Q-band. However, because of the various groups that can be coordinated through the imido-N atom, a very strong dipole moment can be induced. As mentioned above, a strong dipole moment significantly enhances surface ordering of deposited Pc films. Such complexes are therefore also interesting as materials for opto-electronic applications. Considering this aspect and the catalytic potential of metal-imido complexes, the stabilising effect of Pc ligands and the small amount of research done so far in this area, investigating the synthesis and properties of these complexes would be a worthwhile endeavour.

CHAPTER 2 | PURPOSE OF THE WORK

The purpose of this work is divided into several components, each of which will be briefly outlined below.

The major areas of research for phthalocyanines are as photosensitisers in solar cells and in photodynamic therapy. In both of these areas of application, it is desirable that the photosensitiser has an absorption in the near-infrared (NIR) portion of the spectrum, and that predominantly the triplet (T_1) state becomes populated upon photoexcitation. The main component of this work therefore deals with the challenges of synthesising phthalocyanines derivatives that have enhanced light absorbing properties compared to the basic Pc ligand. As already mentioned in the introduction, there are two strategies to extend the range of light absorption of Pc: either the π-system can be extended, as in the case of naphthalocyanines, or the respective energies of the HOMO and LUMO can be altered by substitution of H on the Pc ligand with various groups. Because the stability of the macrocycle decreases upon enlargement of the π-conjugated system, we adopted the latter strategy for altering the photophysical properties of the Pc ligand; in particular, the effect of sulfur substitution was investigated.

In photodynamic therapy, silicon(IV) phthalocyanine derivatives have already been proven successful as photosensitisers. However, their synthesis is often limited to only the simple phthalocyanine ligand, derivatives of it being either synthesised in low yields or not at all. Within the context of the Loewe SynChemBio network financed by the German State of Hesse, new synthetic strategies for silicon phthalocyanine derivatives were explored, and the utility of these derivatives as photosensitisers for PDT was investigated.

Focus shifted in the next research area from biologically relevant complexes to optoelectronics and materials science. This was within the *Sonderforschungsbereich* (SFB) 1083, which deals with the study of internal interfaces, and where phthalocyanines films on metals and semiconductors are being intensively investigated. Additionally, there are many examples of phthalocyanine films prepared on gold surfaces. The phthalocyanines are typically modified with several thioether or thioalcohol groups to promote their chemisorption onto the gold substrate. However in the majority of these studies, the Pc films are not accurately studied, but simply assumed to be ordered SAMs. As part of the SFB 1083,

a phthalocyanine modified with a single thioalcohol was synthesised for the purpose of investigating the phthalocyanine-thiol-gold interface.

In the final more inorganic component of this work, the axial modification of metallo-phthalocyanines was investigated. Most modification of phthalocyanines occurs on the Pc ligand itself. This is because of the large changes in photophysical and photochemical properties that modification here can produce. However, axial modification by coordination of a ligand to a vacant binding site(s) at the central metal ion can have uses, such as linking an acceptor molecule to the Pc complex to facilitate charge transfer. Additionally, because the Pc ligand can stabilise several different redox states of the central metal ion, MPc complexes can be used as catalysts for redox reactions, where the substrate is coordinated at the central metal ion. Hence, the coordination of imido ligands to group 5 and 6 metallo-phthalocyanines was investigated.

CHAPTER 3 | CUMULATIVE SECTION

In the cumulative section of the dissertation, an introduction is given for every presented article. In addition to this, the results of each article are briefly presented and discussed. After this, an explanation of the author's contribution to each article is given.

3.1 Group 10 Metal-Thiocatecholate Capped Magnesium Phthalocyanines – Coupling Chromophore and Electron Donor/Acceptor Entities and its Impact on Sulfur Induced Red-Shifts

Malcolm A. Bartlett and Jörg Sundermeyer

Group 10 Metal-Thiocatecholate Capped Magnesium Phthalocyanines – Coupling Chromophore and Electron Donor/Acceptor Entities and its Impact on Sulfur Induced Red-Shifts.

Dalton Transactions, **2018**, DOI: 10.1039/C8DT03681K

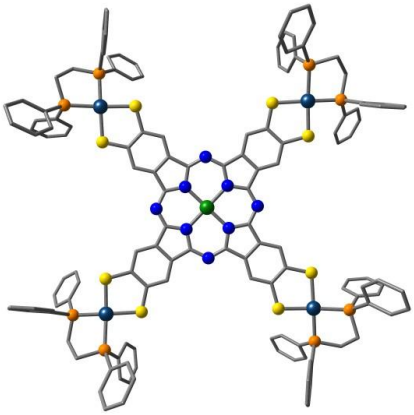

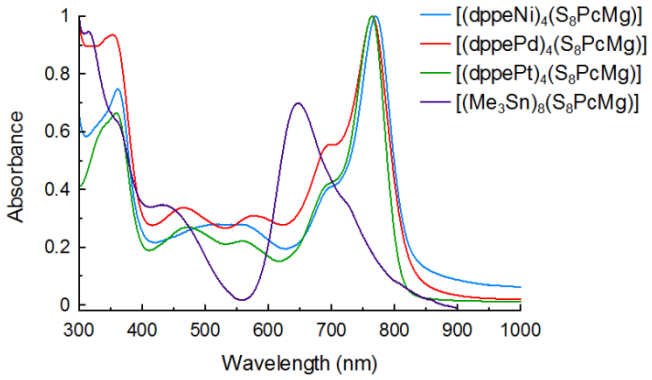

In this publication, the synthesis is described for magnesium phthalocyanine derivatives where –H substituents have been substituted for $–S^-$ at the β-positions of the phthalocyanine ligand. Additionally, the coordination chemistry of the octathiolato complex is explored with transition and main group metals, and the influence that metal coordination has on the electronic and photochemical properties is explored experimentally and by theoretical TD-DFT modelling of the systems. As a background to this publication, there have been several attempts to use heteroleptic complexes to harness solar energy for a range of different functions, from photocatalysis to solar energy production. In these heteroleptic complexes,

there is typically a light harvesting donor ligand that binds a metal through a thiocatecholate group. However, there are very few examples where the donor ligand has good light absorbing properties, such as a phthalocyanine ligand has. The hybrid of both donor ligand and dye are introduced here.

In analogy to hydroxy groups, many thiol/thiolate protecting groups are removed under basic conditions, such as those required for phthalocyanine formation. We were able to develop a facile method of thiolate protection and deprotection by using 2-thiol-benzimidazole groups to introduce thiolether groups onto the dinitrile precursors. Benzimidazole groups are heat stable, and are not removed under basic conditions, and thus remain intact during phthalocyanine formation. The benzimidazole groups can then be quaternerized by *N*-alkylation to benzimidazolium groups. These groups could then be readily cleaved using KOH, or even K_2CO_3 when heated slightly, to give magnesium 2,3,9,10,16,17,23,24-octathiolato-phthalocyanine $K_8[S_8PcMg]$. The octathiolate is extremely air-sensitive, and was therefore complexed directly with an excess of either $MCl_2(dppe)$, where M is Ni^{2+}, Pd^{2+} or Pt^{2+}, or Me_3SnCl to give the corresponding $[(dppeM)_4(S_8PcMg)]$ complexes.

Analogous complexes of [M(dtpn)(dppe)], where dtpn is 4,5-dithio-1,2-dicarbonitrile-benzene and M is Ni^{2+}, Pd^{2+} or Pt^{2+}, were synthesised for comparison. ^{31}P NMR spectroscopy revealed that there are differences in the nature of the bonding in the mono-nuclear and tetra-nuclear complexes, with the biggest difference being for Ni complexes. Analysis of the UV-Vis spectra of the transition metal-capped complexes showed that thiolate formation and metal binding induces a strong Q-band red-shift of *ca.* 70 nm, and gives rise to new broad absorption bands between the B- and Q-bands, so that the complexes have panchromatic absorption over the entire visible region. Conversely, tin coordination causes a blue-shift of the Q-band and alters the Pc ligand's absorption profile. The photophysics of the transition-metal capped complexes where further investigated by measuring their singlet oxygen quantum yields, Φ_Δ. High Φ_Δs for all complexes showed that inter-system crossing is promoted in all of the complexes, with Φ_Δ increase in the order Ni < Pd < Pt. This indicates that the heavy atom effect is present and that the peripheral metal ions interact with the Pc ligand's π system. TD-DFT calculations of the DFT optimised geometries indicated that thiolate formation causes a destabilisation of the HOMO and the LUMO/LUMO+1, but that there is a larger destabilisation of the HOMO. This effectively decreases the HOMO-LUMO energy gap and is therefore responsible for the strong red-shift seen in the UV-Vis absorption

spectra. Interestingly, the Q-band transition shows both the expected π→π* character as well as charge transfer (CT) character from the $[S_8PcMg]^{8-}$ ligand onto the peripheral $[S_2MP_2]$ moieties. Moreover, the higher energy transitions appear to be dominated by CT processes from the indoline-dithiocatehcolate-metal moieties to the peripheral $[S_2MP_2]$ acceptor moieties.

This study showed that it was possible to incorporate the excellent PcMg chromophore with a redox active metal-thiocatecholato complex, thus opening perspectives for the design of photoredox-active complexes.

Explanation of Individual Contributions

The design, synthesis and characterisation of the new metal-capped phthalocyanines and mono-nuclear analogues was done by me as well as the development of the synthetic strategy, *viz*. the use of benzimidazole protecting groups and coordination of metal-ligand fragments. I also performed the spectroscopic analysis, singlet oxygen quantum yield experiments and DFT/TD-DFT calculations and compiled the manuscript. Prof. Dr. Jörg Sundermeyer, as supervisor of the dissertation, provided discussion of the results of this study with me and revised several versions of the manuscript.

3.2 Peripheral Metallation of Phthalocyanine – Inducing New Effects in an Old Chromophore

Malcolm A. Bartlett and Jörg Sundermeyer

Peripheral Metallation of Phthalocyanine – Inducing New Effects in an Old Chromophore

Submitted as communication to: *Dalton Transactions*

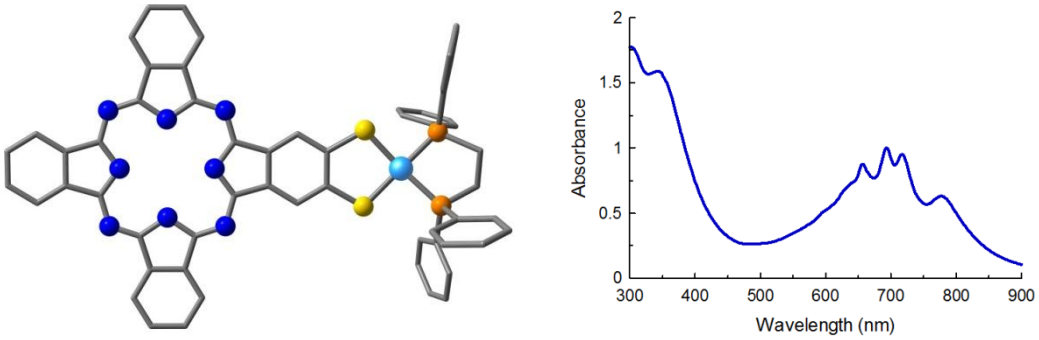

In this publication, the synthesis of an asymmetric phthalocyanine with a single thiocatecholate group and its coordination to nickel 1,2-*bis*(diphenylphosphino)ethane is reported. The electronic properties of the complex were further investigated by spectroscopic and theoretical (TD-DFT) methods.

In a previous publication of ours, we described the synthesis of symmetric A_4-type magnesium phthalocyanine derivatives where thiolate groups were located at every β-position and were used for coordination of transition and main block metals. At the time, an undesired side-reaction made it impossible to synthesise asymmetric phthalocyanine ligands, which are potentially more useful than the symmetric analogues. This problem was overcome by modifying the thiolate protecting groups, 1*H*-benzimidazole, with *n*-butyl groups to form 1-*n*-butyl-benzimidazole. This made the starting dinitrile considerably more soluble in common organic solvents, and lowered the melting point compared to the non-butylated derivative, which was crucial to its use in a melt-type Pc synthesis. The asymmetric A_3B derivative could then be synthesised in a solvent-free cocyclisation of the *n*-butyl derivative with 1,3-diiminoisoindoline. The phthalocyanine derivative was then coordinated to Ni(dppe) by first quaternerisating the protecting groups with methyl iodide to convert them to the labile 1-*n*-

butyl-3-methyl-benzimidazolium groups followed by their cleavage with KOH or NaOH to give the free thiolate groups. The A_3B isomer is significantly more soluble than the other isomers formed, and can thus be readily isolated by extraction and purified by chromatography.

For comparison, a purely organic A_3B phthalocyanine ligand was synthesised with two *t*-butylthiol groups at the β-positions of one isoindoline moiety. The electronic absorption spectra for the two phthalocyanine compounds showed that thiolate formation and metal binding induced both a bathochromic shift of the Q-bands and, more interestingly, caused several new bands in the red and NIR regions to appear. TD-DFT calculations were performed to gain insight into the origin of the new bands. The structures of both [(dppe)Ni(S_2PcH_2)] and $(MeS)_2PcH_2$ were first optimised by DFT methods (B3LYP/6-31G(d,p)) before performing vertical excitations at the same level of theory. TD-DFT calculations showed that the bathochromic shift was a result of increased electron density on the Pc HOMO, which is in keeping with the results seen for related octathiolato Pc systems. However, the asymmetric nature results in a large amount of electron density on a single isoindoline-thiocatecholate-metal moiety. The new transitions are the result of intraligand charge transfer from the electron donating thiocatecholate to the Pc LUMO/LUMO+1. This is surprising, considering that the Pc ligand is itself considered to be an electron donor, and highlights the strong electron donating properties of the thiocatecholate group.

Considering the potential role that these types of complexes have as photocatalysts, the finding that photoexcitation results in the presence of an electron hole at the MO associated with the metal fragment suggests that these complexes could participate in metal-centred photo-oxidative processes. Alternatively, $[S_2PcH_2]^{2-}$ could function as an excellent electron donor in the presence of a suitable electron acceptor.

Explanation of Individual Contributions

The design of the new thiocatecholate phthalocyanine system as well as the required thiol-protected precursor, were done by myself. In addition to this, I also performed the synthesis, spectroscopic examination and theoretical investigation of the complex. As supervisor of this dissertation, Prof. Dr. Jörg Sundermeyer was available for discussion of the scientific results of this project, and helped in compiling the manuscript.

3.3 Synthesis, Spectroscopy and Singlet Oxygen Quantum Yield of a Non-Aggregating Pc*Si Derivative

Malcolm A. Bartlett, Kerstin Mark and Jörg Sundermeyer

*Synthesis, Spectroscopy and Singlet Oxygen Quantum Yield of a Non-Aggregating Pc*Si Derivative*

Inorg. Chem. Comm., **2018**, *98*, 41–43

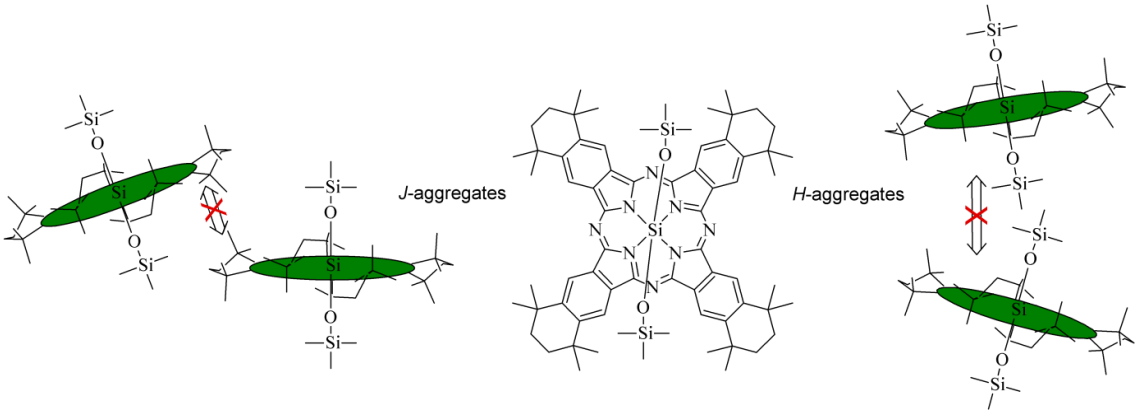

Silicon phthalocyanines derivatives have been extensively studied as photosensitisers for photodynamic therapy (PDT) as two additional groups can be coordinated to the central silicon atom to confer improved solubility, biological targeting or any other function that is also desired. One silicon phthalocyanine derivative with a single axially coordinated ammonium cation, Pc4, has gone so far as to be clinically evaluated. However, it has been shown that aggregation of phthalocyanines quenches their photodynamic activity by preventing them from generating singlet oxygen, and that end-on, or *J*-type, aggregation also occurs for silicon phthalocyanines. In this communication, we described the synthesis of tetra-phthalocyaninato silicon with axial chlorido ligands and OTMS groups. By virtue of the bulky alkyl groups both at the periphery and axially, stacking of the Pc* ligands is prevented. That no aggregation occurred in organic solvents was confirmed by the linear response of absorbance increase with concentration during the determination of the molar attenuation coefficients for Pc*Si(OTMS)$_2$. Singlet oxygen quantum yields, Φ_Δ, were also determined for the Pc*Si(OTMS)$_2$ to assess the effect of alkyl modification of the Pc ligand. Surprisingly, Φ_Δ is reduced by half compared to similar non-alkylated PcSiL$_2$ complexes; this is proposed to be due to the alkyl groups preventing efficient migration of triplet oxygen to the Pc

ligand's T_{1x} MO responsible for energy transfer to oxygen. In conclusion, Pc alkylation decreases Φ_{Δ}, but considering that aggregation completely quenches Φ_{Δ}, it is perhaps necessary that such a compromise be made when designing future PcSi complexes for PDT.

Explanation of Individual Contributions

The design of the systems and synthetic procedures was done me, as well as the electronic absorption spectroscopic characterisation and singlet oxygen quantum yield determination, including reference complexes used for the determination. The synthesis of the Pc* silicon dichloro and di-oxo-trimethylsilyl complexes, as well as other attempted syntheses of Pc*Si complexes reported, were performed by Kerstin Marks within the context of a *Vertiefung* done under my supervision. Scientific results and direction when writing the manuscript were provided by Prof. Dr. Jörg Sundermeyer.

3.4 Zinc(II)Phthalocyanine-Thiol Monolayers on Gold: On the Oxidative Stability of the S–Au Bond

Malcolm A. Bartlett, Michael Kothe, Jörg Sundermeyer and Gregor Witte

Zinc(II)Phthalocyanine-Thiol Monolayers on Gold: On the Oxidative Stability of the S–Au Bond

For submission to: *Journal of Porphyrins and Phthalocyanines*

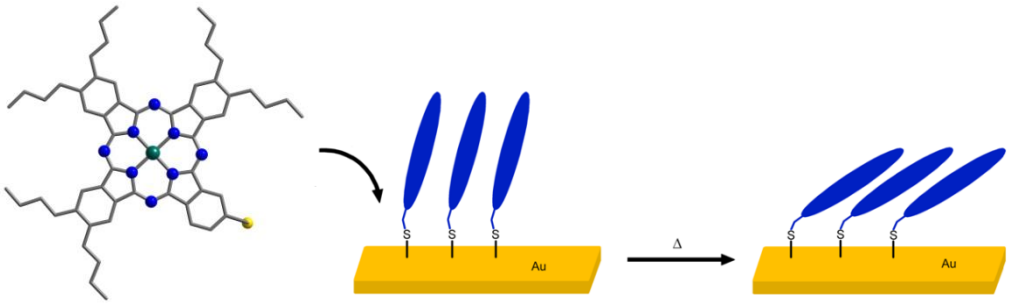

Self assembled monolayers (SAMs) composed of thiols on gold have been used in lithography, molecular electronics and as sensors, to name but a few functions. As such, phthalocyanines have also been modified with multiple thiol groups and used to form SAMs on gold surfaces. However, the characterisation of these monolayers is often poorly done, using only techniques such as cyclic voltammetry and optical absorption and emission spectroscopy; techniques that do not give accurate information as to the molecular structure of the organic compounds on the gold surface. In this publication, we sought to form the first highly ordered SAM derived from a zinc(II) phthalocyanine derivative with a single thiol group connected *via* a flexible linker. To do this, a new dintirile precursor was synthesised, the synthesis of which involved an improved radical bromination of 4-methyl-phthalonitrile. This is also a useful intermediate for the synthesis of other mono-functionalised phthalonitrile precursors. The zinc(II) phthalocyanine was then synthesised by a cocyclisation of 4,5-di-*n*-butyl-phthalonitrile and the newly synthesised S-(3,4-dicyanobenzyl) ethanthioate; the desired A_3B, [$ZnPc^{SH}$], isomer being isolated by chromatography.

[$ZnPc^{SH}$] was then incubated with Au(111)/Mica in both aerobic and anaerobic conditions before being studied by X-ray photoemission spectroscopy (XPS) and near edge X-ray absorption fine structure (NEXAFS) spectroscopy, which gives information on the molecular species bonded to the gold surface and the identity and orientation of the surface bound

compound, respectively. XPS spectra revealed that air oxidation of thiol, largely to sulfonate, occurs in the presence of oxygen, while inorganic gold sulfide species seem to form in large quantity when the sample is annealed under ultrahigh vacuum (10^{-7}–10^{-9} mbar) conditions. Additionally, NEXAFS spectra showed that [Zn(Pc)] was bonded to the surface, but that the films were largely unordered, even after heating to remove entrained solvent molecules. These results therefore show that, despite thiol-bearing phthalocyanines often being deposited on gold surfaces, thiols have a strong tendency to be oxidised in air, probably from light induced production of singlet oxygen. The phthalocyanine deposits cannot be considered well-ordered SAMs without proper analysis. Currently, the synthesis of thiol-anchored well-ordered SAMs of phthalocyanines on Au(111) remains a challenge.

Explanation of Individual Contributions

The design of the target A_3B zinc(II) phthalocyanine was done jointly between Prof. Dr. Jörg Sundermeyer, Prof. Dr. Gregor Witte and me. The synthetic strategy and separation/purification methods were developed and carried out by me. Michael Kothe and I discussed the preparation of the films together, and in some instances – particularly for anaerobically prepared films, prepared the films together. Michael Kothe prepared most of the films under aerobic conditions and also performed all the data collection and analysis using XPS and NEXAFS spectroscopy. All authors discussed the results and the direction of future work.

3.5 Imido Vanadium(IV) and Imido Chromium(IV) Phthalocyanine Complexes: Synthesis, Spectroscopy and Theoretical Investigations

Malcolm A. Bartlett, Elisabeth Seikel and Jörg Sundermeyer

Imido Vanadium(IV) and Imido Chromium(IV) Phthalocyanine Complexes: Synthesis, Spectroscopy and Theoretical Investigations

Manuscript in preparation

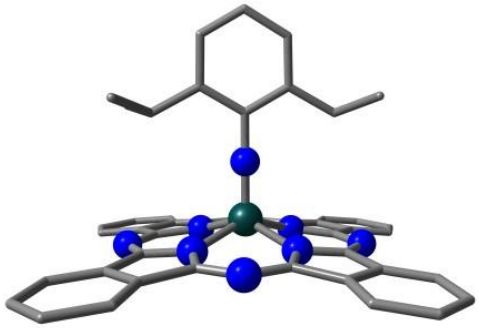

Modification of metallo-phthalocyanine complexes *via* coordination of an addition axial ligand is, in comparison to modification of the Pc ligand structure, far less common. Although axial ligands generally have a minimal influence on the opto-electronic properties of the phthalocyanine ligand, they are ideally located for metal-centred (photo)redox chemisty. In this publication, we investigated the synthesis, as well as the optical and bonding properties, of phthalocyanine complexes with a central imido vanadium(IV) or imido chromium(IV) fragment.

The synthesis of imido vanadium and imido chromium phthalocyanine complexes can be accomplished using several different strategies, depending on the metal used. For [PcV(NR)] complexes, radical chlorination of the Pc ligand by [V(NR)Cl_3] at elevated temperatures required that the starting vanadium-imido-trichloro complex be first reduced prior to cyclotetramerisation, and that a radical savenger, such as 2-methylnaphthalene, also be added to obtain the non-chlorinated product. Alternatively, the [V(NR)Cl_3] starting complex could be directly inserted into the binding cavity of a preformed and deprotonated phthalocyanine ligand, *viz.* [K_2Pc]. The redox activity of [PcCr] enabled it to be oxidized with an organic azide to give the resulting [PcCr(NR)] directly. UV-Vis spectroscopy shows that the Pc ligands' Q-band maxima are red-shifted for all [PcM(NR)] complexes, with a slightly

stronger shift for vanadium compared to chromium, as well as for aromatic compared to aliphatic imido ligands. This can be explained by the more electropositive character of V(IV) compared to Cr(IV) and the interaction of the aromatic imido ligands' π-system with that of the Pc ligand's. DFT calculations of the optimized geometries at the B3LYP/6-311G(d,p) level of theory for the [PcM(NDip)] complexes predict a linear and bent M–N–C(imido) angle of 179.97º and 142.1º for the vanadium and chromium complexes, respectively. To better understand the difference in bonding between these two complexes, a full NBO analysis was performed, which shows that unpaired electrons on chromium 3dz^2 and 3d*yz* orbitals prevent triple bond formation from occurring between the imido ligand and the chromium(IV) ion so that only a double bond can form, which is in contrast to the vanadium complexes, where the unpaired electron on the 3dx^2-y^2 orbital does not interfere with V–N single, double or triple (σ or π) bond formation along the *z*-axis.

Explanation of Individual Contributions

Motivation to synthesise imido metal phthalocyanine complexes came from Prof. Dr. Jörg Sundermeyer. Discovery of the metal-insertion reaction for vanadium imido complexes was made by Elisabeth Seikel. The strategy of oxidative addition of azide to [PcCr] was carried out by Elisabeth Seikel. Development of a classic cyclotetramerisation reaction for, and complete purification and analysis of, vanadium imido complexes using reduced [V(IV)(NR)Cl_2] complexes was done by me. I also carried out the DFT geometry optimisations, NBO population analyses and TDDFT vertical excitation calculations of the complexes. The manuscript was compiled by me. Revisions to the manuscript were made by Prof. Dr. Jörg Sundermeyer.

3.6 Control of Intramolecular Electron Transfer in Perylene Dihydrazides and Perylene Diimides: A Comparative Study by Time-Resolved Spectroscopy

Robin C. Döring, Eduard Baal, **Malcolm A. Bartlett**, Christian Prinzisky, Remco W.A. Havenith, Jörg Sundermeyer and Sangam Chatterjee

Control of Intramolecular Electron Transfer in Perylene Dihydrazides and Perylene Diimides: A Comparative Study by Time-Resolved Spectroscopy

Cornell University Library: **arXiv:1612.05046v1 [physics.chem-ph]**

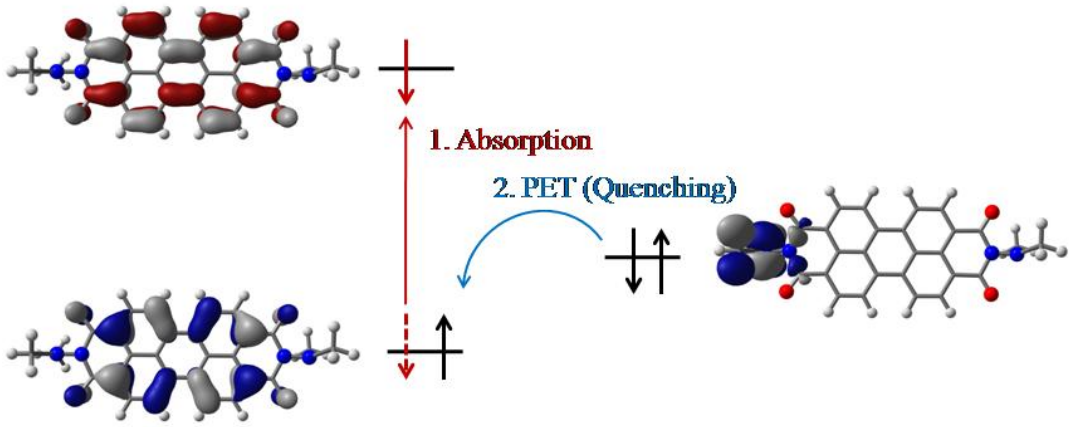

Perylenetetracarboxylic acid dianhydrides and their related diimide analogues are important and well-known pigments that also show strong fluorescence both in the solid state and in solution. By Synthesising diimides with tertiary amines connected either directly or with a spacer to the perylene diimide core, the fluorescence exhibited can be almost completely quenched. However, when the tertiary amines are quaternerised by *N*-methylation, fluorescence is largely restored, while protonation of the tertiary amines causes only a minimal increase in fluorescence despite the protonated compounds being isoelectronic to the methylated species. To better understand this effect, a series of perylene dihydrazines (PDHs) and perylene dimides (PDIs) where synthesised where the distance of the tertiary amine to the PDI core is controlled by using alkyl spacers of varying length from zero to six methylene groups.

That fluorescence quenching is due to the tertiary amines is strongly supported by DFT calculations and electrochemical measurements. DFT calculations of the MO energies for both the ground state and S_1 excited state structures revealed a similar picture. That is, for unprotonated compounds the $\pi \rightarrow \pi^*$ transition responsible for absorption and the corresponding fluorescence is from the HOMO-1 to LUMO, while the tertiary amine lone pair constitutes the HOMO and is

energetically favoured to quench fluorescence through PET. However, when protonated or methylated, the energy of the tertiary/ternary amine is significantly lowered, so that the $\pi \rightarrow \pi^*$ transition is between the HOMO and LUMO. Cyclic voltammetry (CV) and differential pulse voltammetry (DPV) showed that the neutral tertiary amine is more readily oxidised that the perylene core, and therefore constitutes the HOMO, and that protonation does indeed lower the oxidation potential of the amine to a level below the aromatic core.

Further insight could be gained by time-resolved photoluminescence (PL) experiments, which revealed that there is an exponential distance dependence for the fluorescence quenching, meaning that electron transfer is *via* a through-space mechanism. Additionally, the fluorescence decay follows a bi-exponential decay curve, indicating that the decay process is not a simple radiative one. Rather, a dark-shelving state within the system can be inferred from the decay rates. Variation of the excitation energies used also caused a prolongation of the emissive lifetimes by a factor of 1.7. This can best be explained by a reversible inter-system crossing (ISC) process present. DFT calculations revealed multiple triplet states exist around 3.2 eV, which would make it possible for $S_x \rightarrow T_n$ ($X > 1$, $n \geq 1$) transitions to occur.

Explanation of Individual Contributions

Eduard Baal synthesised all the compounds presented in this study. Time-resolved luminescence spectra were recorded by Robin Döring. I performed (TD)DFT calculations of the optimised ground state and S_1 singlet excited state structures and the population analyses for unprotonated, protonated and methylated PDH and PDI compounds. Christian Prinzisky solved the single crystal X-ray structures presented herein. Remco Havenith performed calculations of the singlet and triplet excited states for more precise modelling of the excitation and decay pathways. Prof. Dr. Jörg Sundermeyer and Prof. Dr. Sangam Chatterjee provided the impetus for this collaborative project and were involved in revision of the results and the manuscript.

CHAPTER 4 | SUMMARY

The aim of this doctoral project was the synthesis and characterisation of phthalocyanine compounds with new functionality for optoelectronic and photocatalytic applications. Part of this work was carried out within the collaborative research centre SFB 1083, "Structure and Dynamics of Internal Interfaces." Within the Loewe SynChemBio project, "Innovative Synthetic Chemistry for the Selective Modulation of Biological Processes", phthalocyanine complexes were synthesised and evaluated for use in photodynamic therapeutic applications. As a service to the research group, theoretical chemistry computations were also performed.

4.1 Phthalocyanine ligands with dithiocatecholate functional groups

The major component of this work involved the synthesis of unprecedented phthalocyanine complexes with thiolate groups at the Pc β-position. Methods have previously been reported for introducing thiolate groups onto tetra-aza-porphyrazines, but these methods used thiobenzyl groups to introduce the sulfur atom onto the macrocycle and a harsh Birch reduction to cleave off the benzyl group and give the thiolate. As a first step, a facile and mild method was developed for introducing thiolate groups onto Pc. It was found that 2-thio-benzimidazole was an effective reagent was introducing a thiol functional group onto the dinitrile precursor, 4,5-dichloro-1,2-dicarbonitrile-benzene. More importantly, the benzimidazole group is stable enough to not be cleaved off under the high-temperatures and basic conditions of cyclo-tetramerisation typically required to form phthalocyanines. Once the (2-thio-1H-benzimidazole)-phthalocyanine complex is formed, the benzimidazole protecting groups can be alkylated to form the quaternary benzimidazolium salt. The cationic

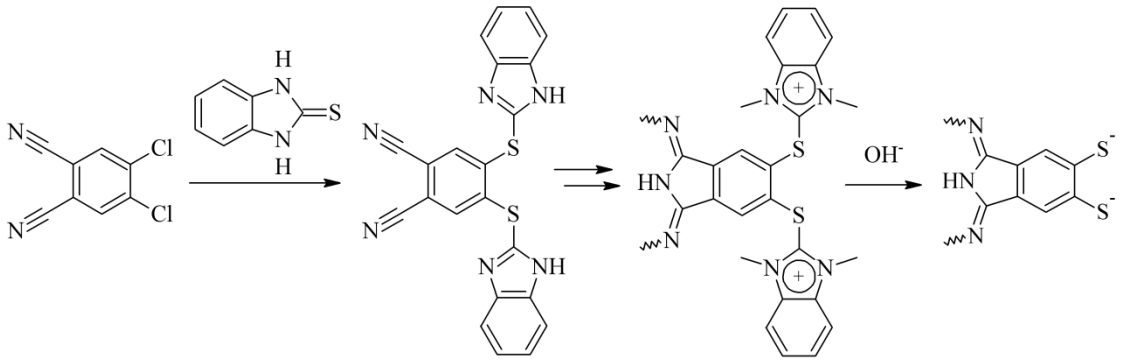

Scheme 4.1: Introduction of thiolate and thiocatecholate groups onto a phthalocyanine ligand *via* substitution of chlorides for 2-thio-benzimidazole groups, alkylation, quaternerisation and cleavage of benzimidazolium with hydroxide

nature of the benzimidazolium made it highly susceptible to nucleophilic attack from hydroxide. The corresponding urea derivative could thus be cleaved off at room temperature to give a soluble Pc thiolate salt. Scheme **4.1** depicts the synthesis of a dithiocatecholate group by the introduction, quaternerisation and cleavage of 2-thio-benzimidazole. Using the above approach, it was possible to synthesise both symmetric A_4-type magnesium octathiolato-phthalocyanine and asymmetric A_3B-type dithiolato-phthalocyanine compounds and to use them for coordination chemistry.

Symmetric compounds were coordinated to both eight $SnMe_3$ groups, as well as four $M(dppe)^{2+}$ fragments of the group 10 metals, Ni^{2+}, Pd^{2+} and Pt^{2+}. Spectroscopically, the light absorption of the $[(dppeM)_4S_8PcMg]$ complexes was significantly enhanced; the Q-band for all complexes is shifted by almost 80 nm compared to normal S-organothioether substitution at the same position in $[(RS)_8PcMg]$ complexes (R = aryl or alkyl). Additionally, two new broad bands arise between the B-band and Q-band regions, so that the complexes have a strong absorption in the entire visible light spectral region, i.e. panchromatic absorption. Figure **4.1** shows the electronic absorption spectra for the complexes $[(dppeM)_4S_8PcMg]$, $[(Me_3Sn)_8S_8PcMg]$ and $[(dppe)Ni(S_2PcH_2)]$.

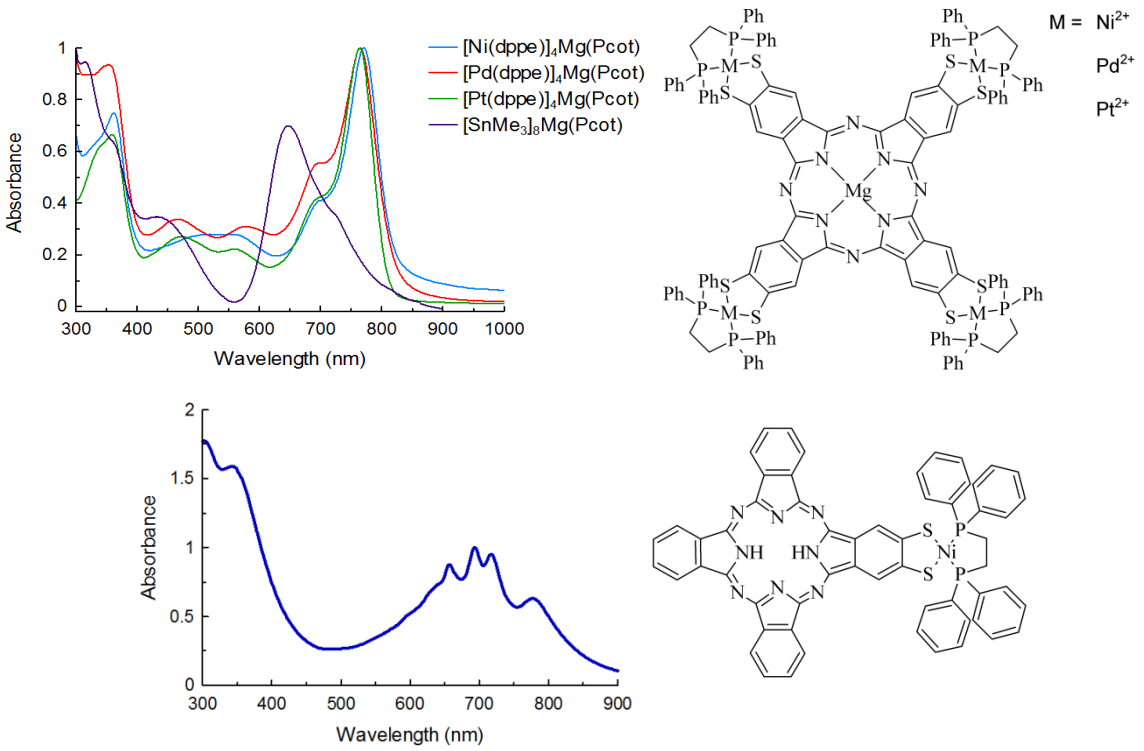

Figure 4.1: UV-Vis absorption spectra and structures for the pentanuclear and mononuclear metal-capped $[S_8PcMg]^{8-}$ (top) and $[S_2PcH_2]^{2-}$ (bottom) complexes, respectively.

This is in contrast to $-SnR_3$ coordination, which has the effect of blue-shifting the Q-band absorption and changing the absorption profile. Also, the absorption spectrum for the A_3B complex, [(dppe)Ni(S_2PcH_2)], was surprisingly very different to that of its symmetric analogue (Figure **4.1**). While the Q-band was significantly red-shifted by the introduction of thiolate groups, as expected, the absorption profile was very different. Several new transitions between 500 and 900 nm appeared. This shows that changes in the peripheral metallation have significant consequences for the electronic processes of the Pc ligand. DFT and TD-DFT calculations were used to determine the geometry of the [(dppeM)$_4$$S_8$PcMg] complexes and [(dppe)Ni(S_2PcH_2)] as well as the origin of the newly observed electronic transitions (Figure **4.2**). For symmetric [(dppeM)$_4$$S_8$PcMg] complexes, the strongly red-shifted Q-band is a result of a narrowing of the destabilisation HOMO → LUMO/LUMO+1 transition, due to greater destabilisation of the HOMO compared to the LUMO/LUMO+1. More interestingly, the Q-band transitions have both π→π* and ligand-to-ligand charge transfer (LLCT) character, as the LUMO/LUMO+1 extends over both the Pc ligand and the thiolate-metal-diphosphine [S_2MP_2] moieties. Furthermore, the new higher energy transitions are predicted to arise mainly from this LLCT process. For the asymmetric complex,

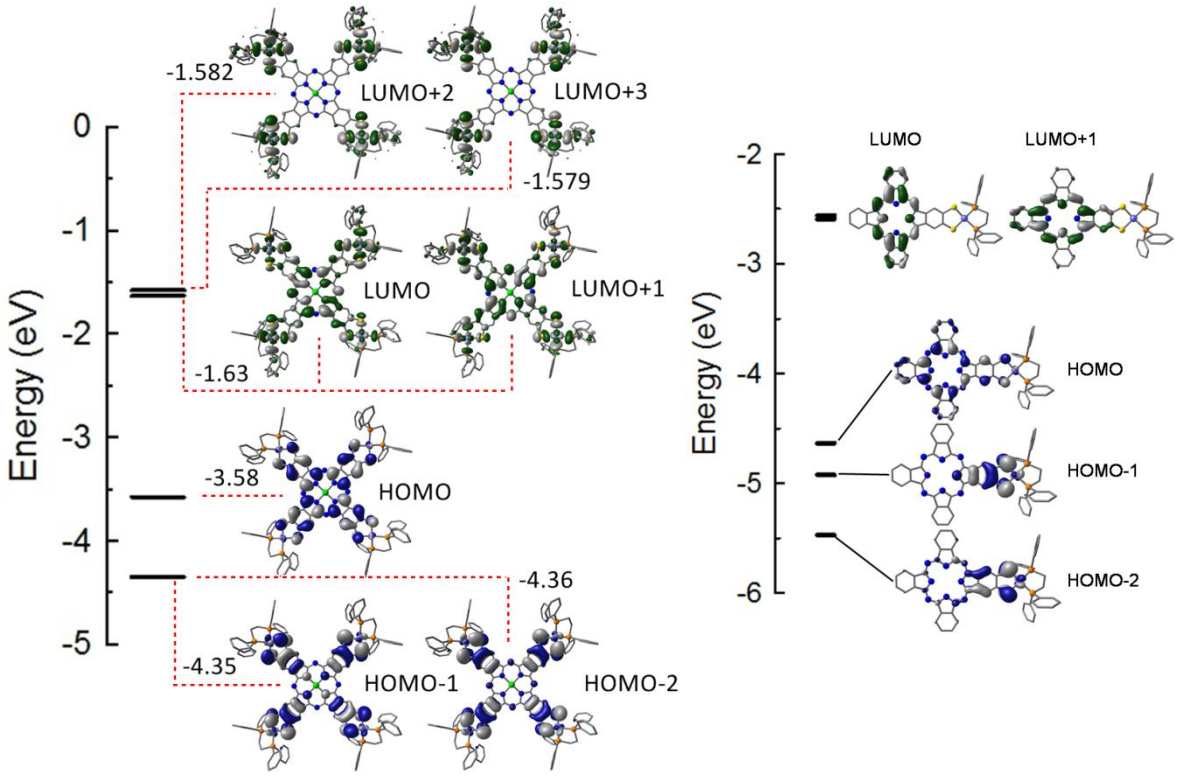

Figure 4.2: MO energy level digram for the HOMO-2 to LUMO+3 for [(dppeM)$_4$(S_8PcMg)] (left) and the HOMO-3 to LUMO+1 for [(dppe)Ni(S_2PcH_2)] (right).

[(dppe)Ni(S_2PcH_2)], the Q-band retains the typical π→π* character. The new bands, however, originate, not from π→π* or LLCT processes, but from intramolecular charge transfer. That is, the isoindoline-dithiolate-metal moiety is an electron rich group with strong electron donor properties, and upon photoexcitation, promotes charge transfer to the Pc LUMO/LUMO+1. MO energy level diagrams for MOs involved in Q-band and new transitions are shown for the symmetric and asymmetric Ni complexes in Figure **4.2**.

Although the identity of the metal ion in the [(dppeM)$_4$$S_8$PcMg] complexes made little difference to their absorbance spectra, they significantly increased the singlet oxygen yields (Φ_Δ) of the complexes. Φ_Δ values of 0.36, 0.76 and 0.91 were obtained for Ni, Pd and Pt complexes, respectively. This trend is well explained by the heavy atom effect, where the heavier atoms promote intersystem (ISC) crossing *via* spin-orbit coupling of the S_1 and T_1 manifolds. Significantly, this result shows that peripherally coordinated metals do indeed interact with the Pc ligand's orbitals, and could therefore be involved in other photophysical and photochemical processes associated with the Pc ligand. The plots of ln(A_0/A_t) vs. time used in determining Φ_Δ values for the complexes are shown below in Figure **4.3**.

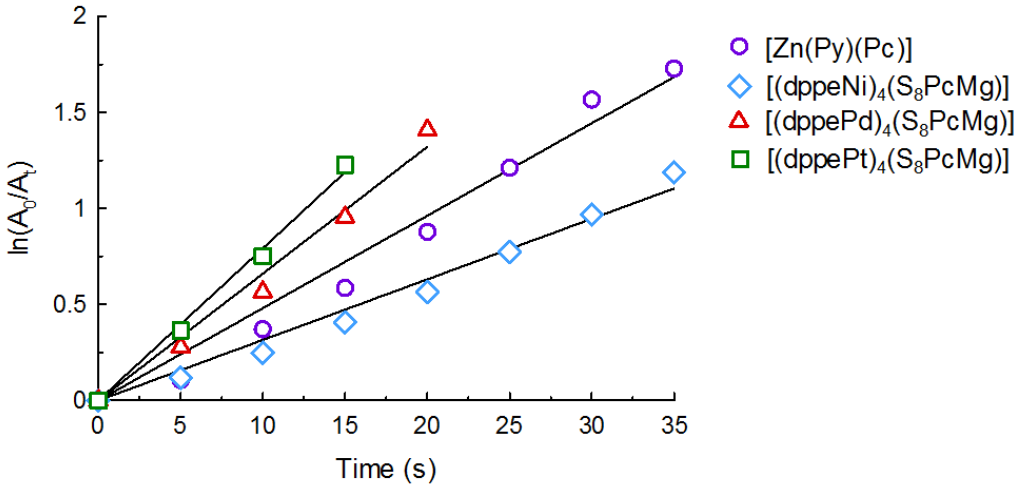

Figure 4.3: Rate of DPBF decay plotted as a function of ln(A_0/A_t) vs. time to determine singlet oxygen quantum yield for [(dppeM)$_4$(S_8PcMg)] complexes; [Zn(Py)(Pc)] (Φ_Δ = 0.56) was used as a standard. The strong dependence of Φ_Δ on the peripheral metal shows that they are intimately involved in the excited state dynamics.

4.2 Coordination of imido ligands axially to metallo phthalocyanine complexes

In addition to metal-coordination at the phthalocyanine ligand periphery, reactivity can also occur at the central metal ion of a metallo-phthalocyanine complex. In a continuation of earlier work, we synthesised vanadium and chromium phthalocyanine complexes with axially coordinated imido ligands (NR^{2-}). Several strategies were available for the synthesis of vanadium imido phthalocyanine ([PcV(NR)]) complexes starting from [$V(NR)Cl_3$]. The trichloro complex could be used as a template for phthalocyanine formation, but required either the addition of a radical scavenger and prior reduction of the starting V(V) complex to a V(III) species to completely prevent chlorination of the Pc ligand. Alternatively, the trichloro complex could be inserted into the preformed phthalocyanine ligand by transmetallation reaction using [K_2Pc]; vanadium is concomitantly reduced in this reaction from V(V) to V(IV). Chromium imido phthalocyanine complexes, [PcCr(NR)], could be prepared by oxidative addition of an organic azide to chromium(II) phthalocyanine. Syntheses of vanadium and chromium complexes are shown in Scheme **4.2**.

The electronic absorption spectra for the vanadium and chromium complexes show only a small red-shift of the Q-band maxima for imido complexes compared to their oxo-

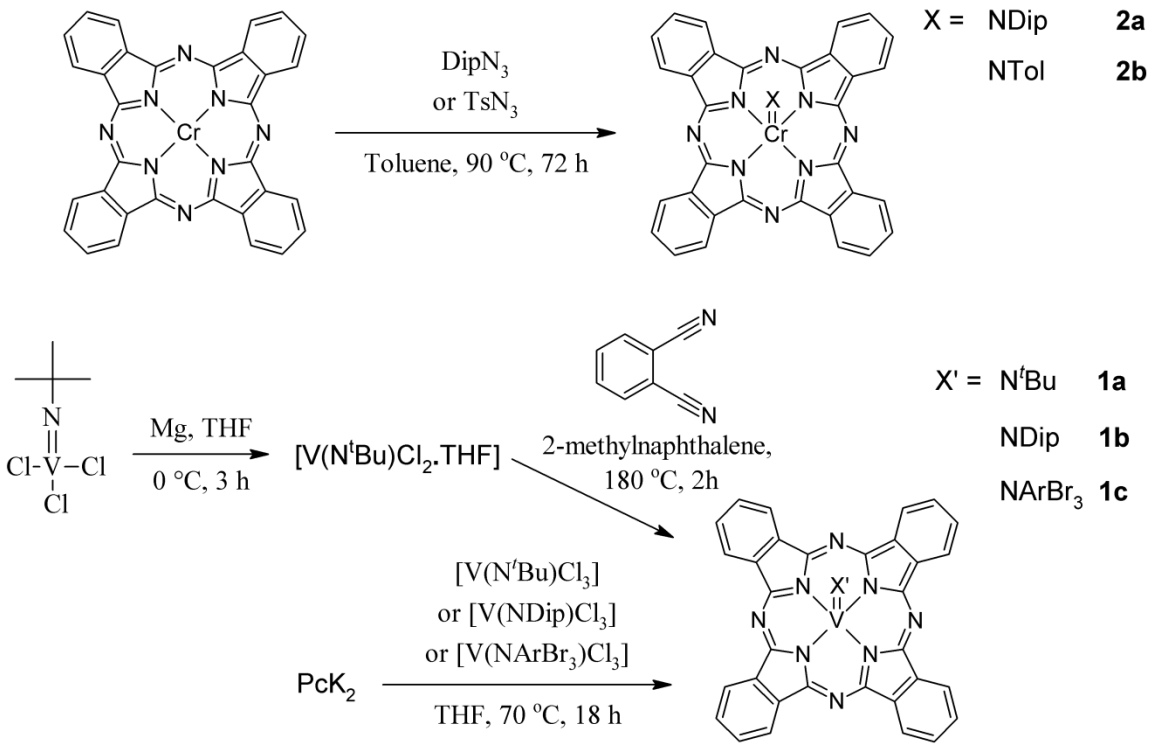

Scheme 4.2: Synthesis of [PcV(NR)] (bottom) and [PcCr(NR)] (top) complexes

derivatives, which is probably a result of interactions of the Pc π-orbitals with those of the axial ligands. Additionally, spectra are also slightly red-shifted for vanadium compared to d^2-chromium(IV) owing to the more electropositive character of d^1-vanadium(IV).

DFT calculations were performed to determine the optimised structures for the complexes. Like previously synthesised imido titanium complexes, [PcV(NR)] complexes had a linear V=N–R bond angle. Surprisingly, the Cr=N–R bond angle was bent at *ca.* 140º. In order to better understand this, a natural bond orbital (NBO) analysis of the imido vanadium and imido chromium complexes was performed (Figure **4.4**). The reason for the non-linear Cr=N–R bond angle was determined to be due to the location of the two non-bonding electrons on chromium, which occupy the $3d_{yz}$ and $3d_{z2}$ orbitals, and thus prevent the M–N bond from having a triple bond character. In vanadium, the unpaired electron is in the $3d_{x2-y2}$ orbital, and therefore does not interfere with vanadium-imido bonding along the z-axis.

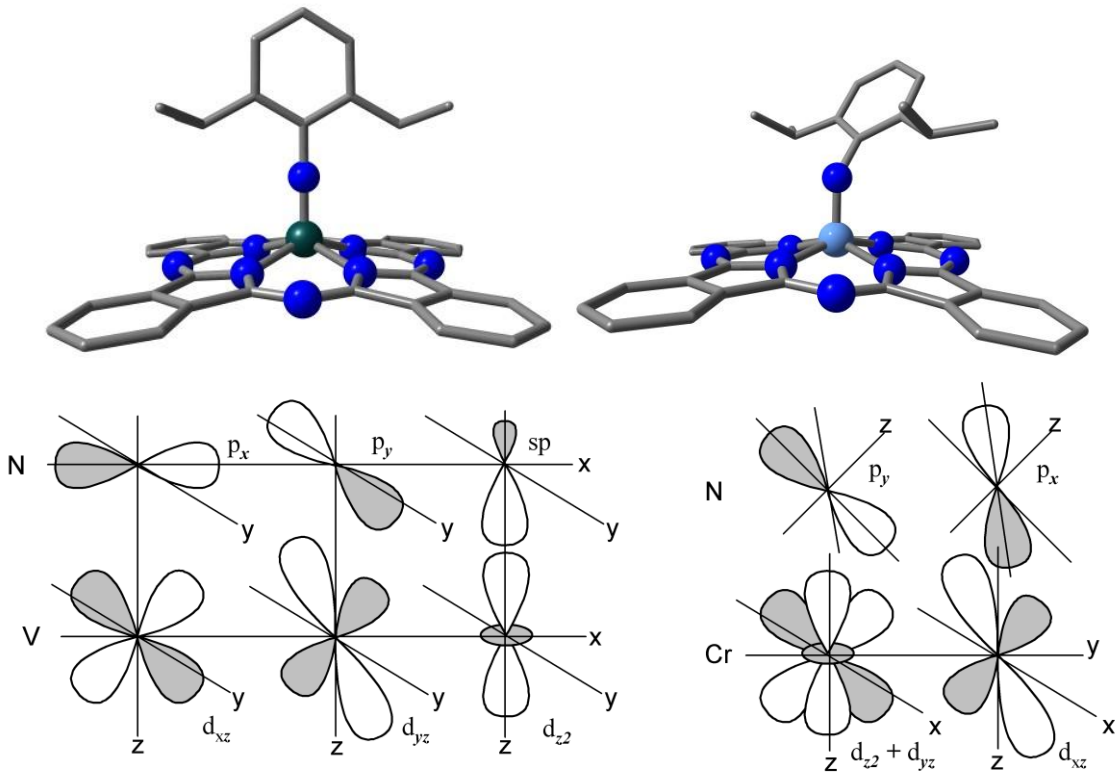

Figure 4.4: DFT gas-phase optimised geometries for [PcV(NDip)] and [PcCr(NDip)] complexes showing the linear and bent M=N–R bond angles for vanadium (left) and chromium (right), respectively, and the respective NBO analysis for the M–N bond in these complexes.

4.3 Mono-thiomethylzinc(II)phthalocyanine for monolayer formation

Within the framework of the SFB 1083, it was attempted to grow well-organised self-assembled monolayers of [Zn(Pc)] on a Au(111) surface. To this end, a new mono-thiomethyldinitrile precursor was synthesised *via* a two-step strategy. 4-Bromomethylphthalonitrile was first synthesised in good yields by a radical bromination of 4-methylphthalonitrile using only NBS and light in acetonitrile, which is a much more environmentally friendly route than that previously described using highly carcinogenic CCl_4 as solvent with chemical radical initiators. Treatment of this product with thioacetic acid gave the S-acylated, thus protected, target dinitrile, which was used in a statistical mixed cocyclisation with 4,5-di-n-butylphthalonitrile to obtain a mixture of Zn(Pc) products. The desired mono-thiomethyl A_3B Zn(Pc) isomer, $ZnPc^{SH}$, could be obtained by column chromatography. The complete synthetic procedure is shown in Scheme **4.3**.

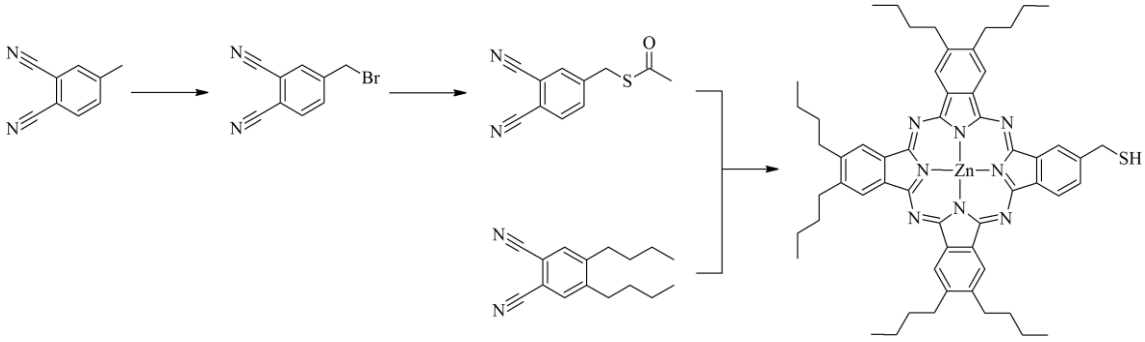

Scheme 4.3: Synthesis of dintriles precursors and A_3B $ZnPc^{SH}$ complex *via* co-cyclisation.

Films were prepared by soaking gold coated Mica sheets in solutions of $ZnPc^{SH}$ under aerobic and anaerobic conditions. NEXAFS spectroscopy revealed that films did consist of [Zn(Pc)]. These films were largely unordered, although annealing under UHV conditions did help to improve their ordering. XPS spectra indicated that thiol (RS–Au) bonds to the surface had formed, but that they were largely oxidised to sulfonate ($–SO_2$) and inorganic gold sulfide (–Au–S–) groups under aerobic and anaerobic conditions, respectively. Oxidation to sulfonate is presumed to be due to the photooxidative properties of the [Zn(Pc)] core, while thermal decomposition to sulfide can be attributed to the lability of the methylene-thio bond.

4.4 Non-aggregating hexadecamethyl phthalocyanine silicon for photodynamic therapy

Silicon phthalocyanine complexes are being extensively investigated for photodynamic therapy, but have been shown to form end-on, or *J*-type, aggregates, which are known to

inhibit their efficacy by quenching energy transfer to triplet oxygen. Here, we synthesised silicon phthalocyanine complexes using a hexadecamethyl substituted phthalocyanine ligand (Pc*) to prevent *J*-type aggregation from occurring. Axial coordination of $OSiMe_3$ groups to the central silicon ion prevents the formation of face-to-face, or *H*-type aggregates, from forming, and significantly enhances the solubility of the complexes. Both a monomeric and dimeric, μ-oxo-bridged complex were isolated and characterised.

The singlet oxygen quantum yield, Φ_Δ, for the monomeric species [Pc*Si(OTMS)$_2$] was also determined by the DPBF decay method, and found to be considerably reduced compared to the unmodified [PcSi(OH)$_2$], Φ_Δ for the two complexes being 0.28 and 0.48, respectively. However, the non-aggregating nature of [Pc*Si(OTMS)$_2$] may mean that their performance in biologically relevant media is in fact superior to unmodified PcSi complexes. The structure of [Pc*Si(OTMS)$_2$] as well as a typical DPBF decay series of spectra is shown in Figure **4.5**.

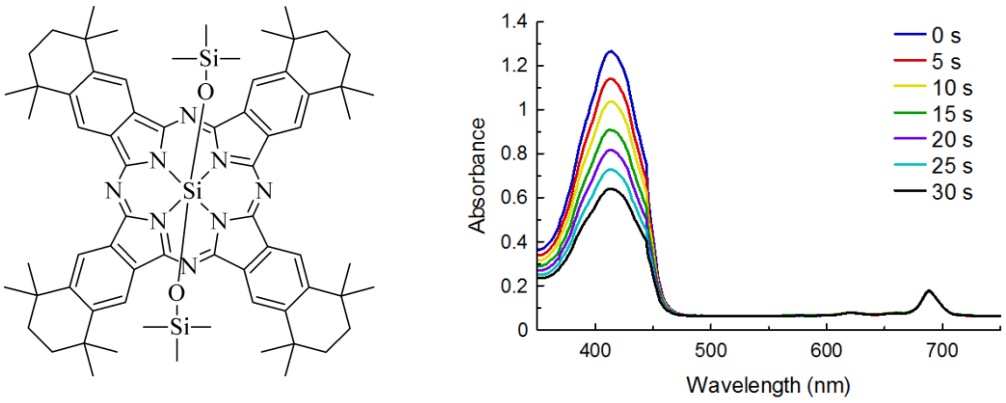

Figure 4.5: The structure of [Pc*Si(OTMS)$_2$] (left) and the decay of DPBF upon exposure of light in the presence of the silicon(IV) photosensitiser

4.5 Density functional theory calculations of the quenching mechanism in perylenediimide-amine conjugates

Fluorescence in perylenediimides (PDI) is typically very high, but was almost completely quenched for perylene dihydrazine (PDH)/PDI-amine conjugates synthesised in our research group. However, quaternerisation of the amine re-established fluorescence. To elucidate the quenching mechanism, the compounds were studied using electrochemistry, steady-state absorption and fluorescence spectroscopy as well as time resolved photoluminescence

spectroscopic techniques. DFT and TDDFT methods were also used to gain insight into the ground and excited state electron dynamics.

As part of this dissertation, DFT and TD-DFT calculations were performed to determine the influence of quaternerisation and protonation of the amine on PDI's ground state and S_1 excited state molecular orbitals. A series of compounds was studied where the tertiary amine was separated from the perylene core by zero, two, three or six methylene (-CH_2-) groups. In all cases, the ground state and S_1 excited state geometries were first optimised before performing a population analysis to determine the energy of the MOs. The results of these calculations showed that, for both the ground and excited state compounds with tertiary amines, the HOMO is located on the amine, and the $\pi \rightarrow \pi^*$ transition associated with absorption and fluorescence is between the HOMO-1 and LUMO. Upon photoabsoprtion, it is assumed that an electron is transferred from the amine centered HOMO to the perylene HOMO-$1^{\bullet+}$, thus preventing any possible fluorescence. Protonation or quaternerisation by N-methylation of the amine stabilises, or lowers, the energy of this orbital below that of the occupied MO on the perylene core, which is now the HOMO. Involvement of the amine MO in photoinduced electron transfer (PET) is therefore no longer energetically favoured, and the absorption and fluorescence processes of the perylene core can occur. This change in the ordering of the MO energy levels is the same, regardless of the length of the alkyl spacer, that is, after protonation or methylation, the HOMO and LUMO are always located on the perylene core. Figure **4.6** shows the energy level diagram for the neutral and protonated PDH compounds, as well as the proposed fluorescence and fluorescence quenching mechanisms.

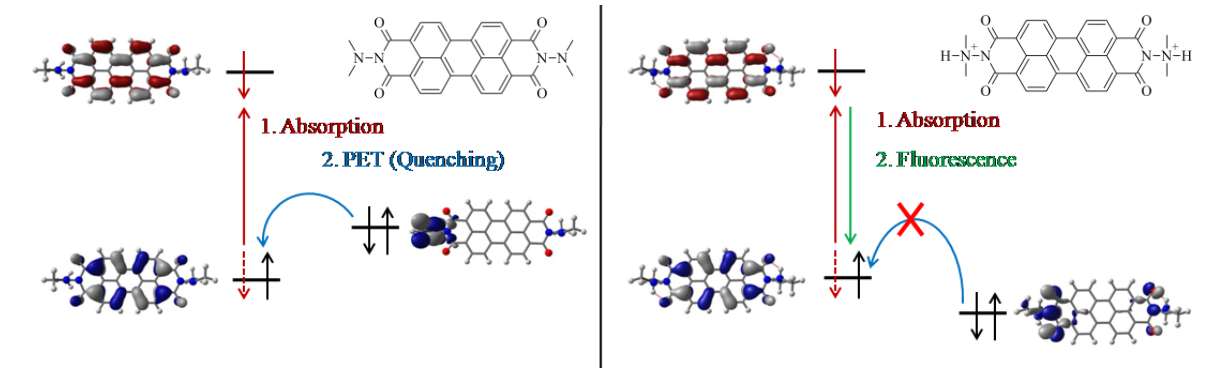

Figure 4.6: Energy level diagram and fluorescence quenching by photoinduced electron transfer (PET) for PDH with neutral (left) and protonated (right) amines.

CHAPTER 5 | ZUSAMMENFASSUNG

Ziel der vorliegenden Doktorarbeit war die Synthese und Charakterisierung neuartig funktionalisierter Phthalocyanine für optoelektronische und photokatalytische Anwendungen. Dieser Arbeit wurde einerseits im Zuge des Sonderforschungsbereichs SFB 1083 „Struktur und Dynamik innerer Grenzflächen“, andererseits für das Loewe SynChemBio Projekt „Innovative Synthesechemie für die selektive Modulation biologischer Prozesse“ bearbeitet. Dazu wurden die hergestellten Phthalocyanine auf ihre Anwendbarkeit in der photodynamischen Therapie hin untersucht. Zudem wurden computergestützte quantenchemische Berechungen und Interpretationen durchgeführt.

5.1 Neue funktionalisiertePhthalocyaninThiolatresten als Ankergruppen

Schwerpunkt der Arbeit war die Synthese bisher unbekannter, in der Pc-β-Position mit Thiolatgruppen funktionalisierterPhthalocyanin-Komplexe.Die bisher bekannten Methoden zur Einführung von Thiolatgruppen in Tetraazaporphyrinazine nutzen Thiobenzylgruppen um das Schwefelatom in den Makrozyklus zu integrieren, und harsche Birch-Reduktionsbedingungen zur Entfernung der Benzylgruppe und Ausbildung der Thiolatfunktion. Zuerst wurde eine mildere Methode auf Basis von 2-Thiobenzimidazol entwickelt, um die Pc-Vorstufe 4,5-dichlor-1,2-dicarbonitrilbenzol mit Thiolatresten zu funktionalisieren. Die Benzimidazolgruppe ist stabil genug am Dinitril gebunden, um durch die hohen Temperaturen und basischen Bedingungen der Cyclotetramerisierung zu den Pc-Verbindungen nicht abgespalten zu werden. Die Benzimidazol-Schutzgruppen des (2-Thio-1H-benzimidazol)-phthalocyanins können unter Ausbildung quaternärer Benzimidazolsalze

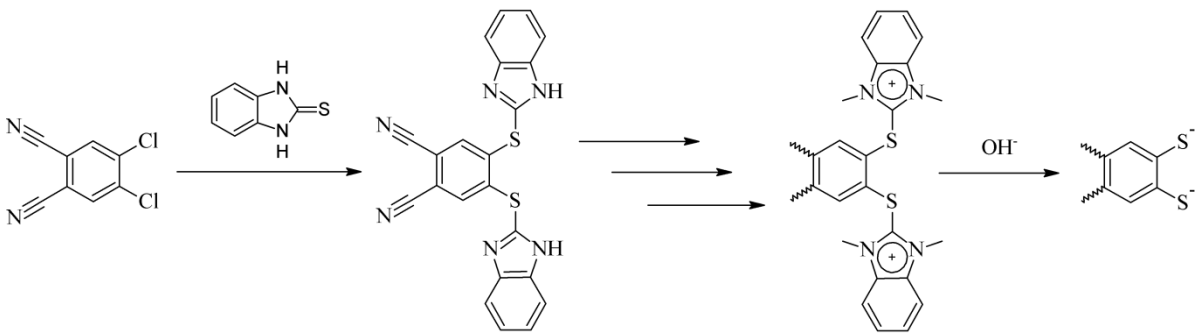

Schema 5.1: Einführung von Thiolat- und Thiocatecholatgruppen in Phthalocyanine durch Substitution der Chloride mit 2-Thio-benzimidazolgruppen. Durch anschließende Alkylierung und basischer Aufarbeitung werden die Benzimidazoliumsubstituenten entfernt.

alkyliert werden. Der kationische Charakter des Benzimidazolrestes impliziert eine hohe Reaktivität gegenüber nukleophilen Hydroxidanionen. Das entsprechende Harnstoffderivat kann bereits bei Raumtemperatur unter Ausbildung eines löslichen Pc-Salzes entfernt werden. In Schema **5.1** ist die Synthese einer Dithiocatecholatgruppe durch Einführung, Quatenisierung und Basischer Abspaltung der 2-thio-benzimidazolgruppe dargestellt.

Die beschriebene Methode ermöglicht einen Zugang zu beiden symmetrischen A_4-artigen Magnesium Octathiolatphthalocyanin-Komplexen, und asymmetrischen, A_3B-artigen, Dithiolat-Pc Verbindungen, sowie deren Koordinationschemie. Die symmetrischen Verbindungen koordinieren 8 $SnMe_3$ Einheiten oder 4 $M(dppe)^{2+}$ Einheiten, mit M = Metall der Gruppe 10, Ni^{2+}, Pd^{2+} und Pt^{2+} (Abbildung **5.1**). Spektroskopisch wird die Absorbanz in $[(dppeM)_4S_8PcMg]$ im Vergleich zu organischen Substituenten an den Schwefelatomen $[(RS)_8PcMg]$ (R = aryl, alkyl) deutlich erhöht, wobei die Q-Bande der Komplexe um ca. 80 nm bathochrom verschoben ist. Zusätzlich sind zwei weitere Banden zwischen der Q- und der B-Bande sichtbar. Dadurch weisen die Komplexe eine starke Absorption über den gesamten sichtbaren Spektralbereich auf (panchromatische Absorption). Im Gegensatz zu den

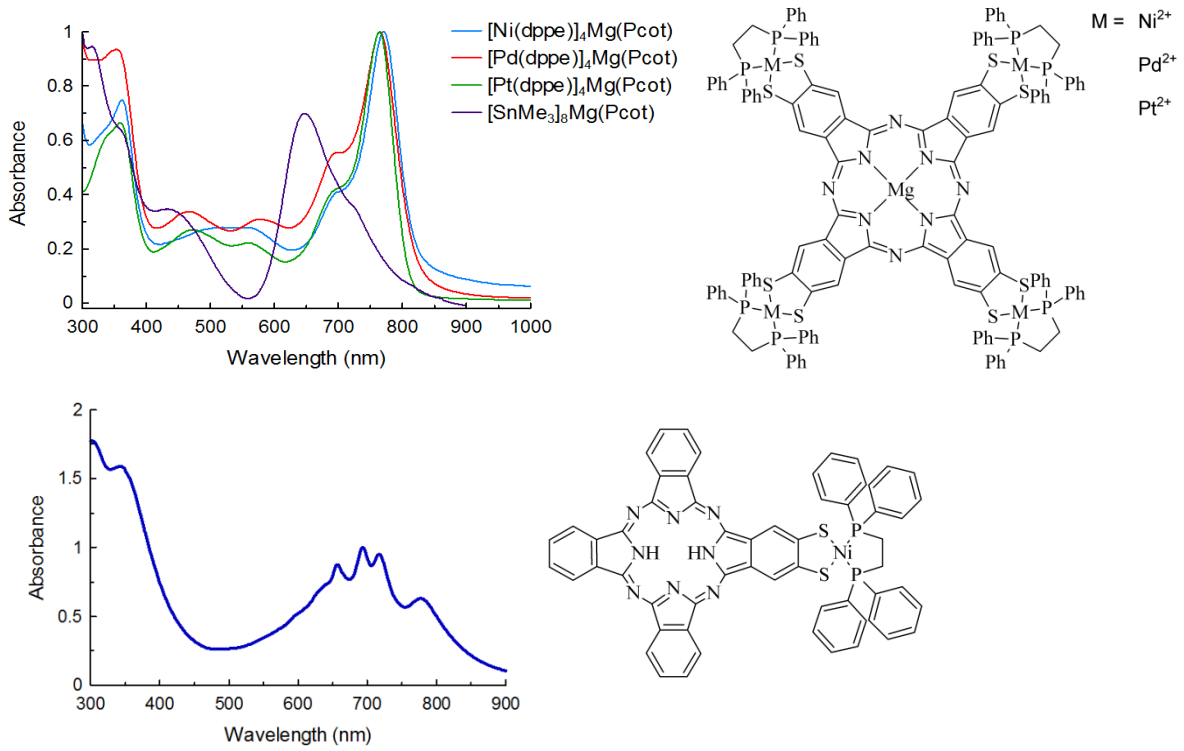

Abbildung 5.1: UV-Vis-Absorptionsspektren und Strukturen derpentanuklearen und mononuklearen Komplexe $[S_8PcMg]^{8-}$ (oben) und $[S_2PcH_2]^{2-}$ (unten).

Metallen der Gruppe 10 verschiebt sich die Q-Bande der Zinnkomplexe hypsochrom. In Abbildung **5.1** sind die elektronischen Absorbanzspektren für die Komplexe [(dppeM)$_4$S$_8$PcMg], [(Me$_3$Sn)$_8$S$_8$PcMg] und [(dppe)Ni(S$_2$PcH$_2$)] dargestellt.

Um die Strukturen der Komplexe [(dppeM)$_4$S$_8$PcMg] und [(dppe)Ni(S$_2$PcH$_2$)], sowie die Ursache für die neu beobachteten, elektronischen Übergänge zu untersuchen, wurden DFT und TD-DFT Berechnungen durchgeführt (Abbildung **5.2**). Die starke Rotverschiebung der Q-Bande symmetrischer [(dppeM)$_4$(S$_2$PcMg)] Komplexe ist auf eine Energiedifferenzerniedrigung zwischen HOMO und LUMO/LUMO+1 zurückzuführen, die aus einer ausgeprägteren energetischen Destabilisierung des HOMOs im Vergleich zu LUMO/LUMO+1 resultiert. Die Q-Bandenübergänge haben π→π*- und Ligand-Ligand Charge Transfer (LLCT)-Charakter, da sich das LUMO/LUMO+1 sowohl über den Pc-Liganden, als auch über die Thiolat-Metall-Diphosphin [S$_2$MP$_2$]-Einheiten erstreckt. Die neu beobachteten, höherenergetischen Übergängesind hauptsächlich auf diesen LLCT-Prozess zurückzuführen. Die Q-Band des asymmetrischen Komplexes [(dppe)Ni(S$_2$PcH$_2$)] behält den üblichen π→π* Charakter bei. Die neu hinzugekommenen Banden sind nicht auf einen

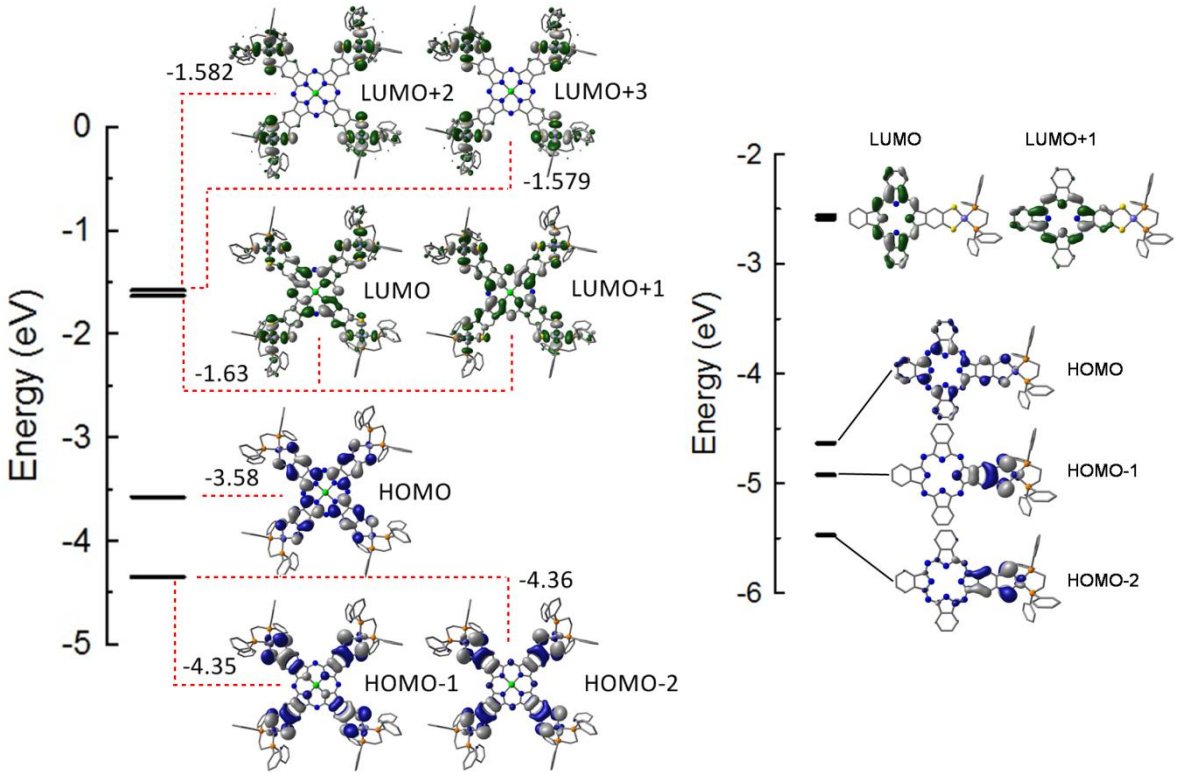

Abbildung 5.2: Energiediagramme der Molekülorbitale HOMO-2 bis LUMO+3 für [(dppeM)$_4$(S$_8$PcMg)] (links) und HOMO-3 bis LUMO+1 für [(dppe)Ni(S$_2$PcH$_2$)] (rechts).

π→π*- oder LLCT-, sondern auf einen intramolekularen Charge Transfer Prozesszurückzuführen. Die Isoindolindithiolat-Metall Einheit ist eine elektronenreiche Gruppe mit starker Elektronendonorfähigkeit. Durch optische Anregung wird eine Ladungsübertragung in das LUMO/LUMO+1 des Pcs initiiert. Abbildung **5.2** zeigt die Energiediagramme der Molekülorbitale, die am Zustandekommen der Q-Bande und der neu beobachteten Übergänge in den symmetrischen und unsymmetrischen Ni-Komplexen involviert sind.

Obwohl das Metall in den untersuchten [(dppeM)$_4$S$_8$PcMg] Komplexen die Absorptionsspektren nur geringfügig beeinflusst, hat es einen starken Einfluss auf die Singulett Sauerstoff Quantenausbeuten (Φ_Δ). Die Singulett Sauerstoff Quantenausbeutenwurden von den Gruppe 10 Komplexen [(dppeM)$_4$S$_8$PcMg] (Φ_Δ= 0.36), [(dppePd)$_4$S$_8$PcMg] (Φ_Δ= 0.76) und [(dppePt)$_4$S$_8$PcMg] (Φ_Δ = 0.91) bestimmt. Dieser Trend kann über den Schweratomeffekt erklärt werden. Schwere Atomkerne fördern Inter-System-Crossing (ISC) Prozesse über eine Spin-Bahn Kopplung der S_1 und T_1 Zustände. Dieses Ergebnis zeigt, dass die an den Thiocatecholateinheiten koordinierten Metallzentren einen ausgeprägten Einfluss auf die Ligandorbitale des Pcs haben, und darum an photophysikalischen und -chemischen Prozesse beteiligt sein können. Die ln(A_0/A_t) - Zeit Diagramme zur Bestimmung der Singulett-Sauerstoff-Quantenausbeute durch Beobachtung des Zerfalls von DPBF (Diphenylbenzofuran) sind in Abbildung **5.3** gezeigt.

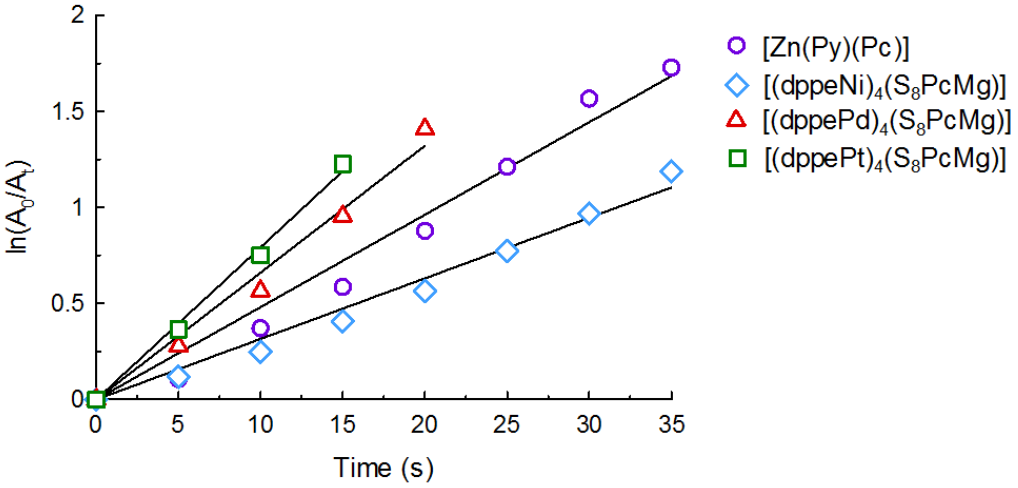

Abbildung 5.3: Der zeitlich aufgelöste Zerfall von DPBF (aufgetragen als Funktion von ln(A_0/A_t)) zur Bestimmung der Singulett-Sauerstoff-Quantenausbeute der [(dppeM)$_4$(S_8PcMg)] Komplexe. [Zn(Py)(Pc)] (Φ_Δ = 0.56) wurde als Standard verwendet.

Die starke Abhängigkeit der Φ_Δ von den thiocatecholatgebundenen Metallen zeigt, dass diese einen ausgeprägten Einfluss auf die Dynamik der angeregten Zustände haben.

5.2 Metallophthalocyaninkomplexe mit axialen Imidoliganden

Nebender periphären Metallkoordination kann auch das Metallzentrum des (Metallo)-phthalocyanin-Komplexes synthetisch modifiziert werden. Als Ergänzung zu früheren Arbeiten werden Vanadium und Chrom-Phthalocyaninkomplexe mit axial koordinierenden Imidoliganden (NR^{2-}) beschrieben. Es gibt mehrere Möglichkeiten, Imido Vanadium-phthalocyanin Komplexe ([PcV(NR)]) ausgehend von [V(NR)Cl_3] herzustellen. [V(NR)Cl_3] dient dabei als Templat für die Integration in ein Pc-System. Allerdings ist dabei eine Zugabe von Radikalfängern und eine vorige Reduktion zur V(III) Verbindung notwendig, um eine Chlorierung des Pc-Liganden zu vermeiden. Alternativ kann [V(NR)Cl_3] mit einem metallierten Pc-Vorläufer [K_2Pc] im Zuge einer Trasmetallierungsreaktion umgesetzt werden. Dabei wird das Vanadiumatom von V(V) zu V(IV) reduziert. Imidochromphthalycyanin Komplexe [PcCr(NR)] konnten durch oxidative Addition organischer Azide an chrom(II)phthalocyanine hergestellt werden. Schema **5.2** zeigt die Synthese der Vanadium- und Chromkomplexe.

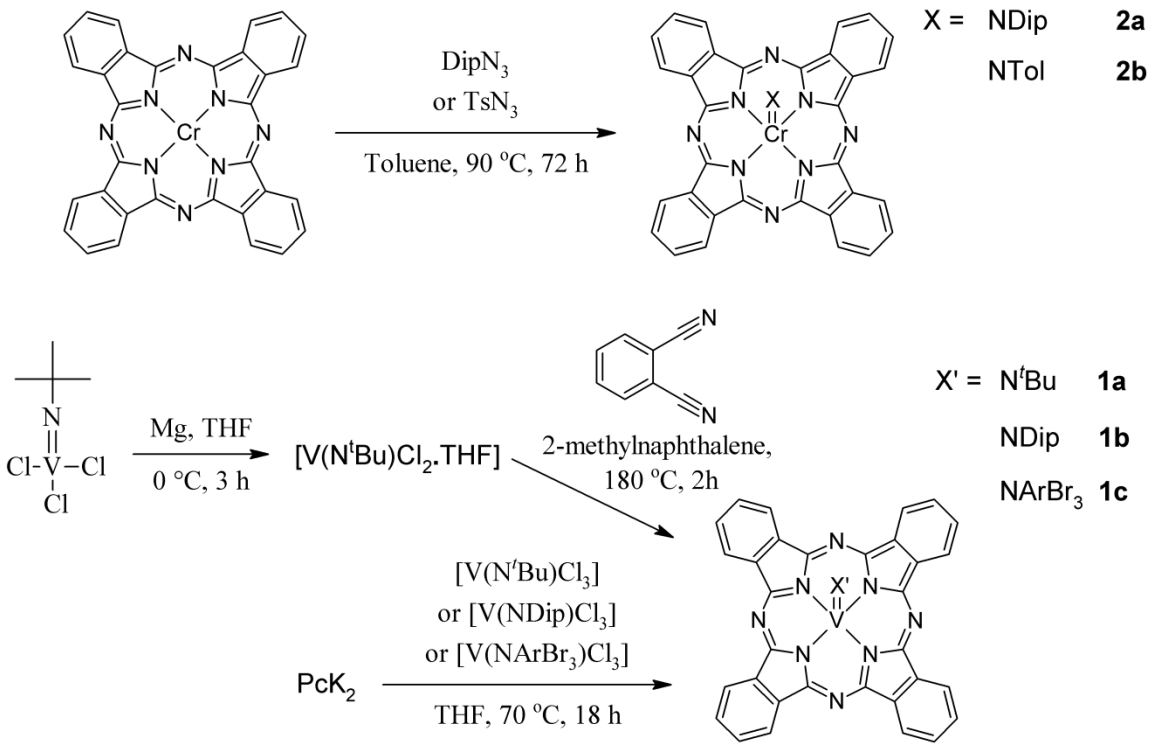

Schema 5.2: Synthese der [PcV(NR)] (unten) [PcCr(NR)] (oben) Komplexe.

Die Absorbanzspektren der Imido Chrom und Imido Vanadium-Pc Komplexe weisen im Vergleich zu ihren Oxo-Derivaten nur eine schwache Rotverschiebung der Q-Bande auf. Diese resultiert wahrscheinlich aus der Wechselwirkung derPc-π-Orbitale mit denen des axialen Liganden. Die leichte Rotverschiebung des Imido-Vanadium-Pcs im Vergleich zum Imido-Chrom-Pc erklärt sich auch über die höhere Elektropositivität des d^1-Vanadium(IV) Atoms.

Im Rahmen dieser Arbeit wurden DFT-Rechnungen durchgeführt um die optimierte Struktur der funktionalisierten Pcs in der Gasphase der Komplexe genauer zu untersuchen. Wie bei bekannten Imidotitan Komplexen, zeigt auch [PcV(NR)] eine lineare V=N-R Bindung. Überaschenderweise ist die Cr=N-R Bindung um ca. 140° gekippt. Um diese Beobachtung genauer zu verstehen, wurde eine *Natural Bond Orbital (NBO) Analysis* durchgeführt (Abbildung **5.4**). Der Grund für die gewinkelte Cr–N–R Bindung wird auf die zwei

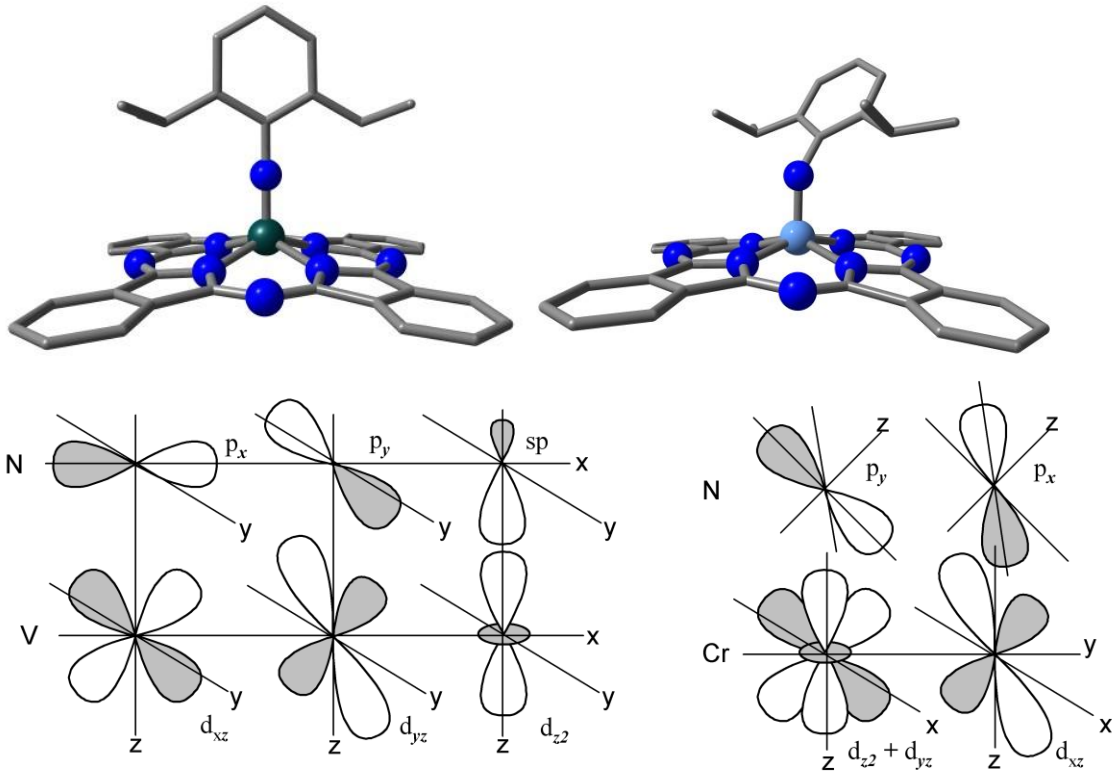

Abbildung 5.4: Gasphasenoptimierte DFT-Geometrien für [PcV(IV)(NDip)] - und [PcCr(IV)(NDip)] - Komplexe, die den linearen und gekrümmt M=N–R Bindungswinkel für Vanadium (links) bzw. Chrom (rechts) und die NBO-Analyse der entsprechenden M–N Bindungen.

nichtbindenden Elektronen am Chrom zurückgeführt, welche die 3d*yz* und das 3dz^2 Orbitale besetzen, und damit dem Dreifachbindungscharakter der M-N Bindung entgegen wirken. Im Vanadium-Komplex befinden sich das nicht bindende Elektron im 3dx^2-y^2 Orbital und wechselwirkt deswegen nicht mit der M-N-Bindung entlang der z-Achse.

5.3 Mono-Thiomethylzink(II)phthalocyanine zur Ausbildung von Monolagen

Im Rahmen des SFB 1083 wurden Untersuchungen zur Bildung von selbstorganisierten Monolagen von [Zn(Pc)] auf einer Au(111) Oberfläche durchgeführt. Dazu wurde ein neuer Monothiomethyldinitril Präkursor über eine zweistufige Reaktion hergestellt (Schema **5.3**).

In der ersten Stufe wurde 4-Bromomethylphthalonitril in guten Ausbeuten über eine radikalische Bromierung von 4-Methylphthalodinitril mit N-Bromsuccinimid (NBS) in Acetonitril erhalten. Diese umweltfreundlichere Synthese verbessert dabei die bisher etablierte Route, die chemische Radikalbildner und das giftige Lösungsmittel CCl_4 notwendig machte. Im zweiten Schritt wird das 4-Bromomethylphthalonitril mit Thioessigsäure umgesetzt, um das S-acylierte, geschützte, Dinitril zu erhalten. Dieses wurde in einer statistisch gemischten Co-Zyklisierung mit 4,5-di-n-Butylphthalonitril verwendet, um eine Mischung aus Zn(Pc)-Produkten zu erhalten. Die Zielverbindung Mono-thiomethyl A_3B Zn(Pc), [Zn(Pc^{SH})] konnte säulenchromatographisch isoliert und aufgereinigt werden.

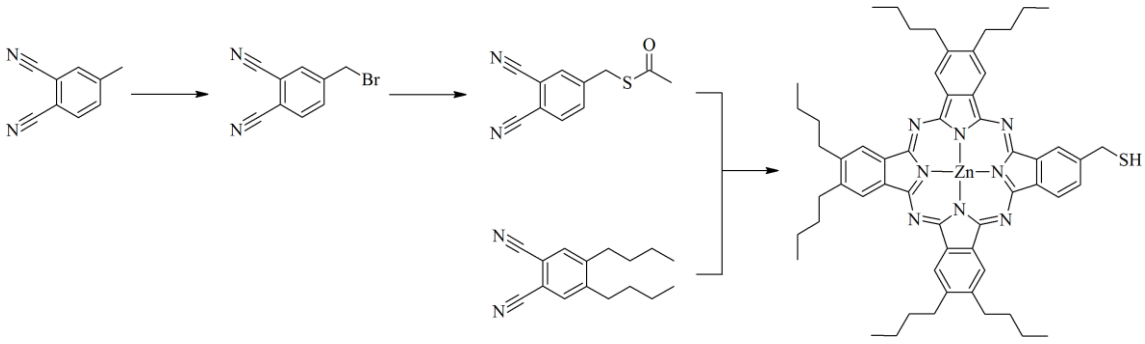

Schema 5.3: Synthesen der Dinitrilvorstufe und der A_3B-[Zn(Pc^{SH})]-Komplexe durch Co-Zyklisierung.

Es wurde unter aeroben und anaeroben Bedinungenversucht, Monolagen durch Eintauchen einer goldbeschichteten Micaprobe in [$ZnPc^{SH}$] Lösungen aufzubringen. Durch Röntgen-

Nahkanten-Absorptions-Spektroskopie (NEXAFS) konnte gezeigt werden, dass die Oberfläche mit [ZnPc] beschichtet war, jedoch größtenteils ungeordnet, was durch thermische Nachbehandlung nur unwesentlich verbessert werden konnte. Über XPS-Spektren konnte gezeigt werden, dass RS-Au Bindungen an der Oberfläche ausgebildet werden, diese sich jedoch unter aeroben Bedingungen zu Sulfonaten (Au-SO_2), und unter anaeroben Bedingungen zu anorganischem Goldsulfid (-Au-S-) zersetzen. Die Oxidation zum Sulfonat kann auf die photooxidativen Eigenschaften des [Zn(Pc)] zurückgeführt werden, während die thermische Zersetzung zum Sulfid auf die Labilität der Methylen-Schwefel-Bindung zurückzuführen ist.

5.4 Nichtaggregierendes Hexadecamethylphthalocyaninsilicium für die photodynamische Therapie

Siliziumphthalocyanine sind aufgrund ihrer potenziellen Eignung in der photodynamischen Theraphie. Da diese jedoch *End-on* oder *J*-Typ Aggregate ausbilden, die die Singulett-Sauerstoff-Quantenausbeute verringern. In dieser Arbeit wurde ein Siliziumphthalocyanin Komplex mit hexadecamethylsubstituiertem Phthalocyaninligand (Pc*) hergestellt, der keine *J*-Typ Aggregation ausbildet. Durch die axialen $OSiMe_3$ Liganden am Siliziumatom wird die Ausbildung von *face-to-face* oder *H*-Type Aggregaten unterbunden, und die Löslichkeit des Komplexes drastisch erhöht. Sowohl ein monomerer, als auch ein µ-oxo-verbrückter dimerer Komplex wurden isoliert und charakterisiert.

Für die monomere Spezies [Pc*Si$(OTMS)_2$] (Φ_Δ = 0.48) konnte die Singulett-Sauerstoff-Quantenausbeute auch hier über den zeitaufgelösten DPBF-Zerfall bestimmt werden. Im Vergleich zum unsubstituierten [PcSi$(OH)_2$] (Φ_Δ = 0.28) ist die Singulett-Sauerstoff-Quantenausbeute erheblich reduziert. Die verringerte Aggregation von [Pc*Si$(OTMS)_2$] hat somit einen starken Einfluss auf ihre Wirksamkeit in biologischer Umgebung. Die Struktur des [Pc*Si$(OTMS)_2$] und die DPBF Spektren sind in Abbildung **5.5** gezeigt.

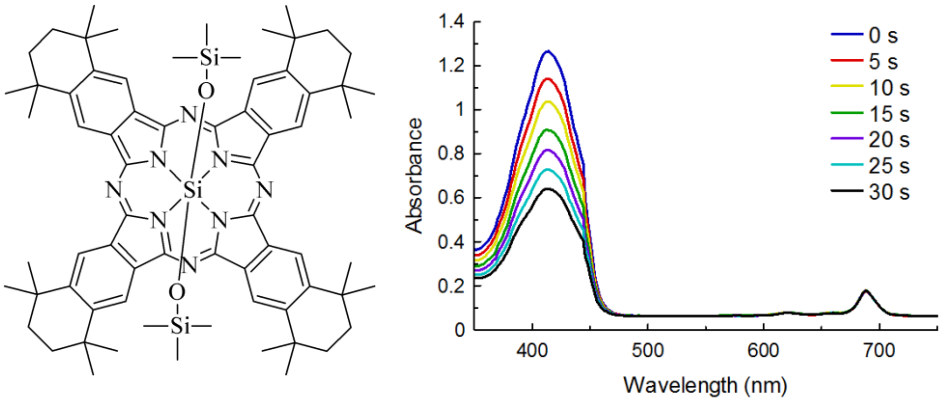

Abbildung 5.5: Die Struktur von [Pc*Si(OTMS)$_2$] (links) und der Zerfall von DPBF bei Belichtung in Gegenwart des Silicium(IV)-Photosensibilisators.

5.5 DFT Berechnungen des Quenching-Mechanismus in Perylendiimid-Amin-Konjugaten

Die Fluoreszenz von Perylenediimidien (PDIs) ist typischerweise sehr hoch, wird aber fast gänzlich für alle arbeitskreisintern hergestellten, aminkonjugierten PDIs gequencht. Um näher zu untersuchen wie dieser Quechning Mechanismus abläuft, wurden die Verbindungen über elektrochemische Methoden, Absorbanz- und Fluoreszenz-, sowie zeitaufgelöster Photolumineszenzspektroskopie untersucht. Auch DFT und TD-DFT Methoden wurden genutzt, um die Elektronendynamik in den Grundzuständen und den angeregten Zuständen zu verstehen.

Die Ergebnisse dieser Berechnungen zeigen, dass für Verbindungen mit tertiärem Amin das HOMO sowohl im Grundzustand als auch im angeregten Zustand am Amin lokalisiert ist, und der $\pi \rightarrow \pi^*$ Übergang, der für die Fluoreszenz verantwortlich ist, zwischen HOMO-1 und LUMO stattfindet. Es ist anzunehmen, dass bei optischer Anregung ein Elektron vom aminzentrierten HOMO in das HOMO-1$^{\bullet+}$ übergeht, welches sich über das Perylengerüst erstreckt, wodurch jede mögliche Fluoreszenz gequencht wird. Durch Protonierung oder Quaternisierung durch N-Methylierung des Amins, senkt sich die Energie des aminzentrierten Orbitals unterhalb der Energie des perylenzentrierten Molekülorbitals, dass nun dem HOMO entspricht. Darum ist eine Beteiligung des aminzentrierten Orbitals an photoinduziertem Elektronentransfer (PET) energetisch nicht mehr begünstigt und der Absorptions-Fluoreszenz-Prozess des Perylengerüstes kann stattfinden. Die energetische Umstrukturierung der Molekülorbitale ist unabhängig von der Entfernung zwischen Amin und Perylengrundgerüst, was anhand von PDIs/PDHs mit verschieden langen Alkylspacern

gezeigt wurde. Abbildung **5.6** zeigt das Molekülorbitalenergiediagram für neutrale und protonierte PDH Verbindungen, und den angenommenen Mechanismus für das Auslöschender Fluoreszenz.

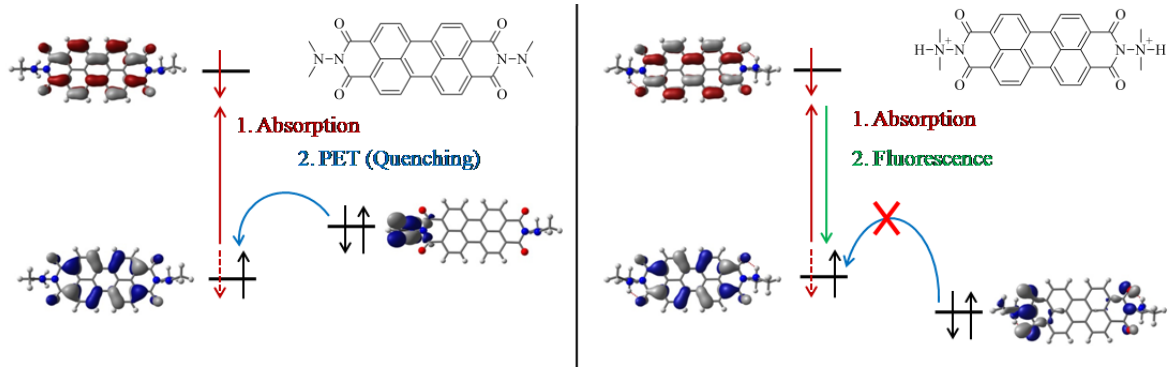

Abbildung 5.6: MO-Energieniveaudiagramm und Fluoreszenzlöschung durch photoinduzierten Elektronentransfer (PET) für PDH mit neutralem (links) und protoniertem(rechts) Amin.

CHAPTER 6 | FULL TEXTS OF THE DISCUSSED MANUSCRIPTS

The six manuscripts appear here in the same order as they were discussed in the cumulative section. The manuscripts already published are presented in their form as found online. Manuscripts that have been accepted, but are not available online are presented in the template of the journal that they have been accepted to. For manuscripts 2 and 3, supplementary information for the relevant spectroscopic and synthetic procedures is included. Figures of FTIR, NMR and MS spectra have not been reproduced here. Manuscripts 5 and 6 have not yet been submitted to a journal for publication.

1) "Group 10 Metal-Thiocatecholate Capped Magnesium Phthalocyanines – Coupling Chromophore and Electron Donor/Acceptor Entities and its Impact on Sulfur Induced Red-Shifts" Reproduced from: Malcolm A. Bartlett and Jörg Sundermeyer, *Dalton Trans.*, **2018**, DOI: 10.1039/C8DT03681K

2) "Peripheral Metallation of Phthalocyanine – Inducing New Effects in an Old Chromophore", Malcolm A. Bartlett and Jörg Sundermeyer, *submitted.*

3) "Synthesis, Spectroscopy and Singlet Oxygen Quantum Yield of a Non-Aggregating Pc*Si Derivative" Reproduced from: Malcolm A. Bartlett, Kerstin Mark and Jörg Sundermeyer, *Inorg. Chem. Comm.*, **2018**, *98*, 41–43

4) "Zinc(II) Phthalocyanine-Thiol Monolayers on Gold: On the Oxidative Stability of the S–Au Bond", Malcolm A. Bartlett, Michael Kothe, Jörg Sundermeyer and Gregor Witte, *in preparation*

5) "Imido Vanadium(IV) and Imido Chromium(IV) Phthalocyanine Complexes: Synthesis, Spectroscopy and Theoretical Investigations", Malcolm A. Bartlett, Elisabeth Seikel and Jörg Sundermeyer, *in preparation*

6) "Control of Intramolecular Electron Transfer in Perylene Dihydrazines and Perylene Diimides: A Comparative Study by Time-Resolved Spectroscopy" Robin C. Döring, Eduard Baal, Malcolm A. Bartlett, Christian Prinzisky, Remco W. A. Havenith, Jörg Sundermeyer and Sangam Chatterjee, Cornell University Library: arXiv:1612.05046v1 [physics.chem-ph]

6.1 Group 10 Metal-Thiocatecholate Capped Magnesium Phthalocyanines – Coupling Chromophore and Electron Donor/Acceptor Entities and its Impact on Sulfur Induced Red-Shifts

Malcolm A. Bartlett and Jörg Sundermeyer

Group 10 Metal-Thiocatecholate Capped Magnesium Phthalocyanines – Coupling Chromophore and Electron Donor/Acceptor Entities and its Impact on Sulfur Induced Red-Shifts.

Dalton Transactions, **2018**, DOI: 10.1039/C8DT03681K, *in press*

Dalton Transactions

Accepted Manuscript

This article can be cited before page numbers have been issued, to do this please use: M. A. Bartlett and J. Sundermeyer, *Dalton Trans.*, 2018, DOI: 10.1039/C8DT03681K.

ROYAL SOCIETY OF CHEMISTRY

rsc.li/dalton

View Article Online
DOI: 10.1039/C8DT03681K

Journal Name

ARTICLE

Group 10 Metal-Thiocatecholate Capped Magnesium Phthalocyanines – Coupling Chromophore and Electron Donor/Acceptor Entities and its Impact on Sulfur Induced Red-Shifts‡

Received 00th January 20xx,
Accepted 00th January 20xx

DOI: 10.1039/x0xx00000x

www.rsc.org/

Malcolm Alan Bartlett[a] and Jörg Sundermeyer*[a]

A new and facile method of generating thiolate groups at the phthalocyanine (Pc) β-position is presented as well the unique properties that these groups confer on the Pc ligand upon coordination of group 10 metals Ni, Pd and Pt(dppe) or $SnMe_3$. In particular, the Q-band is shifted to almost 800 nm for all group 10 metals used, and the complexes show panchromatic absorption owing to new absorbance bands that appear between 400 and 650 nm. Enhanced intersystem-crossing for all transition metal coordinated Mg(Pc) complexes was demonstrated by the moderate to very high singlet oxygen quantum yields of 0.36, 0.76 and 0.91 for the Ni, Pd and Pt coordinating complex, respectively, which show that the heavy metals have direct influence on the Pc π-system and inter-system-crossing (ISC). This was further confirmed by MO calculations, which show mixing of metal and ligand orbitals, as well as suggest that the Q-band transition has both π→π* and ligand-to-metal charge transfer character. Furthermore, the origin of the Q-band red-shift was shown to be due to greater destabilization of the HOMO compared to LUMO/LUMO+1, thus decreasing the HOMO-LUMO band gap.

1. Introduction

Heteroleptic complexes, where one of the ligands binds a metal *via* a thiolate groups, have relevance for energy conversion in dye-sensitized solar cells[1] or for energy storage, e.g. water splitting,[2] or the reduction of H^+ to H_2.[3d] In these applications, the thiolato or endithiolato ligand is often an electron donor, and the process can be driven either photo- or electrochemically.[3] It is therefore desirable that such ligands have both good electron-donating and, for photo-driven processes, good light absorbing properties. Examples of such endithiolato or dithiocatecholato ligands with extended π-systems ranging from simple maleonitrile[4] and benzene[3d,5] groups to BODIPY[6] derivatives can be found in the literature; some representative examples are shown in Figure 1.

Phthalocyanines (Pcs) are known for their strong light absorbing properties as well as general chemical and physical stability.[7] Consequently their application in optoelectronic devices, such as near-infrared (NIR) imagers and dye-sensitized-solar-cells, continues to be extensively investigated.[8] In particular, increasing the light absorption of Pc and promoting charge transfer to an acceptor moiety[9,10] is a topical area of research, as this would enable a more efficient utilization of the full solar spectrum and more efficient photo-driven processes. Many strategies have been employed to improve light harvesting, such as incorporating additional chromophores onto the Pc to create a donor with absorbance between the B- and Q-bands to create a so-called panchromatic-absorber.[11,12,13,14] Additionally, many strategies involve shifting the Q-band absorption maximum to longer wavelengths to harvest NIR light energy. Although it has been known for many years that derivatisation of the Pc ligand at the α and β positions (Figure 2) with organochalcogenide substituents –ER, where E =

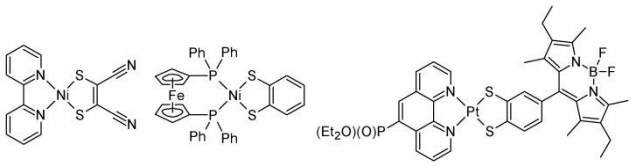

Fig. 1 Heteroleptic complexes employing a dithiolate-containing ligand as a donor ligand for photo- or electrochemically active intermolecular charge transfer: [(dtmn)Ni(bpy)],[4] [Ni(bdt)(dppf)][3d] and a [(BODIPY)Pt(phen)][6] derivative.

[a] Department of Chemistry, Philipps-Universität Marburg, Hans-Meerwein St 4, 35032, and Wissenschaftliches Zentrum für Materialwissenschaften (WZMW), Marburg, Germany.

*Email: Prof. Dr. Jörg Sundermeyer jsu@chemie.uni-marburg.de

Electronic Supplementary Information (ESI) available: [copies of NMR, FTIR and UV-Vis spectra and MS data are given in the supplementary information]. See DOI: 10.1039/x0xx00000x

View Article Online
DOI: 10.1039/C8DT03681K

S, Se and Te, causes a bathochromic (red-) shift of the Q-band, it was only recently demonstrated how strong this effect can be, inducing red-shifts of over 100 nm.[15,16] This is believed to be due to an increase in the size of the effective π-system, caused by mixing of the valence p-orbital with the macrocycle's π-system. Inclusion of anionic thiolate/thiocatecholate groups $-E^-$ onto the Pc scaffold should therefore result in a Pc based chromophore with unique optical properties that is, at the same time, a capable donor in the synthesis of photoactive heteroleptic complexes with good charge-transfer activity.

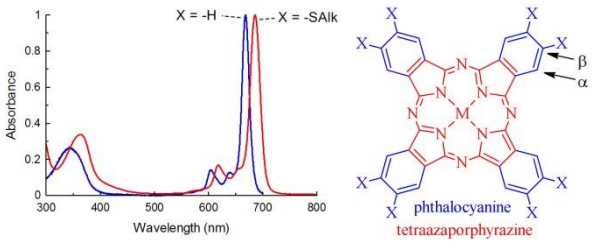

Fig. 2 (left) The typical UV-Vis-NIR absorbance spectra for a metallated Pc (X=H) and a Pc derivative with eight thiol groups at the β-positions (X = SAlk). (right) The structure of a metallated tetraazaporphyrazine (Pz; red) and phthalocyanine (Pc; blue) with the common positional labelling system for benzene substitution

Despite this, there is only one example of a Pc compound bearing formally anionic thiolate groups.[17] The thiolate salt is generated by cleavage of benzyl thioether groups under harsh conditions of a Birch-type reduction ($Na/NH_3(l)$). There are also few examples of tetraazaporphyrazine (Pz) complexes bearing formally anionic thiolate groups (Figure 2 shows the core structure of a Pz compound). These were also generated under the same Birch-type conditions.[18] So far, the high temperatures and the use of super-bases, e.g. DBU, often associated with Pc or Pz ring formation precludes the use of ideal thiolate protecting groups, which later on are readily cleaved under mild conditions.[19] To date, there has been no convincing alternative but to mask the thiolate as a robust PcS-benzyl functionality, followed by cyclisation of the dinitrile and deprotection of the resulting dye-benzylthioether under extremely harsh Birch conditions not compatible with the goal of trapping the sodium thiolate *in statu nascendi* with a wide range of transition metal complexes. A much milder deprotection strategy would open a multitude of perspectives in using such dyes as thiolate or thiocatecholate ligands in heteronuclear transition metal chemistry.

Here, we present both a new facile method of generating thiocatecholate groups on the Pc ligand and show how coordination of metals, in particular group 10 metal ions, by these thiocatecholate groups can have a strong influence on the Pc ligand's optoelectronic properties, which are considerably stronger than those observed for thioether substitution. Given the broad range of potential applications of thiol-substituted Pc derivatives, these findings, while broadening the perspectives for coordination chemistry with Pc ligands, have relevance for the design and synthesis of chromophore complexes for photo-driven redox chemistry.

2. Experimental

2.1 Methods and materials

4,5-dichlorophthalonitrile was prepared from 4,5-dichlorophthalic acid (Sigma Aldrich) according to literature procedures.[20] 1,3-dihydro-2*H*-benzimidazole-2-thione was prepared using the method of Zhivotova et al.[21]

Photo-irradiation was performed using a halogen lamp with an adjustable power rating, which was set to 100 W. Light was filtered through a water filter for removal of infrared light and then through a glass filter with a cut-on wavelength of 500 nm. NMR spectra were obtained on a Bruker AVANCE 300 spectrometer. Chemical shifts are reported in δ (ppm) values. ^1H and ^{13}C NMR values were referenced to residual solvent as an internal standard, while ^{119}Sn NMR values were referenced to Me_4Sn. The following abbreviations were used: s = singlet, d = doublet, t = triplet, q = quartet, m = multiplet and br = broad singlet. Mass spectra were recorded on a Thermo Fischer Scientific LTQ-FT Ultra, or on a Bruker Biflex III-Spectrometer (MALDI matrix DHB). UV-Vis spectra were recorded on a Varian Cary Eclipse 5000. FTIR spectra were measured using a Bruker Alpha Platinum ATR single reflection diamond spectrometer.

2.2 Singlet oxygen quantum yields

Singlet oxygen quantum yield measurements were performed using the set-up described above. In a typical measurement, a cuvette was filled with 2 ml of sample solution containing the sensitizer and DPBF, the concentrations of which were such that the absorbance of each was ca. 0.2 and ca. 1.0, respectively. The samples were saturated with O_2 by bubbling a stream of O_2 gas through the sample solution in the dark for one minute before beginning the measurements under light irradiation. The singlet oxygen quantum yield, Φ_Δ, was determined by using the following equation:[22]

$$\Phi_\Delta = \Phi^{Std}_\Delta (k I^{Std}_{Abs} / k^{Std} I_{Abs}) \qquad (1)$$

where k and k^{Std} are the slopes of the plot of $\ln(A_0/A_t)$ versus time, for the sensitizer and standard, respectively, where A_0 and A_t are the measure of DPBF absorbance at time "0" and time "t", and I_{Abs} and I^{Std}_{Abs} are the rates of light absorption by the sensitizer and standard, respectively, and are determined using the equation:[23]

$$I_{abs} = \alpha((AP)/N_A) \text{ with } \alpha = 1 - 10^{-E} \qquad (2)$$

Where E is the absorbance of the sensitiser at the irradiation wavelength, A is the irradiated area (2.2 cm^2), P is the intensity

View Article Online
DOI: 10.1039/C8DT03681K

of light and N_A is Avogadro's constant. Zn(Pc) was used as a standard (Φ_Δ = 0.56 in DMF).[23]

2.3 Molecular orbital calculations

The gas-phase structures of [(dppeM)$_4$(S_8PcMg)], where M = Ni, Pd or Pt, were optimized at the B3LYP/LanL2DZ level of theory. TDDFT calculations solving for 20 states were then performed at the same level of theory using the gas-phase optimized structures as input structures. All calculations were performed on the MaRC2 computing cluster using the Gaussian09 software package.[24]

2.4 Syntheses

2.4.1 4,5-bis(1-H-benzimidazol-2-ylsulfanyl)benzene-1,2-dicarbonitrile (dbtpn): 4,5-dichlorophthalonitrile (2.00 g; 10.15 mmol) and benzimidazole-2-thione (3.20 g; 21.30 mmol) were dissolved in DMF (30 ml). K_2CO_3 (8.5 g; 61.50 mmol) was finely ground before being added to the solution. The resulting suspension was stirred at rt for 18 h. H_2O (80 ml) was then added, causing a yellow solid to precipitate out of solution. The solids were collected by filtration and washed thoroughly with H_2O before being dried *in vacuo*. Mass: 3.75 g. Yield: 87 %. ^{1}H NMR (DMSO-*d6*; 300 MHz, 298 K): δ (ppm) 7.21-7.26 (m, 4H, benz); 7.54-7.59 (m, 4H, benz); 8.19 (s, 2H, phthalonitrile).^{13}C NMR: (DMSO-*d6*; 75 MHz; 298 K): δ (ppm) 143.11; 149.54; 135.66; 122.60; 115.22; 113.91. HRMS (APCI+, MeOH): Calcd. for $C_{22}H_{12}N_6S_2$ $[M+H]^+$: 425.0639; Found: 425.0638.

2.4.2 4,5-bis(1-methyl-benzimidazol-2-ylsulfanyl)benzene-1,2-dicarbonitrile (Dmbtpn): Dbtpn (0.25 g; 0.59 mmol) was dissolved in DMF (10 ml). Crushed KOH pellets (0.35 g; 6.25 mmol) were added to this solution, which was stirred for 5 min at rt. MeI (0.8 ml; 2.5 mmol) was added, and stirring was continued for 10 min. H_2O (30 ml) was added, and the precipitate that formed was collected by filtration and washed thoroughly with H_2O. The solids were extracted into $CHCl_3$, dried over $MgSO_4$ and the solvent was evaporated to leave a white crystalline solid. Mass obtained: 0.23 g. Yield: 85 %. ^{1}H NMR (300 MHz, DMSO-*d6*): δ (ppm) 3.82 (s, 6H, -CH3); 7.26-7.38 (dt, 4H, Ar); 7.63-7.69 (t, 4H, Ar); 7.93 (s, 2H, phthalonitrile). ^{13}C NMR (75 MHz, DMSO-*d6*): δ (ppm) 30.85 (-CH3); 110.92, 114.04, 115.05, 119.04, 122.44, 123.37, 134.96, 136.58, 140.36, 142.80, 143.77. HRMS (APCI+; MeOH): Calcd for $C_{24}H_{17}N_6S_2$ $[M+H]^+$: 453.0951; Found: 453.0952.

2.4.3 Magnesium(2,3,9,10,16,17,23,24-octa(1-H-benzimidazol-2-ylsulfanyl)-phthalocyanine) ([(RS)$_8$PcMg]): Dbtpn (0.800 g; 1.88 mmol) was mixed with $Mg(OEt)_2$ (0.200 g; 1.75 mmol) under N_2. 1-Octanol (3 ml) was then added to the mixture, which was then homogenised in an ultrasound bath for 15 min. The suspension was then heated at 160°C for 10 min to afford a dark green solid. This was then cooled to rt before washing with hexane, $CHCl_3$, EtOH and H_2O. Mass: 0.602 g. Yield: 74%. ^{1}H NMR (DMSO-*d6*; 300 MHz): δ (ppm) 9.29 (s, 8H, PcH); 8.15 (s, 6H, NH); 7.52- 7.48 (m, 32H, Ar); 7.18-7.14 (m, 32H, Ar). MS (MALDI+, CH_3CN): Calcd. for $C_{88}H_{49}MgN_{24}S_8$ $[M+H]^+$: 1723.32; Found: 1723.32. UV-Vis (DMSO): 702 (s), 664 (sh), 628 (s), 368 (s). FTIR: ν/cm^{-1} = 1060 (s), 1265 (s), 1395 (s), 1595 (s), 2850 (s), 2920 (s), 3051 (m).

2.4.4 Magnesium(2,3,9,10,16,17,23,24-octa[(1-methyl-benzimidazol-2-yl) sulfanyl]-phthalocyanine ([(^{Me}RS)$_8$PcMg]): (Method a) ([(RS)$_8$PcMg] (0.700 g; 0.406 mmol) was dissolved in DMF (10 ml). MeI (1 ml) was then added, followed by crushed KOH pellets (0.500 g; 8.911 mmol). The suspension was stirred for 25 min at rt before being added to H_2O (90 ml). The precipitate that forms was collected by filtration and washed thoroughly with H_2O before being dried *in vacuo*.

(Method b) Dmbtpn (1.01 g; 2.21 mmol) was mixed with $Mg(OEt)_2$ (0.48 g; 4.19 mmol) under N_2. Octanol (10 ml) was added, and the resulting suspension was homogenised using an ultrasound bath. The suspension was then placed in an oil bath preheated to 170°C for 35 min. The resulting green suspension was allowed to cool before washing the solids with hexane (3 x 40 ml). Washing was repeated using $CHCl_3$, Me_2CO, EtOH and H_2O until all washings were colourless. The remaining dark green solids were then dried to yield the final product. Mass: 0.874 g. Yield: 86 % (Method a). Mass: 0.635 g. Yield: 62 % (Method b). ^{1}H NMR (DMSO-*d6*, 300 MHz, 298 K): δ (ppm) = 3.92 (s, 24H, -CH3); 7.05-7.19 (m, 16H, Ar); 7.56-7.54 (m, 16H, Ar); 8.89 (s, 8H, Pc). LRMS (MALDI+, CH_3CN): Calcd. for $C_{96}H_{64}MgN_{24}S_8$ $[M]^+$: 1832; Found: 1832. UV-Vis (DMSO): λ/nm = 704 (s), 670 (sh), 632 (s), 375 (s). FTIR: v/cm^{-1} = 1064 (s), 1277 (s), 1321 (s), 1370 (s), 1396 (s), 1448 (s), 1595 (w), 2920 (w), 3051 (w).

2.4.5 Magnesium(2,3,9,10,16,17,23,24-octa[(1,3-dimethyl-1H-benzimidazol-2-yl)sulfanyl]-phthalo-cyanine octaiodide ([(^{Me2}RS)$_8$PcMg]I$_8$): [(^{Me}RS)$_8$PcMg] (0.800 g; 0.463 mmol) was dissolved in DMF (15 ml). MeI (4 ml; 64.25 mmol) was then added, and the solution was heated at 80°C for 16 h. The solution was then added to THF (200 ml), and the precipitate was collected by filtration and washed with THF. The sample was cleaned by repeated dissolution in DMF followed by precipitation from THF. Mass: 1.049 g. Yield: 81 %. ^{1}H NMR (DMSO-*d6*, 300 MHz, 298 K): δ (ppm) 4.28 (s, 48H, -C*H*3); 7.89-7.92 (m, 16H, Ar); 8.23-8.26 (m, 16H, Ar); 9.45 (s, 8H, Pc). UV-Vis (DMSO): λ/nm = 705 (s), 630 (s), 362 (sh). FTIR: ν/cm^{-1} = 1019 (s), 1079 (m), 1120 (s), 1281 (m), 1393 (s), 1478 (s), 1590 (m), 1699 (s), 2935 (w), 3014 (w), 3283 (w).

View Article Online
DOI: 10.1039/C8DT03681K

2.4.6 Magnesium(2,3,9,10,16,17,23,24-octa[(trimethyltin)sulfanyl]-phthalocyanine) ([(Me$_3$Sn)$_8$(S$_8$PcMg)]: [(^{Me2}RS)$_8$PcMg]I$_8$ (0.100 g; 0.0337 mmol) and K_2CO_3 (0.160 g; 1.158 mmol) were mixed together, and then suspended in degassed H_2O (3 ml). The suspension was gently heated until a purple solution of K_8[S_8PcMg)] free of any solids was obtained. This solution was then added to a stirred solution of Me_3SnCl (0.540 g; 0.271 mmol) in degassed $CHCl_3$ (5 ml). The two phases were mixed until the aqueous phase became clear and the organic phase became green. The organic portion was separated, dried over $MgSO_4$ and filtered. Solvents were then removed from the filtrate to leave a dark green solid. This was washed with hexane and EtOH before being dried *in vacuo*(10^{-3} mbar). Mass: 0.0664 g. Yield: 94 %. ^{1}H NMR ($CDCl_3$,300 MHz, 298 K): δ (ppm) 0.667 (s, -C*H*$_3$). ^{119}Sn NMR (187 MHz, $CDCl_3$, 298 K): δ (ppm) 173.79. MS (MALDI+, CH_2Cl_2): Calcd. for $C_{53}H_{71}MgN_8S_7Sn_7$ [M – [SSnMe$_3$]]$^+$: 1906.69; Found: 1906.69. UV-Vis(CH_2Cl_2; 298 K) λ/nm: 321, 358 sh, 434, ~645 sh, 663, 699, 732.

2.4.7 General Procedure for the synthesis of K$_8$[S$_8$PcMg] and its coordination to [M(dppe)]$^{2+}$: [(^{Me2}RS)$_8$PcMg] (0.070 g; 2.4 x 10^{-2}mmol) was treated with a solution of KOH (0.05 g; 0.9 mmol) in degassed H_2O (10 ml). Once all solids had dissolved and a blue solution was obtained, it was added drop-wise to a concentrated solution of [MCl_2(dppe)] (0.13 mmol) in THF (20 ml) with vigorous stirring. The suspension that forms was then stirred at rt for 18 h. The sample was then diluted with H_2O and centrifuged to collect the solids. The solids were then washed with MeOH, EtOH, Me_2CO and hexane before being extracted into DCM and filtered. Evaporation of the filtrate left the pure compound.

[(dppeNi)$_4$(S$_8$PcMg)]: ^{1}H NMR (DMSO-*d6*, 300 MHz, 298 K): δ (ppm) 1.35 (s, 16H, -C*H*$_2$C*H*$_2$-), 7.34-7.94 (m, 80H, Ph), 9.04 (br, 8H, Pc). ^{31}P NMR (DMSO-*d6*, 101 MHz, 298 K): δ (ppm) 30.24. MS (MALDI-TOF): Calcd. for $C_{136}H_{105}N_8Ni_4P_8S_8$ [M+H$^+$-Mg]$^+$: 2590.43; Found: 2590.55. UV-Vis (DMSO): λ/nm = 770 (s), 700 (sh), 534 (br), 362 (s).

[(dppePd)$_4$(S$_8$PcMg)]: ^{1}H NMR (300 MHz, DMSO-*d6*, 298 K): δ (ppm) 1.35 (s, 16H, -C*H*$_2$C*H*$_2$-), 7.53-7.65 (m, 40H, Ph); 7.91-7.97 (m, 40H, Ph); 8.24 (s, 8H, Pc). ^{31}P NMR (DMSO-*d6*, 101 MHz, 298 K):δ (ppm) 53.76. MS (MALDI-TOF): Calcd. for $C_{136}H_{105}N_8Pd_4P_8S_8$ [M+H$^+$-Mg]$^+$: 2781.3406; Found: 2782.6098. UV-Vis (DMSO): λ/nm = 765 (s), 698 (sh), 580 (br), 468 (br), 354 (s).

[(dppePt)$_4$(S$_8$PcMg)]: ^{1}H NMR (300 MHz, DMSO-*d6*, 298 K): δ (ppm) 1.24 (s, 16H, -C*H*$_2$C*H*$_2$-), 7.63 (br, 40H, Ph), 7.98 (br, 40H, Ph), 9.27 (br, 8H, Pc).^{31}P NMR (DMSO-*d6*, 101 MHz, 298 K): δ (ppm) 48.34 ($^1J_{Pt\text{-}P}$ = 1160 Hz). UV-Vis (DMSO): λ/nm =764 (s), 702 (sh), 559 (br), 473 (br), 360 (s).

2.4.8 (Bis(1,2-diphenylphosphino)ethane)(4,5-dithiolatophthalonitrile)nickel(II) ([Ni(dppe)(dtpn)]): [$NiCl_2$(dppe)] (0.150 g; 0.28 mmol) was dissolved in $CHCl_3$ (10 ml) and added to a solution of H_2dtPN (0.054 g; 0.28 mmol) in $CHCl_3$ (10 ml). Triethylamine (0.035 g; 0.35 mmol) was then added drop-wise, and the resulting solution was stirred for 180 min. The solution was concentrated by rotary evaporation and then loaded onto a silica column. The product was then purified by column chromatography (silica/$CHCl_3$); it elutes as the first coloured band. Solvent was evaporated to leave a pale orange solid. Mass: 0.141 g. Yield: 78 %. ^{1}H NMR ($CDCl_3$, 300 MHz, 298 K): δ (ppm) 2.43 (d,^1J = 8.4 Hz, 4H, -C*H*$_2$C*H*$_2$-), 7.52 (m, 12H, Ph), 7.66 (s, 2H, phthalonitrile), 7.75 (br, 8H, Ph). ^{13}C NMR ($CDCl_3$, 75 MHz, 298 K): 100.89, 101.45, 105.95, 106.35, 125.99, 129.09, 129.16, 129.27, 131.72, 131.88, 133.41, 133.48, 175.06.^{31}P NMR ($CDCl_3$, 101 MHz, 298 K): 60.05. HRMS (APCI+; CH_2Cl_2): Calcd. for $C_{34}H_{27}N_2NiP_2S_2$ [M+H]$^+$: 647.0439; Found: 647.0436.

2.4.9 (Bis(1,2-diphenylphosphino)ethane)(4,5-dithiolatophthalonitrile)palladium(II) ([Pd(dppe)(dtpn)]: [$PdCl_2$(dppe)] (0.085 g; 0.15 mmol) and H_2dtpn (0.028 g; 0.15 mmol) were suspended in DCM (5 ml). NEt_3 (0.2 ml; 0.15 g; 1.4 mmol) was added, and the suspension was stirred at rt for 18 h. Solvent was evaporated and the solids remaining were washed with hexane. The product was then purified by column chromatography (silica/DCM), being collected as the major yellow band. Mass: 0.085g. Yield: 82 %. ^{1}H NMR ($CDCl_3$, 300 MHz, 298 K): δ (ppm) 2.58 (d, 1*J* = 10.52 Hz, 4H, -C*H*$_2$C*H*$_2$-), 7.46-7.55 (m, 12H, Ph), 7.61 (s, 2H, phthalonitrile), 7.71-7.78 (m, 8H, Ph). ^{13}C NMR ($CDCl_3$, 75 MHz, 298 K):27.83, 106.34, 117.27, 128.64, 129.24, 129.31, 129.39, 132.08, 133.02, 133.19, 133.26, 133.34, 156.06. ^{31}P NMR ($CDCl_3$, 101 MHz, 298 K): δ (ppm) 53.19. HRMS (APCI+; CH_2Cl_2): Calcd. for $C_{34}H_{27}N_2PdP_2S_2$ [M+H]$^+$: 695.0132; Found: 695.0132.

2.4.10 (Bis(1,2-diphenylphosphino)ethane)(4,5-dithiolatophthalonitrile) platinum(II) ([Pt(dppe)(dtpn)]): $PtCl_2$(dppe)] (0.074 g; 0.11 mmol) was mixed with H_2dtpn (0.029 g; 0.15 mmol). The mixture was then dissolved in DCM (5 ml) and NEt_3 (0.2 ml; 0.15 g; 1.4 mmol) was added. The solution was then stirred for 22 h at rt. Solvent was evaporated to leave a yellow-brown solid, which was subsequently washed with MeOH. The solids were then dissolved once more in DCM and loaded onto a silica-gel column. The product was eluted as the second colourless band using DCM. Mass: 0.055g. Yield: 62 %. ^{1}H NMR ($CDCl_3$, 300 MHz, 298 K): δ (ppm) 2.46-2.62 (m, 4H, - C*H*$_2$C*H*$_2$-), 7.47-7.52 (m, 12H, Ph and phthalonitrile); 7.73-7.79 (m, 10H, Ph). ^{13}C NMR ($CDCl_3$, 75 MHz, 298 K):δ (ppm) 106.18, 117.05, 128.91, 129.09, 129.11,

View Article Online
DOI: 10.1039/C8DT03681K

129.19, 132.04, 133.33, 133.40, 133.48, 151.36. ^{31}P NMR ($CDCl_3$, 101 MHz, 298 K): δ (ppm) 44.60 ($^1J_{Pt,P}$= 1399 Hz). HRMS (APCI+; CH_2Cl_2): Calcd. for $C_{34}H_{27}N_2PtP_2S_2$ $[M+H]^+$: 784.0736; Found: 784.0735.

2.4.11 Synthesis of 4,5-disulfanylbenzene-1,2-dicarbonitrile (H_2dtpn): To solid dmbtpn (2.00 g; 2.72 mmol) was added solid KOH (0.5 g; 8.9 mmol) and H_2O (5 ml) to give a suspension. This was sonicated for 15 min, or until all solids dissolved, to give a dark yellow solution. The solution was then diluted with H_2O (25 ml) and acidified with HCl (37 %, aq) to cause a yellow solid to separate. This solid was extracted with DCM (3 x 10 ml). The DCM fractions were combined, dried ($MgSO_4$), filtered and the filtrate was evaporated to leave the pure product as a bright yellow solid. Mass: 0.48 g. Yield: 92 %. ^{1}H NMR (300 MHz; DMSO-*d6*): δ (ppm) 8.60 (s, Ar). ^{13}C NMR (75 MHz; DMSO-*d6*): δ (ppm) 114.5, 114.8, 135.5, 137.5.

3. Results and discussion

3.1 Synthesis

Thiolate protecting groups that can be easily removed are typically not stable under basic conditions, such as those required for phthalocyanine synthesis.[19] We therefore employed a two-step strategy where, first, a stable 2-thio-benzimidazole group was used to introduce a thiol group onto a dinitrile precursor by reacting with readily available 4,5-dichlorophthalonitrile. After normal cyclisation to the Pc dye, a two-fold N-methylation leads to benzimidazol-2-thiuronium groups, that are activated for C-S bond cleavage. These are cleaved with even weakly basic aqueous potassium carbonate to afford an N,N'-dimethylbenzimidazole urea derivative as stable leaving group and a highly reactive and air sensitive potassium thiolate salt $K_8[S_8PcMg]$ for coordination studies.

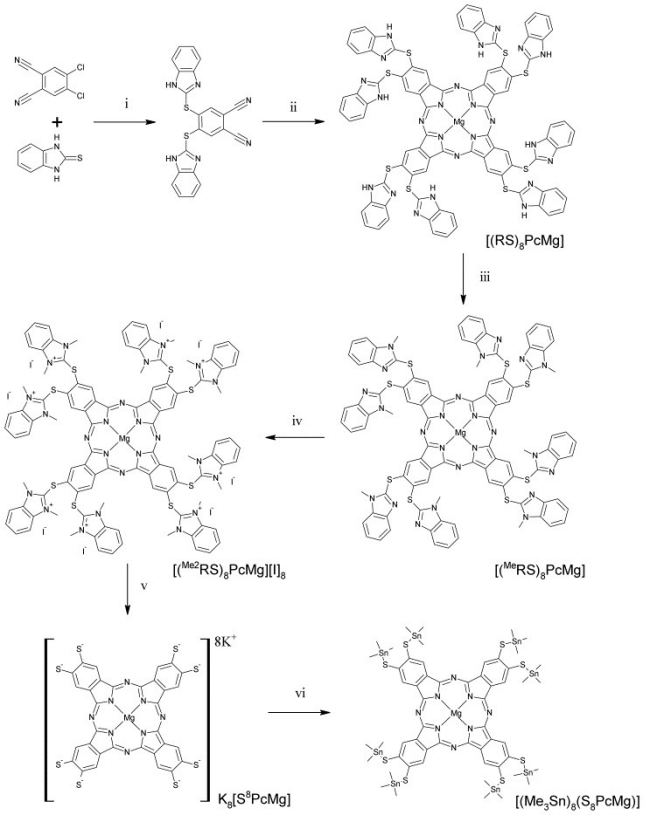

Scheme 1 Synthesis of $[(Me_3Sn)_8(S_8PcMg)]$ *via* the octathiolato intermediate $K_8[S_8PcMg]$. (i) K_2CO_3, DMF, rt; (ii) $Mg(OEt)_2$, 1-Octanol, 160 °C, 10 min; (iii) MeI, DMF, rt, 25 min; (iv) MeI, DMF, 80 °C, h, 16 h; (v) KOH (aq), rt or K_2CO_3 (aq), 80 °C; (vi) Me_3SnCl, THF, rt, 5 min.

This strategy is demonstrated by the *in situ* synthesis of octathiolato Pc complex $K_8[S_8PcMg]$ and its conversion into Ni, Pd, and Pt(dppe) complexes or trimethylstananes. The dinitriledithioether was synthesised by reaction of 4,5-dichlorophthalonitrile with benzimidazole-2-thione in DMF in the presence of K_2CO_3 (Scheme 1). Cyclisation with $Mg(OEt)_2$ in octanol led to the formation of corresponding octa(2-thiobenzimidazol)phthalocyaninato magnesium complex ($[(RS)_8PcMg]$). Quaternerization of the benzimidazole groups was then accomplished *via* two successive *N*-methylations with MeI in DMF, the first one being with the aid of KOH at room temperature and the second one at elevated temperatures. The second *N*-methylation proceeds very slowly at room temperature, with little product formation after several days of stirring. Substitution of the imidazole-H atom with a methyl group can be readily monitored by disappearance of the strong N-H stretching frequency at 2950and 2850 cm^{-1} in the FTIR spectrum of $[(RS)_8PcMg]$. When quaternerisation *via* double methylation of $[(RS)_8PcMg]$ is attempted directly in one step, a by-product is formed that causes concomitant decomposition of the chromophore, hence the need for a two-step approach. The generated benzimidazolium groups are readily cleaved by KOH (aq) at 0°C

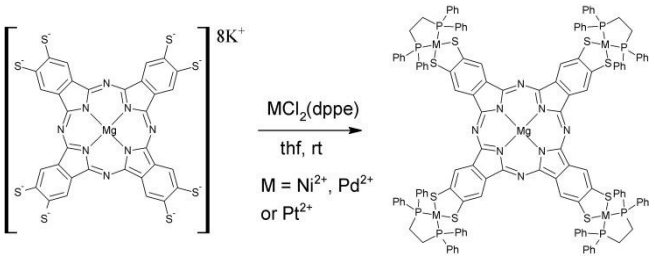

Scheme 2. Synthesis of group 10 metal-capped complexes $[(dppeM)_4(S_8PcMg)]$.

to yield the purple octathiolato Pc complex, $K_8[S_8PcMg]$. Alternatively, this complex can be formed using a milder base, such as K_2CO_3 (aq), at elevated temperatures. $K_8[S_8PcMg]$ is extremely air sensitive, and precipitates from aqueous solution as an insoluble blue-green material when exposed to air. When a THF solution of Me_3SnCl is added to an aqueous solution of $K_8[S_8PcMg]$ in the presence of K_2CO_3, the Sn-capped complex $[(Me_3Sn)_8(S_8PcMg)]$ forms immediately (Scheme 1). This complex

View Article Online
DOI: 10.1039/C8DT03681K

is soluble in common non-polar organic solvents, such as $CHCl_3$. It is a moderately air stable complex, decomposing within days to an unidentified insoluble green compound. Treatment of freshly synthesised $K_8[S_8PcMg]$ with an excess of either Ni-, Pd-, or $[PtCl_2(dppe)]$, gave the tetradiphosphinometal-capped complexes, $[(dppeNi)_4\text{-}(S_8PcMg)]$, $[(dppePd)_4(S_8PcMg)]$, and $[(dppePt)_4(S_8PcMg)]$ (Scheme 2). It is important though that $K_8[S_8PcMg]$ is added to the dichlorido metal complex, and not *vice versa*, to ensure that the latter is always in excess, or else precipitation of an unknown blue-green solid occurs, which we postulate to be a coordination polymer. The complexes are air-stable in DMSO solutions for days and show no aerobic decomposition in the solid state after several months. They show limited solubility in polar organic solvents, such as DMF and DMSO, as well as in a few non-polar solvents, such as DCM. Because of their insolubility in many common solvents, it is possible to remove excess of $[MCl_2(dppe)]$ or other impurities by washing, and then to extract the product into DCM. Filtration of the extract removes polar impurities to give the pure product as a dark purple (Ni) or dark brown (Pd and Pt) solids.

For comparison, smaller heteroleptic complexes of 4,5-dithiolatophthalonitrile ($dtpn^{-2}$) and $[MCl_2(dppe)]$ were prepared. H_2dtpn was synthesised *via* a similar method to that described for the synthesis of $K_8[S_8PcMg]$; namely, the 4,5-(benzimidazole-2-thiol)-phthalonitrile was quaternerised using methyl iodide by heating in DMF. Unlike for $[(RS)_8PcMg]$, both methylations can be performed in a single step by heating the starting dinitrile in a MeI/DMF solution. The benzimidazolium groups were then readily cleaved by KOH in a DMF/H_2O solution. Neutralization of the solution with HCl (aq)

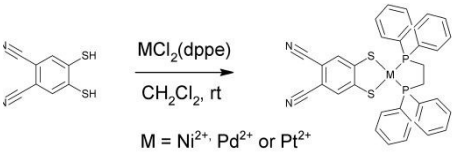

Scheme 3 Synthesis of heteroleptic dithiocatecholato complexes of group 10 metals for comparison.

precipitated H_2dtpn. A solution of H_2dtpn and the desired dichloro metal diphosphine in the presence of an organic base, e.g. NEt_3, gave the corresponding heteroleptic complexes, [Ni(dppe)(dtpn)], [Pd(dppe)(dtpn)], and [Pt(dppe)(dtpn)], in good yield. The general synthesis of these complexes is shown in Scheme 3. The complexes are all air-stable solids that have good solubility in common organic solvents.

3.2 ^{31}P NMR Spectroscopy

^{31}P NMR spectra were recorded for the pentanuclear Pc complexes and their mononuclear analogues, as this gives an insight into the M–P and consequently the M–S bonding environment. For the mononuclear [M(dtpn)(dppe)] complexes, a clear trend in the ^{31}P NMR chemical shifts can be seen, with the signal being shifted downfield in the order Pt < Pd < Ni (Table 1). This trend in shifts appears to follow the trend in size and electropositive character of the metals used. However, this trend in ^{31}P shifts is broken for the pentanuclear complexes, with the order of shifts being Ni < Pt < Pd. Furthermore, while the ^{31}P NMR signals are shifted slightly downfield for the Pd- and Pt-capped complexes, the signal for the Ni-capped complex is rather surprisingly shifted by ca. 30 ppm up-field compared to the mononuclear analogue. The reason for this remarkable change in ^{31}P NMR shifts caused when a benzene group is replaced by Pc is at present unclear, and will be the subject of further investigation.

Table 1 ^{31}P NMR chemical shifts (ppm) for the heteroleptic complexes $[(dppeM)_4(S_8PcMg)]$ and [M(dppe)(dtpn)]

Compound	^{31}P δ (ppm)	$^{1}J_{Pt,P}$ (Hz)
[Ni(dppe)(dtpn)]	60.1	-
$[(dppeNi)_4(S_8PcMg)]$	30.2	-
[Pd(dppe)(dtpn)]	53.2	-
$[(dppePd)_4(S_8PcMg)]$	53.3	-
[Pt(dppe)(dtpn)]	44.6	1399
$[(dppePt)_4(S_8PcMg)]$	48.3	1160

3.3 Electronic absorption spectroscopy

All three octa-2-thiobenzimidazole/iumsubsitituted PcMg complexes showed the typical absorption spectra for inner core metallated Pc complexes with eight peripheral thioether groups, with an absorption maximum at *ca.* 700 nm.[25] Absorption spectra for these complexes are shown in the supplementary information. Of greater interest in this study is the effect that metal coordination to $K_8[S_8PcMg]$ has on the complexes' spectra, as this has never before been examined. Sn is known to form covalent bonds to S, and therefore the effect that Sn has on the overall energy of the transition was not expected to be as great as that of the group 10 metals. Additionally, the methyl groups of $SnMe_3$ should not participate strongly in the excited state dynamics. This was indeed the case, as can be seen in the absorption spectrum for $[(Me_3Sn)_8(S_8PcMg)]$ (Figure 3), where the region of absorbance is approximately the same as for $[(^{Me}RS)_8PcMg]$. Of interest, though, is how the spectral profile has been significantly

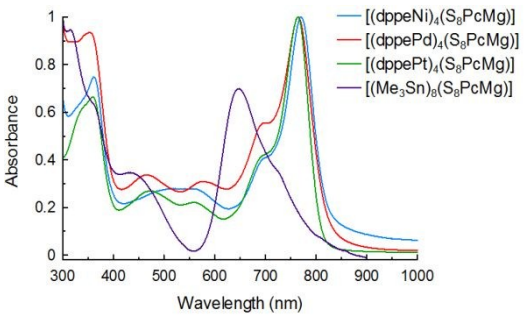

View Article Online
DOI: 10.1039/C8DT03681K

Fig. 3 Normalised absorption spectra for [(dppeM)$_4$(S$_8$PcMg)] (M = Ni, Pd, Pt) and [(Me$_3$Sn)$_8$(S$_8$PcMg)].

altered upon Sn coordination, and that the Q-band absorbance maximum has been both hypsochromically (blue-) shifted by 56 nm to 648 nm and at the same time reduced in strength to below that of the B-band. This unusual profile does somewhat resemble that for an aggregated Pc, but this could be ruled out during the determination of the molar absorption coefficient, where a linear response between concentration and absorbance was observed (see supplement, Figure S2). These changes suggest that the p-orbitals of the thiolates preferentially mix with the Me$_3$Sn groups rather than with the Pc π-system, giving a similar effect to β-alkoxy substitution.[10]

Like Sn, coordination of diphosphino metal ions at the free thiolates of K$_8$[S$_8$PcMg] causes several changes to the absorption spectra compared to [(MeRS)$_8$PcMg], including the appearance of two new broad bands between the B- and Q-bands. However, unlike for the Sn complex, it is the energy of the major features of the absorption spectra that are altered and not so much the profile. Most notably, the Q-band is strongly bathochromically (red-) shifted to 770, 765 and 764 nm for the Ni, Pd and Pt complex, respectively. These values are very similar, and show that the nature of the metal ion has little effect on the HOMO-LUMO energy gap. The magnitude of the red-shift at *ca.* 70 nm is also greater than the observed red-shift of 50 nm seen for octathiolato-porphyrazine complexes coordinated to diphosphino metal fragments prepared earlier.[18f] The normalized absorption spectra for all metal-capped [S$_8$PcMg]$^{8-}$ complexes are shown in Figure 3, and the absorbance maxima and their associated molar attenuation coefficients are given in Table 2.

Table 2. Absorbance wavelength and molar attenuation coefficients measured in DMF.

Complex	Wavelength /nm (ε / dm^3 mol^{-1} cm^{-1})[a],[b]				
[(dppeNi)$_4$(S$_8$ PcMg)]	770 (70000)	700 (28000) (sh)	534 (19000) (br)	362 (51000)	
[(dppePd)$_4$(S$_8$ PcMg)]	765 (71000)	698 (39000) (sh)	580 (22000) (br)	468 (24000) (br)	354 (66000)
[(dppePt)$_4$(S$_8$ PcMg)]	764 (68000)	702 (29000) (sh)	559 (15000) (br)	473 (18000) (br)	360 (45000)

[a] sh denotes a shoulder on a larger peak. [b] br denotes a broad peak.

3.4 Singlet oxygen quantum yields

Although the identity of the coordinated transition metal made little difference on the absorption properties of the complexes, we were interested to see if they would have a different effect on the excited state dynamics. We therefore measured the rate of decay of the singlet oxygen quencher diphenylbenzofuran (DPBF) in the presence of the [(dppeM)$_4$(S$_8$PcMg)] complexes to indirectly determine the population of the T_1 state, and hence the amount of inter-system crossing (ISC), upon photoexcitation.

Figure 4 shows the plot of ln(A_0/A_t) vs. time (s) for [(dppeM)$_4$(S$_8$PcMg)] (M = Ni, Pd, Pt) versus [Zn(py)(Pc)], which was used as the standard. All the metal-phosphine complexes show higher than usual singlet oxygen quantum yields (Φ_Δ) for Mg(Pc) complexes, which are known to be poor sensitizers for singlet oxygen production.[26] [(dppeNi)$_4$(S$_8$PcMg)] shows the lowest activity, which, at Φ_Δ = 0.36, is lower than that of [Zn(Py)(Pc)] (0.56 in DMF[22]). [(dppePd)$_4$(S$_8$PcMg)] and [(dppePt)$_4$(S$_8$PcMg)], however, both show very high activity, with Φ_Δ values of 0.76 and 0.91, respectively.

Typically, [PcMg] and its derivatives have very low Φ_Δ values, which are ascribed to the inability of the Mg^{2+} ion to facilitate ISC through spin-orbit coupling of the S_1 and T_1 manifolds.[27] Additionally, it is known that diamagnetic heavy transition metals coordinated in the Pc cavity facilitate ISC through their d-orbitals. The heavier the metal, the greater the amount of ISC will be. This is often referred to as the heavy atom effect.[28] In the series synthesised here, the only difference between the complexes is the group 10 metal used, and therefore the higher Φ_Δ values can only be attributed to the presence of diamagnetic heavier d^8 M^{2+} ions. These results show that the metals peripherally coordinated through thiolate groups also interact with the Pc π-system to increase ISC. It is therefore possible that they could also be involved in other photophysical and photochemical processes of the Pc ligand.

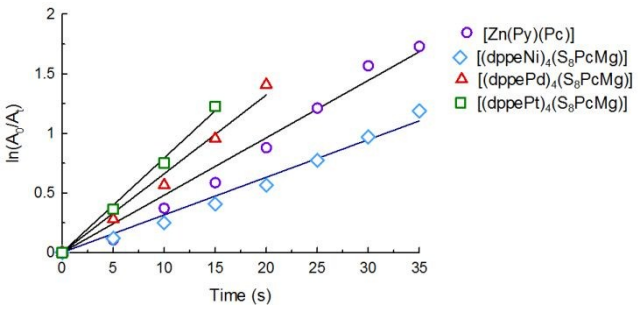

Fig. 4 Plot of ln(A_0/A_t) vs. time (s) for [(dppeNi)$_4$(S$_8$PcMg)], [(dppePd)$_4$(S$_8$PcMg)], [(dppePt)$_4$(S$_8$PcMg)] and [Zn(Py)(Pc)] determined from the decay of DPBF under irradiation by visible light of wavelengths >500 nm.

3.5 MO calculations

TDDFT calculations were performed at the B3LYP/LANL2DZ level of theory on the optimized gas-phase structures for the complexes [(dppeNi)$_4$(S$_8$PcMg)], [(dppePd)$_4$(S$_8$PcMg)] and[(dppePt)$_4$(S$_8$PcMg)] to gain insight into how the coordination of the diphosphinometal ions affects the Pc's electronic properties; in particular, how the energy of the molecular orbitals (MOs) associated with complexes' absorption is altered.

View Article Online
DOI: 10.1039/C8DT03681K

For comparison, a TDDFT calculation at the B3LYP/LANL2DZ level of theory was performed on the gas-phase optimized structure of Mg(octamethylthiophthalocyanine) ([(MeS)$_8$PcMg]). [(MeS)$_8$PcMg] was chosen because it has an identical core structure to the studied complexes, but differs in that the thiol groups are methylated. For the simple complex [(MeS)$_8$PcMg], the calculation results match well with the four-orbital model of Goutermann,[29] where the HOMO is significantly more destabilized than the HOMO-1, and the LUMO and LUMO+1 are degenerate. Here, the transitions HOMO→LUMO/LUMO+1 give rise to the Q-band absorption.

Comparison of the metal-capped complexes to [(MeS)$_8$PcMg] shows that formation of thiocatecholates and coordination of d^8 metal ions causes a destabilization of both the HOMO and the degenerate LUMO/LUMO+1 by 1.7 eV and 1.5 eV for the Ni, 1.7eV and 1.6 eV for the Pd, and 1.7 eV and 1.6 eV for the Pt complexes, respectively. The red-shift of the Q-band in these complexes arises because the HOMO is destabilised more than the LUMO by formation of the dithiolatometal heterocycle, which causes a narrowing of the band gap by about 0.12 eV. Calculations also predict what is observed by UV-Vis spectroscopy; that Ni, Pd, and Pt have almost the same amount of influence on the energy of the Q-band absorption. As expected, the Q-band transitions have mostly π→π* character. However, the LUMO/LUMO+1 are dispersed over both the macrocycle and the dithiocatecholate metal diphosphine moieties [S$_2$MP$_2$], so that there is also a small charge transfer contribution to the

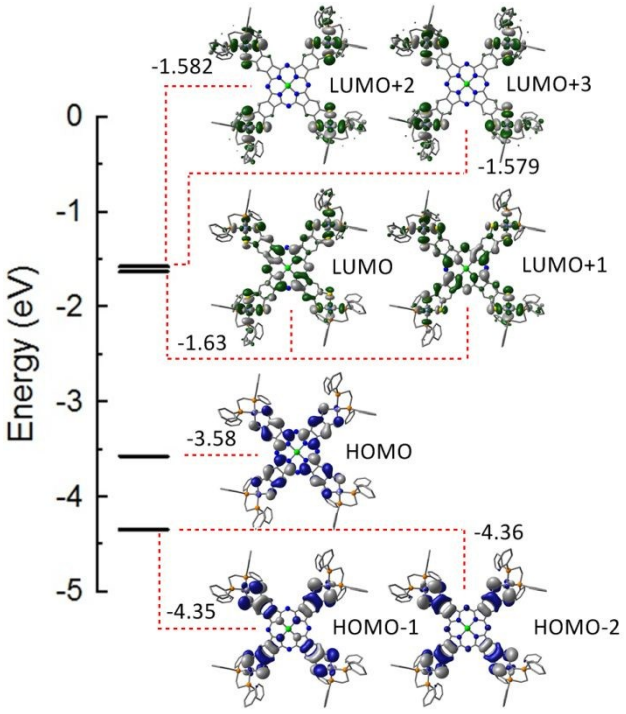

Fig. 5 Contour plots for the HOMO-2 to LUMO+3 for [(dppeNi)}$_4$(S$_8$PcMg)]. The Q-band transition involves MOs with mostly π/π* character, while the higher energy transitions are predominantly charge transfer processes.

Table 3 Calculated energies (eV) and wavelengths (nm) for the HOMO-LUMO transitions and their associated oscillator strengths (f) for the metal-capped and model complex studied.

Complex	Δ(E_{LUMO}-E_{HOMO}) (eV)	λ (nm)	*f*
[(dppeNi)$_4$(S$_8$PcMg)]	1.86	665.8	0.72
[(dppePd)$_4$(S$_8$PcMg)]	1.86	665.4	0.76
[(dppePt)$_4$(S$_8$PcMg)]	1.85	671.6	0.78
[(MeS)$_8$PcMg]	1.98	626.8	0.56

Q-band transitions. Additionally, the higher energy transitions associated with the new bands between 400 and 650 nm are predicted to be largely charge transfer processes between the isoindoline-dithiolate moieties and the peripheral [S$_2$MP$_2$] moieties. This is in keeping with the well-known, good electron donating properties of dithiocatecholato ligand systems. Furthermore, while the HOMO-1/-2 and LUMO+2/+3 are not strictly degenerate MOs, they are separated by only a small predicted energy difference of 0.01 eV and 0.003 eV, respectively. Contour plots for the HOMO-2 to LUMO+3 and for [(dppeNi)$_4$(S$_8$PcMg)] as a representative example are shown in Figure 5. The calculated transition energies (eV and nm) and oscillator strengths (*f*) for all pentanuclear complexes studied are given in Table 3.

4. Conclusions

We have demonstrated that the synthesis and cleavage of S-benzimidazolium groups is a mild, facile and viable option for introducing anionic thiolato and dithiocatecholate groups onto the Pc ligand scaffold and other aromatic systems. The deprotection protocol under weakly basic conditions is compatible with the presence of Lewis acidic transition metal complex fragments, which act as scavengers for thiocatecholate. This offers new perspectives in coupling such chromophores with a variety of transition metals *via* thiocatecholate bridges. Coordination of group 10 metals significantly enhances the Pc ligand's absorption by inducing a strong red-shift of the Q-band to almost 800 nm. Additionally, the absorbance in the entire visible region is increased by the emergence of new broad bands between 400 and 650 nm, so that the metal-capped complexes display truly panchromatic absorbance. Along with this light absorption, the transition metal-capped complexes show a strong increase in their singlet oxygen quantum yields. Φ_Δ values increase in the order Ni > Pd > Pt, indicating that the heavy atom effect is clearly present, and, more importantly, that the peripheral metal ions interact with the Pc ligand's π-system and support ISC. This mixing is further supported by TDDFT calculations of the electronic transitions for the optimised structures of these complexes, which predict that the Q-band transitions have both π→π* and CT character. CT is proposed to

View Article Online
DOI: 10.1039/C8DT03681K

be a result of the strong electron donor properties of the dithiocatecholate metal system. The strong red-shift observed is due to an increased destabilisation of the HOMO compared to the LUMO/LUMO+1 in the title compounds. Finally, the incorporation of an excellent chromophore, *viz.* PcMg, into a heteroleptic tetra-thiocatecholato complex both enhances the optical absorption of the chromophore and combines the strong absorbance of the Pc dye with the redox activity of metal thiocatecholate functionalities, thus opening perspectives for the design of photo-active complexes for energy transfer and photoredox catalysis. Analysis of their photo-redox chemistry will be the focus of further studies.

Conflicts of interest

There are no conflicts to declare.

Acknowledgements

MAB would like to thank the German Academic Exchange Service (DAAD) for a doctoral scholarship.

Notes and references

‡ This paper is dedicated to the occasion of the ninetieth birthday of Prof. Wolfgang Sundermeyer, Heidelberg.

1 a) C. Browning, J. M. Hudson, E. W. Reinheimer, F. -L. Kuo, R.N. McDougald, Jr., H. Rabaâ, H. Pan, J. Bacsa, X. Wang, K. R. Dunbar, N. D. Shepherd and M. A. Omary, *J. Am. Chem. Soc.*, **2014**, *136*, 16185- 16200; b) C. L. Linfoot, P. Richardson, K. L. McCall, J. R. Durrant, A. Morandeira and N. Robertson, *Solar Energy*, **2011**, *85*, 1195-1203.

2 a) L. Gan, T. L. Groy, P. Tarakeshwar, S. K. S. Mazinani, J. Shearer, V. Mujica, A. K. Jones, *J. Am. Chem. Soc.*, **2015**, *137*, 1109-1115; b) K. E. Rosenkoetter, J. W. Ziller, A. F. Heyduk, *Inorg. Chem.*, **2016**, *55*, 6794- 6798; (c) P. Du and R. Eisenberg, *Energy Environ. Sci.*, **2012**, *5*, 6012.

3 a) J. M. Bevilacqua, J. A. Zuleteandand R. Eisenberg, *Inorg. Chem.*, **1994**, *33*, 258-266; b) R. Benedix, D. Pitsch, K. Schone and H. Hennig, *Z. anorg. allg. Chem.*, **1986**, *542*, 102-116; c) R. L. Cowan, D. B. Pourreau, A. L. Rheingold, S. J. Geiband W. C. Trogler, *Inorg. Chem.,* **1987**, *26*, 259-265; d) L. Gan, T. L. Groy, P. Tarakeshwar, S. K. S. Mazinani, J. Shearer, V. Mujica, and A. K. Jones, *J. Am. Chem. Soc.*, **2015**, *137*, 1109-1115.

4 S. D. Cummings and R. Eisenberg, *J. Am. Chem. Soc.*, **1996**, *118*, 1949- 1960.

5 D. Espa, L. Pilia, L. Marchiò, F. Artizzu, A. Serpe, M. L. Mercuri, D. Simão, M. Almeida, M. Pizzotti, F. Tessore and P. Deplano, *Dalton Trans.,* **2012**, *41*, 3485.

6 B. Zheng, R. P. Sabatini, W. -F. Fu, M. S. Eum, W. W. Brennessel, L. Wang, D. W. McCamantand R. Eisenberg, *PNAS*, **2015**, E3987-E3996.

7 D. Wöhrle, G. Schnurpfeil, S. Makarovand O. Suvora, *Chem. Unserer Zeit*, **2012**, *46*, 12-24.

8 a) L. Martin-Gomis, F. Fernández-Lázaro and A. Sastre-Santos, *J. Mater. Chem. A.*, **2014**, *2*, 15672-15682; b) X. Zhang, T. Peng and S. Song, *J. Mater. Chem. A*, **2016**, *4*, 2365-2402.

9 C. K. C. Bikram, N. K. Subbaiyan and F. D'Souza, *J. Phys. Chem. C*, **2012**, *116*, 11964-11972.

10 T. Kawata, Y. Chino, N. Kobayashi and M. Kimura, *Langmuir,* **2018**, *34*, 7294-7300.

11 X. -F. Chen, M. E. El-Khouly, K. Ohkubo, S. Fukuzumi and D. K. P. Ng, *Chem. Eur. J.,* **2018**, *24*, 3862-3872.

12 J. Fernandez-Ariza, M. Urbani, M. S. Rodriguez-Morgade and T. Torres, *Chem. Eur. J.*, **2018**, *24*, 2618-2625.

13 J. Demuth, R. Kucera, K. Kopecky, Z. Havlinova, A. Libra, V. Novakova, M. Miletin and P. Zimčík, *Chem. Eur. J.*, **2018**, *24*. 9658-9666.

14 E. A. Ermilov, J. -Y. Liu, R. Menting, Y. -S. Huang, B. Röding and D. K. P. Ng, *Phys. Chem. Chem. Phys.*, **2016**, *18,* 10964-10975.

15 N. Kobayashi, H. Ogata, N. Nonaka, and E.A. Luk'yanets, *Chem, Eur. J.*, **2003**, *9*, 5123-5134.

16 T. Furuyama, K. Satoh, T. Kushiya, and N. Kobayashi, *J. Am. Chem. Soc.,* **2014**, *136*, 765-776.

17 a) T. Kimura, A. Yomogita, T. Matsutani, T. Suzuki, I. Tanaka, Y. Kawai, Y. Takaguchi, T. Wakahara, and T. Akasaka, *J. Org. Chem.*, **2004**, *69*, 4716-473.

18 a) C. S. Velázquez, W. E**.** Broderick, M. Sabat, A. G. M. Barrett, and B. M. Hoffman, *J. Am. Chem. Soc.*, **1990**, *112*, 7408-7410; b) T. F. Baumann, J. W. Sibert, M. M. Olmstead, A. G. M. Barrett, and B. M. Hoffman, *J. Am. Chem. Soc.,* **1994**, *116*, 2639-2640; c) S. L. J. Michel, D. P. Goldberg, C. Stern, A. G. M. Barrett and B. M. Hoffman, *J. Am. Chem. Soc.*, **2001**, *123*, 4741-4748; d) T. F. Baumann, M. S. Nasir, J. W. Sibert, A. J. P. White, M. M. Olmstead, D. J. Williams, A. G. M. Barrett and B. M. Hoffman, *J. Am. Chem. Soc.,* **1996**, *118*, 10479-10486; e) J. W. Sibert, T. F. Baumann, D. J. Williams, A. J. P. White, A. G. M. Barrett and B. M. Hoffman, , *J. Am. Chem. Soc.,* **1996**,*118*, 10487-10493; f) C. S. Velazquez, T. F. Baumann, M. M. Olmstead, H. Hope, A. G. M. Barrett and B. M. Hoffman, *J. Am. Chem. Soc.*, **1993**, *115*, 9997-10003.

19 a) J. M. Tour, L. Jones II, D. L. Pearson, J. J. S. Lamba, T. P. Burgin, G. M. Whitesides, D. L. Allara, A. N. Parikh and S. V. Atre, *J. Am. Chem. Soc.*, **1995**, *117*, 9529-9534; b) L. Cai, Y. Yao, J. Yang, D. W. Price, Jr., and J. M. Tour, *Chem. Mater.*, **2002**, *14*, 2905-2909.

20 D. Wöhrle, M. Eskes, K. Shigehara and A. Yamada, *Synthesis*, **1992**, 194-196.

21 T. S. Zhivotova, A. M. Gazaliev, S. D. Fazylov, Z. K. Aitpaeva and D. M. Turdybekov, *Russ. J. Org. Chem.,* **2006**, *42*, 448-450.

22 D. Çakir, M. Göksel, V. Çakir, M. Durmuş, Z. Biyikhoğlu and H. Kantekin, *Dalton Trans.*, **2015**, *44*, 9646-9658.

23 W. Spiller, H. Kliesch, D. Wohrle, S. Hackbarth, B. Roder and G. Schnurpfeil, *J. Porph. Phthalo.*, **1998**, *2*, 145-158.

24 Gaussian 09, Revision C.01, M. J. Frisch, G. W. Trucks, H. B. Schlegel, G. E. Scuseria, M. A. Robb, J. R. Cheeseman, G. Scalmani, V. Barone, B. Mennucci, G. A. Petersson, H. Nakatsuji, M. Caricato, X. Li, H. P. Hratchian, A. F. Izmaylov, J. Bloino, G. Zheng, J. L. Sonnenberg, M. Hada, M. Ehara, K. Toyota, R. Fukuda, J. Hasegawa, M. Ishida, T. Nakajima, Y. Honda, O. Kitao, H. Nakai, T. Vreven, J. A. Montgomery, Jr., J. E. Peralta, F. Ogliaro, M. Bearpark, J. J. Heyd, E. Brothers, K. N. Kudin, V. N. Staroverov, T. Keith, R. Kobayashi, J. Normand, K. Raghavachari, A. Rendell, J. C. Burant, S. S. Iyengar, J. Tomasi, M. Cossi, N. Rega, J. M. Millam, M. Klene, J. E. Knox, J. B. Cross, V. Bakken, C. Adamo, J. Jaramillo, R. Gomperts, R. E. Stratmann, O. Yazyev, A. J. Austin, R. Cammi, C. Pomelli, J. W. Ochterski, R. L. Martin, K. Morokuma, V. G. Zakrzewski, G. A. Voth, P. Salvador, J. J. Dannenberg, S. Dapprich, A. D. Daniels,

View Article Online
DOI: 10.1039/C8DT03681K

O. Farkas, J. B. Foresman, J. V. Ortiz, J. Cioslowski and D. J. Fox, Gaussian, Inc., Wallingford CT, **2010**.
25 N. Kobayashi, H. Ogata, N. Nonaka and E.A. Luk'yanets, *Chem. Eur. J.*, **2003**, *9*, 5123-5134.
26 M. Kostka, P. Zimcik, M. Miletin, P. Klemera, K. Kopecky and Z. Musil, *J. Photochem. Photobio. A: Chem.*, **2006**, *178*, 16-25.
27 M. Kostka, P. Zimcik, M. Miletin, P. Klemera, K. Kopecky and Z. Musil, *J. Photochem. and Photobio. A: Chem.,* **2006**, *178*, 16-25.
28 P. S. Vincett, E. M. Voigt and K. E. Rieckhoff, *J. Chem. Phys.*, **1971**, *55*, 4131-4140.
29 C. Weiss, H. Kobayashi and M. Gouterman, *J. Mol. Spec.*, **1965**, *16*, 415- 450.

View Article Online
DOI: 10.1039/C8DT03681K

Graphical Abstract

Four thiocatecholate groups at a magnesium phthalocyanine can coordinate transition metals, strongly red-shifting the Q band and promoting charge-transfer to peripheral groups.

.

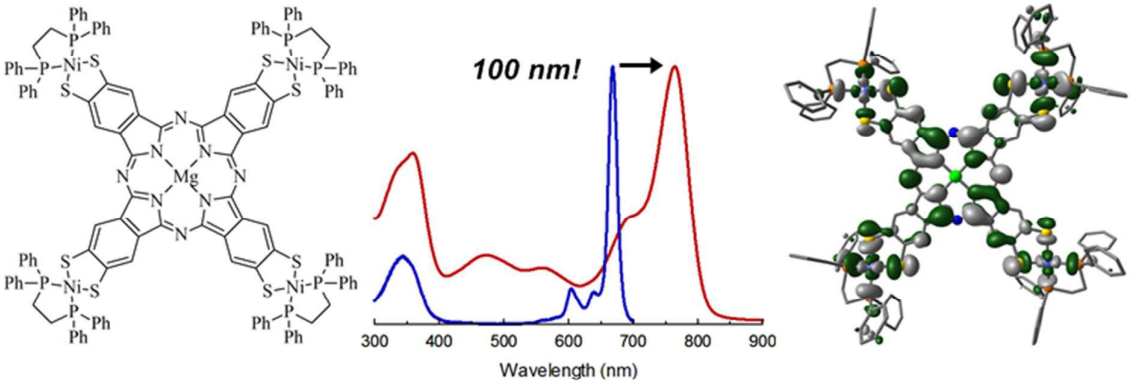

6.2 Peripheral Metallation of Phthalocyanine – Inducing New Effects in an Old Chromophore

Malcolm A. Bartlett and Jörg Sundermeyer

Peripheral Metallation of Phthalocyanine – Inducing New Effects in an Old Chromophore

Submitted as communication to *Dalton Transactions*

Journal Name

COMMUNICATION

Peripheral Metallation of Phthalocyanine – Inducing New Effects in an Old Chromophore

Received 00th January 20xx,
Accepted 00th January 20xx

DOI: 10.1039/x0xx00000x

www.rsc.org/

Malcolm Alan Bartlett[a] and Jörg Sundermeyer*[a]

A single thiocatecholate group has been combined with a phthalocyanine and used to coordinate a $[Ni(dppe)]^{2+}$ fragment to give the unprecedented title complex $[(dppe)Ni(S_2PcH_2)]$. UV-Vis spectroscopy shows new strong transitions near the Q-band, which TDDFT calcualtions predict result from internal charge transfer processes. Insights are gained with respect to designing future photocatalytic systems.

Electron rich redox-active thiocatecholate ligands in both homoletpic and heteroleptic complexes have been extensively studied because of their ability to alter the reactivity of the metal center to which they are coordinated[1,2]. They have the effect of stabilizing various metal oxidation states, and promoting redox reactions[3] and ligand-to-ligand charge transfer (LLCT) processes[4]. Moreover, the ubiquitous nature of dithiolate ligands in nature has also prompted the use of thiocatecholate groups in the biomimetic studies of the active sites of hydrogenase[5], oxidase and reductase[6] enzymes.

The electron transfer process can also be photo-driven by coupling a chromophore to the thiocatecholate ligand. Most of these systems, however, use multi-component approaches, often incorporating either inorganic semiconductors, such as CdS, ZnS or TiO_2[8], or metal-organic dyes, such as Ru(III)tris-bpy derivatives[9]. Consequently, there are very few examples of thiocatecholate[9b] or dithiolate[9c] ligands incorporated directly into the chromophore. Donor substituted phthalocyanines (Pc), as excellent light absorbing organic dyes with electron donating character[10], are an obvious choice to combine and conjugate with a thiocatecholate group to promote photo-driven electron donation from a single ligand. We previously described a method[11] of generating thiocatecholate groups on Pc complexes that is significantly milder than established methods involving cleavage of benzylthioester groups under Birch-type conditions[12]. In this communication, we describe for the first time the synthesis of an A_3B-type Pc complex with only a single thiocatecholate group, which allows for the inclusion of other functional groups on the so far non-metallated Pc ligand. The effect on the optical properties is investigated by means of spectroscopy and theory with respect to its potential use in photo-redox chemistry.

We previously showed how dinitrile **3** could be cyclised using $Mg(OEt)_2$ in a high boiling alcoholic solvent to obtain the corresponding symmetric (A_4) tetra-thiocatecholate $K_8[S_8PcMg]$ derivative. However, under these conditions the alcohol also reacts with the 2-thio-benzimidazolium groups to replace the S-benzimidazolyl by S-alkyl groups of the alcohol as a side reaction. For synthesis of the symmetrical A_4-type system, this is acceptable, as the alkyl-substituted by-products can be easily removed by washing with a non-polar solvent owing to their increased solubility. This method is however not suitable for co-cyclisation of different phthalonitrile synthons, as, in addition to the six expected products, a significant number of S-alkylated side-products are formed as well. This greatly complicates the separation and drastically lowers the yield of the desired A_3B-type complex. The solubility of dinitrile **3** is too low in the high-boiling non-alcoholic solvents typically employed for Pc synthesis. Hence, **3** was N-butylated to give the more soluble derivative **4** (Scheme 1).

To obtain the asymmetric phthalocyanine, dinitrile **4** was co-cyclised with 1,3-diiminoisoindoline in a 1:4 molar ratio at 180 °C for six hours. The product mixture was separated from any decomposition products by filtration through silica using EtOAc before being directly heated with MeI in DMF to N-methylate both benzimidazole functionalities to benzimidazolium leaving groups. The quaternerized mixture of compounds was deprotected using a degassed solution of NaOH (aq), to give a blue-colored solution. The deprotected sodium salt of thiocatecholato-Pc is extremely air sensitive, and was therefore reacted directly with $[NiCl_2(dppe)]$. From the solid residue of this reaction, the A_3B isomer is readily extracted using $CHCl_3$. Final purification is accomplished by preparative

[a] *Fachbereich Chemie, Philipps-Universität Marburg, Hans-Meerwein Str. 4, Marburg 35032, Germany.*
† Prof. Dr. Jörg Sundermeyer. E-mail: jsu@chemie.uni-marburg.de
Electronic Supplementary Information (ESI) available: experimental procedures, copies of NMR, FTIR, UV-Vis and mass spectra and additional computational details. See DOI: 10.1039/x0xx00000x

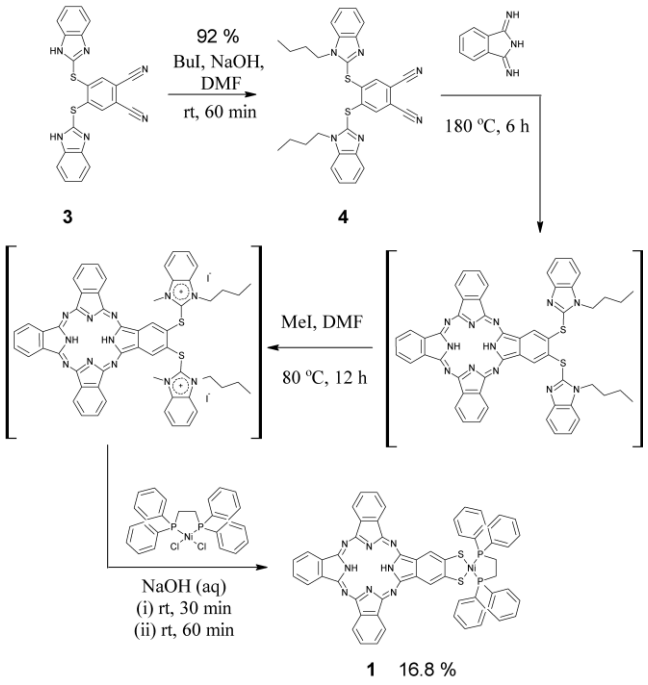

Scheme 1. Synthesis of asymmetric H_2Pc-derivative, its quaternerization, deprotection and coordination to $[NiCl_2(dppe)]$ to form $[(dppe)Ni(S_2PcH_2)]$.

TLC (DCM/EtOH; 10:1), collecting the product as the dark blue-green band. Isolation of the A_3B isomer is thus greatly simplified compared to the initially formed purely organic product mixture, which is why it is beneficial to work with a mixture until the final product has been synthesised. The complete synthetic pathway is shown in Scheme 1.

The unique title compound **1** could be isolated in an overall yield of 16.8 %, which is very impressive for this chemistry, and its purity could be confirmed by ^{1}H, ^{13}C and ^{31}P NMR spectroscopy, as well as MALDI-TOF MS. In addition to the Ni complex **1**, a purely organic A_3B-type Pc with two *tert*-butyl thiol groups at β-positions, $(t\text{BuS})_2PcH_2$ (**2**), was synthesised for comparison (Fig. 1). This compound was obtained by melting one equivalent of 4,5-di(*tert*-butylthiol)-phthalonitrile with four equivalents of 1,3-diiminoisonidoline to obtain almost exclusively the A_3B product. Details of this compound's synthesis, purification and characterization can be found in the supplementary information.

1,2-Bis(diphenylphosphino)ethane (dppe) was chosen as neutral ligand for **1**, because it is a weak electron acceptor for LLCT processes compared to N-containing heterocycles, such as 2,2'-bipyridine (bpy), which are often used to promote LLCT processes[13]. By using a relatively redox inert ligand, we hoped to minimize any potential LLCT and observe only the effect that thiocatecholate formation and metal coordination has on the Pc ligand's optical and electronic properties. Therefore, better electron acceptor ligands at the peripheral metal, such as bpy, will be explored in future work with this ligand.

The absorption spectrum for **1** shows strong absorption bands in both the ultraviolet (300-400 nm) and the visible (Q-band) regions. Typically, the strength of the absorption between 300 and 400 nm is less than that of the absorptions in

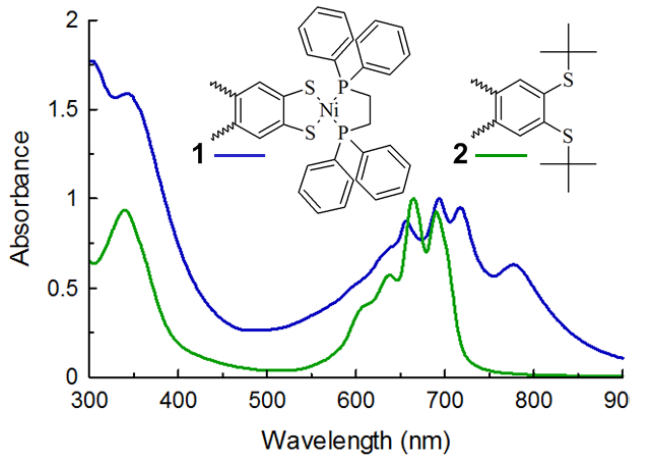

Fig. 1. The normalized UV-Vis-NIR absorption spectra for the organic A3B Pc $(t\text{BuS})_2PcH_2$ (green) and the mononuclear complex $[(dppe)Ni(S_2PcH_2)]$ (blue).

the Q-band region. The strong absorption seen in the UV region for **1** compared to **2** is possibly due to the combination of the allowed π→π* transitions of the four phenyl rings of the dppe ligand, the typical B-band absorption of the Pc ligand and metal-to-ligand (MLCT) Ni→P transitions seen in similar complexes[14]. The absorption of the Q-band region of **1** is also significantly altered compared to **2**. The Q-band of **1** is broadened by more than 100 nm and is split into four major peaks with maxima at 656, 693, 718 and 777 nm. The two major Q-band maxima for **2** are located at 664 and 690 nm, similar to other A_3B-type Pc compounds.[15] Figure **1** shows the UV-Vis-NIR absorption spectra for both **1** and **2**. The large differences between the profiles of the Q-band transitions for **1** and **2** show that thiocatecholate formation and metal coordination does not simply change the energy of these transitions, although the Q-band is mostly bathochromically (red) shifted for **1** compared to **2**. Rather, the new bands indicate that the distribution of electron density on the Pc ligand has been affected. That is, electron density is most likely localized over certain regions of the macrocycle instead of being evenly distributed over the entire HOMO.

Time-dependent (TD)-DFT calculations were performed on the DFT optimized structure of **1** to ascertain whether or not the coordinated [Ni(dppe)] fragment is directly or indirectly involved in the electronic transitions of the Q-band. That is, if these transitions involve orbitals located over both the Pc ligand and Ni and/or the dppe ligand, or if coordination of [Ni(dppe)] only has an inductive electronic effect on the electronic density on the Pc ligand. DFT and TD-DFT calculations of **2** were also performed for comparison.

Table 1. Q-band absorption maxima for the Ni-dppe complex **1** and the comparable, purely organic compound $(t\text{BuS})_2PcH_2$.

Compound	Wavelength (nm)			
$[(dppe)Ni(S_2PcH_2]$	777 (s)	718 (s)	693 (s)	656 (s)
$(t\text{BuS})_2PcH_2$	690 (s)	664 (s)	638 (s)	607 (sh)

[a] (s) denotes a sharp peak. [b] (sh) denotes a shoulder.

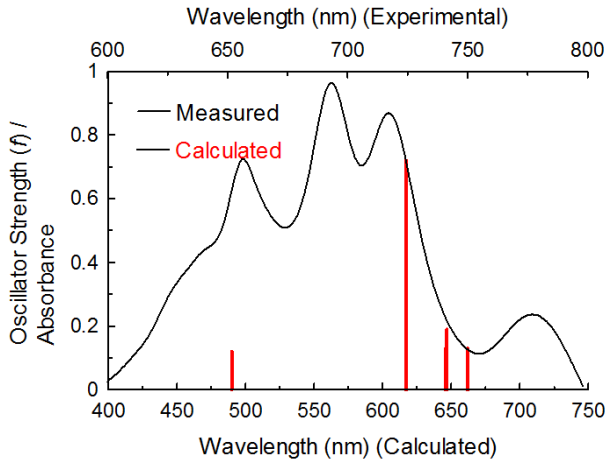

Fig. 2 Overlay of measured electronic absorption spectrum (black) and calculated transitions (red bars) for complex **1**.

Evaluation of the calculated and the experimentally obtained absorption spectrum of **1** shows that there is a reasonably good agreement between the observed and predicted absorption profiles, with there being four major transitions present in both. Theory does, however, overestimate the broadness of the Q-band region as well as the energies of the various transitions. An overlap of the observed and calculated electronic transitions is shown in Figure **2**. Analysis of the orbital contributions for the Q-band transitions of **1** (Table **2**) shows that they involve the HOMO, HOMO-1, HOMO-2, LUMO and LUMO+1 MOs. From the contour plots for these MOs (Figure **3**), it is clear that thiocatecholate formation and [Ni(dppe)] coordination have little influence on the energy of the unoccupied MOs, which are more strongly associated with

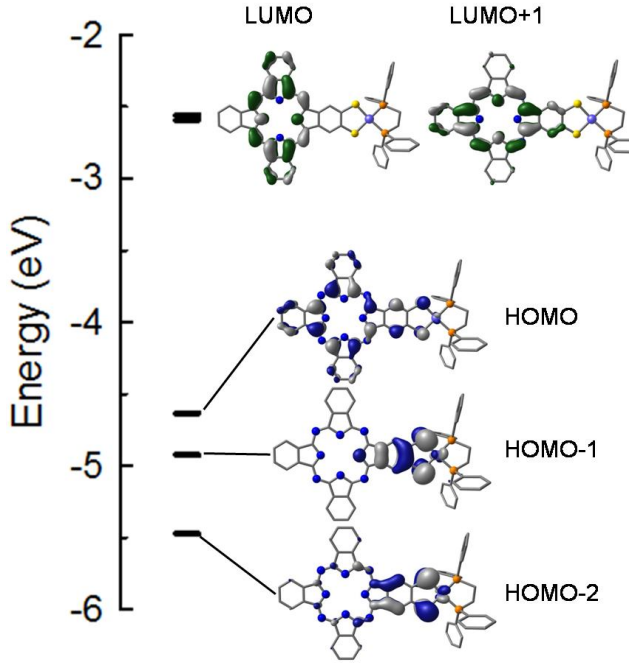

Fig. 3 Calculated energy levels of Q-band MOs and their contour plots. Contour plots are coloured blue and green for occupied and unoccupied MOs, respectively. Calculations were performed at the B3LYP/6-31G(d,p) level of theory.

the inner porphyrazine ring rather than the benzene rings. Instead, it is the occupied orbitals that are destabilized by the addition of the [S_2Ni(dppe)] moiety. In particular, the HOMO-1 and HOMO-2 are located almost exclusively over the dithiolato-isoindoline moiety, with a significant amount of electron density on the sulfur atoms. Small portions of the HOMO-1/HOMO-2 MOs are also located on the Ni^{2+} ion.

From these results, it is clear that the [Ni(dppe)] fragment does not participate in the electronic Q-band transitions of **1**. Q-band transitions instead originate from MOs located only on the Pc ligand. Thus, the Q-band absorptions involve not only the expected π→π* transitions, but also have an intramolecular charge transfer component from the dithiolate-metal heterocycle moiety to the inner porphyrazine core. This is probably due to the previously described strong donor properties of dithiolate-metal systems. Here, where a typical electron accepting group is absent, donation is even seen to the electron-rich Pc ligand, although it is itself considered to be an electron donor ligand. These results also confirm the above interpretation of the experimentally observed absorption spectrum that the electron density is unevenly distributed over the Pc ligand.

Table 2. Calculated Q-band transitions and oscillator strengths with orbital contributions for **1** and $(MeS)_2PcH_2$.

Transition	ΔE (eV)	f	Composition (%)
[(dppe)Ni(S_2PcH_2)]			
661.72	1.87	0.13	H→L (58), H-1→L+1 (37)
646.77	1.917	0.19	H-1→L (54), H→L+1 (43)
645.91	1.920	0.13	H-1→L+1 (60), H→L (35)
617.13	2.00	0.72	H-1→L (40), H→L+1 (49)
490.15	2.53	0.12	H-2→L (93)
$(MeS)_2PcH_2$			
615.32	2.02	0.45	H→L (40), H→L+1 (51)
600.82	2.06	0.41	H→L (53), H→L+1 (41)

Conclusions

For the first time, we have demonstrated a synthesis combining the excellent Pc chromophore with a single thiocatecholate group, and its use in the synthesis of a heteroleptic Ni(II) complex. The yield of greater than 16 % makes this approach a valuable entry into yet unexplored heteronuclear phthalocyanine chemistry. Additionally, the same co-cyclisation method can also be used to synthesise the corresponding purely organic A_3B-type $(RS)_2PcH_2$ with good selectivity. Formation of thiocatecholate groups and coordination of $[Ni(dppe)]^{2+}$ has the effect of significantly broadening the region of the Q-band transitions by more than 100 nm. TD-DFT calculations show that electron density in the HOMO-1 and HOMO-2 is highly localised to the metal-dithiolato-isoindoline moiety, which causes the extensive broadening of the Q-band as well as the general red-shift observed for this region. Thus, in comparison to the A_3B-type compound $(t\text{BuS})_2PcH_2$, **2**, the region of visible light absorption is increased by thiocatecholate formation and metal

coordination. Furthermore, the intramolecular charge transfer from the thiocatecholate to the inner porphyrazine ring of the macrocycle shows that the thiocatecholate-metal units are still effective electron donor substituents when incorporated into a Pc ligand scaffold. These results further support the vision of using $[H_2PcS_2]^{2-}$ as a photoactive donor ligand for photo-redox chemistry.

Conflicts of interest

There are no conflicts to declare.

Notes and references

‡Footnotes relating to the main text should appear here. These might include comments relevant to but not central to the matter under discussion, limited experimental and spectral data, and crystallographic data.

§

§§

etc.

1 D.L.J. Broere, R. Plessius, and J. I. van der Vlugt, *Chem. Soc. Rev*., 2015, **44**, 6886-6915.

2 [2] H. Fei and S.M. Cohen, *J. Am. Chem. Soc.*, 2015, **137**, 2191-2194.

3 [3] S. Pullen, H. Fei, A. Orthaber, S.M. Cohen and S. Ott, *J. Am. Chem. Soc.*,2013, **135**, 16997-17003.

4 [4] S.D. Cummings, R. Eisenberg, *J. Am. Chem. Soc.*,1996, **118**, 1949-1960.

5 [5] M. Wang, L. Chen, X. Li and L. Sun, *Dalton Trans.*, 2011, **40**, 12793-12800.

6 A.M. Appel, J. E. Bercaw, A. B. Bocarsly, H. Dobbek, D. L. DuBois, M. Dupuis, J. G. Ferry, E. Fujita, R. Hille, P. J. A. Kenis, C. A. Kerfeld, R. H. Morris, C. H. F. Pedent, A. R. Portis, S. W. Ragsdale, T. B. Rauchfuss, J. Reek, L. C. Seefeldt, R. K. Thauer, and G. L. Waldrop, *Chem. Rev.*, 2013, **113**, 6621-6658.

7 P. Du and R. Eisenberg, *EnergyEnviron. Sci.*, 2012, **5**, 6012-6021.

8 [8] F. Wen and C. Li, *Accounts of Chemical Research*, 2013, **46**, 2355-2364.

9 [9] Y. Na, M. Wang, J. Pan, P. Zhang, B. Akermark andL. Sun, *Inorg. Chem.*, 2008, **47**, 2805-2810.

10 [9b] B. Zheng, R. P. Sabatini, W.-F. Fu, M. S. Eum, W. W. Brennessel, L. Wang, D. W. McCamantand R. Eisenberg, *PNAS*, 2015, E3987-E3996.

11 [9c] L.-C. Song, L.-X. Wang, M.-Y. Tang, C.-G. Li, and Q.-M. Hu, *Organometallics*, 2009, **28**, 3834–3841.

12 [10] D. Wöhrle, G. Schnurpfeil, S. Makarovand O. Suvorova, *Chemie unser Zeit*, 2012, **46**, 12-24

13 [11] Our publication for A4 system.

14 [12] C.S. Velazquez, T.F. Baumann, M.M. Olmstead, H. Hope, A.G.M. Barrett and B.M. Hoffman, *J. Am. Chem. Soc.*, 1993, **115**, 9997-10003; T. Kimura, A. Yomogita, T. Matsutani, T. Suzuki, I. Tanaka, Y. Kawai, Y. Takaguchi, T. WakaharaandT. Akasaka, *J. Org. Chem*., 2004, **69**, 4716-4723 (as representative examples)

15 [13] W. W. Kramer, L. A. Cameron, R. A. Zarkesh, J. W. Ziller, and A. F. Heyduk, *Inorg. Chem.*, 2014, **53**, 8825-8837

16 [14] V. Koç, S.Z. Topal, D.A. Tekdaş, Ö.D. Ateş, E. Önal, F. Dumoulin, A.G. Gürek, and V. Ahsen, *New J. Chem.*, 2017, **41**, 10027-10036.

17 [15] a) G.A. Bowmaker, P.D. Boyd, G.K. Campbell, *Inorg. Chem.*, 9182, **21**, 2403-2412; b) C.S. Velázquez, T.F. Baumann, M.M. Olmstead, H. Hope, A.G.M. Barrett, and B.M. Hoffman, *J. Am. Chem. Soc*., 1993, **115**, 9997-10003.

Supplementary Information to

Peripheral Metallation of Phthalocyanine: Inducing New Effects in an Old Chromphore

Authors

Malcolm Alan Bartlett and Jörg Sundermeyer

Contents: **Page**

S1. General Comments 1

S2. Syntheses 2

S1. General Comments

Methods and Materials

^{1}H and ^{13}C NMR spectra were obtained on a Brüker AVANCE 300 spectrometer. Chemical shifts are reported in δ (ppm) values. ^{1}H and ^{13}C NMR values were referenced to residual solvent as an internal standard, while ^{31}P NMR values were referenced to_____. The following abbreviations were used: s = singlet, d = doublet, t = triplet, q = quartet, m = multiplet and br = broad singlet. Mass spectra (MS) were recorded on either a Thermo Fischer Scientific LTQ-FT Ultra or on a Bruker Biflex III-Spectrometer. UV-Vis spectra were recorded on a Varian Eclipse. FTIR spectra were measured using a Bruker Alpha Platinum ATR single reflection diamond spectrometer. Quantum chemical calculations were performed using the MaRC2 computing cluster.

The following chemicals were used as received from their respective suppliers. 1,3-diiminoisoindoline and 1-iodomethane were purchased from Acros Organics. 4,5-dichlorophthalic acid and 2-Methyl-2-propanethiol was purchased from Sigma Aldrich. Carbon disulfide, 1,2-diamino-*ortho*-benzene and 1-iodobutane were purchased from Merck, dppe was purchased from Fluka and nickel dichloride hexahydrate was purchased from VWR Chemicals. Preparative silica TLC plates were purchased from Merck. 4,5-Dichlorophthalonitrile[S1], 4,5-bis(*tert*-butylsulfanyl)benzene-1,2-dicarbonitrile[S2] and 2-thione-benzimidazole[S3] were synthesised according to literature procedures.

Theoretical Calculations

Geometries of **1** and **2** were first optimized in the gas phase at the B3LYP/6-31G(d,p) level of theory. Frequency calculations were then performed on the optimized structures at the same level of theory; no negative eigenvalues were obtained. TD-DFT calculations were also performed at the B3LYP/6-31G(d,p) level of theory solving for 20 states. All calculations were performed using the Gaussian09 suite of software[S4].

S2. Syntheses

*Synthesis of 4,5-bis(1H-benzimidazol-2-ylsulfanyl)benzene-1,2-dicarbo-nitrile (dbtpn) (**3**)*: 4,5-dichlorophthalonitrile (0.500 g; 2.54 mmol), 1,3-dihydro-2H-benzimidazole-2-thione (0.762 g; 5.07 mmol) and K_2CO_3(1.50 g; 10.85mmol) were mixed together and dissolved in DMF (10 ml). The solution was then warmed to 80 ºC for 3 h; reaction progress was monitored by TLC. H_2O was then added, and the precipitate that formed was collected by filtration, washed with H_2O and dried *in vacuo* (10^{-3} mbar). Mass: 0.960 g. Yield: 89 %. ^{1}H NMR (DMSO-*d6*; 300 MHz, 298 K): δ (ppm) 7.21-7.26 (m, 4H, benz); 7.54-7.59 (m, 4H, benz); 8.19 (s, 2H, phthalonitrile).^{13}C NMR(DMSO-*d6*; 75 MHz; 298 K): δ (ppm) 143.11; 149.54; 135.66; 122.60; 115.22; 113.91.

*Synthesis of 4,5-bis(1-butyl-benzimidazol-2-ylsulfanyl)benzene-1,2-dicarbonitrile (dBubtpn) (**4**)*: Dbtpn (0.900 g; 2.12 mmol) was dissolved in DMF (3 ml). NaOH(0.15 g) was crushed and added to this solution with stirring. After 5 minutes, 1-iodobutane (1.0 ml; 8.8 mmol) was added, and stirring was continued for 1 h. H_2O (50 ml) was then added, causing a very fine precipitate to form. The suspension was then extracted into DCM (3 x 50 ml). The organic portions were combined, dried ($MgSO_4$) and filtered. Volatiles were then evaporated to leave an oil, which was washed with hexane to leave a beige solid. Mass: 1.06 g. Yield: 93 %^{1}H NMR (300 MHz; $CDCl_3$; 298 K): 0.85 (t, 6H, -CH_3); 1.17-1.29 (hex, 4H, -CH_2-); 1.69 (p, H, -CH_2-); 4.19 (t, 4H, -CH_2-); 7.28-7.40 (m, 6H, benzo); 7.63 (s, 2H, phthalonitrile); 7.73-7.76 (dd, 2H, benzo). MS(APCI+): Calcd for $C_{30}H_{29}N_6S_2$ $[M+H]^+$: 537.1890; Found: 537.1906.

Synthesis and quaternerisation of asymmetrical (SR)$_2$PcH$_2$: dBubtpn (**4**) (1.05 g; 1.95 mmol) and 1,3-diiminoisoindoline (1.65 g; 11.40 mmol) were thoroughly ground together using a mortar and pestle before being added to a Schlenck tube. The mixture was then heated under N_2 with stirring for 6 h, during which time it forms a dark green paste. TLC analysis showed the presence of several colored products, but all were produced in trace amounts except for the two with the smallest R_f values. The paste was cooled to rt and then dissolved in EtOAc.

This solution was filtered through a short silica gel column. Solvent was then removed to leave a blue-green solid, which was subsequently dissolved in DMF (10 ml). MeI (2.0 ml) were then added, and the solution was heated at 80 ºC in a sealed vessel for 12 h. The solution was then added to THF, and the solids that precipitated were collected by filtration and washed with THF. Solids were repeatedly dissolved in a minimal amount of DMF and precipitated with THF until the filtrate obtained from washing was colourless. Drying the precipitate *in vacuo* (10^{-3} mbar) left a blue-green coloured solid.

*Synthesis of [(dppe)Ni(S_2PcH_2)] (**1**)*: A degassed aqueous solution of NaOH was added to a portion of the blue-green solid obtained (0.200 g). The solution colour very quickly turns blue as the thiolate groups are formed/deprotected. The suspension was placed in an ultrasound bath for 30 min to ensure complete deprotection had taken place. This suspension was then added dropwise with vigorous stirring to a separately prepared solution of $NiCl_2$(dppe) (0.300 g ; 0.568 mmol) in THF (20 ml). The resulting suspension was then stirred at rt for 60 min before removing the solvent *in vacuo*. The residue was then extracted with $CHCl_3$ and filtered. The filtrate was concentrated and loaded onto a silica gel column. The product was eluted using DCM/EtOH (10:0.5) as the dark blue-green band. Mass: 0.085 g.Yield over three steps: 16.8 %. ^{1}H NMR (300 MHz; $CDCl_3$; 298 K): δ (ppm) = 2.53 (s, 4H, ethyl); 7.41-7.50 (m, 14H, Pc and Ph); 7.70 (m-br, 10 H, Pc and Ph).^{13}C NMR (75 MHz; $CDCl_3$; 298 K): δ (ppm) = 30.33 (ethyl), 125.51, 128.85 (t, J = 5.90 Hz, Ph), 130.83 (t, J = Hz, Ph), 132.08, 135.83, 151.52.^{31}P NMR (MHz; $CDCl_3$; 298 K): δ (ppm) = 33.26. MS(MALDI+): Calcd for $C_{56}H_{41}N_8NiP_2S_2$ ($[M+H]^+$): 1033.17; Found: 1033.17. FTIR: 508 (s); 533 (s); 688 (s); 733 (s); 1027 (m); 1101 (m); 1121 (m); 1176 (s); 1435 (m); 2850 (w); 2915 (w); 3054 (w). UV-Vis ($CHCl_3$): 777 (s); 718 (s); 693 (s); 656 (s); 341 (sh)

*Synthesis of (ButS)$_2$PcH$_2$ (**2**)*: 4,5-bis(*tert*-butylsulfanyl)benzene-1,2-dicarbonitrile(0.300 g; 0.985 mmol) and 1,3-diiminoisoindoline (0.575 g ; 3.96 mmol) were mixed together under N_2. The mixture was then heated at 200 ºC in a sealed vessel for 14 h. Once cool, the dark green mass was dissolved in DCM and loaded onto a silica gel column. The product was eluted used DCM and collected as the large dark blue band. Solvent was then evaporated and the dark blue solid remaining was washed with MeOH before being dried *in vacuo* (10^{-3} mbar). ^{1}H NMR (300 MHz; CD_2Cl_2; 298 K): 1.26 (s, 18H, -CH_3); 7.00-8.06 (m, 14H, Pc). MS (APCI+):Calcd for $C_{40}H_{35}N_8S_2$ $[M+H]^+$: 691.2421; Found: 691.2442.UV-Vis (DCM): 690 (s), 664 (s), 638 (s), 607 (sh).

6.3 Synthesis, Spectroscopy and Singlet Oxygen Quantum Yield of a Non-Aggregating Pc*Si Derivative

Malcolm A. Bartlett, Kerstin Mark and Jörg Sundermeyer

*Synthesis, Spectroscopy and Singlet Oxygen Quantum Yield of a Non-Aggregating Pc*Si Derivative*

Inorg. Chem. Comm., **2018**, *98*, 41–43

Inorganic Chemistry Communications 98 (2018) 41–43

Contents lists available at ScienceDirect

Inorganic Chemistry Communications

journal homepage: www.elsevier.com/locate/inoche

Short communication

Synthesis, spectroscopy and singlet oxygen quantum yield of a non-aggregating hexadecamethyl-substituted phthalocyanine silicon(IV) derivative

Malcolm Alan Bartlett[a], Kerstin Mark[b], Jörg Sundermeyer[a,*]

[a] Department of Chemistry and Material Sciences Center, Philipps-Universität Marburg, Hans-Meerwein-Straße 4, 35032 Marburg, Germany
[b] Institut für Pharmazeutische Chemie und Zentrum für Tumor-und Immunbiologie (ZTI), Philipps-Universität Marburg, Hans-Meerwein-Straße 3, 35043 Marburg, Germany

GRAPHICAL ABSTRACT

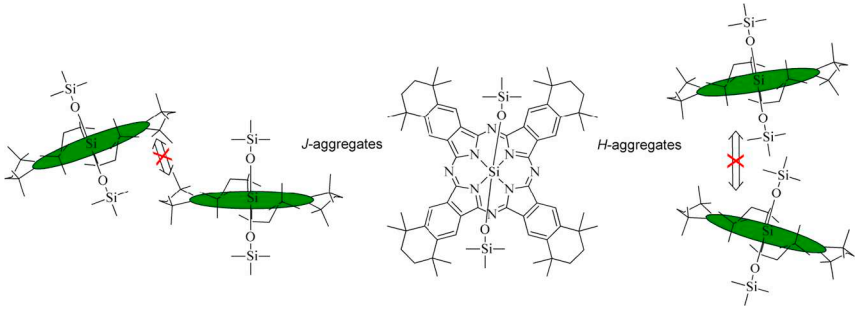

ARTICLE INFO

Keywords:
Silicon
Phthalocyanine
Singlet oxygen
Photosensitiser

ABSTRACT

A rigid hexadecamethyl substituted phthalocyanine (Pc*) silicon(IV) dichloride was synthesized by template cyclization of corresponding 1,3-diiminoisoindoline derivative with $SiCl_4$. Attempts to prepare the same compound by insertion of $HSiCl_3$ into preformed H_2Pc^* in the presence of bases were unsuccessful. Exchange of the axial chloride ligands with trimethylsiloxy groups made the molecular complex $Pc^*Si(OTMS)_2$ very soluble and non-aggregating, as shown by UV–Vis experiments. The effect of such peripheral alkyl substitution on the singlet oxygen quantum yield of the $Pc^*Si(OTMS)_2$ complex was determined and found to be 0.28; significantly lower than that for unsubstituted parent $PcSi(OTMS)_2$. The merit of improving solubility over reduced singlet oxygen quantum yields is discussed.

Photodynamic therapy is a well-established method for the treatment of cancer that reduces unwanted side-effects by using light, typically tissue-penetrating IR-laser light, to activate a photosensitiser (PS) in a specific region where activity is desired [1]. Therapeutic activity is achieved by the excitation of triplet oxygen present in the cell to singlet oxygen, which then oxidizes the surrounding biomolecules; the effectiveness of a compound to do this is measured as its singlet oxygen quantum yield, Φ_Δ. Whereas the first generation of compounds consisted mainly of porphyrins, such as photofrin, phthalocyanine (Pc) compounds have received considerable attention as second and third generation drugs, as they have superior optical properties compared to porphyrins, namely, the ability to absorb light of longer wavelengths, which allows for deeper tissue penetration and an increased region of activity [2]. Additionally, silicon Pc complexes have been extensively

* Corresponding author.
E-mail address: jsu@chemie.uni-marburg.de (J. Sundermeyer).

https://doi.org/10.1016/j.inoche.2018.07.032
Received 24 May 2018; Received in revised form 13 July 2018; Accepted 24 July 2018
Available online 25 July 2018

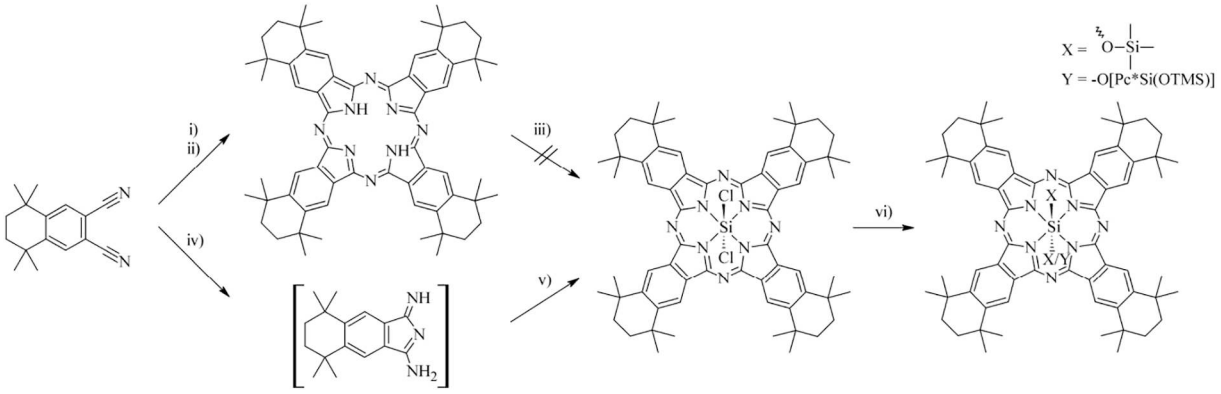

Scheme 1. Synthesis of Pc*Si(OTMS)$_2$ from PN*. Route A) – insertion of Si into the cavity of Pc*. Route B) – cyclization with Si template. Conditions: i) Mg(OEt)$_2$, *n*OctOH, 180 °C, 2 h; ii) H_2SO_4, H_2O, 0 °C; iii) M[HMDS] (M = Li, Na, K), $HSiCl_3$, 3 days; iv) NaOMe, NH_3, MeOH, 50 °C; v) $SiCl_4$, quinoline, 240 °C, 2 h; vi) TMS-ONa, pyridine, 60–80 °C, 4 h.

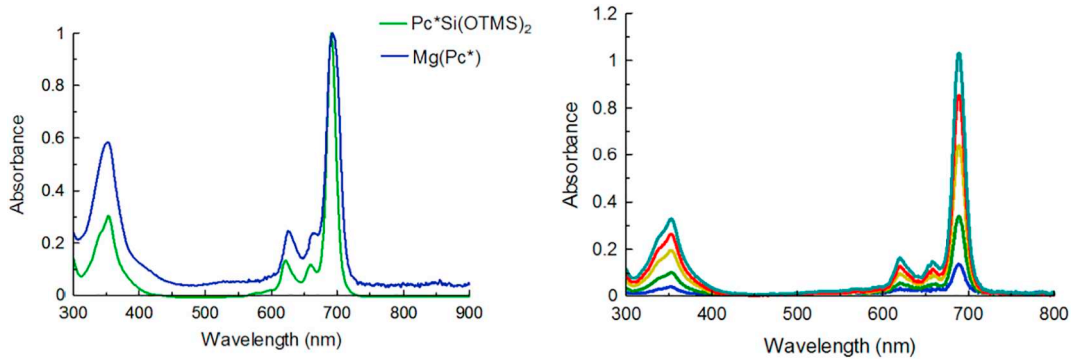

Fig. 1. (Left) Normalized UV–Vis absorption spectra for Pc*Si(OTMS)$_2$and Mg(Pc*). (Right) Absorbance versus concentration for Pc*Si(OTMS)$_2$; the linear correlation between absorbance and concentration (see inset box) shows that no aggregation occurs at the concentrations used.

investigated by the group of Kenney, with Pc 4, a PcSi derivative with an axially coordinated-O-SiMe$_2$-C$_3$H$_6$-NMe$_2$ ligand functionality, having progressed to clinical trials [3]. An advantage of PcSi complexes is the two axial coordination sites on Si that allow for the attachment of groups that can improve the complex's solubility while at the same time preventing the formation of H-/co-facial aggregates. Aggregation is a well-known phenomenon of Pcs that results because of the large Pc π-system, and can be either co-facial (H-type), head-to-tail (*J*-type) or a combination of both. However, H-aggregates are predominantly favored in solution, as this allows for the greatest overlapping of π-systems, and consequent equilibration of dispersion and electrostatic interactions [4]. In general, it is sought to reduce aggregation as this lowers both the solubility and the light absorption of Pc. More importantly for PDT, it has been known for many years that when aggregation occurs within a biologically relevant medium, the Φ_Δ of a compound can be effectively reduced to zero [5]. Recently, it was shown by Doane et al. that Pc 4 also forms *J*-aggregates in basic aqueous media [6]. In our group, we have made use of a phthalonitrile derivative with bulky alkyl substitution at the 4 and 5 positions that was first described by Mikhalenko [7]; the synthesis of this phthalonitrile was later optimized in our group [8]. Phthalocyanines synthesized using this phthalonitrile derivative show very good solubility in most organic solvents and, importantly, prevent both H- and *J*-type aggregation. Owing to their good solubility, we have termed the phthalonitrile and phthalocyanine synthesized from it PN* and Pc*, respectively. In this communication, we present a method for synthesizing non-aggregating Pc*SiX$_2$(X = Cl, OTMS), where TMS = trimethylsilyl, complexes and show that the singlet oxygen quantum yield for this peripherally alkyl substituted derivative compares well to unmodified Pc.

Initially, insertion of Si into the cavity of Pc* was attempted. For this, Pc*Mg was first synthesized by heating PN* with Mg(OEt)$_2$ in 1-octanol. The complex Pc*Mg was obtained in a yield of 51%, and was characterized by ^{1}H NMR, HRMS (APCI+), FTIR, and UV–Vis spectroscopy. To obtain the metal-free H$_2$Pc* ligand, Pc*Mg was treated with trifluoroacetic acid in the dark; complete demetallation was confirmed by UV–Vis spectroscopy. For the insertion reactions, H$_2$Pc* was treated with a base followed by addition of $HSiCl_3$. For all insertion reactions, complete deprotonation could be observed by monitoring the UV–Vis spectrum of the reaction solution. Li-, Na-, or *K*-hexamethyldisilane (HMDS) were used as bases in order to promote Pc* dianion formation, however, no transmetallation towards silicon was observed regardless of the base used.

Pc*SiCl$_2$ could, however, be synthesized directly by reaction of $SiCl_4$ with PN* via a two-step synthesis involving the 1,3-diiminoisoindoline derivative of PN*. PN* was therefore first reacted with ammonia in a methanolic solution of NaOMe. Heating the product of this reaction with $SiCl_4$ in quinoline gave the product Pc*SiCl$_2$ as a green solid, which was sparingly soluble in most common organic solvents. Pc*SiCl$_2$ was reacted with TMS-ONa in pyridine to give highly soluble Pc*Si(OTMS)$_2$ in 37% yield. The good solubility of this complex enabled analysis by both ^{1}H and ^{13}C NMR, as well as HRMS (LIFDI$^+$), FTIR and UV–Vis spectroscopy. Scheme 1 shows the successful and unsuccessful synthetic pathways for the synthesis of Pc*Si(OTMS)$_2$. In addition to the desired product, we could also isolate a μ-oxo-bridged dimer, O([Pc*Si(OTMS)])$_2$ in a yield of 18%. Dimer formation between PcSi(OH)$_2$ and PcSiCl$_2$ is well known [9], and it is therefore likely that some Pc*SiCl$_2$ was hydrolyzed during its work-up, which could then react to form the dimeric species. No other higher oligomeric species were observed in the reaction (Fig. 1).

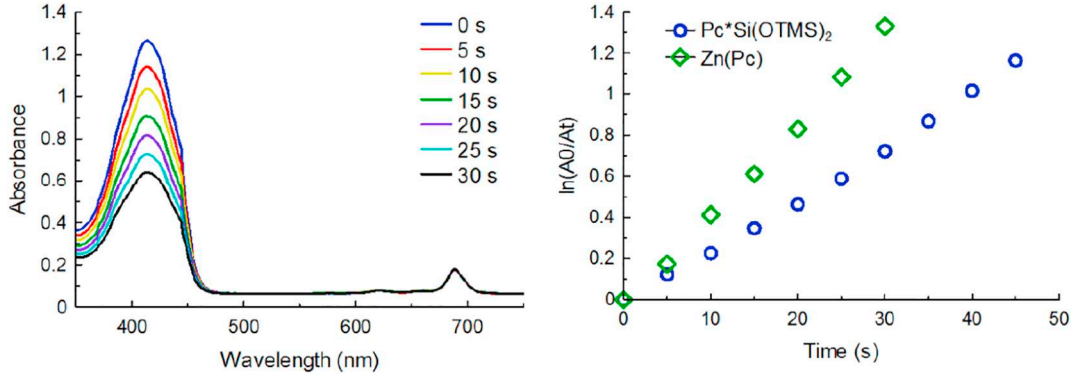

Fig. 2. (Right) Decrease of DPBF absorbance upon irradiation with light (> 590 nm) in the presence of $Pc^*Si(OTMS)_2$. (Left) Plot of the rates of DPBF decay in the presence of the standard $PcZn(py)_2$ (green diamonds) or $Pc^*Si(OTMS)_2$ (blue circles) versus time to determine the singlet oxygen quantum yield, Φ_Δ, for $Pc^*Si(OTMS)_2$. (For interpretation of the references to color in this figure legend, the reader is referred to the web version of this article.)

UV–Vis absorption spectra were measured for the Mg and Si Pc* complexes. The Q-band absorption maxima, at 693 nm and 691 nm for Pc*Mg and $Pc^*Si(OTMS)_2$, respectively, are very close in energy, the slight difference being explained by the less electronegative character of Mg [10]. The Q-band absorption maximum for $PcSi(Cl)_2$ is located at 685 nm [11], and therefore substitution with alkyl groups at the Pc β-positions results in the expected bathochromic shift [12] of 20 nm for the Pc*Si complex [13]. This is, of course, an advantage for PDT, where the use of longer wavelengths for PS excitation is preferred. The molar attenuation for $Pc^*Si(OTMS)_2$ was determined by measuring the absorbance at incrementally increased concentrations in DCM; a linear response was observed, indicating that no aggregation occurred within the concentration range used. The molar attenuation coefficient for absorption maxima are listed in Table S1 in the Supplementary information.

In addition to being able to prevent aggregation, it is important that the complex still have an ability to generate singlet oxygen in sufficient quantity so as to be useful for PDT. Therefore, the singlet oxygen quantum yield for $Pc^*Si(OTMS)_2$ was determined. 1.3-diphenylisobenzofuran (DPBF) decay under visible irradiation above 550 nm was monitored in toluene. $PcZn(py)_2$, with a known Φ_Δ value of 0.49 in toluene [14], was used as a standard. Fig. 2 shows an example decay curve of DPBF in the presence of $Pc^*Si(OTMS)_2$ as sensitizer, as well as a comparison of the decay rates of DPBF for the standard $PcZn(py)_2$ and $Pc^*Si(OTMS)_2$ monitored at 414 nm.

From the plot of decay rates, it is clear that the PcSi derivative does not have as high an activity as does $PcZn(py)_2$. Instead, the value of Φ_Δ calculated for $Pc^*Si(OTMS)_2$ is 0.28. This is significantly less than the value of $\Phi_\Delta = 0.48$ for unmodified $PcSi(OH)_2$ [14]. This result is at first surprising, considering that alkyl substitution at the Pc β-positions is not expected to have such a large impact on the photophysics of the Pc complexes. Furthermore, the substitution of H- for C- at the periphery should cause a slight improvement on inter-system crossing (ISC), which would result in a slightly higher Φ_Δ value. Instead, it is possible that the large steric bulk of the alkyl groups, while preventing aggregation, also prevents triplet oxygen from coming into contact the Pc ligand's T_{1x} MO responsible for energy transfer to oxygen. [15].

In conclusion, Si can be used to template a cyclization with PN* to give Pc*, whereas attempts to insert Si into Pc^{*2-} were unsuccessful. Pc^*SiCl_2 can be axially functionalized with siloxy groups; the combination of axial siloxy groups and peripheral rigid “alkyl” groups can prevent H- and *J*-type aggregation, but it lowers the singlet oxygen quantum yield, Φ_Δ, of the Pc*Si derivative by almost half. While this lowering of Φ_Δ is a drawback for application as a PS in PDT, the prevention of aggregation may prove to be of greater value when used in a biologically relevant medium.

Acknowledgements

Financial support by the State of Hesse (LOEWE, SynChemBio) is gratefully acknowledged.

Appendix A. Supplementary material

Experimental procedures and characterisation data (NMR, FTIR, and mass spectra) to this article can be found online at https://doi.org/10.1016/j.inoche.2018.07.032.

References

[1] C.A. Robertson, D. Hawkins, E.A. Abrahamse, J. Photochem. Photobiol. B Biol. 96 (2009) 1–8.
[2] N. Sekkat, H. van den Bergh, T. Nyokong, N. Lange, Molecules 17 (2012) 98–144.
[3] T.J. Kinsella, E.D. Baron, V.C. Colussi, K.D. Cooper, C.L. Hoppel, S.T. Ingalls, M.E. Kenney, X. Li, N.L. Oleinich, S.R. Stevens, S.C. Remick, Front. Oncol. 1 (2011) 1–6 (Article 14).
[4] F. Würthner, T.E. Kaiser, C.R. Saha-Möller, Angew. Chem. Int. Ed. 50 (2011) 3376–3410;
A.W. Snow, Phthalocyanine aggregation, in: K.M. Kadish, K.M. Smith, R. Guilard (Eds.), The Porphyrin Handbook, Vol. 17 Academic Press, San Diego, 2003(Chapter 109).
[5] D.S. Lawrence, D.G. Whitten, Photochem. Photobiol. 64 (1996) 923–935.
[6] T. Doane, A. Chomas, S. Srinivasan, C. Burda, Chem. Eur. J. 20 (2014) 8030–8039.
[7] S.A. Mikhalenko, L.I. Solov'eva, E.A. Luk'yanetz, J. Gen. Chem. USSR 64 (1991) 996–1003.
[8] M.B. Liebold, Ph.D. Thesis, Synthesis and Hotophysical Characterization of New Azaphthalocyanines and Azanaphthalocyanines for Semiconductor Interface Design, Philipps-University Marburg, 2016.
[9] E. Ciliberto, K.A. Doris, W.J. Pietro, G.M. Reisner, D.E. Ellis, I. Fragalà, F.H. Herbstein, M.A. Ratner, T.J. Marks, J. Am. Chem. Soc. 106 (1984) 7748–7761.
[10] M.J. Gouterman, Chem. Phys. 30 (1959) 1139–1161.
[11] B.H. Lessard, R.T. White, M. Al-Amar, T. Plint, J.S. Castrucci, D.S. Josey, Z.-H. Lu, T.P. Bender, ACS Appl. Mater. Interfaces 7 (2015) 5076–5088.
[12] E.A. Cuellar, T.J. Marks, Inorg. Chem. 20 (1981) 3766–3770.
[13] C.W. Dirk, T. Inabe, K.F. Schoch Jr., T.J. Marks, J. Am. Chem. Soc. 105 (1983) 1539–1550.
[14] X.-F. Zhang, Y. Rong, J. Photochem. Photobiol. A Chem. 222 (2011) 141–145.
[15] K. Ishii, H. Itoya, H. Miwa, M. Fujitsuka, O. Ito, N. Kobayashi, J. Phys. Chem. A 109 (2005) 5781–5787.

Supplementary Information to:

*Synthesis, Spectroscopy and Singlet Oxygen Quantum Yield of a Non-Aggregating Pc*Si Derivative*

Authors

Malcolm A. Bartlett and Jörg Sundermeyer

Contents Page

General Comments 1
Syntheses 2
Molar Attenuation Coefficients 3
References 3

General Comments

All reactions were carried out under a protective N_2 atmosphere unless otherwise stated. Solvents were dried by distillation over either CaH_2 (for alcohols) or Na before use. $SiCl_4$ and $HSiCl_3$ were purchased from Sigma Aldrich and used as received. NMR Spectra were recorded on a Bruker Avance 300 NMR spectrometer. UV-Vis absorption spectra were recorded either with an AvaSpec-2048 or a Cary Eclipse Spectrometer. FTIR spectra were recorded on a Bruker Alpha II spectrometer. Mass spectra were recorded on a Thermo Fischer Scientific LTQ-FT Ultra for ESI and APCI ionized samples, and on a JEOL AccuTOF GCv for LIFDI ionized samples. Photo-irradiation was performed using a halogen lamp with an adjustable power rating, which was set to 100 W. Light was filtered through a water filter for removal of infrared light and then through a glass filter with a cut-on wavelength of 500 nm.

Singlet Oxygen quantum yields

Singlet oxygen quantum yield measurements were performed using the set-up described above. In a typical measurement, a cuvette was filled with 2 ml of sample solution containing the sensitizer and DPBF, the concentrations of which were such that the absorbance of each was ~ 0.2 and ~ 1.0, respectively. The samples were saturated with O_2 by bubbling a stream of O_2 gas through the sample solution for 1 minute before beginning the measurements. The singlet oxygen quantum yield, Φ_Δ, was determined by using the following equation[S1]:

$$\Phi_\Delta = \Phi_\Delta^{Std}\left(kI_{Abs}^{Std}/k^{Std}I_{Abs}\right)$$

$$\Phi_\Delta = \Phi_\Delta^{Std}\left(kI_{Abs}^{Std}/k^{Std}I_{Abs}\right)$$

Where k and k^{Std} are the slopes of the plot of $\ln(A_0/A_t)$ versus time, for the sensitizer and standard, respectively,where A_0 and A_t are the measure of DPBF absorbance at time "0" and time "t", and I_{Abs} and I_{Abs}^{Std} are the rates of light absorption by the sensitizer and standard, respectively.

Syntheses

Synthesis of Mg(Pc)*

$Mg(OEt)_2$ (0.25 mg; 2.14 mmol) and 6,7-dicyano-1,1,4,4-tetramethzltetralin (0.50 mg, 2.11 mmol) were mixed together in 1-octanol (5 ml), and the resulting suspension was heated to 150 ºC for 16 h. Volatiles were then removed in vacuo, and the residue was extracted into DCM. The extract was then filtered and loaded onto a neutral alumina column. After passing hexane and DCM through the column to remove non-polar impurities, the product was eluted using $CHCl_3$/DCM (4:1). The product, Mg(II)(Pc*), was isolated as a dark blue-green powder. Mass obtained: 0.263 g. Yield = 51 %.

^{1}H NMR (300 MHz, $CDCl_3$, 298 K): δ (ppm) 9.46 (s, 8H, H_{Ar}), 2.05 (s, 16H, CH_2), 1.81 (s, 48H, CH_3)
HRMS (APCI+): m/z+ calculated for $C_{64}H_{73}MgN_8$ ($M+H^+$): 977.5803, Found: 977.5803.
FTIR(ATR): ν = 2955 (m), 2911 (m), 2856 (m), 1617 (w), 1483 (m), 1456 (s),1427 (s), 1393 (m), 1384 (m), 1361 (m), 1328 (s), 1304 (w), 1259(m), 1215 (w), 1187 (m), 1112 (m), 1075 (s), 1048 (s), 1020 (m), 982 (m), 950 (w), 895 (m), 864 (m), 793 (m), 778 (m), 763 (s), 752 (m), 728 (s), 704 (w), 665 (m), 621 (w), 530 (m) cm−1.
UV-Vis ($CHCl_3$) λ = 693 (s),

Synthesis of Pc$SiCl_2$*

Sodium (0.027 g; 1.2 mmol) was dissolved in MeOH (40 ml). Once all Na had dissolved, PN* (0.50 g; 2.12 mmol) was added, and ammonia gas was bubbled through the suspension with stirring and gentle heating (50 ºC) for 6 h. Solvent was then evaporated and the residue was dissolved in DCM and filtered. The filtrate was evaporated, and the residue was dissolved in quinoline. $SiCl_4$ (0.10 ml: 0.87 mmol) was then added, and the resulting suspension was heated at 240 ºC for 2 h. The green-brown solution obtained was then diluted with hexane, and the precipitate that formed was collected by filtration and washed with hexane, $CHCl_3$ and EtOH. In this way, 0.225 g of Pc*$SiCl_2$ was obtained as a green powder. Yield over two steps = 40 %.

Comment: the solubility of the dichloro complex is very low, so that no 1H NMR of MS spectra could be obtained.

FTIR(ATR): $\tilde{\nu}$ = 2961 (m), 2923 (m), 2862 (m), 1620 (w), 1531 (m), 1457 (m), 1438 (m), 1412 (m), 1388 (m), 1365 (w), 1344 (w), 1309 (s), 1203 (s), 1190 (m), 1121 (w), 1094 (w), 1073 (m), 1049 (s) , 1003 (s), 956 (s), 936 (w), 907 (w), 878 (m), 799 (m), 768 (w), 756 (w), 747 (m), 714 (w), 665 (w), 551 (m), 540 (m), 458 (s), 411 (m) cm−1.

*Synthesis of Pc*Si(OTMS)$_2$*

Pc*$SiCl_2$ (0.098 g; 0.09 mmol) was suspended in pyridine (7 ml). TMSONa (0.043 g; 0.38 mmol) was added, and the suspension was heated to 80 ºC for 4 h to give a dark blue-green solution. Solvent was removed *in vacuo*, and the residue was loaded and separated on a preparative silica TLC plate using DCM. Both the product, Pc*Si$(OTMS)_2$, and the mono-substituted dimer, (Pc*Si$(OTMS))_2O$, could be obtained as green-blue solids.

<u>Pc*Si$(OTMS)_2$</u>
Mass: 0.040 g
Yield = 37 %
^{1}H-NMR (300 MHz, CDCl3, 298 K) δ(ppm) = 9.54 (s, 8H, H_{Ar}), 2.08 (s, 16H, CH_2), 1.81 (d, 48H, CH_3),2.68 (d, 18H, Si(C$H_3)_3$).

^{13}C-NMR (300 MHz, CDCl3, 298 K) δ(ppm) = 148.8, 148.6, 134.0, 121.6, 36.2, 35.6, 33.1, -1.0 ppm.
HRMS (LIFDI+)**:** *m/z* Calculated for $C_{70}H_{90}N_8O_2Si_3$ ($[M+H]^+$): 1158.6495. Found: 1158.6463.
IR (ATR): $\tilde{\nu}$ = 2957 (m), 2922 (m), 2857 (w), 1522 (m), 1458 (m), 1436 (m), 1407 (m), 1354 (m), 1306 (s), 1259 (m), 1188 (s), 1071 (s, br), 1017 (s, br), 894 (m), 869 (s), 795 (s), 756 (m), 708 (m), 622 (w), 581 (w), 548 (w), 467 (w) cm−1.
UV-Vis ($CHCl_3$) : λ (nm) = 691(s), .

$(Pc*Si(OTMS))_2O$
Mass : 0.019 g
Yield = 18 %
^{1}H NMR (300 MHz, $CDCl_3$, 298 K): δ (ppm) 9.55 (s, 16H, H_{Ar}), 2.08 (s, 32H, CH_2), 1.81 (d, 96H, CH_3), 2.68 (d, 18H, $Si(CH_3)_3$)
^{13}C NMR (MHz, $CDCl_3$, 298 K): δ (ppm) 152.8, 149.1, 134.0, 121.6, 36.2, 35.6, 33.1, 1.0.
HRMS (LIFDI+): *m/z* Calculated for $C_{67}H_{81}N_8OSi_2$ ($[1/2M-O]^+$): 1069.6066, Found: 1069.6072.
IR (ATR) = 2958 (m), 2922 (m), 2857 (m), 1773 (w), 1724 (m), 1619 (w), 1520 (m), 1457 (m), 1435 (m), 1407 (m), 1349 (m), 1305 (s), 1259 (w), 1188 (s, br), 1017 (s, br), 895 (w), 870 (s), 795 (s), 758 (s), 708 (m), 666 (m), 622 (m), 542 (m), 507 (w), 466 (w) cm−1.
UV-Vis ($CHCl_3$):

Attempted insertion of Si into Pc*
H_2Pc* (0.050 g; 0.05 mmol) were mixed with base(Note 1) (0.12 mmol) in either THF, Toluene or Diethylether. $HSiCl_3$ was then added dropwise, and the solution was stirred at rt. Reaction progress was monitored by UV-Vis spectroscopy; even after 3 days, no formation of $Pc*SiCl_2$ could be detected.

Note 1: base used was LiHMDS, NaHMDS or KHMDS.

Molar Attenuation Coefficients

Table **S1**: Electronic absorption spectral data for $Pc*Si(OTMS)_2$

Absorption maximum (nm)	Molar Attenuation ($dm^3\ mol^{-1}\ cm^{-1}$)
689	176573
657	22473
619	25153
352	56185

References

S1: D. Çakir, M. Göksel, V. Çakir, M. Durmuş, Z. Biyikhoğlu and H. Kantekin, *Dalton Transactions*, **2015**, *44*, 9646-9658.

6.4 Zinc(II)Phthalocyanine-Thiol Monolayers on Gold: On the Oxidative Stability of the S–Au Bond

Malcolm A. Bartlett, Michael Kothe, Gregor Witte and Jörg Sundermeyer

Zinc(II)Phthalocyanine-Thiol Monolayers on Gold: On the Oxidative Stability of the S–Au Bond

Manuscript in preparation – for submission to: *Journal of Porphyrins and Phthalocyanines*

TITLE

Zinc(II)Phthalocyanine-Thiol Monolayers on Gold: On the Oxidative Stability of the Thiol-Au Bond.

AUTHORS

Malcolm Alan Bartlett[1], Michael Kothe[2], Gregor Witte[2], and Jörg Sundermeyer[1]

1 Fachbereich Chemie, Philipps-Universität Marburg, Hans-Meerwein Str. 4, 35032
2 Fachbereich Physik, Philipps-Universität Marburg, Renthof 5, 35032

ABSTRACT

In order to understand and tune charge transfer dynamics between surface bound molecules and their substrate, control of the molecular orientation and resultant electronic coupling is essential. Zn phthalocyanine (Pc) is already well studied in this regard, but lacks the ability to bind covalently in a highly ordered fashion to a substrate. Here, we demonstrate that the addition of an anchoring unit, namely a thiolalcohol, enables covalent attachment, and thus control of the molecular orientation, of thin films of ZnPc. For this study, an asymmetric ZnPc derivative bearing six *n*-butyl groups and a single peripheral thiol group (Zn(Pc^{SH})) was synthesised. The optimised structure of the synthesized Zn complex was calculated using DFT methods. The binding and orientation of Zn(Pc^{SH}) on Au(111) was investigated using XPS and NEXAFS, respectively. XPS data revealed that films prepared under air showed significant sulfonate formation, while those prepared under N_2 showed considerable compound decompostion to leave gold sulfide. These results show that Zn(Pc)-containing S-Au films are not inherently robust, but are susceptible to oxidation under aerobic conditions.

INTRODUCTION

Self-assembled monolayers (SAMs) represent an easy and convenient way to combine metals, semiconductors, and inorganic compounds with organic and biological compounds; that is, materials that have very different physical and chemical properties.[1] SAMs composed of alkyl thiols and dithiols on gold have found many different applications, including: inks or resists for lithography,[2] in molecular electronics as transistors and switches,[3] in sensors and biosensors,[4] and in the stabilization of gold nanoparticles.[5] It is therefore not surprising that phthalocyanines (Pcs) have also been functionalized with one or more thiol groups and used for SAM formation.[6] However, although there are many techniques available for surface characterization that together provide a very complete picture of the structure, composition and orientation of the organic compounds of the SAM, only a limited number of techniques have been used for analyzing the proposed SAMs formed by thiol-Pcs on gold surfaces. These techniques typically generally include atomic force microscopy (AFM), electron microscopy (EM), electrochemical techniques, such as cyclic voltammetry (CV), and optical absorption and emission spectroscopy. While these methods can show whether or not Pc is present at the gold surface, they do not provide information as to the molecular composition of the bound compounds. Rather, it is generally assumed that the molecular structure remains unchanged during, not only SAM formation, but also subsequent reactions or processes at the SAM surface. Additionally, Revell *et al.* demonstrated that Pc containing SAMs formed *via* S–Au bonds were stable towards oxidation only when tight packing between and separation of the Pc molecules from the gold surface was increased.[7]

In this short paper, we have attempted to better understand the nature of surface bound phthalocyanine by synthesizing asymmetric Zn(Pc) derivative with a single peripheral methylene thiol (-CH_2SH) functionality, and depositing it on Au(111) surfaces under different conditions. Films grown were

then examined through X-ray photoemission spectroscopy (XPS) and near edge X-ray absorption fine structure (NEXAFS) spectroscopy to probe the binding and orientation, respectively, of the phthalocyanine.

RESULTS AND DISCUSSION

Compound design

In this study, we wished to develop a Zn phthalocyanine derivative that would not simply adsorb onto the Au surface, but would bind in such a way that the aromatic system would be largely decoupled from the substrate. We therefore incorporated a single thioalcohol group attached to the Zn(Pc) *via* a methylene group to ensure that binding would be specific. The peripheral Pc'-CH_2-SH binder was selected in order to provide a flexible, but nevertheless constrained, hinge for aiding chemisorptions of Pc molecules on the surface. Additionally, *n*-butyl groups were used for improving solubility, as they would not significantly affect tight packing of Zn(Pc) in a SAM.

Synthesis

***Dinitriles*:** Literature known procedures were used for the syntheses of **1**, **2** and **3**. The synthesis of **4** required the radical bromination of the commercially available 4-methylphthalonitrile. At first, a literature method was used that involved a radical initiator (AIBN) in CCl_4 followed by treatment of the products with diethyl phosphate to obtain the product in moderate yields.[8] We found that it was possible to obtain the product in much higher yields when only light was used as the initiator at ambient temperatures; MeCN could also be used as the solvent instead of the highly carcinogenic CCl_4. Additionally, only a small amount of dibrominated by-product could be detected, and no tri-brominated species could be identified by ^{1}H NMR. Synthesis of **5** was then readily accomplished by treatment of **4** with HSAc in the presence of a mild base. N,N,N',N'-tetramethylpropylamine was chosen, as the doubly protonated salt precipitates readily from DCM solutions, and can therefore be conveniently removed by filtration.

***Asymmetric Zn phthalocyanine derivative*:** The unsymmetrical ZnPc derivative (**6**) was synthesized by the cross-condensation of **3** and **5** in the presence of $Zn(OAc)_2$, DBU and 1-octanol, with **3** being in a large excess (8:1) compared to **5** (Scheme 1). Interestingly, **5** does not react to form the related symmetric Pc complex under the same conditions when it alone is used for Pc synthesis. Rather, it is only incorporated into the Pc when a second phthalonitrile derivative is present. Because of the large differences in solubility of the isomers, the A_4[9] and A_3B isomers can be eparated from the other isomers by extraction into DCM or $CHCl_3$, although some other asymmetric isomers are also present in the extract in small amounts. During the cyclization however, the thiolester is deacylated into a thiolalcohol. The A_4 and A_3B isomers can be separated from each other using chromatography, but when silica is used it must first be deactivated using a tertiary amine, such as *N,N,N',N'*-tetramethyl-1,3-propaneamine, and washed thoroughly with hexane or else the A_3B isomer cannot be separated from the other asymmetric isomers present nor can it be effectively removed from the silica. The structure of **6** was confirmed by ^{1}H NMR spectroscopy and MALDI-TOF mass spectrometry.

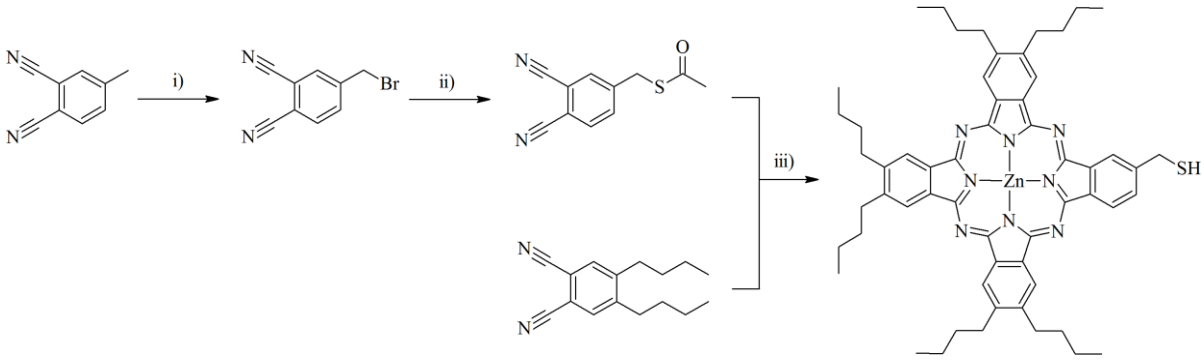

Scheme 1: Synthesis of asymmetric Zn(Pc) **6** and its phthalonitrile precursors **3** and **5**: i) NBS, MeCN, *hv* (300 W), 28 h, 40 °C; ii) 1,3-$(Me_2N)_4Pr$, $H_3CC(O)SH$, THF, rt, 30 min; iii) $Zn(OAc)_2$, DBU, 1-OctOH, 190 °C, 70 min.

DFT structure optimization

The gas-phase structure of **6** was optimized by DFT calculations at the B3LYP/6-311G level of theory. Calculations predict that **6** has a planar structure as expected, and importantly, that the n-butyl groups project away from the Zn(Pc) core, and therefore should not cause significant steric hindrance between Zn(Pc) complexes as they pack together on the Au(111) surface. The thiol group projects away from the Pc at an angle of 113 º, while the angle transcribed between the thiol-H atom and the plane of Pc core is 30.5 º. This suggests that the Zn(Pc) would be orientated at an angle of ca. 60 º to the Au(111) surface. Figure 1 shows the optimized gas-phase structure of **6**.

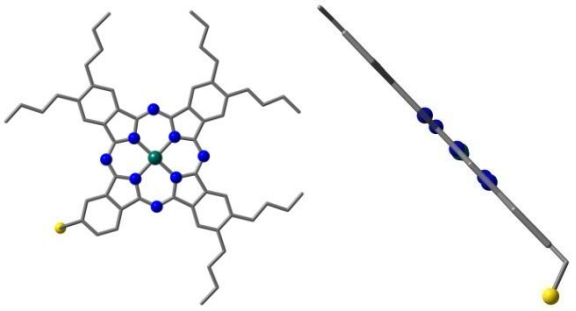

Figure 1: DFT optimization of the gas-phase structure of **6** showing the Zn(Pc) core (left) and the planarity of the complex (right). H-atoms have been omitted for clarity. Calculations were performed at the B3LYP/6-311G level of theory.

Substrate binding studies

Samples were prepared by immersion of Au(111)/Mica into a chloroform/octanole solution of **6** for one week at room temperature. Additionally, some samples were prepared under normal atmospheric conditions while others were prepared under anaerobic conditions. The results for the two sample groups are summarized below.

Samples prepared under normal atmospheric conditions were analyzed by XPS. The chemical shift of the S2p binding energy with respect to the chemical binding situation was used to determine if the

molecules do bind to the surface by deprotonation of their thiol group to a thiolate, according to the assignment by Khalid *et al.*[10] Even though unreacted thiol (R-SH, 163.5eV) and thiolate (AuS-R,162.0eV) species are present on these samples the strongest contribution origins from unwanted sulfonates ($AuSO_x$, 169eV) [see Supporting Information]. The observed degree of oxidation is assumed to be enhanced by Zn(Pc) itself because Zn(Pc) is known to catalyze oxidation *via* photo-induced singlet oxygen production.[11]

Additional samples were prepared under anaerobic conditions. The corresponding XP spectrum in Figure XPS1 b) with no sulfonate species present (169 eV) proves the successful suppression of the unwanted oxidation to sulfonates under inert N_2 gas conditions. The molecular orientation of compound **6** was further analyzed by NEXAFS, because NEXAFS, in contrast to many other methods, is able to detect the orientation even for non-crystalline samples. The corresponding spectrum for a sample of **6** prepared under anaerobic conditions is shown in Figure 2 a). Even though resonances in the π*-region at 284.4 eV and 285.3 eV indicate that the presence of a Zn(Pc) derivate (compare with unmodified ZnPc (b) grey curve)), are present, the spectrum shows different contributions that may be originating from solvent inclusions. Additionally, there is almost no dichroism visible in the spectra, meaning that the molecular thin film is not ordered.

Subsequently the sample prepared under anaerobic conditions was heated in ultrahigh vacuum (UHV) (10^{-7} – 10^{-9} mbar) to increase the ordering and remove the solvent inclusions. Performing heating steps of 30 °C a significant change in the spectrum was observed after heating to 260 °C. The resulting spectrum in Figure 2 shows the resonances at 284.4 eV and 285.3 eV strengthened, indicating that the majority of the solvent inclusions were desorbed. In addition the appearing of a dichroism indicates an increased ordering of the film. The evaluation of the intensities of the peak at 284.4 eV results in an average orientation of the molecular plane of 29° ±6° with respect to the Au(111) surface, meaning the Zn(Pc) molecules are in a more lying-down orientation.

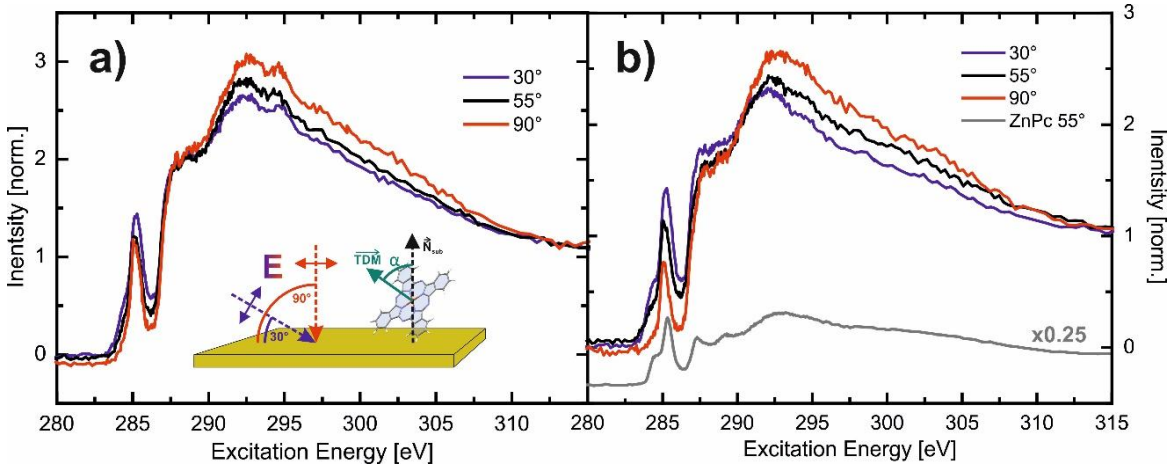

Figure 2: NEXAFS spectra for **6** at orientations of 30º, 55º, and 90º respectively for films prepared at room temperature (a) and after *in situ* heat treatment at 260 ºC (b). Furthermore in graph a) the orientation of TDM and sample is shown schematically. The signature of 3 nm Zn(Pc) is added in b) for comparison (grey curve).

In the XP spectrum of the unheated sample one can identify a thiol (R-SH, 163.5 eV) and a thiolate species (AuS-R, 162.0 eV) as well as a strong additional species at 161.3 eV that can be assigned to inorganic gold sulfides or disulfide. This oxidation of thiols to sulfide species has already been well documented[12] and could therefore very likely have occurred during the incubation period for these samples. An upcoming question is, if the thiolate bound with the substrate can withstand a temperature treatment at 260 °C, which is necessary to desorb the solvent inclusions. Comparing the first spectrum with the spectrum Figure 3 d) of the heated sample, a strong reduction of the thiolate signal and an increase in the sulfide signal is observable, showing that the thiolate bond is broken by the heating process leaving an inorganic gold sulfide at the surface.

The analysis has shown that it is mandatory to work under anaerobic conditions to prevent unwanted oxidation of the thiol group to sulfonates, but even under inert gas conditions the formation of sulfides and disulfides can't be prevented. When samples are prepared by immersion of the substrate the resulting monolayer shows solvent inclusions that lead to disorder. Annealing the samples at 150 – 260 °C will lead to the desorption of intercalated solvent residuals and an increased ordering of the molecules in a rather lying molecular orientation. Nevertheless such a heat treatment leads to the breaking of the arene-thiolate bond leaving gold sulfide on the surface.

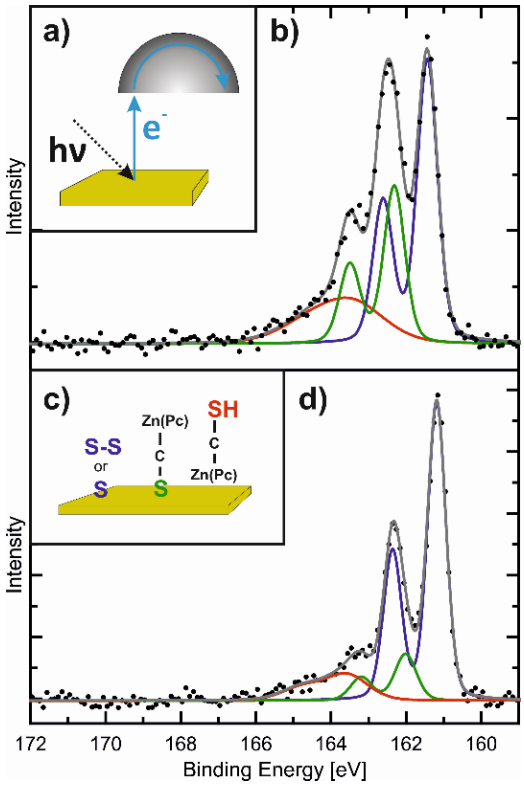

Figure 3: XP spectra of the S2p region taken from the sample prepared under anaerobic conditions without further heat treatment b) and after *in situ* heating to 260 °C d). The inset a) shows the experiment setup, inset c) a schematic drawing of the observed sulfur species.

SUMMARY

A soluble asymmetric Zn(Pc) derivative with a single peripheral methylenethiol group was successfully synthesized by a statistical mixed cyclisation. Synthesis of the mono-thioacetate dinitrile

precursor was accomplished in good yield, and can be used for the synthesis of additional phthalocyanine complexes were a single thiol functional group is required. DFT calculations showed that the *n*-butyl groups lie within the plane of the Zn(Pc) core, and should therefore not prevent tight packing of the Zn(Pc) complexes within the SAM. Physical investigations, however, revealed that SAM formation is not a trivial process when densely packed phthalocyanines are concerned. Particularly, XPS showed that oxidation of the thiol groups occurs both in and excluding the presence of oxygen. Oxidation processes are most likely photo-induced, being auto-catalyzed by Zn(Pc) within the SAM. This work has implications for thiol-gold-based SAMs incorporating phthalocyanines, especially where the SAMs are to be exposed to heat, oxygen or light. It is mandatory to determine binding state and actual orientation of the molecules before they may be considered to form a SAM. As demonstrated in this short communication, this is not necessarily trivial.

EXPERIMENTAL

General remarks

All reactions were carried out under a protective N_2 atmosphere unless otherwise stated. Solvents were dried by distillation over either CaH_2 (for alcohols) or Na before use. 4-methylphthalonitrile and thioacetic acid were purchased from Sigma Aldrich and used as received. NMR Spectra were recorded on a Bruker Avance 300 NMR spectrometer. UV-Vis absorption spectra were recorded either with an AvaSpec-2048 or a Cary Eclipse Spectrometer. FTIR spectra were recorded on a Bruker Alpha II spectrometer. Mass spectra were recorded on a Thermo Fischer Scientific LTQ-FT Ultra for ESI and APCI ionized samples, and on a JEOL AccuTOF GCv for FD ionized samples.

Synthesis

1,2-dibutylbenzene (**1**),[13] **1,2-dibutyl-4,5-dibromobenzene** (**2**)[14] and **1,2-dicarbonitrile-4,5-dibutylbenzene**[15] (**3**) were synthesized according to known literature procedures.

Synthesis of 4-(bromomethyl)benzene-1,2-dicarbonitrile (**4**)**.** 4-methylphthalonitrile (1.50 g; 10.55 mmol) and NBS (1.91 g; 10.73 mmol) were dissolved in MeCN (100 ml). The solution was irradiated with a 300 W halogen lamp (Osram) for 28 h. Light was filtered through a water-tank to prevent over-heating of the reaction vessel. A yellow color began developing shortly after irradiation was initiated. The solvent was then removed *in vacuo* to leave a pale brown solid, which was extracted with toluene. The extracts were filtered and then eluted through a short silica path before evaporating the solvents to leave a beige colored solid. This solid is a mixture of mono- and dibrominated product, as well as some unhalogenated starting material. It was not possible to remove the by-products by chromatography; instead, the obtained product mixture was used directly in the next step. The composition of the product mixture was determined by ^{1}H NMR to consist of mostly mono-brominated product (92 %) with the remainder being dibrominated product (5.5 %) and starting material (2.5 %).

Synthesis of S-acetyl-1-mercaptomethyl-(3,4-dicyanobenzene) (**5**)**. 4** (3.92 g; 17.71 mmol) was dissolved in DCM (20 ml). N,N,N',N'-tetramethyl-1,3-diaminopropane (technical grade) (1.20 g; 9.21 mmol) was added, which caused a white precipitate to begin forming. Thioacetic acid (1.40 g; 18.39 mmol) was then added; the addition is exothermic, and a large amount of white precipitate forms simultaneously. The suspension was stirred for 30 min before removing the THF *in vacuo*. The solids were then dissolved in DCM, and the resulting solution was eluted through silica. The coloured

fractions that elute first were discarded. The solvent was evaporated to leave a pale brown solid. The product was then purified by column chromatography (toluene/silica) to yield the product as a white solid. Mass obtained: 2.10 g. Yield = 55 %. ^{1}H NMR (DMSO-*d6*; 300 MHz, 298 K): 2.37 (s, 3H, -CH_3); 4.23 (s, 2H, -CH_2S-); 7.84 (dd, J_1 = 8.13, J_2 = 1.68 Hz, 1H, Ar); 8.06-8.09 (m, 2H, Ar).^{13}C NMR (DMSO-*d*6; 75 MHz, 298 K): 30.16, 31.56, 112.99, 114.63, 120.69, 126.01, 133.95, 134.12, 134.15, 134.18, 145.31. HRMS (FD+): Calcd for $C_{11}H_8N_2O_1S_1^+$ 216.0357. Found 216.0351.

Synthesis of 2,3,9,10,16,17-hexabutyl-23-(2-mercaptomethyl)phthalocyaninatozinc(II) (6). 3 (3.25 g; 13.51 mmol), **5** (0.36 g; 1.65 mmol), $Zn(OAc)_2$ (1.24 g; 6.76 mmol) and DBU (0.2 ml) were suspended in 1-OctOH (20 ml). The suspension was then placed in an oil bath, which had been pre-heated to 190 °C, and was stirred for 70 min at this temperature. All solids rapidly dissolved at this temperature to give a dark red-colored solution, which soon turns dark blue-green. The solution was then allowed to cool to room temperature, before removing the volatiles by vacuum distillation. The solids were then extracted using $CHCl_3$. The extract was concentrated and loaded onto a neutral alumina column, and the product was eluted using DCM/EtOH (10:0.5) as the second blue band. Alternatively, a silica gel column is prepared and *N,N,N',N'*-tetramethyl-1,3-propylamine is eluted through followed by extensive washing with hexane to remove un-adsorbed amine. The extracts are then loaded onto the column using DCM and eluted with the same solvent system as for the alumina column to obtain the product as the second blue band. Some excess amine does elute with the product, thus complicating the purification; therefore, the use of an alumina solid phase is advised. Both the A_4 and A_3B isomers are blue complexes that show moderate solubility in a limited range of organic solvents, such as DCM, THF, DMSO and DMF.

$ZnPc^{nBu6/CH2SH}$ (A_3B isomer): ^{1}H NMR ($CDCl_3$, 300 MHz, 298K): δ (ppm) 0.92-1.26 (m, 18H, -CH_3); 1.38-1.89 (m, 24H, -CH_2CH_2CH$_3$); 2.15 (s, 1H, -SH); 2.44-2.93 (m, 14H, -CH_2CH$_2$CH$_2$CH$_3$ and –CH_2SH); 7.15-8.22 (m, 8 H, Pc); 8.81-8.88 (m, 1H, Pc). MS(MALDI+): Calc. for $C_{57}H_{67}N_8Zn$ [M–SH]$^+$: 929.61; Found: 929.60.

$ZnPc^{nBu8}$(A_4 isomer): ^{1}H NMR ($CDCl_3$; 300 MHz; 298 K): 1.03 (t, 24H, -CH_3), 1.03 (t, 16H, -CH_3), 9.70 (s, 8H, Pc). MS (HRMS-ESI+): Calc. for $C_{64}H_{81}N_8Zn$ [M+H]$^+$ (Found): 1025.5870 (1025.5871).

Computational details

Gas phase geometry optimizations were performed using the B3LYP functional with the 6-311G basis set. The optimization step was immediately followed by a frequency calculation at the same level of theory, from which no negative eigenvalues were found, indicating that the structure had optimized to a global minimum. Calculations were performed on the MaRC2 computer cluster.

Substrate and monolayer formation

Au(111) substrates was prepared by UHV evaporation of 100-200 nm gold onto Mica sheets leading to epitaxially grown Au(111) surfaces. Monolayers were prepared by impregnation of Au(111) with solutions of **6** (10^{-4} M) in $CHCl_3$. For anaerobically prepared monolayers, dry $CHCl_3$ was stored with molecular sieves under a N_2 atmosphere before use. Schlenck techniques were used during the impregnation of Au(111) substrates with **6**.

Physical measurements

XPS and NEXAFS measurements, including high temperature annealing of the samples, where performed under UHV conditions at the HE-SGM beamline at the BESSY II facility. NEXAFS spectra where recorded using a home-built double channel plate detector in PEY mode with a

retarding field set to 150 eV. Energy was calibrated by the known carbon signal on a gold grid placed directly behind the exit slit. For further details on the NEXAFS setup the reader is advised to the work of Breuer et al.[16]

A hemispheric electron energy analyzer (Scienta R3000) was used to record XPS under normal electron exit angle. The photon energy was set to 330 eV with an incidence angle of 45°. Energy was calibrated by the Au4f substrate signal.

Acknowledgements

We acknowledge support by the Deutsche Forschungsgemeinschaft (Grant SFB 1083) and the Helmholtz-Zentrum Berlin (electron storage ring BESSY II) for provision of synchrotron radiation at beamline HE-SGM and financial support. MAB thanks the German Academic Exchange Service (DAAD) for a doctoral scholarship.

REFERENCES*

[1] Vericat, C, Vela, ME, Benitez, G, Carro, P, and Salvarezza, RC, *Chem. Soc. Rev.*, 2010; **39**: 1805-1834.

[2] Wilbur, JL and Whitesides, GM, in *Nanotechnology*, ed. Timp, G, Springer Verlag, New York, 1999; (b) Love, JC, Estroff, LA, Kriebel, JK, Nuzzo, RG, and Whitesides, GM, *Chem. Rev.*, 2005; **105**: 1103–1169; (c) Gates, BD, Xu, Q, Stewart, M, Ryan, D, Willson, CG, and Whitesides, GM, *Chem. Rev.*, 2005; **105**: 1171–1196.

[3] (a) Bumm, LA, Arnold, JJ, Cygan, MT, Dunbar, TD, Burgin, TP, Jones, L, II, Allara, DL, Tour, JM, and Weiss, PS, *Science*, 1996; **271**: 1705–1707.(b) Tour, JM, *Acc. Chem. Res.*, 2000, **33**: 791–804. (c) Sugawara, T, and Matsushita, MM, *J. Mater. Chem.*, 2009; **19**: 1738–1753. (d) Lio, A, Charych, DH, and Salmeron, M, *J. Phys. Chem. B*, 1997; **101**: 3800–3805.

[4] Bonanni, B, Bizzarri, AR, and Cannistraro, S, *J. Phys. Chem. B*, 2006; **110**: 14574–14580.

[5] Brust, M, Walker, M, Bethell, D, Schiffrin, DJ, and Whyman, R, *J. Chem. Soc., Chem. Commun.*, 1994: 801–802.

[6] (a) Chambrier, I, Cook, MJ, and Russell, DA, *Synthesis*, 1995: 1283-1286. (b) Moeno, S, Antunes, E, and Nyokong, T, *J. Photochemistry Photobiology A: Chemistry*, 2011; **222**: 343-350.

[7] Revell, DJ; Chambrier, I.; Cook, MJ; Russell, DA, *J. Mater. Chem.*, 2000; **10**: 31–37.

[8] Enes RF; Cid J-J; Hausmann, A; Trukhina, O; Gouloumis, A; Vázquez, P; Cavaleiro, JAS; Tomé, AC; Guldi, DM; Torres, T; *Chem. Eur. J.*, 2012; **18**: 1727.

[9] Davidenko, NA, Spitsyna, NG, Lobach, AS, Breusova, MO, Kalashnikova, IP, Kostenko, LI, Get'manchuk, YP, Mokrinskaya, EV, Gumenyuk, LN, Chuprina, NG, Pavlov, VA, Studzinskii, SL, *High Energy Chem.*, 2008; **42**: 45–50.

[10] Khalid, W, el Helou, M, Murböck, T, Yue, Z, Montenegro, JM, Schubert, K, Göbel, G, Lisdat, F, Witte, G, and Parak, WJ, *ACS Nano*, 2011; **5(12)**: 9870-9876.

[11] Zhao, X, Kong, A, Shan, C, Wang, P, Zhang, X, Shan, Y, *Catal. Lett.*, 2009; **131**: 526.

[12] Wöhrle, D, Baziakina, N, Suvorova, O, Makarov, S, Kutureva, V, Schupak, E, and Schnurpfeil, G, *J. Porphyrins Phthalocyanines*, 2004; **8**: 1390-1401.

[13] Kumada M, Tamao K, Sumitani K, *Organic Synthesis, Coll.* 1988; **6**: 407

[14] Cuellar EA, Marks TJ, *Inorg. Chem.* 1981; **20**: 3766

[15] Iqbal Z, Lyubimtsev A, Hanack M, *SYNLETT*, 2008; **15**: 2287

[16] Breuer, T, Klues, M and Witte, G, *J. Electron. Spectrosc. Relat. Phenom.*, 2015; **204**: 102-115.

***Journal of Porphyrins and Phthalocyanines format**

6.5 Imido Vanadium(IV) and Imido Chromium(IV) Phthalocyanine Complexes: Synthesis, Spectroscopy and Theoretical Investigations

Malcolm A. Bartlett, Elisabeth Seikel and Jörg Sundermeyer

Imido Vanadium(IV) and Imido Chromium(IV) Phthalocyanine Complexes: Synthesis, Spectroscopy and Theoretical Investigations

Manuscript in preparation

Title: *Imido Vanadium(IV) and Imido Chromium(IV) Phthalocyanine Complexes: Synthesis, Spectroscopy and Theoretical Investigations*

Authors: Malcolm Alan Bartlett, Elisabeth Seikel and Jörg Sundermeyer

Philipps-Universität Marburg, Hans-Meerwein Str 4, 35032

Abstract

The coordination of imido vanadium(IV) and imido chromium(IV) moieties $[M(NR)]^{2+}$ by the ubiquitous phthalocyanine (Pc) ligand is described for the first time. Vanadium(V) imido precursors can be reductively inserted in the Pc cavity of [K_2Pc], while oxidative azide addition and N_2 elimination to [PcCr(II)] gives the corresponding imido chromium complexes. Axial imido ligation causes a moderate red-shift of the Pc ligands' optical absorption, which is more pronounced for vanadium complexes. Structures for all complexes were elucidated by DFT methods, which found an unexpected non-linear M=N–C bond angle for chromium complexes. NBO analysis revealed that unpaired electrons on chromium preventing bonding *via* a second π orbital between imido ligands and chromium(IV) in contrast to vanadium(IV) imido complexes.

Introduction

Metallo-phthalocyanine complexes are one of the most important classes of metal-organic chromophores,[1] given their huge versatility in both low- and high-tech applications, from simple pigments in paints, thermoplastics and fabrics, to semiconductors in organic field effect transistors (OFETs),[2] photosensitizers in dye-sensitized solar cells (DSSCs)[3] and optical limiters in non-linear optical materials (NLOs).[4] The phthalocyanine (Pc) ligand is readily synthesized by the reductive cyclotetramerization of four phthalic acid derivatives, typical phthalonitriles. Moreover, many different organic groups can be attached to the phthalonitrile prior to cyclotetramerization to afford the corresponding Pc derivative, of which there exist a huge variety of reported examples in the literature. The Pc ligand is also capable of coordinating almost all d-block metals, metalloids and many p-block elements, which opens the possibility for the coordination of additional ligands at the coordinatively unsaturated metal centre. This property has been exploited to use phthalocyanines in molecular wires,[5] photoactive therapeutics,[6] photosensitisers in renewable energy production[7] and catalysis.[8] Even the presence of a dipole induced by the axial PcM–X

ligand can have a significant effect on the ordering of Pc films.[9] Despite the myriad of new applications that axial ligation can have, comparatively little work has done in this area compared to modifications of the Pc ligand itself. We previously reported the synthesis of several imido metal phthalocyanine ([PcM(NR)]) complexes of early transition metals using both aliphatic and aromatic imido ligands.[10] Imido ligands are capable of stabilising various metal oxidation states, and imido metal complexes have already been shown to be effective catalysts for olefin polymerisation reactions,[11] ring opening of epoxides,[12] aziridines[13] and cyclopropanation of olefins.[14] For instance, it was shown how [PcTi(NR)] complexes effectively catalysed metathetical carbodiimide synthesis from isocyanates.[10, a)]

Chromium phthalocyanine ([PcCr]) is an attractive compound for axial modification because of the different oxidation states that the central metal ion can have, as has been recently demonstrated by the group of Leznoff.[15] For the analogous chromium porphyrin complexes, oxidation states from +2 to +6 are known, which allow the complexes to undergo both photooxidation and photoreduction reactions at the metal centre.[16] Phthalocyanine, with its increased range of light absorption compared to porphyrin, is therefore a very attractive ligand to use with chromium. [PcCr] has also been shown to function as a Lewis-acid catalyst[17] and as an oxidation catalyst;[8] reactivity being located at the central metal ion. The redox active nature of the chromium ion was further demonstrated by the ability of [PcCr] complexes to oxidatively react with organolithium reagents to form complexes of the type [PcCr(Alk)].[18] In contrast, there are few different oxidation states known for vanadium phthalocyanine, although its activity as an oxidation catalyst has been shown several times.[19] In most phthalocyanine complexes of vanadium reported contain the highly stable vanadyl ion, i.e. vanadium(IV) with an axial oxo-ligand (V=O). In this publication, we describe our recent progress in synthesizing imido chromium and vanadium Pc complexes, with particular attention to their structural and electronic properties. In these complexes, both V and Cr are in the +4 oxidation state, and are thus in the $[Ar]d^1$ and $[Ar]d^2$ electron configuration, respectively. It is therefore of interest to understand how this difference affects the coordination of the axial imido ligand and the potential reactivity at the metal centers.

Results and Discussion

Synthesis

Despite the similarities between the chromium and vanadium complexes, very different strategies were required for their synthesis. For the vanadium complexes, two separate

methods were developed. In previous publications, we have described the synthesis of [PcM(NR)Cl] complexes, where M is Mo, W or Re[10b,c], using imido metal chloro complexes as templating reagents for a cyclotetramerization reaction. Alternatively, the metal-imido moiety was inserted into the cavity of a preformed and deprotonated Pc ligand. For the vanadium complexes, both of the above strategies could be used to obtain the desired [PcV(NR)] complexes. When using a [V(N*t*Bu)Cl_3] to template Pc synthesis, vanadium is reduced from V(V) to V(IV). In this way, it also acts as a strong chlorinating reagent so that, according to FD MS analysis, mono-, di-, tri-, and tetra-chlorination of the Pc ligand occurs, while no un-chlorinated Pc complex is observed. Addition of a radical scavenger, such as 2-methylnaphthalene, to the reaction mixture prevents multiply chlorinated species from forming, but the mono-chlorinated species is still formed in large yield. Synthesis of non-chlorinated [PcV(NtBu)] is possible when [V(NtBu)Cl_3] is first reduced using Mg turnings, as described by Preuss *et al.*;[20] the addition of a chlorine radical scavenger is still necessary. A simpler procedure was found by coordinating [V(NR)Cl_3] with [K_2Pc] to obtain the desired [PcV(NR)] complexes in good yields. This does not however represent a simple salt-elimination reaction, as there is a concomitant reduction of V(V) to V(IV) by [K_2Pc] as the reducing agent. This is clear from the EPR spectrum obtained for [PcV(NDip)], which shows the typical eight line spectrum for ^{51}V (I = 7/2) and has a g_{iso} value of 1.9906, which is typical for V(IV) Pc complexes. These two methods for the synthesis of [PcV(NR)] complexes are shown in Scheme 1.

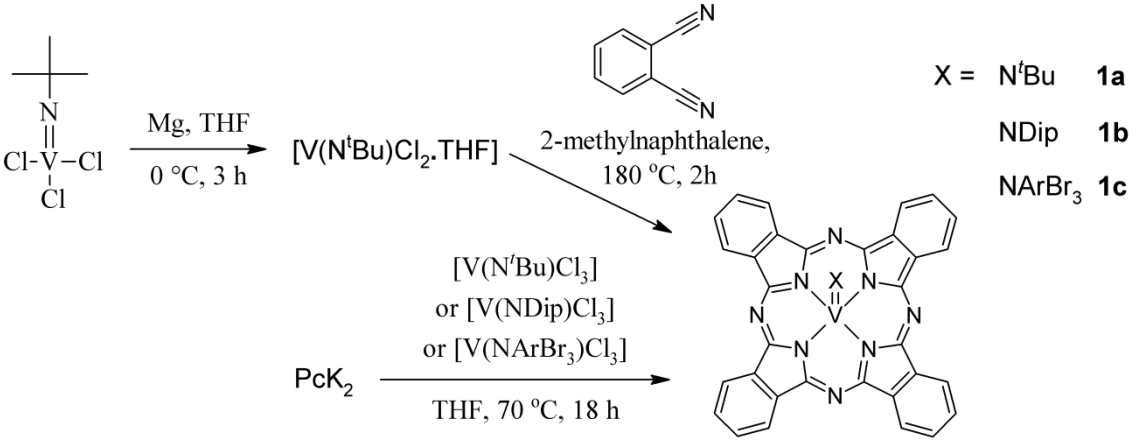

Scheme 1: Alternative methods for the synthesis of PcV(NR) complexes. Top: tetracyclization reaction using a reduced V(NR)Cl_n template. Bottom: reductive insertion of V(NR)Cl_3 into K_2Pc.

In contrast, a completely different strategy that makes use of the redox active nature of chromium in [PcCr] proved to be successful for the synthesis of [PcCr(NR)] complexes. Addition of ArN_3 to a solution of [PcCr] results in the oxidation of Cr(II) to Cr(IV) and the simultaneous reduction of the azide, as evidenced by the generation of gas during the reaction, with the result that [PcCr(NR)] complex is formed in good to moderate yield. Surprisingly though, the addition of TsN_3 did not result in the formation of [PcCr(NTs)], but rather SO_2 was also lost, so that [PcCr(NTol)] was formed instead. The solution changes colour during the reaction from purple to blue and the products are obtained as blue solids. The synthesis of [PcCr(NR)] complexes is shown in Scheme 2.

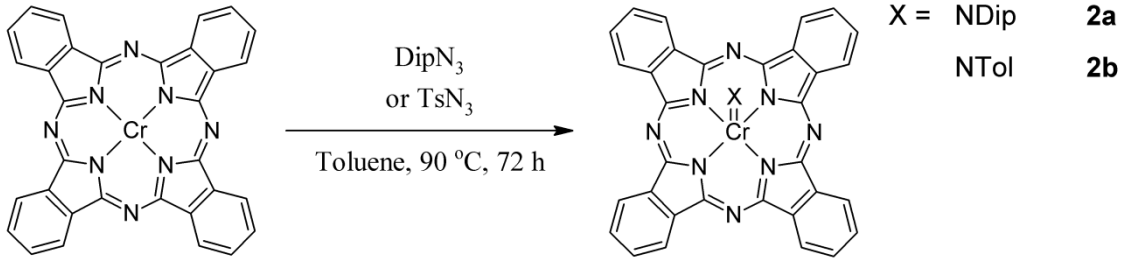

Scheme 2: Oxidative addition of RN_3 to [PcCr] to form [PcCr(NR)].

UV-Vis Spectroscopy

For vanadium complexes, aromatic imido ligands cause a red-shift of 12-13 nm compared to the aliphatic imido ligand. This same effect has been seen for imido molybdenum phthalocyanine and porphyrazine complexes previously synthesized in our group.[10] Additionally, there is little difference in the Q-band absorption maxima between the NDip and $NC_6H_2Br_3$ ligands. There are two possibilities for the observed red-shift, *viz.* either the electron density at the vanadium centre is significantly different so as to affect the electron density on the Pc ligand, or the axial aromatic groups are interacting with the aromatic π-system of the Pc ring. Considering that the Q-band absorption maximum is almost identical for the two aromatic imido ligands, despite them having very different electron donating or withdrawing groups, the second possibility is the more likely cause of the red-shift. A similar effect has been observed upon axial coordination of neutral and anionic ligands to zinc(II)porphyrin complexes, where axial ligation always results in a red-shift of the

absorption spectra, the magnitude of which depends upon the charge and polarizability of the axial ligand.[21]

Comparison of the [PcM(NDip)] complexes of V and Cr shows that the Q-band absorption maximum is red-shifted by a modest 4 nm for V compared to Cr. This is not surprising, considering the similar electronegativites of the two metals and that they are both in the same 4+ oxidation state. Figure 1 shows the UV-Vis absorption spectra for the [PcCr(NR)] and [PcV(NR)] complexes discussed here; absorption maxima of the Q-band region are given in Table 1.

Table 1: Absorption maxima of the Q-band region for the [PcCr(NR)] and [PcV(NR)] complexes.

Complex (solvent)	λ (nm)		
[PcCr(NTol)](CNP)	683	653 (sh)	614
[PcCr(NDip)](CNP)	686	634 (sh)	619
[PcV(N^{t}Bu)] (DCM)	676	645	610
[PcV(NDip)] (DCM)	690	654	631
[PcV(N-2,4,6-$Br_3C_6H_2$)] (DCM)	689	656	623

Theoretical Calculations

To better understand the bonding situation for the complexes, the gas phase optimizations of the geometries were performed for the comparable complexes [PcV(NDip)] and [PcCr(NDip)]. Optimized geometries show the typical planar structure for a Pc ligand, the central metal ion being displaced from the plane of the Pc ligand (Figure **2**). As expected from previously synthesis imido vanadium complexes,[22] there is an almost linear V–N–C bonding angle of 179.97º for both [PcV(N-2,4,6-Br_3-C_6H_2)] and [PcV(NDip)]. Unexpected, however, is the nonlinear Cr–N–C bonding angle of 142.1º for the imido chromium complex. This divergence from linearity was seen before for several [$Cr(NR)_2Cl_2$] complexes previously synthesized in our group[23] and was ascribed to steric repulsion between substituents on the imido ligands. This cannot be the case here, though, given the almost perfect linear structure of the corresponding [PcV(NDip)] complex.

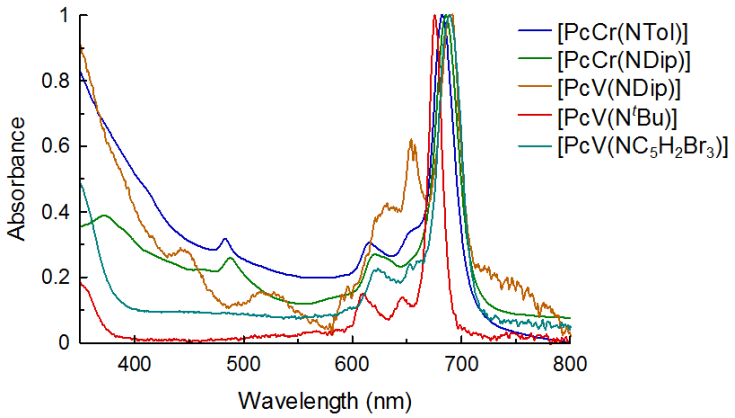

Figure 1: UV-Vis absorption spectra for [PcV(NR)] and [PcCr(NR)] complexes measured in DCM and chloro-naphthalene, respectively.

Natural bond order (NBO) analysis of the [PcV(NDip)] and [PcCr(NDip)] showed that the linear V–N–C axis had a M–N triple bond character, while that for Cr–N–C had only a double bond character (Figure **2**). The imido nitrogen bonds *via* a hybrid sp orbital to the vanadium d_{z2} orbital, and through the p_x and p_y orbitals to the vanadium's d_{xz} and d_{yz} orbitals, respectively. The unpaired electron is predicted to be in the d_{x2-y2}, and so does not interact with the V–N bonding, although this is not the typical location for unpaired electron on V(IV).[24]

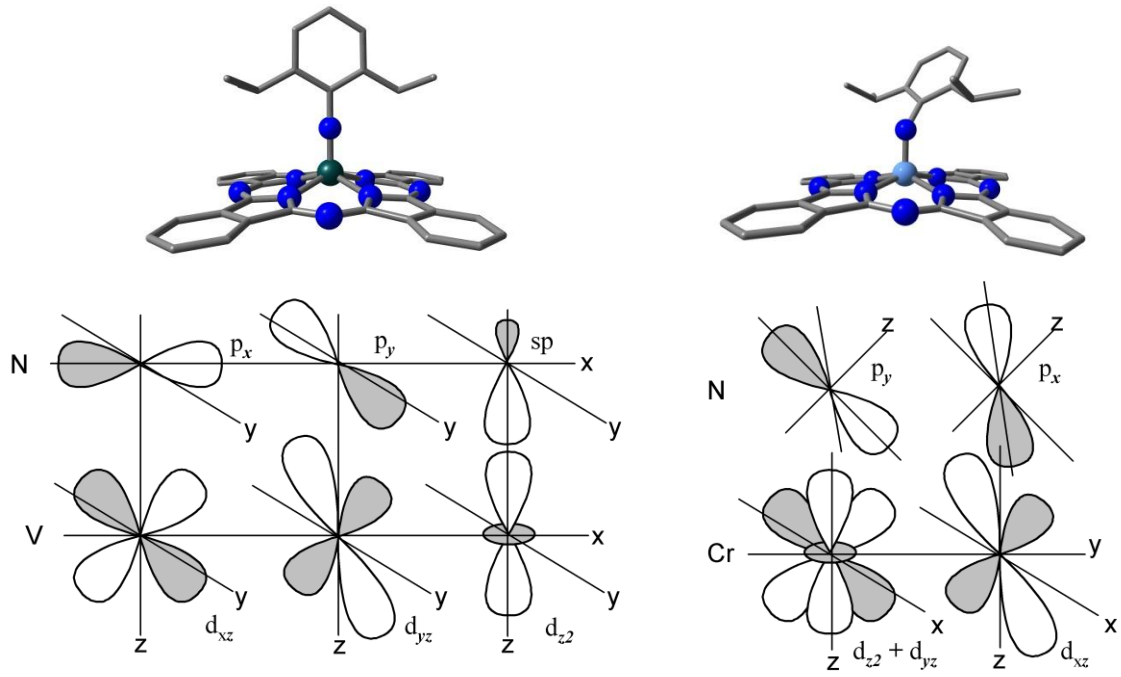

Figure 2: DFT optimized geometries for [PCV(NDip)] (left) and [PcCr(NDip)] (right), and the calculated M–N bonding in each complex shown below the respective complexes.

In the non-linear Cr–N–C bond, the imido nitrogen bonds via three π-dative orbital interactions, where the N p_x orbital interacts with the Cr d_{xz} orbital, and the N p_y orbital interacts with both the Cr d_{yz} and d_{z2} orbitals. The Cr d_{yz} and d_{z2} orbitals are also the location of the two non-bonding electrons on d^2 Cr(IV), and are the postulated reason for the bent Cr–N–C bond angle. The orbitals diagrams for both the V–N and Cr–N bonds are shown in Figure 2.

TDDFT calculations at the B3LYP/6-311G(d) level of theory revealed that the strong (Q-band) transitions in the experimentally observed spectra are the result of a π→π* transition from the HOMO-1 to the LUMO and LUMO+1 (Figure 3). These MOs are located over the expected regions of the Pc ligand, and do not involve the metal ion or imido ligand. In the case of Cr complexes, where the M=N-Ar angle is not linear, the LUMO and LUMO+1 are

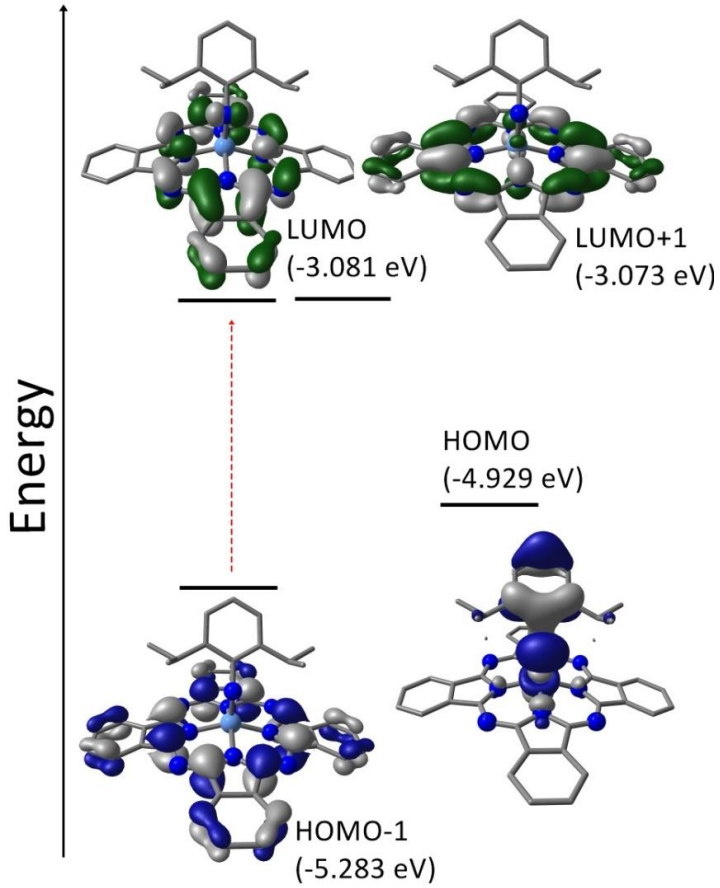

Figure 3: Electronic transitions from the HOMO-1 to the LUMO/LUMO+1 that give rise to the Q-band absorption in [PcCr(NDip)]. The HOMO is isolated on the metal-arylimido moiety, and is consequently not involved in the Q-band transition.

non-degenerate. This is probably due to the asymmetry caused by the aromatic ring. The HOMO is located on the central metal-aryl imido moiety for both vanadium and chromium complexes, and does not participate in the electronic transitions of these complexes. The MOs involved in the Q-band transition and the HOMO are shown for [PcCr(NDip)] in Figure 3.

Conclusions

The synthesis of imido vanadium(IV) and imido chromium(IV) phthalocyanine complexes can be accomplished using several different strategies, depending on the metal used. For [PcV(NR)] complexes, radical chlorination of the Pc ligand at elevated temperatures required that the starting material, [V(NR)Cl_3] be either pre-reduced using magnesium or alternatively inserted into preformed [K_2Pc] ligand cavity. The redox activity of [PcCr] enabled it to be oxidized with an organic azide to give the resulting [PcCr(NR)] directly. UV-Vis spectroscopy shows that the Pc ligands' Q-band maxima are red-shifted for all imido metal Pc complexes, with a slightly stronger shift for vanadium compared to chromium, as well as for aromatic compared to aliphatic imido ligands. This trend can be explained by the electropositive character of the central metal ion and the interaction of the aromatic imido ligands' π-system. DFT calculations of the optimized geometries for the [PcM(NDip)] complexes predict a linear and bent M–N–C(imido) angle for the vanadium and chromium complexes, respectively. This effect is explained by NBO analysis, which show that unpaired electrons on chromium prevent triple bond formation from occurring between the imido ligand and the chromium(IV) ion so that only a double bond can form, which is in contrast to the vanadium complexes, where the unpaired electron localized on the dz^2 orbital does not interfere with V–N single, double or triple bond formation.

Experimental

Methods and Materials

NMR spectra were obtained on a Bruker AVANCE 300 spectrometer. Chemical shifts are reported in δ (ppm) values. ^{1}H and ^{13}C NMR values were referenced to residual solvent as an internal standard. Mass spectra (MS) were recorded on either a Thermo Fischer Scientific LTQ-FT Ultra or on a Bruker Biflex III-Spectrometer. UV-Vis spectra were recorded on a Varian Cary Eclipse 5000. FTIR spectra were measured using a Bruker Alpha Platinum ATR single reflection diamond spectrometer. Theoretical calculations were performed on the MaRC2 computing cluster using the Gaussian 09 software package.[25]

The synthesis of vanadium(V) tert-butyl imido trichloride and vanadium(V) "Ar" imido trichloride were described previously.[2223] K_2Pc[2326] was synthesised by deprotonating H_2Pc using Schlosser's base.[2427]

Syntheses

General procedure: salt elimination reaction with [K_2Pc]

[K_2Pc] (0.210 g: 0.36 mmol) was dissolved in THF (60 ml) and stirred for 60 min before filtering the solution through Celite® onto [V(NR)Cl_3] (1.3 eq). The resulting solution was stirred overnight at 50 ºC. The solution was then filtered through Celite® to remove insoluble components. Volatiles were then removed *in vacuo* to leave a dark blue powder, which was washed with toluene and hexane before being dried at 60 °C at 10^{-3} mbar.

[PcV(N*t*Bu)]: Mass obtained: 0.148 g. Yield: 65 %. Elemental Anal.: Calc. (Found) C: 68.93% (68.14%), H: 2.90% (3.97%), N: 16.48% (19.86%). MS (MALDI-TOF): *m/z* = 633.9 $[M]^+$, 618.9 [M-(Me)]$^+$, 574.5 [M-(*t*Bu)]$^+$. MS (APCI-HRMS): *m/z* = 635.1736 $[M+H]^+$, Calc. for $C_{36}H_{26}N_9V$: 635.1745. UV/Vis (DCM): λ/nm = 698 (s), 665 (sh), 635 (w). FTIR**:** $\bar{\nu}$/cm^{-1} = 1606 (w), 1499 (m), 1438 (m), 1333 (w), 1313 (m), 1276 (m), 1157 (w), 1117 (m), 1066 (m), 1001 (s), 947 (m), 872 (m), 778 (m), 753 (m), 729 (s).

[PcV(NDip)]: Mass obtained: 0.156 g. Yield: 59 %. Elemental Anal.: Calc. for $C_{44}H_{33}N_9V$ (Found): C: 69.10% (71.54%), H: 2.89% (4.50%), N: 17.19% (17.06%). EPR (chloronaphthalene/toluene 1:3, 40 K): g_{iso} = 1.9906. MS (MALDI-TOF): *m/z* = 737.7 $[M]^+$, 574.5 [M-(Dip)]$^+$. MS (APCI-HRMS): *m/z* = 739.2372 $[M+H]^+$, Calc. for $C_{44}H_{34}N_9V$: 739.2371. UV/Vis (CNP): λ/nm = 699 (s), 668 (sh), 631 (w). FTIR: $\bar{\nu}$/cm^{-1} = 1608 (w), 1497 (m), 1416 (m), 1331 (s), 1286 (m), 1259 (m), 1159 (w), 1117 (s), 1074 (s), 1001 (s), 896 (m), 799 (m), 752 (m), 725 (m).

[PcV($NC_6H_2Br_3$)]: Mass obtained: 0.144 g. Yield: 45 %. MS (APCI-HRMS): *m/z* = 892.8731 $[M+H]^+$, Calc. for $C_{38}H_{18}Br_3N_9V$: 892.8714. UV-Vis (DCM):689 (s), 656 (sh), 623 (w).

Mono-chlorinated phthalocyanine vanadium(tert-butyl imido) [(ClPc)V(NtBu)]

[V(N*t*Bu)Cl_3] (0.055 g; 0.241 mmol), PN (0.160 g; 1.25 mmol) and 2-methylnaphthalene (0.185 g: 1.30 mmol) were mixed together in dichlorobenzne (5 ml) and heated at 190 ºC for 2 h. Hexane was then added, and the solids that formed were collected by filtration and washed with hexane before being dissolved in DCM and purified by column chromatography (silica/DCM). Only one major product was obtained that was identified as the monochlorinated species by MS (FD+). MS (FD+): Calc. for $C_{36}H_{24}N_9ClV$ $[M]^+$: 668.1277; Found: 668.1269.

Phthalocyanine vanadium(tert-butyl imido) [PcV(NtBu)]

[V(N*t*Bu)Cl_3] (0.050 g; 0.22X mmol) was mixed with Mg(s) (0.030 g; 1.30 mmol) in THF (40 ml) and stirred at rt for 15 h. The solution colour rapidly changes from yellow to green, and then gradually to dark brown by the end of the reaction. Solvent was removed *in vacuo* to leave a dark brown solid, which was subsequently dissolved in DCM and filtered through a glass frit (G4). Solvent was removed and the solids were redissolved in DCB. This solution was added to a mixture of PN (0.155 g; 1.21 mmol) and 2-methylnaphthalene (0.174 g; 1.22 mmol); the resulting solution was heated at 190 ºC for 3 h. Volatiles were then removed *in vacuo* and the dark blue solid remaining was extracted with DCM and purified by column chromatography (silica/DCM). Mass obtained: 0.103 g. Yield = 71 %. MS (HR-FD): m/z = 634.16606 $[M^+]$; Calc. for $C_{36}H_{25}N_9V$: 634.16726.

General Procedure for phthalocyanine chromium(imido)([PcCr(NR)]) complex synthesis

1.0 eq of [PcCr] and 2.0 eq of ArN_3 were added to toluene. The resulting suspension was heated at 90 ºC for 3 days, during which time constant gas evolution was observed. Volatiles were removed *in vacuo*, and the remaining solids were washed with pentane and THF before being dried (100 ºC; 10^{-3} mbar). A violet powder was thus obtained.

[PcCr(NDip)]: Mass obtained 56 mg. Yield = 42 %. Elemental Anal.: Calc. for $C_{44}H_{33}N_9Cr$ (Found): C: 61.16% (71.44%), H: 3.66% (4.50%), N: 14.73% (17.04%). MS (MALDI-TOF): *m/z* = 737.7 $[M]^+$, 574.5 $[M\text{-}(Dip)]^+$. MS (APCI-HRMS): *m/z* = 740.2342 $[M+H]^+$, Calc. for $C_{44}H_{34}N_9Cr$: 740.2337. UV/Vis (CNP): λ/nm = 677 (s), 363 (s). FTIR: $\bar{\nu}/cm^{-1}$ = 2959 (w), 1609 (w), 1558 (w), 1488 (m), 1412 (m), 1330 (s), 1259 (m), 1162 (m), 1117 (s), 1080 (s), 899 (m), 800 (w), 751 (m), 720 (s), 569 (w).

[PcCr(NTol)]: Mass obtained 112 mg. Yield = 49 %. Elemental Anal.: Calc. for $C_{39}H_{23}N_9Cr$ (Found): C: 63.97% (69.95%), H: 3.76% (3.46%), N: 16.82% (18.82%). MS(APCI-HRMS): *m/z* = 669.1475 $[M+H]^+$, Calc. for $C_{39}H_{24}N_9Cr$: 669.1477. UV-Vis (CNP): λ/nm = 682 (s), 616 (sh), 346 (s). FTIR (ATR): $\bar{\nu}/cm^{-1}$ = 1608 (w), 1488 (m), 1412 (m), 1330 (s), 1248 (m), 1201 (w), 1162 (m), 1117 (s), 1077 (s), 936 (m), 900 (w), 868 (m), 800 (w), 753 (m), 726 (s), 559 (w).

Supporting Information

Copies of FTIR and mass spectra are given for the complexes synthesized.

References

[1] D. Wöhrle, G. Schnurpfeil, S. Makarov, O. Suvora, *Chem. unserer Zeit*, **2012**, *46*, 12-24.

[2] J. Zaumseil, H. Sirringhaus, *Chem. Rev.*, **2007**, *107*, 1296−1323.

[3] L. Martín-Gomis, F. Fernández-Lazaro, Á. Sastre-Santos, *J. Mater. Chem. A*, **2014**, *2*, 15672-15682.

[4] (a) G. de la Torre, P. Vazquez, F. Agullo-Lopez, T.J. Torres, *Mater. Chem.*, **1998**, *8*, 1671-1683. (b) S.M.O. Flaherty, S.V. Hold, M.J. Cook, T. Torres, M. Hanack, W. Blau, *J. Adv. Mater.*, **2003**, *15*, 19-32. (c) G. de la Torre, P. Vazquez, F. Agullo-Lopez, T. Torres, *Chem. Rev.* **2004**, *104*, 3723-3750. (d) M. Hanack, T. Schneider, M. Barthel, J.S. Shirk, S.R. Flom, R.G.S. Pong, *Coord. Chem. Rev.*, **2001,** *219*, 235-258.

[5] V. N. Nemykin, A. A. Purchel, A. D. Spaeth and M. V. Barybin, *Inorg. Chem.*, **2013**, *52* (19), 11004–11012

[6] J.-D. Huang, S. Wang, P.-C. Lo. W.-P. Fong, W.-H. Ko and D. K. P. Ng, *New J. Chem.*, **2004**, *28*, 348-354.

[7] (a) H.B. Gobeze, T. Tram, C.B. KC, R.R. Cantu. P.A. Karr, F. D'Souza, *Chin. J. Chem.*, **2016**, *34*, 969-974. (b) C.B. KC, F. D'Souza, *Coordination Chemistry Reviews*, **2016**, *322*, 104-141; (c) K.-C. Lin, L. Wang, T. Doane, A. Kovalsky, S. Pejic andC. Burda, *J. Phys. Chem. B*, **2014**, *118*, 14027-14036.

[8] A.B. Sorokin, *Chem. Rev.*, **2013**, *113* (10), 8152–8191.

[9] a) L. Fernandez, S. Thussing, A. Mänz, J. Sundermeyer, G. Witte and P. Jakob, *Phys. Chem. Chem. Phys.*, **2017**, *19*, 2495–2502; b) A. Lerch, L. Fernandez, M. Ilyn, M. Gastaldo, M. Paradinas, M. A. Valbuena, A. Mugarza, A. B. M. Ibrahim, J. Sundermeyer, U. Hofer and F. Schiller, *J. Phys. Chem. C.*, **2017**, *121*, 25353–25363.

[10] (a) W. Darwish, E. Seikel, R. Kasmarker, K. Harms, J. Sundermeyer, *Dalton Trans.* **2011**, *40*, 1787-1794. (b) W. Darwish, E. Seikel, K. Harms, O. Burghaus, J. Sundermeyer *Dalton Trans.*, **2011**, *40*, 1183-1188. (c) E. Seikel, B. Oelkers, O. Burghaus, J. Sundermeyer, *Inorg. Chem.*, **2013**, *52*, 4451-4457.

[11] (*a*) M. P. Coles and V. C. Gibson, *Polym. Bull.*, 1994, **33**, 529; (*b*) M. P. Coles, C. I. Dalby, V. C. Gibson, W. Clegg and M. R. J. Elsegood, *J. Chem. Soc., Chem. Commun.*, 1995, 1709; (*c*) M. P. Coles, C. I. Dalby, V. C. Gibson, I. R. Little, E. L. Marshall, M. H. Ribeiro da Costa and S. Mastroianni, *J. Organomet. Chem.*, 1999, **591**, 78; (*d*) V. C. Gibson, *Eur. Pat. Appl. EP 641804 A2*BP Chemicals Ltd., UK, 1995; (*e*) U. Siemeling, L. K¨ olling, A. Stammler, H.-G. Stammler, E. Kaminski and G. Fink, *J. Chem. Soc., Chem. Commun.*, 2000, 1177; (*f*) M. Schopf, J. Sundermeyer, J. Kipke, K. A. Rufanov, W. Heitz, U. Peucker, *EP1200453* (*B1*), Basell Polyolefine GmbH, 2003; (*g*) M. Schopf, J. Sundermeyer, J.Kipke,K.A.Rufanov,W. Heitz,U. Peucker, *WO 01/09148* (*A1*), Elenac GmbH, 2001; (*h*) V. R. Jensen and K. J. Børve, *Organometallics*, 2001, **20**, 616.

[12] W.-H. Leung, E.K. F. Chow, M.-C. Wu, P. W. Y. Kumand L.-L. Yeung, *Tetrahedron Lett.*, 1995, **36**, 107.

[13] W.-H. Leung, M.-T. Yu, M.-C. Wu and L.-L. Yeung, *Tetrahedron Lett.*, 1996, **37**, 891.

[14] D. Jan, F. Simal, A. Demonceau, A. F. Noels, K. A. Rufanov, N. A. Ustynyuk and D. N. Gourevitch, *Tetrahedron Lett.*, 1999, **40**, 5695.

[15] W. Zhou, J.R. Thompson, C.L. Leznoff, D.B. Leznoff, *Chem. Eur. J.*, **2016**, *23*(10), 2323-2331.

[16] D.M. Roundhill, *Photochemistry and Photophysics of Metal Complexes*, Plenum Press, New York, 1994.

[17] K. Suda, S.-I. Nakajima, Y. Satoh, T. Takanami, *Chem. Commun.*, **2009**, 1255-1257.

[18] (a) J.E. Lyons, P.E. Ellis, *Applied Catalysis A: General*, **1992**, *84*(2), L1-L6. (b) A. Junkaew, J. Meeprasert, B. Jansang, N. Kungwan, S. Namuangruk, *RSC Adv.*, **2017**, *7*, 8858-8865.

[19] W. Zhou, D.B. Leznoff, *Chem. Commun.*, **2018**, *54*, 1829-1832.

[20] F. Preuss, E. Tabellion, G. Overhoff, and G. Reiss, *Z. Anorg. Allg. Chem.*, **2000**, *626*, 1665-1675.

[21] M. Nappa and M. Valentine, *J. Am. Chem. Soc.*, **1978**, *100*, 5075-5080.

[22] J.K.F. Buijink and J. H. Teuben, *Organometallics*, **1994**, *13*, 2922–2924.

[23] K.A. Rufanov, J. Kipke and J. Sundermeyer, *Dalton Trans.*, **2011**, *40*, 1990-1997.

[24] T. S. Smith II, R. LoBrutto and V. L. Pecoraro, *Coord. Chem. Rev.*, **2002**, *228*, 1–18.

[25] M. J. Frisch, G. W. Trucks, H. B. Schlegel, G. E. Scuseria, M. A. Robb, J. R. Cheeseman, G. Scalmani, V. Barone, B. Mennucci, G. A. Petersson, H. Nakatsuji, M. Caricato, X. Li, H. P. Hratchian, A. F. Izmaylov, J. Bloino, G. Zheng, J. L. Sonnenberg, M. Hada, M. Ehara, K. Toyota, R. Fukuda,J. Hasegawa, M. Ishida, T. Nakajima, Y. Honda, O. Kitao, H. Nakai, T. Vreven, J. A. Montgomery Jr., J. E. Peralta, F. Ogliaro, M. Bearpark, J. J. Heyd, E. Brothers, K. N. Kudin, V. N. Staroverov, T. Keith, R. Kobayashi, J. Normand, K. Raghavachari, A. Rendell, J. C. Burant, S. S. Iyengar, J. Tomasi, M. Cossi, N. Rega, J. M. Millam, M. Klene, J. E. Knox, J. B. Cross, V. Bakken, C. Adamo, J. Jaramillo, R. Gomperts, R. E. Stratmann, O. Yazyev, A. J. Austin, R. Cammi, C. Pomelli, J. W. Ochterski, R. L. Martin, K. Morokuma, V. G. Zakrzewski, G. A. Voth, P. Salvador, J. J. Dannenberg, S. Dapprich, A. D. Daniels, O. Farkas, J. B. Foresman, J. V. Ortiz, J. Cioslowski and D. J. Fox, *Gaussian 09, Revision C.01*, Gaussian, Inc., Wallingford CT, 2010.

[26] a) P. A. Barrett, C. E. Dent and R. P. Linstead, *J. Chem. Soc.*, **1936**, 1719–1736; b) J. A. Cissell and T. P. Vaid, *Inorg. Chem.*, **2007**, *46*, 4360–4361.

[27] M. Schlosser, J. Hartmann, *Angew. Chem. Int. Ed.*, **1973**, *12*, 508–509.

6.6 Control of Intramolecular Electron Transfer in Perylene Dihydrazides and Perylene Diimides: A Comparative Study by Time-Resolved Spectroscopy

Robin C. Döring, Eduard Baal, Malcolm A. Bartlett, Christian Prinzisky, Remco W.A. Havenith, Jörg Sundermeyer and Sangam Chatterjee

Control of Intramolecular Electron Transfer in Perylene Dihydrazides and Perylene Diimides: A Comparative Study by Time-Resolved Spectroscopy

Cornell University Library: arXiv:1612.05046v1 [physics.chem-ph]

Control of Intramolecular Electron Transfer in Perylene Dihydrazides and Perylene Diimides: A Comparative Study by Time-Resolved Spectroscopy

Robin C. Döring[1], Eduard Baal[2], Malcolm A. Bartlett[2], Christian Prinzisky[2], Remco W. A. Havenith[3,4], Jörg Sundermeyer[2,*], and Sangam Chatterjee[1,5,*]

[1]Faculty of Physics and Materials Sciences Center, Philipps-Universität Marburg, Renthof 5, D-35032 Marburg, Germany

[2]Faculty of Chemistry and Materials Sciences Center, Philipps-Universität Marburg, Hans-Meerwein-Straße, D-35032 Germany

[3]Zernike Institute for Advanced Materials, Stratingh Institute for Chemistry, University of Groningen, Nijenborgh 4, NL-9747 AG Groningen, The Netherlands

[4]Ghent Quantum Chemistry Group, Department of Inorganic and Physical Chemistry, Ghent University, Krijgslaan 281 (S3), B-9000 Gent, Belgium

[5]Institute of Experimental Physics I, Justus-Liebig-University Giessen, Heinrich-Buff-Ring 16, D-35392 Giessen, Germany

ABSTRACT Electron transfer (ET) in molecular donor-acceptor dye systems is crucial for charge transport in organic semiconductors. Classically, rates should decrease with increasing donor-acceptor distance while the microscopic mechanism is more complex and shows intricate dependencies on the excitation conditions. In this paper, we introduce highly soluble *N,N'*-dialkylperylenedihydrazides (PDH) – perylene dyes with a dialkylamino -NR_2 donor functionality directly bonded to both of their imide nitrogen atoms. We compare the PDH ET dynamics with a group of classical *N,N'*-dialkylperylenediimides (PDI) equipped with a -NR_2 donor linked to the PDI acceptor core *via* alkyl chains with a varying number of methylene -(CH_2)- groups, thus at distinctly different distances. Special physicochemical design features of our study objects include, i) amine moieties as donor group to minimize spin-orbit coupling, ii) substitution solely at both imide positions to avoid major impact on HOMO and LUMO levels and distortions of the PDI backbone, and, iii) control of donor-acceptor separation by non-conjugated alkyl groups to exclude any additional effects due to delocalized π electron systems. All materials show non-single-exponential photoluminescence decay dynamics. An analytically solvable three-level system is employed to explain the photoluminescence decay dynamics. Additionally our findings indicate ET efficiency across the intramolecular interface strongly depends on the surplus excitation energy.

Perylene derivatives such as the perylenediimides (PDIs) where initially synthesized in the 1910's. From the 1950's onward, they found a broad range of industrial dye applications, *e.g.* as high-grade pigments in industrial applicationns such as automotive finishes.[1] Since these early days, PDIs have developed into one of the most valuable material classes of organic electronics.[2-4] They have proven their value as versatile building blocks for functional opto-electronic supramolecular architectures.[5,6] Recently, advanced uses in contactless pH measurements, as metal cation sensors[7],and as active layers in organic photovoltaics (OPV) have been proposed.[8]

Beyond their technological benefit, PDIs are also model systems for charge and energy transport studies. Their high thermal and photochemical stability along with their preferable spectral range and electron acceptor properties favor such fundamental investigations.[6] For example, such systems provide insight into the time scales for charge generation by exciton dissociation and competing relaxation processes such as photoluminescence (PL), internal conversion (IC) or intersystem crossing (ISC). The intricate interplay between the different relaxation channels should be controllable by the chromophore type, its set of push (donor) and pull (acceptor) substituents and, in particular, by the supramolecular assembly of these organic semiconductor systems.

In general, perylene core substituents at either the bay- (1-, 6-, 7-, 12-) or the headland-/ortho- (2-, 5-, 8-, 11-) positions govern the triplet energy levels, the triplet quantum yields, and the potential to undergo carrier multiplication, *e.g.*, by singlet fission (SF). Recently, such multiple exciton generation is reported in slip-stacked thin-films of ortho-phenyl-substituted PDIs[9] and it is also expected to occur in rigidly linked dimers.[10] Rapid ISC with up to 53 % yield in heavy-atom-free, bay-substituted PDIs is observed in solution and attributed to vibronically assisted spin-orbit coupling.[11] The intrinsic $S_1 \rightarrow T_1$ ISC efficiency of unsubstituted PDIs, however, is below 1 %.[3] Hence, its phosphorescence has only recently been reported in a glassy butyronitrile matrix containing methyl iodide at 77 K.[12] Consequently, triplet formation is not expected to play a major role in the excited-state dynamics of core-unsubstituted PDIs.

While a vast number of publications investigated core- and imide-*N*-substituted PDIs, only very few focus on perylenedihydrazides (PDHs). Early works used PDHs as fluorescence sensors for different organic targets.[13-15] More recent studies focus on nitrogen-nitrogen covalently linked multichromophore PDI systems. Utilizing a short fluorophore-fluorophore distance, nitrogen-nitrogen linked perylene and naphthalene imide dyads and triads are used as model systems for the investigation of (single-)molecular wires and intramolecular energy transfer.[16-19] Their use as dyes in p-type dye sensitized solar cells leads to a sharp increase of solar cell efficiency: the formation of dye-localized long-lived charge separated states enabled increased hole injection.[20-23] Unfortunately, planar PDIs are not yet able to compete with fullerenes as electron transporting materials despite their high electron mobility, thermal stability, and structural variety. This is mainly due to their strong tendency to form aggregates that reduces the overall charge separation and global transport.[24]The aggregation tendency was overcome by covalently linking PDIs *via* an imide nitrogen-nitrogen bond, which results in a perpendicular fluorophore orientation and therefore a reduced tendency for molecular stacking. The resulting im-

proved material properties make nitrogen-nitrogen linked PDIs a promising alternative to fullerenes.[24-27]

In this paper, we present the hydrazinolysis of PTCDA with *N,N*-dialkylhydrazines leading to new and soluble PDHs. We focus on the electron transfer across molecular-scale internal-interfaces between the amino moiety and the perylenecore in PDIs and PDHs with direct nitrogen-nitrogen linkage. Three different routes to control the electron transfer rate are employed: i) variation of the orbital energies of the introduced donor moiety by means of protonation and methylation, ii) variation of the (electron) donor – acceptor distance, and iii) variation of the excitation energy used in the optical experiments. In all cases, we use time-resolved photoluminescence as a direct probe for the population decay of the lowest-energy bright transition $S_1 \rightarrow S_0$. A careful analysis of the transient luminescence dynamics reveals the presence of a shelving reservoir (SR) state interacting with the bright $S_1 \rightarrow S_0$ transition. This is manifested in intrinsic deviations from the commonly reported single-exponential photoluminescence decay.[28, 29]

The basis of these experiments is tailored samples which enable systematic investigations. We are able to obtain the smallest possible donor-acceptor distance at the imide position, *i.e.*, a direct nitrogen-nitrogen bond by using unsymmetrical *N,N*-dialkylhydrazines as donor-bearing moieties. Alkyl chains of increasing length control the spatial nitrogen-nitrogen separation and reveal the distance dependence of the photophysical properties. We chose electronically isolating and non-conjugating bridge units instead of the commonly used phenyl groups. This eliminates the potential influence of their conjugated π-electron systems which, themselves, provide rich carrier dynamics. The imide position of the PDIs is selected for substitution due to the presence of a node in the MOs of the PDIs ground state and excited state.[5] This further reduces the orbital overlap and electronic interactions and, thereby, presumably also the rate of electron transfer.[5]

Scheme 1. Synthetic route and chemical structures of the studied **PDH-1** and **-2**, **PDI-1** to **-4**, the corresponding protonated **H_2PDH-1** and **-2**, **H_2PDI-2** to **-4** and methylated **Me_2PDI-2**[a].

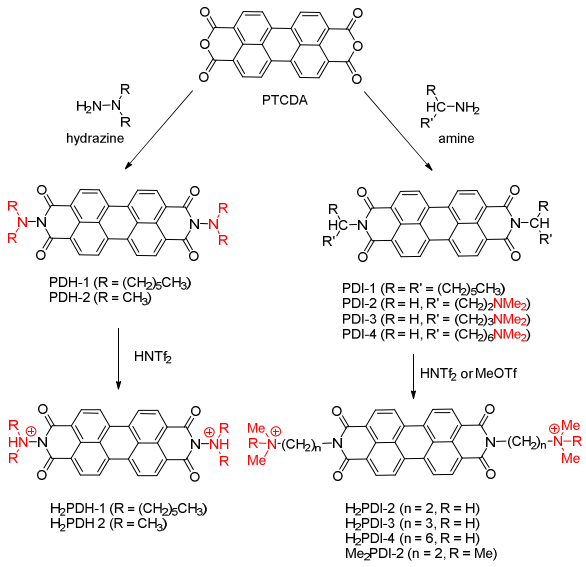

[a] Reagents and conditions: **PDH-1**, **PDH-2**, and **PDI-1 - PDI-4**are synthesized in molten imidazole at 130 °C and purified by column chromatography. Protonated **H_2PDH-1, H_2PDH-2,** and **H_2PDI-2** to **H_2PDI-4**are obtained from the corresponding PDHand PDIby reaction with bis(trifluoromethane)sulfonimide($HNTf_2$) in toluene.

Two series of samples are synthesized for this comprehensive study: PDHs with a nitrogen-nitrogen bond (no spacer) and dimethyl amino-alkyl-substituted PDIs with different alkyl spacer lengths, an ethylene (C_2), a propylene (C_3) and a hexylene (C_6) chain (Scheme 1). Highly soluble **PDH-1** was obtained from *N,N*-dihexylhydrazine and PTCDA. **PDH-2** was synthesized accordingly as a model system. For the protonation we chose the weakly coordinating bistriflimide (TFSI) anion to ensure a minimum of ionic interactions. The synthetic procedure is described in the Methods Section and Supporting Information.

We investigate the influence of protonation on the spectroscopic properties of the individual molecules dissolved in organic solvents. Therefore, we first turn to **PDH-1**. This new compound is related to the well-known reference compound, the "swallow tail" **PDI-1**.[31] In **PDH-1**, a [=CH-] unit of **PDI-1** is formally substituted by [=N-]. Generally, all samples under study have numerous spectroscopic properties in common: The spectral signatures, as obtained by absorption and steady-state fluorescence, barely differ, *cf.* Figure 1a) and Figure 5a). In line with literature[32], the absorption maximum is located at 2.36 eV (526 nm) for all samples, when dissolved in chloroform ($CHCl_3$). The typical absorption-emission mirror symmetry is observed, owing to the Franck-Condon principle. Three vibronic progressions of the fundamental transition are observed, spaced equidistantly by ~170 meV. They are associated with a family of intramolecular C-C vibrations which couple to the optical transitions in these types of aromatic molecules. The relatively small Stokes shift of ~40 meV (8 nm) between the absorption and emission maxima indicates that the reorganization energy and changes in geometry are negligible for optical transitions. Hence, the perylene backbone governs the optical properties of the samples despite the chemical substitutions at the imide positions. This behavior is expected as the substituents are linked to the backbone in a non-conjugating manner. The influence that donor moieties linked by conjugated bridges have on the optical properties has been extensively studied.[31-33] The minor spectral shift of 30 meV (*cf.* Figure 1b) for samples dissolved in acetonitrile (MeCN) is attributed to a change of the dielectric constant due to the higher polarity of MeCN, compared to $CHCl_3$.

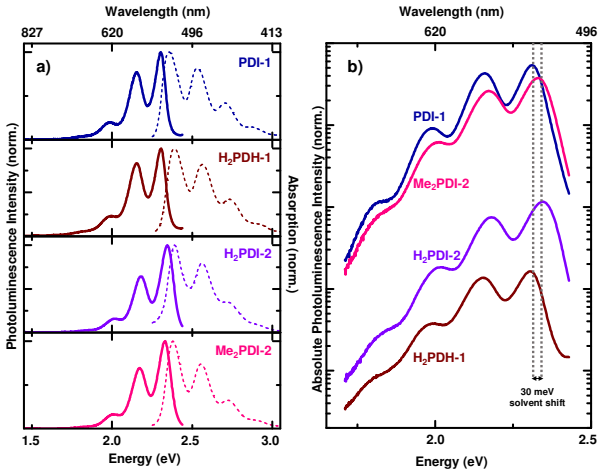

Figure1. (a) Normalized absorption (dashed) and photoluminescence (solid) spectra of **PDI-1**(as reference), **H_2PDH-1, H_2PDI-2** and **Me_2PDI-2**. (b) Absolute photoluminescence of the same samples on a semi-logarithmic scale.

However, the photoluminescence quantum yield (PLQY) of **PDH-1** is almost zero (<1 %), while **PDI-1** shows a near-unity quantum yield (> 90.0 %). Upon protonation of the hydrazide $–NR_2$ group, making protonated dication **H_2PDH-1** isoelectronic to **PDI-1**, the PLQY shows only a negligible change. The quantum yields and photoluminescence lifetimes of **H_2PDI-2** (ϕ=10.3 %) deviate from

those of **PDI-2** (ϕ=5.4 %) The PLQY improves by a factor of two, accompanied by a lifetime increase by a factor of four (*cf.* Table 3). For the methylated compound, **Me$_2$PDI-2**, the situation is drastically changed. Its PLQY as well as the mono-exponential lifetime almost match that of reference **PDI-**1.

The protonation is expected to increase the oxidation potential of the donating amine, lowering the relative energy of the donor-located molecular orbital (MO) below that of the acceptor highest molecular orbital (HOMO), thus making electron transfer thermodynamically unfavorable. However, we observe only a minor increase of the PLQY for e.g. **H$_2$PDH-1**.

One possible explanation could be a partial deprotonation upon excitation as it has been observed in excited state hydrogen transfer processes.[(a] A second explanation is the nonradiative decay from $a^1\pi\sigma^*$ excited state to the ground state[(b,c)], which is observed in many N-heterocylces with acidic protons that are present in the protonated perylenes under study. To disentangle the influence of both mechanisms we perform different methods of analysis.

IR spectroscopy reveals a hydrogen bond for protonated perylenes, which is indicated by a weaker C-O bond of the neutral perylenes (Figure SX /Table SX). Protonation of **PDIs 2-4** has a small but still distinct influence on the C-O bond, while the hydrogen bonding in **H$_2$PDH-1** is especially strong, leading to the weakest recovery of PLQY upon protonation.

We used **H$_2$PDH-2** as model compound to further investigate the hydrogen bonding in the crystal structure, since **H$_2$PDH-1** has a very low tendency to crystallize due to its long alkyl chains. In the crystal structure, an intramolecular hydrogen bond between the acidic proton and the carbonyl oxygen is found, which is confirmed by slightly longer carbonyl bonds for the participating carbonyl moieties. This hydrogen bond locks the conformation and results in a perpendicular orientation of the dimethylamino moiety to the perylene core and a minimalized steric repulsion. DFT calculations also reveal that a perpendicular amine orientation with a hydrogen bond is the energetically most favorable structure (*cf.* inset in Figure 4). With these findings, a reversible elongation and possibly breaking of the hydrogen bond along the N-H-O bond, instead of a intermolecular deprotonation, is reasonable, making **H$_2$PDH-1** a "intramolecular photoacid". In such a situation the hydrogen would be oxygen and not nitrogen centered. Further insight is gained by identifying the redox potentials. Therefore, we investigated the electrochemical properties by cyclic voltammetry (CV). **PDH-1** shows two reversible reduction peaks as does reference **PDI-1**. While CV only shows one oxidation potential for **PDH-1**, like for **PDI-1**, differential pulse voltammetry (DPV) reveals an additional oxidation potential $E_{oxd,1}$ for **PDH-1** at 1.59 V, 0.2 V lower than E_{Oxd} of **PDI-1**and $E_{Oxd,1}$ of **PDH-1,** which are almost identical. The first oxidation potential is therefore assigned to the oxidation of the amine moiety and the second potential $E_{Oxd,2}$ to the oxidation of the aromatic core, which is observed for **PDI-1** as well. This results in a $E_{Oxd,2} - E_{Red,1}$ difference of 2.46 V for **PDH-1** (see Figure S8), which is identical to the $E_{Oxd,1} - E_{Red,1}$ of **PDI-1** and indicates that the ground state (GS) of the amine moiety is energetically higher than the π orbital of the aromatic core, in good agreement with our DFT calculations. The observation of the second oxidation potentials in **PDI2-4** is desired but limited by the electrochemical window of the solvent. For **H$_2$PDH-1** no second oxidation potential is observed, which can be explained by the lower energy of the protonated amine moiety. No redox potentials of deprotonated perylenes are observed. Figure 3 shows the CV data of the reference compound **PDI-1** as well as those of **PDH-1** and **H$_2$PDH-1** in dichloromethane (DCM) Further evidence is provided when considering the respective ratios of PLQYs, $\frac{\Phi(H_2PDH-1)}{\Phi(PDH-1)} \approx \mathbf{1}$and $\frac{\Phi(H_2PDI-2)}{\Phi(PDI-2)} \approx \mathbf{2}$, of the protonated and unprotonated version of **PDH-1** and **PDI-2**, respectively. If de-protonation was the origin, the ratios should be approximately the same. However, as also evidenced by the IR measurements, hydrogen bonding becomes less likely with increasing distance between nitrogen and carboxyl. This is reflected by the fact that protonation is more effective for the fluorescence recovery for the sample bearing a C_2-spacer (**H2PDI-2**). Combining IR and CV measurements, we assume that the absent recovery of PLQY in **H$_2$PDI-1** is caused by the hydrogen bond.

Table 1. Half-Wave redox potentials of PDHs and PDI-1 given in V *vs.* SCE.

	$E_{Red,2}$(V)	$E_{Red,1}$(V)	$E_{Oxd,1}$(V)	$E_{Oxd,2}$(V)	$E_{Oxd,1-Red,1}$(V)
PDH-1	-0.87	-0.67	1.59	1.79[a]	2.26
H$_2$PDH-1	-	-0.12	1.92	-	2.04
H$_2$PDH-1[b]					2.14
PDI-1	-0.84 (0.83)[b]	-0.64 (0.62)[b]	1.82 (1.77)[b]	-	2.46 (2.39)[c]

Potentials are calculated with E(Fc/Fc+) = +0.46 V*vs.* SCE in DCM and with E(Fc/Fc+) = +0.40 V*vs.* SCE in MeCN.[34a]Determined by DPV in DCM. [b] Values determined in DCM. Absolute oxidation and reduction potentials were not determined because a reaction of **H$_2$PDH-1** with the internal standard ferrocene occurs.[c] Taken from literature.[35]

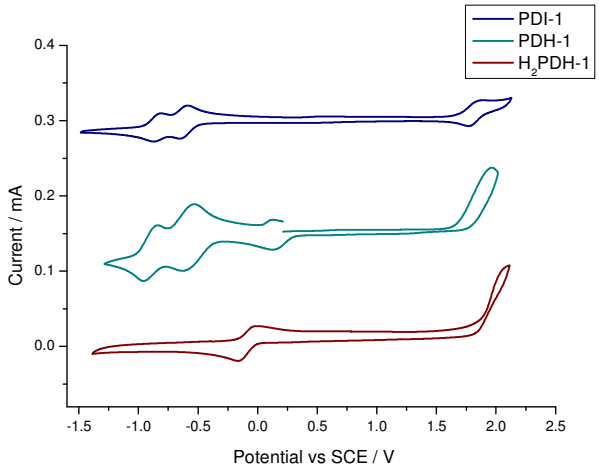

Figure 3. CV data of **PDI-1**, **PDH-1** and **H$_2$PDH-1** measured in DCM versus SCE.

Our assignment of the oxidation potentials is supported by DFT and TDDFT calculations for the neutral and dicationic compound. The results show that the MO associated with the terminal amine moiety (HOMO) is energetically intermediate to the aromatic π (HOMO-1) and π* (LUMO) orbitals of the perylene core. However, protonation stabilizes the nitrogen located MO to a level below that of the aromatic π orbital. These results also show how fluorescence quenching is expected to be energetically favored for the neutral compound but not for the protonated one. Figure 4 summarizes the results of these calculations.

Additional proof for our assumptions is given by investigating methylation of the donor group. Firstly, this should virtually ex-

clude even the slightest de-protonation in an equilibrium due to the stable bond between the amine and the methyl group. For the same reason, methylation should also prevent hydrogen bonding. Unfortunately, even the strongest methylation agent MeOTf did not yield *N*-methylated PDHs in refluxing 1,2-dichloroethane (12h, 80°C). Hence, neither **PDH-1** nor **PDH-2** are obtained as methylated species. (*cf.* Scheme 1). Instead we compare three related samples: the neutral sample **PDI-2**, as well as protonated **H_2PDI-2** and methylated **Me_2PDI-2**. As mentioned earlier, the PLQY of **Me_2PDI-2** almost matches that of **PDI-1**.

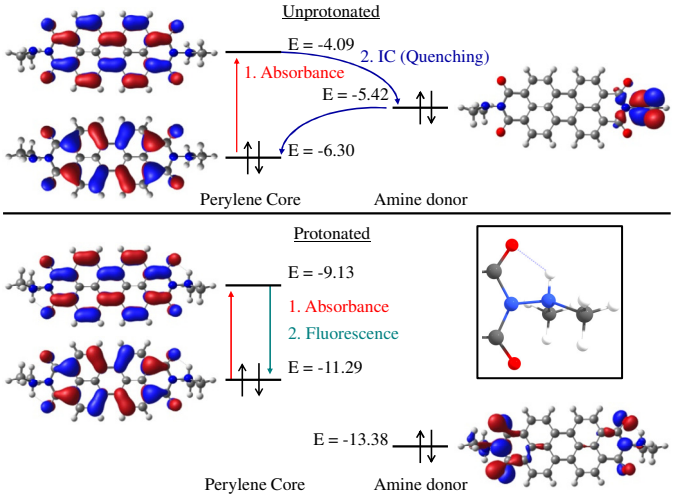

Figure 4. MO energy level diagram based on the S_1 excited state B3LYP/6-31G* calculated for **PDH-2** and **H_2PDH-2**showing the effect of protonation upon the amine donor MO. Protonation stabilizes the amine MO and energetically favors fluorescence rather than internal conversion. Energies are given in eV. Inset: hydrogen bond.

Systematically varying the distance between the nitrogen and the amino donor moiety provides further insight into the electrontransfer dynamics. Therefore, we use a series of samples with spacers introduced in between the nitrogen-nitrogen pairs of the reference compounds **PDH-1** and **PDH-2**. The spacers are alkyl chains of two, three and six methylene (–CH_2–) groups for **PDI-2**, **PDI-3**, and **PDI-4**, respectively.

The CV data allows us to extract the change in Gibbs free energy of the charge separation ΔG_{CS} using the redox potentials (complete data given in the Supporting Information) and the calculated donor-acceptor distances in the equation developed by Weller (eq 1).[36] The change in Gibbs free energy ΔG_{CS} is determined relative to the energy level of the PDI S_1 ($E_{0,0}$) which is obtained in the optical measurements.

$$\Delta G_{CS} = e(E_{ox} - E_{red}) - E_{0,0} - \frac{e^2}{4\pi\varepsilon_0\varepsilon_s R_{ee}} - \frac{e^2}{8\pi\varepsilon_0}\left(\frac{1}{r_+} + \frac{1}{r_-}\right)\left(\frac{1}{\varepsilon_{ref}} - \frac{1}{\varepsilon_s}\right). \quad (1)$$

E_{red} is attributed to the first reduction potential and E_{ox} to the first oxidation potential. $E_{0,0}$ is the energy of the $S_1 \rightarrow S_n$excited state, R_{ee} is the edge to edge distance which corresponds to the nitrogen-nitrogen distance determined from DFT calculations. These values are only the upper limit of the donor-acceptor distance, since DFT calculations show stretched alkyl chains. ε_{ref} is the dielectric constant of the solvent in the electrochemical measurements and is ε_s the dielectric constant of the solvent used in the photophysical measurements ($CHCl_3$ for neutral PDIs and MeCN for charged PDIs); r^+ and r^- are the ionic radii of the amino cation and the PDI-anion (estimated 200 nm for the cation and 471 nm for the anion[37]).

Table 2. Estimates for the Gibbs free energy ΔG_{CS} for the formation of a charge separated state relative to $E_{0,0}$.

	$E_{0,0}$(eV)	R_{ee}(pm)	ΔG_{CS}(eV)
PDH-1	2.305	143	-1.64
PDH-2	2.329	143	-1.43
PDI-2	2.302	373	-0.34
PDI-3	2.304	458	-0.37
PDI-4	2.297	797	0.08

ε ($CHCl_3$) = 4.81, ε (DCM) = 8.93, ε(MeCN) = 37.5

The results of the calculation indicate that the $S_1 \rightarrow$ **CSS** decay becomes more favorable with decreasing donor-acceptor distances. While for **PDH-1** and **PDH-2** (no alkyl spacers) energy of the CSS is well below that of the S_1 state. For C_2 and C_3, alkyl spacer bearing **PDI-2** and **PDI-3** the energy win is given but lower than for PDHs. In the case of **PDI-4** decay to the CSS even becomes energetically unfavorable. This formation of CS states suggests a PL quenching. Note that the Gibbs free energy for **PDI-4** is calculated assuming a stretched alkyl chain. Calculations using shorter donor-acceptor distances for **PDI-4** result in a more favorable CS with $\Delta G_{CS} = -0.14$ eV (for $R_{ee} = 500$ pm) and emphasize the importance of the donor-acceptor distance on the formation of the CS state.

These findings agree with the optical measurements. As shown in Figure 5, all samples show virtually identical absorption spectra, similar to the first series shown in Figure 2. Spectral shapes and positions again show no effect on the appendage of substituents. However, the quantum yields depend heavily on the distance between perylene backbone and donating amines (illustrated in Figure 5b which shows the absolute emission intensities of **PDH-1** and **PDI-1** – **PDI-4**). The addition of the amine groups and their electron lone electron pairs invoke a drop in PL intensity (and in quantum efficiency) of more than two orders of magnitude compared to **PDI-1**. The systematic introduction of alkyl chains as spacer units leads to a recovery of the quantum efficiencies. Eventually, **PDI-4** with a C_6 spacing unit reaches efficiencies of about 0.64, even in its unmasked neutral form.

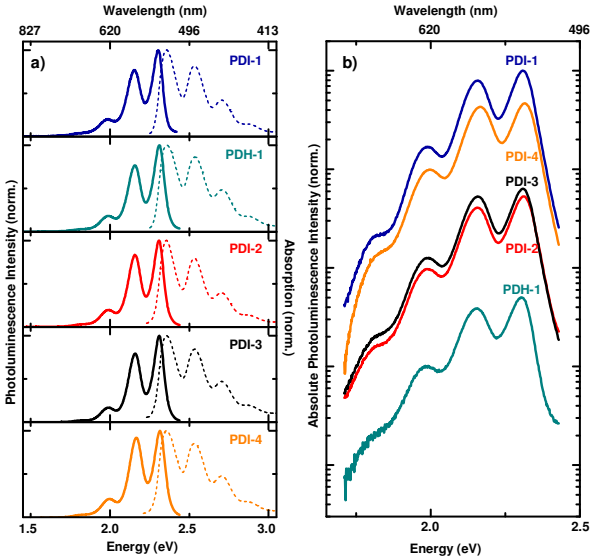

Figure 5. (a) Normalized absorption (dashed) and photoluminescence (solid) spectra of **PDI-1 – PDI-4** and **PDH-1**. (b) Absolute photoluminescence of the same samples on a logarithmic scale.

Time-resolved photoluminescence measurements provide further insight into the temporal dynamics of the population of the emissive S_1 state. Characteristic decay profiles are shown in Figure 6b). The reference compound **PDI-1** shows a single-exponential decay as is expected due to its virtually exclusively radiative decay. Drastic deviations from this behavior are found for the amino-substituted compounds. Samples **PDH-1**, **PDI-2** and **PDI-3** no longer show single-exponential behavior but rather more complex dynamics which are well-described bi-exponentially. While the initial decay (t_{fast}) is fastest for **PDH-1**, the lifetime recovers for larger distances and is almost single-exponential again for sample **PDI-4**, incorporating the longest (C_6) spacer.

Table 3. Spectroscopic properties of the studied samples. Photoluminescence Quantum Efficiencies (Φ_{PL}) and decay times measured by time-resolved photoluminescence. All values for E_{exc} = 2.8 eV

	Solvent	Φ_{PL}(%)	t_{fast}(ps)	t_{slow}(ps)	A_{fast}	A_{slow}	R^2
PDI-1	$CHCl_3$	> 90.0	3908 ± 92 (= t_{Ref})		0.83[a]		0.98
PDH-1	$CHCl_3$	0.5	18 ± 0	269 ± 26	0.929 ± 0.007	0.068 ± 0.002	0.98
PDI-2	$CHCl_3$	5.4	59 ± 0	1345 ± 14	0.837 ± 0.003	0.144 ± 0.001	1
PDI-3	$CHCl_3$	6.1	132 ± 1	729 ± 20	0.951 ± 0.005	0.092 ± 0.006	1
PDI-4	$CHCl_3$	64.0	591 ± 122	2179 ± 374	0.271 ± 0.116	0.715 ± 0.115	1
H_2PDH-1	$CHCl_3$	0.5	30 ± 1	2090 ± 529			
H_2PDI-2	MeCN	10.3	254 ± 87	6368 ± 561			
Me_2PDI-2	MeCN	89.0	3472 ± 84				

[a] Value is not 1 because of offset before time-zero caused by "backsweeping" effect in the streak camera.

As already mentioned, CV measurements and theoretical calculations indicate that an electron transfer from the amine is responsible for the PL quenching. More precisely, the molecule rapidly decays from its S_1 state to the radical anion ($PDI^{\bullet-}$) charge separated state (CSS). In accordance with previous reports, we assign the fast quenching gives a figure for the rate of electron transfer and thus decay to the CSS.[28,29,38] As the intrinsic radiative lifetime is expected to be unchanged for all samples, the k_{CS} is corrected by the lifetime of reference **PDI-1**:

$$k_{CS} = 1/t_{PL} - 1/t_{Ref} \qquad (2)$$

This yields the rate of charge separation in the case of mono-exponential photoluminescence decay (*i.e.* **Me_2PDI-2**). Consequently, the quantum yields recover along with the lifetimes, indicating that increased distance not only actually affects the electron transfer rate but also its efficiency.

The observation of a non-single-exponential behavior for **PDH-1** and **PDI-3** – **PDI-4** can have various physical origins. The majority of which can be excluded due to careful measures taken during the experiments. Table 4 summarizes all possible non-intrinsic mechanisms, which lead to such an observed long-lived component. Dependencies on experimental conditions and observable effects respective mechanisms would show are also given. Additionally, the ^{1}H-NMR spectra (Supporting Information Figure S1 to S4) rule out sample contaminations by another soluble PDI-specimen which then could provide the long-lived photoluminescence component. Aggregation as an explanation for a non-single-exponential behavior seems unlikely for **PDH-1**, since a strong structural similarity to **PDI-1** is given. Moreover, the respective amplitudes of the fast and slow decay component vary for the different samples, showing generally an increased A_{slow}/A_{fast} ratio with increasing spacer length (*cf.* Table 3).

Table 4. Non-intrinsic mechanisms leading to non-single-exponential decay dynamics.

Mechanism	Dependency		
	Sample Concentration	Excitation power	Spectral shift
FRET	++	o	0
Two-Photon absorption	o	++	o
Multi-electron excitation (same or consecutive pulse)	o	++	o
Aggregation	++	o	++
Dimerization	o	o	++

"o": minor effect; "+": intermediate effect; "++": strong effect

The decay dynamics provide further insight into the ET dynamics of individual molecules as bimolecular or other aggregation effects and other extrinsic origins are excluded: varying the excitation fluence and concentrations in the sample solutions over several orders of magnitude provide identical results. Intriguingly, the PL decay is non-single-exponential for all samples.

This infers the existence of an additional, reservoir, state in the molecule feeding the bright transition: the emission from an optical two-level system of localized states will always yield a single-exponential decay. Adding a second, possibly non-radiative decay channel again results in a single exponential decay. The combined decay rate in the law of decay is given by the sum of the two individual rates ($1/t_{combined} = 1/t_1 + 1/t_2$). Consequently, an additional reservoir needs to be involved to invoke a bi-exponential decay. A bi-exponential decay will result exclusively from the independent population of this reservoir, which is able to feed the originally considered emissive state. Taking into account this mathematical fact sheds new light on the obtained experimental results.

The CSS is a viable candidate for the proposed shelving state. Photoinduced charge separation is accompanied by the reverse process. This re-population of the emissive state leads to the observed bi-exponential photoluminescence decay, the CSS acting as shelving state. Following the method of Lor *et al.* the three rates k_{CS}, k_{rCS} and k_{CR}(*c.f.* Figure 6) can be obtained from the two lifetimes t_{fast} and t_{slow} and the ratio A_{fast}/A_{slow} of the respective amplitudes. The value for k_{PL} is taken from the inverse mono-exponential lifetime $1/t_{Ref}$ of reference **PDI-1**.The obtained rate constants are given in Table 3. A clear dependence of the k_{CS} and k_{rCS} on the donor-acceptor distance is observed, both increasing with distance. The fact thatk_{CS} and k_{rCS} are correlated and not anti-correlated is intriguing at first. A possible explanation is that the forward and reverse charge-separation both occur at or near the Marcus optimum regime and thus activation-less. In this case the electron transfer rate is mainly governed by the electronic contribution and will decrease exponentially with donor-acceptor distance. The previous assumption is partially supported by the temperature-dependent measurements of **PDH-1** in a poly(methyl methacrylate) (PMMA) matrix (Figure S10). The spectral and temporal emission characteristics are temperature-independent in the range from 10-300 K, again indicating that the activation of CS is barrier-less. However, the very large ΔGibbs of **PDH-1** argues against this interpretation, at least for the aforementioned sample. Finally, for the rate for charge recombination k_{CR} we observe far lower dependence on the donor-acceptor distance.

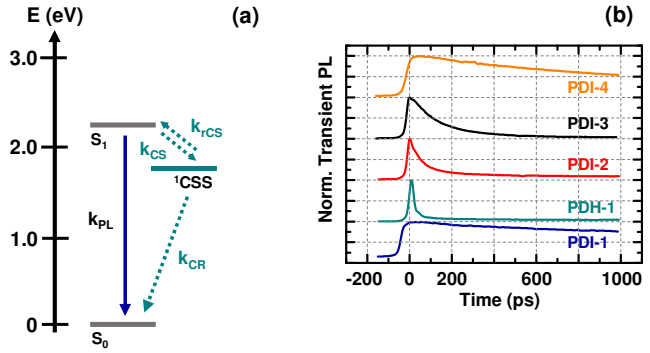

Figure 6. (a) Proposed energy level diagram for the decay of the excited S_1 state.(b) Transients of the reference sample **PDI-1** as well as the samples from the distance-series, **PDH-1** and **PDI-2** – **PDI-4**, respectively.

Femtosecond transient Absorption (fsTA) measurements were carried out to further elucidate the excited state dynamics. All samples commonly share the bleaching of the ground state at 2.36 eV (525 nm) and an induced absorption at 1.75 eV(710 nm). The induced absorption has been attributed to excited state $S_1 \rightarrow S_X$ absorption (ESA)of the PDI core[cite].

Intriguingly, no distinct $PDI^{\bullet-}$ induced absorption signal is observed. The CV measurements and theoretical considerations suggest such a state should be present. Also the lifetime of the CSS as determined by the analysis of the PL decay show that charge recombination is slow enough for $PDI^{\bullet-}$to be observable. However it can be assumed that the absorption of *PDI resembles that $PDI^{\bullet-}$ because the energy of the LUMO is widely unchanged regardless whether it is occupied by one or by two electrons [**cite Gosztola 2000**]. Indeed, steady-state spectro-electrochemical measurements range the $PDI^{\bullet-}$absorption between1.77 eV (715 nm) and 1.84 eV (675 nm)[**cite Gosztola 2000; Salbeck 1989; Weiser 2015; Kircher 1999**]. Thus the energies overlap with those of the ESA of *PDI. However, no broadening or shoulder around the ESA feature is observed, the end-of-pulse spectra look identical for all samples, **PDH-1** forming the only exception .For **PDH-1**within the first 2 ps after excitation a shoulder at 1.91 eV (650 nm) appears in the high energy flank of the ESA. For the other samples charge recombination appears to be much faster than the respective separation and thus no significant population can accumulate.

Finally, we explored the dependence of the photoluminescence decay and, therefore, the electron transfer rate constants (k_{CS}), on the excitation photon energy. Four different excitation energies are used in time-resolved measurements, 2.5 eV, 2.8 eV, 3.3 eV, and 4.5 eV (*cf.*Figure 7a). Pumping at 2.5 eV and 2.8 eV excites the system into the S_1 electronic state, while the higher-lying singlet states, denoted S_X, are excited with excitation photon energies of 3.3 and 4.5 eV. The CS rates of all samples peak at 2.8 eV excitation energy. They subsequently decrease again for higher and lower excitation energies, respectively. **PDI-4** shows only a very weak dependence. This is probably owed to the overall low CS rate; the quantum yield already approaches that of **PDI-1**. The initial increase of k_{CS} is most pronounced for **PDH-1**. For an excitation with 2.8 eV the system is transferred to a higher vibrational sublevel of the S_1 state (compared to $E_{exc} = 2.5$ eV). Thus, relaxation time from the excited vibrational sublevel to the emissive vibrational-ground level is elongated. Additionally the surplus excitation vibrational energy might facilitate the transition to the CSS and thus increase the charge transfer rate and efficiency. Both mechanisms would lead to the observed increased k_{CS} value, while at the same time PL intensity is reduced. Vibrational relaxation within the S_1 excited state of perylene in solution has been measured to occur on a timescale of 30 ps, very well on a timescale comparable to $1/k_{CS}$ of **PDH-1**.[40]For**PDI-2** – **PDI-4**k_{CS}($E_{exc} = 2.5$ eV) is lowered, compared to **PDH-1**. The dependence of $1/k_{CS}$ on the excited vibrational level within the electronic S_1 state is a lot less pronounced. To explain the successive decrease of k_{CS} for $E_{exc} = 3.3$ eV and$E_{exc} = 4.5$ eV, we must pay attention to the behavior of donor-free **PDI-1**.

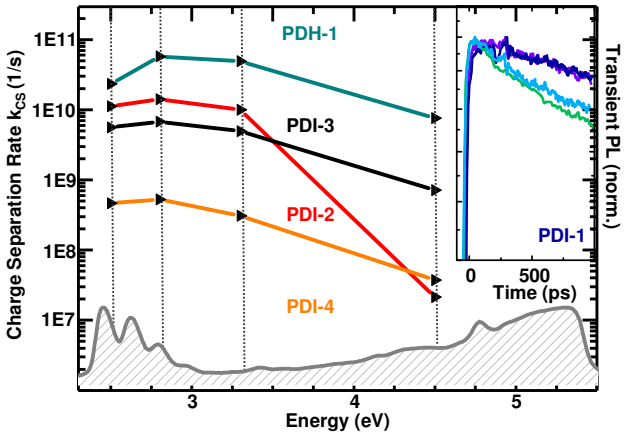

Figure 7.(a) Logarithmic plot of the Charge Separation Rate determined by TRPL measurements for samples **PDH-2** (squares), **PDI-2** (circles), **PDI-3** (up-pointing triangles) and **PDI-4** (down-pointing triangles). The dashed vertical lines indicate the respective excitation energies into the S_1 and higher energy S_X absorption regions. *Inset*: Excitation energy dependence of the reference sample **PDI-1** plotted on a logarithmic scale. The color of the traces represent the color of the respective excitation wavelength. A clear increase of lifetime (fitting yields a 1.7-fold increase from 2.5 eV to 4.5 eV) with excitation energy is observed.

As the TRPL measurement probes the dynamics of the S_1 state, the dependence of the rates k_{CS}, k_{rCS} and k_{CR} on the excitation energy (Fig. 7a) and Fig. S a), b)) intruiging. This either infers that the donor-acceptor distance is elongated, possibly due to higher energy vibrational modes. Alternatively, photoionization of either one or both donating groups could occur, thus lowering the electrontransfer probability. We rule out the second possibility as the rates for investigated excitation energies are reversible for the investigated energies (the only exception being **PDI-2** for $E_{exc} = 4.5$ eV).

No CS occurs for **PDI-1** (transient PL shown in the inset of Figure 7a). Nevertheless, the transients depend on the excitation energy, showing increased lifetimes for higher excitation energies. If a slow IC from $S_X \rightarrow S_1$was the origin of the delayed fluorescence, the emission from $S_X \rightarrow S_0$ transition should be at least weakly observable. Such emission is demonstrated, *e.g.*, for matrix-isolated SeO_2 molecules.[41]Yet, we observe no higher energy emission for an excitation with 3.3 and 4.5 eV laser light. For pure perylene in liquid solution, the $S_3 \rightarrow S_1$ vibrational relaxation takes only as long as 60 ps.[33] Consequently, a slow IC alone is insufficient to explain a 1.7-fold lifetime-increase, assuming rates comparable to those observed in perylene. An ISC, however, is a possible explanation and is observed for similar systems, *i.e.*, in PDIs and NDIs lacking heavy atoms.[7,42] Significant ISC rates are observed especially for $S_x \rightarrow T_n(x > 1, n \geq 1)$ transitions.[7] Among others, a small singlet–triplet energy splitting is the key factor for efficient ISC.[7]According to DFT calculations, multiple triplet states exist around 3.2 eV for the studied samples (see Supporting Information Table S3). The photoluminescence excitation (PLE) spectrum deviates significantly from the absorption spectrum (Supporting Information Figure S12), indicating a partial breakdown of Kasha-Vavilov's rule. The deviations become particularly pronounced in the vicinity of the probed excitation energies. In the lower energy regions ranging from 2.2 - 3.0 eV, however, PLE and absorption data show no difference. This corroborates our assumption of an additional relaxation pathway, namely $S_x \rightarrow T_n(x > 1, n \geq 2)$transitions. As the lifetime of the $S_1 \rightarrow S_0$ transition is increased for large E_{Exc}, the forward ISC must be accompanied by reverse ISC. Only the combination of both can lead to the observed 1.7-fold lifetime increase of the emissive state. The extended energy level diagram is shown in Figure 7b).

Strikingly, in the case of **PDI-2**, k_{CS} at 4.5 eV excitation is lowered by more than one order of magnitude compared to the other excitation energies. An irreversible transition occurs under excitation with UV light accompanied by a drastic increase of fluorescence intensity. Mass spectroscopy revealed that the probable origin of this observation lies the cleavage of the bond connecting the PDI-core and the electron donating imide group. It remains unclear why a breach occurs exclusively for the sample bearing the C_2spacer.

In summary, we present the synthesis and characterization of two new PDHs, chromophores with a directly nitrogen bound donor – NR_2 attached to the acceptor perylene imide core. In particular, a well soluble **PDH-1**is investigated, which is isoelectronically related to reference "swallowtail" **PDI-1**. These PDHs with very short donor-acceptor distances exhibit a very efficient fluorescence quenching. Upon double-protonation with bistriflylimide (HTFSI), the reported PDHs show partially recovered fluorescence. Such $[H_2\text{-PDH}]^{2+}$ salts reveal weak fluorophore-fluorophore interactions in solution and in the single-crystalline state as shown for bay-unsubstituted$[H_2\text{PDH-2}][TFSI]_2$.

The intramolecular electron transfer of these PDH is compared with a series of classical *N,N*'-bisalkylperylenediimides (PDI) equipped with an extra -NR_2 donor linked to the PDI acceptor core via a varying number of –(CH_2)- spacer groups, thus at distinctively different distances. Control of the transfer across the intramolecular interfaces is achieved by three different methods. Donor methylation proved to be the most efficient, as indicated by quantum efficiency and time-resolved measurements. The donor-acceptor distances for the ground and excited state compounds are determined by DFT and TDDFT calculations, and used to calculate k_{CS}. The elongation of the spacer effectively prevents overlap of the donor and acceptor orbitals. The IC process responsible for fluorescence quenching in unprotonated compounds could be attributed to the MO associated with the terminal amine at an energy intermediary to the π and π^* orbitals; protonation and/or methylation reduce the energy of this MO to below that of the π and π^* orbitals, reducing the PL quenching.

The observed exponential distance dependence is in accordance with a through-space type mechanism. This experimental observation is unaffected by spurious effects in the spacer units from, *e.g.*, delocalized π-electron systems. The excitation energy dependence of k_{CS} reveals the intricate interplay of charge-separation and IC processes. The pronounced non-single-exponential decay dynamics infer the presence of a dark shelving state within the system as extrinsic effects can be excluded. Furthermore, the excitation-energy dependent decay dynamics and bi-exponential nature of the transient PL strongly hint efficient ISC in these heavy-atom free, imide-substituted PDIs.

Experimental Methods

Synthesis. Synthesis of**PDI-1** to**PDI-4** and **Me_2PDI-2**has been reported previously.[31, 43-45]The synthesis of unsymmetrical *N,N*-dialkylhydrazines is accomplished by the nitrosylation of secondary amines, followed by lithium aluminium hydride reduction of the cancerogenic*N*-nitrosamines.[30]Protonated PDHs and PDIs (H_2PDHs and H_2PDIs) are obtained analytically pure by protonation with bis(trifluoromethane)sulfonimide ($HNTf_2$) in toluene. The precipitated H_2PDH and H_2PDIsalts are characterized by NMR spectroscopy and elemental analysis. Methylated **Me_2PDI-2** was obtained by reaction of **PDI-2** with methyl trifluoromethanesulfonate (MeOTf). Methylated PDHsare not accessible by reaction with methylation agents like methyl iodide, dimethyl sulfate or methyl triflate. Details of syntheses and characterization are found in the Supporting Information.

Electrochemistry. Cyclic voltammetry (CV) and differential pulse voltammetry (DPV) of neutral compounds are performed in dichloromethaneand of charged H_2PDHs and H_2PDIs in acetonitrileon arhd instruments TSC 1600 closed electrochemical workstation (see supporting information). All samples are measured at a concentration of 5 mM or as saturated solutions for less soluble dyes in 100 mMtetrabutylammoniumhexafluorophosphate solutions with a scan rate of 100 mVs^{-1}withferrocene as an internal standard. Half-wave redox potentials are summarized in Table 1 (a complete overview is given in the Supporting Information) and are given in V *vs.* SCE.

Steady-state spectroscopy. All steady-state absorption measurements are performed using a commercial double-beam spectrophotometer (Varian Cary 3) in the range from 190 – 900 nm. The steady-state emission spectra are obtained in a custom-built setup. A broad area diode laser operating at 2.8 eV (445 nm) is used for excitation and a compact spectrometer with 0.3 nm resolution (OceanOptics USB2000) for detection. The sample is mounted inside a 15 mm inner-diameter integrating sphere for the quantum-efficiency measurements. The detector is calibrated against a traceable tungsten-halogen white-light source; details are reported elsewhere.[46]

Time-resolved spectroscopy.A standard streak-camera setup is used for the time-resolved measurements. A pulsed titanium-sapphire

laser (Spectra Physics Tsunami HP) acts as excitation source. Its sub-100-fs pulses are tunable between 690 and 1080 nm while operating at a fixed repetition rate of 78 MHz The excitation wavelength range is further increased by including a frequency doubler and tripler unit. It provides the desired excitation energy of 2.8 eV (445 nm). An achromatic lens with f = 150 mm is used to focus the exciting laser beam on the sample. The emitted light is collected in backscattering geometry through the same lens and it is propagated towards a Czerny-Turner-type grating spectrometer yielding a spectral resolution of 2 nm. The streak camera equipped with a S20 photocathode that yields a time-resolution of 1.5 ps within the time window of 1.5 ns.

Solution sample preparation.The sample concentrations are kept well below the saturation limit for all samples and solvents (0.05 mM – 0.1 mM) to exclude aggregation effects, which would distort the optical spectra. The effect of oxygen induced fluorescence lifetime quenching is known to be negligible for **PDI-1** under air equilibration.[32]This assumption was verified by preliminary comparative measurements of O_2-free and air equilibrated samples. Hence, no further efforts are undertaken to avoid air equilibration. The samples are measured in standard cuvettes (Hellma Analytics) with an optical path length of 1 mm.

Quantum Chemical Studies. All calculations are performed using the Guassian09 software package.[47] The ground state (GS) structure for all compounds in both their protonated and unprotonated forms was optimized using DFT with the B3LYP functional[48–51]and the 6-31+G(d)[52, 53]basis set. Frequency calculations were performed at the same level of theory as for the geometry optimizations; the absence of negative eigenvalues is considered as confirmation that the state obtained is a true global potential energy minimum and not a transition state. A full population analysis was then performed on the optimized GS structures using DFT with the B3LYP functional and cc-pVDZ[54]basis set. ESS structures are found by optimizing the GS structures using TDDFT with the B3LYP functional and 6-31+G(d) basis set. A full population analysis of these ESS structures was then performed at same level of theory as for their optimizations. Additional geometry optimizations (B3LYP/6-31G**) were performed using GAMESS-UK[55], and TDDFT (B3LYP/6-31G**) calculations for the first ten singlet and triplet excitation energies were performed using DALTON 2.0.[56,57]

Acknowledgment

Funding by the Deutsche Forschungsgemeinschaft through SFB 1083 is gratefully acknowledged. C.P acknowledges funding by DFG through GRK 1782. M.A.B. acknowledges funding by a DAAD doctoral fellowship.

Supporting Information Available

Details on the synthetic procedures, NMR spectra, electrochemisty TRPL, temperature- and distance-dependenceof the electron transfer, details on the rate equation model, PLE data and DFT calculated singlet and triplettenergies.This material is available free of charge *via* the Internet at http://pubs.acs.org.

References

(1) W. Herbst and K. Hunger, Industrial Organic Pigments: Production, Properties, Applications, 2nd ed., Wiley-VCH, Weinheim, 1997.

(2) Zhan, X.; Facchetti, A.; Barlow, S.; Marks, T. J.; Ratner, M. A.; Wasielewski, M. R.; Marder, S. R.Rylene and Related Diimides for Organic Electronics. *Adv. Mater.* **2011**, 23, 268– 284.

(3) Würthner, F.; Stolte, M.Naphthalene and PeryleneDiimides for Organic Transistors. *Chem. Commun.***2011**, 47, 5109– 5115.

(4)Liu, Z.; Zhang, G.; Cai, Z.; Chen, X.; Luo, H.; Li, Y.; Wang, J.; Zhan g, D.New Organic Semiconductors with Imide/Amide-Containing Molecular Systems. *Adv. Mater.* **2014**, 26, 6965– 6977.

(5) Würthner, F.; Struijk, C. W.; Sieval, A. B.; Dakhorst, J. E. J.; Dijk, M. Van; Kimkes, P.; Koehorst, R. B. M.; Donker, H.; Schaafsma, T. J.; Picken, S. J.; et al. PeryleneBisimide Dyes as Versatile Building Blocks for Functional Supramolecular Architectures. *Chem. Commun.***2004**, 122, 1564–1579.

(6) Würthner, F.; Saha-Möller, C. R.; Fimmel, B.; Ogi, S.; Leowanawat, P.; Schmidt, D. PeryleneBisimide Dye Assemblies as Archetype Functional Supramolecular Materials. *Chem. Rev.***2016**, *116*, 962–1052.

(7) Georgiev, N. I.; Sakr, A. R.; Bojinov, V. B. Design and synthesis of novel fluorescence sensing perylenediimides based on photoinduced electron transfer. *Dyes Pigm.***2011**, 91, 332–339.

(8) Shoer, L. E.; Eaton, S. W.; Margulies, E. A.; Wasielewski, M. R. Photoinduced Electron Transfer in 2,5,8,11-Tetrakis-Donor-Substituted Perylene-3,4:9,10-bis(dicarboximides). *J. Phys. Chem. B***2015**, 119, 7635-7643.

(9) Eaton, S. W.; Shoer, L. E.; Karlen, S. D.; Dyar, S. M.; Margulies, E. A.; Veldkamp, B. S.; Ramanan, C.; Hartzler, D. A.; Savikhin, S.; Marks, T. J.; et al. Singlet Exciton Fission in Polycrystalline Thin Films of a Slip-Stacked Perylenediimide. *J. Am. Chem. Soc.***2013**, *135*, 14701–14712.

(10) Mirjani, F.; Renaud, N.; Gorczak, N.; Grozema, F. C. Theoretical Investigation of Singlet Fission in Molecular Dimers: The Role of Charge Transfer States and Quantum Interference. *J. Phys. Chem. C***2014**, *118*, 14192–14199.

(11) Yang, W.; Zhao, J.; Sonn, C.; Escudero, D.; Karatay, A.; Yaglioglu, H. eG.; Küçüköz, B.; Hayvali, M.; Li, C.; Jacquemin, D. Efficient Intersystem Crossing in Heavy-Atom-Free Perylenebisimide Derivatives. *J. Phys. Chem. C* 2016, 120, 10162–10175.

(12)Fukuzumi, S.; Ohkubo, K.; Ortiz, J.; Gutiérrez, A. M.; Fernández-Lázaro, F.; Sastre-Santos, A. Control of Photoinduced Electron Transfer in Zinc Phthalocyanine-Perylenediimide Dyad and Triad by the Magnesium Ion. *J. Phys. Chem. A***2008**, *112*, 10744–10752.

(13)Langhals, H.; Jona, W., The Identification of Carbonyl Compounds by Fluorescence: A Novel Carbonyl-Derivatizing Reagent. *Chemistry – A European Journal* **1998,***4*, 2110-2116.

(14) Mohr, G. J.; Spichiger, U. E.; Jona, W.; Langhals, H., Using N-Aminoperylene-3,4:9,10-tetracarboxylbisimide as a FluorogenicReactand in the Optical Sensing of Aqueous Propionaldehyde. *Analytical Chemistry* **2000,***72*, 1084-1087.

(15) Langhals, H.; Pust, T., Axially Extended Perylene Dyes. *European Journal of Organic Chemistry* **2010,***2010*, 3140-3145.

(16) Langhals, H.; Jona, W., Intense Dyes through Chromophore–Chromophore Interactions: Bi- and Trichromophoric Perylene-3,4:9,10-bis(dicarboximide)s. *Angew. Chem. Int. Ed.***1998,***37*, 952-955.

(17) Holman, M. W.; Liu, R.; Zang, L.; Yan, P.; DiBenedetto, S. A.; Bowers, R. D.; Adams, D. M., Studying and Switching Electron Transfer: From the Ensemble to the Single Molecule. *J. Am. Chem. Soc.***2004,***126*, 16126-16133.

(18)Wilson, T. M.; Tauber, M. J.; Wasielewski, M. R., Toward an n-Type Molecular Wire: Electron Hopping within Linearly Linked Perylenediimide Oligomers. *J. Am. Chem. Soc.***2009,***131*, 8952-8957.

(19) Menelaou, C.; Schiphorst, J. t.; Kendhale, A. M.; Parkinson, P.; Debije, M. G.; Schenning, A. P. H. J.; Herz, L. M., Rapid Energy Transfer Enabling Control of Emission Polarization in PeryleneBisimide Donor–Acceptor Triads.*J. Phys. Chem. Lett.* **2015,***6*, 1170-1176.

(20) Morandeira, A.; Fortage, J.; Edvinsson, T.; Le Pleux, L.; Blart, E.; Boschloo, G.; Hagfeldt, A.; Hammarström, L.; Odobel, F., Improved Photon-to-Current Conversion Efficiency with a Nanoporous p-Type NiO Electrode by the Use of a Sensitizer-Acceptor Dyad. *J. Phys. Chem. C* **2008,***112*, 1721-1728.

(21) Gibson, E. A.; Smeigh, A. L.; Le Pleux, L.; Fortage, J.; Boschloo, G.; Blart, E.; Pellegrin, Y.; Odobel, F.; Hagfeldt, A.; Hammarström, L., A p-Type NiO-Based Dye-Sensitized Solar Cell with an Open-Circuit Voltage of 0.35 V. *Angew. Chem. Int. Ed.***2009,***48*, 4402-4405.

(22) Le Pleux, L.; Smeigh, A. L.; Gibson, E.; Pellegrin, Y.; Blart, E.; Boschloo, G.; Hagfeldt, A.; Hammarstrom, L.; Odobel, F., Synthesis, photophysical and photovoltaic investigations of acceptor-functionalized perylenemonoimide dyes for nickel oxide p-type dye-sensitized solar cells. ***Energy Environ. Sci*. 2011,***4*, 2075-2084.

(23) Warnan, J.; Gardner, J.; Le Pleux, L.; Petersson, J.; Pellegrin, Y.; Blart, E.; Hammarström, L.; Odobel, F., Multichromophoric Sensitizers

Based on Squaraine for NiO Based Dye-Sensitized Solar Cells. *J. Phys. Chem. C* **2014,***118*, 103-113.

(24) Rajaram, S.; Shivanna, R.; Kandappa, S. K.; Narayan, K. S., NonplanarPeryleneDiimides as Potential Alternatives to Fullerenes in Organic Solar Cells. *J. Phys. Chem. Lett.***2012,***3*, 2405-2408.

(25) Shivanna, R.; Rajaram, S.; Narayan, K. S., Interface engineering for efficient fullerene-free organic solar cells. *Appl. Phys.Lett.***2015,***106*, 123301.

(26) Wu, C.-H.; Chueh, C.-C.; Xi, Y.-Y.; Zhong, H.-L.; Gao, G.-P.; Wang, Z.-H.; Pozzo, L. D.; Wen, T.-C.; Jen, A. K. Y., Influence of Molecular Geometry of PeryleneDiimide Dimers and Polymers on Bulk Heterojunction Morphology Toward High-Performance Nonfullerene Polymer Solar Cells. *Adv.Funct. Mater.***2015,***25*, 5326-5332.

(27) Ye, L.; Sun, K.; Jiang, W.; Zhang, S.; Zhao, W.; Yao, H.; Wang, Z.; Hou, J., Enhanced Efficiency in Fullerene-Free Polymer Solar Cell by Incorporating Fine-designed Donor and Acceptor Materials. *ACS Appl. Mater. Interfaces* **2015,***7*, 9274-9280.

(28) Wiberg, J.; Guo, L.; Pettersson, K.; Nilsson, D.; Ljungdahl, T.; Mårtensson, J.; Albinsson, B. Charge Recombination versus Charge Separation in Donor-Bridge-Acceptor Systems. *J. Am. Chem. Soc.***2007**, 129, 155–163.

(29) Pettersson, K.; Wiberg, J.; Ljungdahl, T.; Mårtensson, J.; Albinsson, B. Interplay between Barrier Width and Height in Electron Tunneling: Photoinduced Electron Transfer in Porphyrin-Based Donor-Bridge-Acceptor Systems. *J. Phys. Chem. A***2006**, 110, 319–326.

(30) Zimmer, H.; Audrieth, L. F.; Zimmer, M.; Rowe, R. A., The Synthesis of Unsymmetrically DisubstitutedHydrazines. *J. Am. Chem. Soc.***1955**, 77, 790-793.

(31)Demmig, S.; Langhals, H., Leichtlösliche, lichtechte Perylen-Fluoreszenzfarbstoffe. *Chem. Ber.* **1988,***121*, 225-230.

(32) Langhals, H.; Karolin, J.; Johansson, L. B.-Å. Spectroscopic Properties of New and Convenient Standards for Measuring Fluorescence Quantum Yields. *J. Chem. Soc. Faraday Trans.***1998**, *94*, 2919–2922.

(33) An, Z.; Odom, S. A.; Kelley, R. F.; Huang, C.; Zhang, X.; Barlow, S.; Padilha, L. A.; Fu, J.; Webster, S.; Hagan, D. J.; *et al.*Synthesis and Photophysical Properties of Donor- and Acceptor-Substituted 1,7-Bis(arylalkynyl)perylene-3,4:9,10-Bis(dicarboximide)s. *J. Phys. Chem. A***2009**, *113*, 5585–5593.

(34) Connelly, N. G.; Geiger, W. E., Chemical Redox Agents for Organometallic Chemistry. *Chem. Rev.***1996,***96*, 877-910.

(35) Flamigni, L.; Zanelli, A.; Langhals, H.; Bock, B., Photoinduced processes in a dyad made of a linear and an angular perylenebisimide. ***Photochem. Photobiol. Sci.*****2013,***12*, 2137-2145.

(36) Weller, A. Photoinduced Electron Transfer in Solution: Exciplex and Radical Ion Pair Formation Free Enthalpies and Their Solvent Dependence. *Zeitschrift für Phys. Chemie***1982**, *133*, 93–98.

(37) Neuteboom, E. E.; Meskers, S. C. J.; Van Hal, P. A.; Van Duren, J. K. J.; Meijer, E. W.; Janssen, R. A. J.; Dupin, H.; Pourtois, G.; Cornil, J.; Lazzaroni, R.; et al. Alternating Oligo(p-PhenyleneVinylene)-PeryleneBisimide Copolymers: Synthesis, Photophysics, and Photovoltaic Properties of a New Class of Donor-Acceptor Materials. *J. Am. Chem. Soc.***2003**, *125*, 8625–8638.

(38) Huang, J.; Fu, H.; Wu, Y.; Chen, S.; Shen, F.; Zhao, X.; Liu, Y.; Yao, J. Size Effects of Oligothiophene on the Dynamics of Electron Transfer in pi-Conjugated Oligothiophene-PeryleneBisimide Dyads. *J. Phys. Chem. C***2008**, *112*, 2689–2696.

(39) Closs, G. L.; Miller, J. R. Intramolecular Long-Distance Electron Transfer in Organic Molecules. *Science***1988**, *240*, 440–447.

(40) Rulliere, C.; Declemy, A.; Kottis, P. Picosecond Spectroscopic Investigation of the Internal Conversion Rate of Excited Perylene in Solution. *Chem. Phys. Lett.***1984**, *110*, 308–314.

(41) Voigt, E. M.; Meyer, B.; Morelle, A.; Smith, J. The Spectrum of Matrix Isolated SeO_2: Evidence for Slow Internal Conversion between Excited States. *J. Mol. Spectrosc.***1970**, *34*, 179-189.

(42) Yushchenko, O.; Licari, G.; Mosquera-Vazquez, S.; Sakai, N.; Matile, S.; Vauthey, E. Ultrafast Intersystem-Crossing Dynamics and Breakdown of the Kasha–Vavilov's Rule of Naphthalenediimides. *J. Phys. Chem. Lett.***2015**, *6*, 2096–2100.

(43) Ryan, S. T. J.; Del Barrio, J.; Ghosh, I.; Biedermann, F.; Lazar, A. I.; Lan, Y.; Coulston, R. J.; Nau, W. M.; Scherman, O. A., Efficient Host–Guest Energy Transfer in PolycationicCyclophane–PeryleneDiimide Complexes in Water. *J. Am. Chem. Soc.***2014,***136*, 9053-9060.

(44) Schnurpfeil, G.; Stark, J.; Wöhrle, D., Syntheses of uncharged, positively and negatively charged 3,4,9,10-perylene-bis(dicarboximides). *Dyes Pigm.***1995,***27*, 339-350.

(45) Deligeorgiev, T.; Zaneva, D.; Petkov, I.; Timcheva, I.; Sabnis, R., Synthesis and properties of fluorescent bis-quaternizedperylene dyes. *Dyes Pigm.***1994,***24*, 75-81.

(46) Rosemann, N. W.; Metzger, B.; Kunert, B.; Volz, K.; Stolz, W.; Chatterjee, S. Temperature-Dependent Quantum Efficiency of Ga(N,As,P) Quantum Wells. *Appl. Phys. Lett.***2013**, *103*, 252105.

(47) Frisch, M. J.; Trucks, G. W.; Schlege, H. B.; Scuseria, G. E.; Robb, M. A.; Cheeseman, J. R.; Scalman, i. G.; Barone, V.; Mennucci, B.; Petersson, G. A. et al. Gaussian 09, Revision C.01; Gaussian, Inc.: Wallingford, CT, 2010.

(48) Becke, A. D. Density-Functional Thermochemistry. III. The Role of Exact Exchange. *J. Chem. Phys.***1993**, *98*, 5648.

(49) Lee, C.; Yang, W.; Parr, R. G. Development of the Colle-Salvetti Correlation-Energy Formula into a Functional of the Electron Density. *Phys. Rev. B***1988**, *37*, 785-789.

(50) Vosko, S. H.; Wilk, L.; Nusair, M. Accurate Spin-Dependent Electron Liquid Correlation Energies for Local Spin Density Calculations: A Critical Analysis. *Can. J. Phys.***1980**, *58*, 1200–1211.

(51) Stephens, P. J.; Devlin, F. J.; Chabalowski, C. F.; Frisch, M. J. Ab Initio Calculation of Vibrational Absorption and Circular Dichroism Spectra Using Density Functional Force Fields. *J. Phys. Chem.***1994**, *98*, 11623–11627.

(52) Hehre, W. J.; Ditchfield, R.; Pople, J. A. Self-Consistent Molecular Orbital Methods. XII. Further Extensions of Gaussian-Type Basis Sets for Use in Molecular Orbital Studies of Organic Molecules. *J. Chem. Phys.***1972**, *56*, 2257.

(53) Rassolov, V. A.; Pople, J. A.; Ratner, M. A.; Windus, T. L. 6-31G∗ Basis Set for Atoms K through Zn. *J. Chem. Phys.***1998**, *109*, 1223.

(54) Dunning, T. H. Gaussian Basis Sets for Use in Correlated Molecular Calculations. I. The Atoms Boron through Neon and Hydrogen. *J. Chem. Phys.***1989**, *90*, 1007.

(55) Guest, M. F.; Bush, I. J.; Van Dam, H. J. J.; Sherwood, P.; Thomas, J. M. H.; Van Lenthe, J. H.; Havenith, R. W. A.; Kendrick, J. The GAMESS-UK Electronic Structure Package: Algorithms, Developments and Applications. *Mol. Phys.***2005**, *103*, 719–747.

(56) Helgaker, T.; Jensen, H. J. A.; Jorgensen, P.; Olsen, J.; Ruud, K.; Ågren, H.; Andersen, T.; Bak, K. L.; Bakken, V.; Christiansen, O. Dalton, A Molecular Electronic Structure Program, release 2.0 2005.

(57) Aidas, K.; Angeli, C.; Bak, K. L.; Bakken, V.; Bast, R.; Boman, L.; Christiansen, O.; Cimiraglia, R.; Coriani, S.; Dahle, P.; et al. The Dalton Quantum Chemistry Program System. *Wiley Interdiscip. Rev. Comput. Mol. Sci.***2014**, *4*, 269–284.

(a) Pino, G. A.; Oldani, A. N., Marceca, E.; Fujii, M.; Ishiuchi, S.-I.; Miyazaki, M.; Broquier, M; Dedonder, C; Jouvet. C., Excited state hydrogen transfer dynamics in substituted phenols and their-complexes with ammonia:$\pi\pi^*$-$\pi\sigma^*$energy gap propensityand ortho-substitution effect.*J. Chem. Phys.* 133, **2010**, 124313.

(b) Sobolewski, A. L.; Domcke, W.; Dedonder-Lardeux, C.;Jouvet, C., Excited-state hydrogen detachment and hydrogen transfer driven by repulsive$^1\pi\sigma^*$states: A new paradigm for nonradiativedecay in aromatic biomolecules. *Phys. Chem. Chem. Phys.*, **2002**, 4, 1093–1100.

(c) Ashfold, M. N. R.; King, G. A.; Murdock, D.; Nix, M. G. D.;Oliver, T. A. A; Sage, A.G., $\pi\sigma^*$excited states in molecular photochemistry. *Phys. Chem. Chem. Phys.*, **2010**, 12, 1218–1238.

Supplementary Information to

Control of Intramolecular Electron Transfer in Perylene Dihydrazines and Perylene Diimides: A Comparative Study by Time-Resolved Spectroscopy

Authors

Robin C. Doring, Eduard Baal, Malcolm A. Bartlett, Christian Prinzisky, Remco W. A. Havenith, Jorg Sundermeyer and Sangam Chatterjee

(TD)DFT optimisations of ground state (GS) and S_1 excited singlet state (ESS) structures and population analyses thereof.

Table S1. MO energies of the π, π* and highest lying non-perylene core MOs for the excited singlet state PDI and PDH derivatives calculated at the B3LYP/6-31G* level of theory. The energy difference between the π* and π orbitals represents the $S_1 \rightarrow S_0$ (fluorescence) transition.

Compound	Energy (eV)			
	π	π*	DA[†]	Δ(π*→π)
PDH-2	-6.301	-4.090	-5.420	2.211
H_2PDH-2	-11.286	-9.125	-13.384	2.161
PDI-2	-6.317	-4.112	-4.743	2.205
H_2PDI-2	-10.426	-8.291	-12.236	2.135
PDI-3	-6.335	-4.136	-4.492	2.463
H_2PDI-3	-10.236	-8.088	-11.997	2.148
PDI-4	-6.279	-4.071	-4.651	2.207
H_2PDI-4	-8.560	-6.385	-10.147	2.175
Me_2PDI-2	-10.171	-8.010	-11.957	2.161

[†]DA = donor amine. This represents the highest lying non-aromatic MO associated with the alkyl group. For neutral compounds, this MO is centered on the tertiary amine.

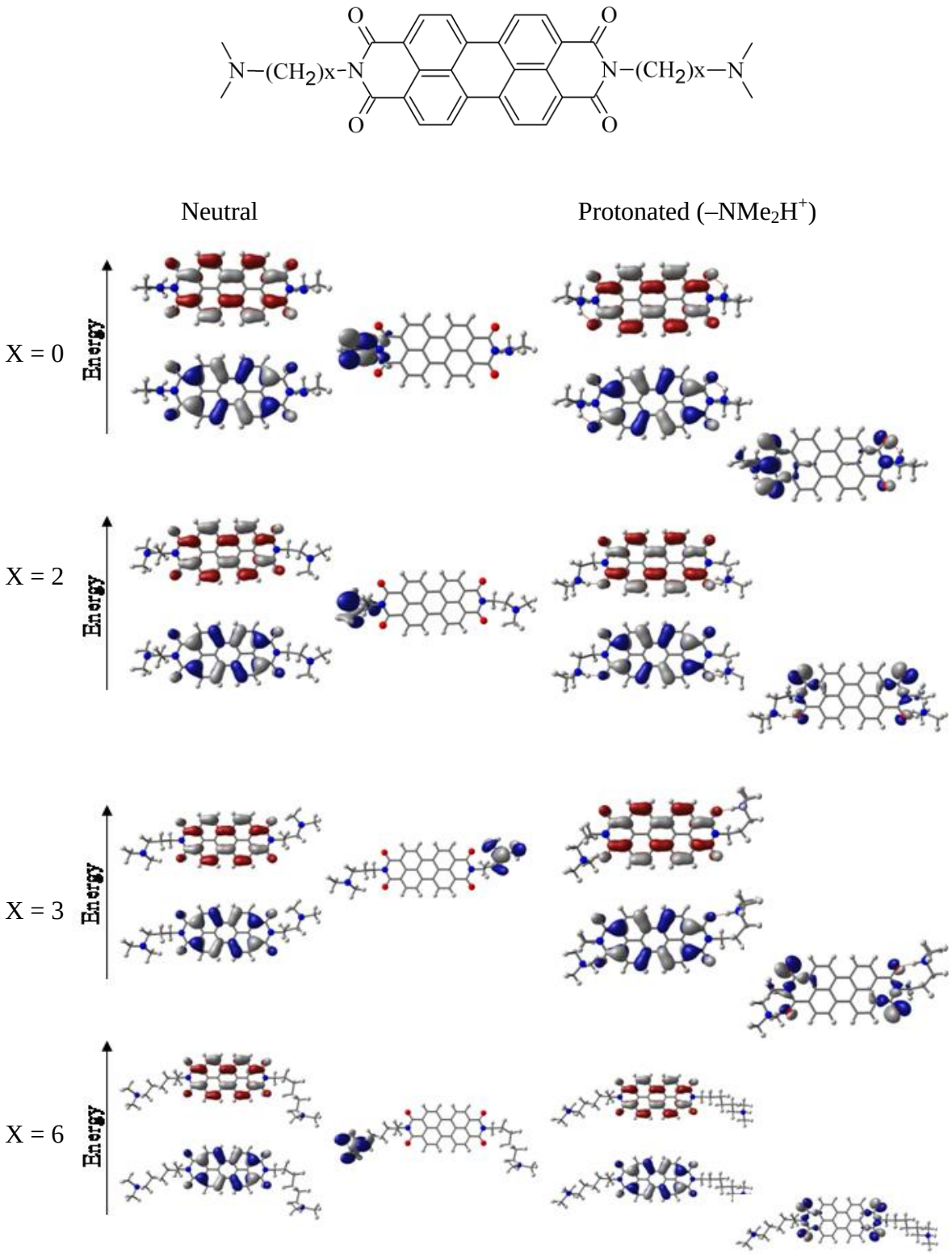

Figure S1. Contour plots of MOs involved in the π→π* transitions for the neutral and protonated PDH and PDI compounds, as well as the amine centered donor orbital involved in photoinduced electron transfer (PET). The first MO not located on the perylene core is shown for the protonated compounds. Occupied MOs are coloured blue-grey, while occupied MOs are colored red-grey.

Changes in the geometry of the alkyl chain, and terminal/donor amine in particular, are observed upon excitation from the GS to the ESS. These changes are demonstrated for the ethylene-bridged compound, PDI-2 and its protonated and methylated derivatives.

Table S2. Comparison of C-N-C bond angles of terminal amines in PDI-2, H2PDI-2 and Me2PDI-2 for the GS and ESS compounds. Excitation induces a change in the geometry resembling a change in hybridisation on nitrogen from sp^3 to sp^2.

Compound	C-N-C angle (°)	
	GS	ESS
PDI-2	112.5	121.0
H_2PDI-2	110.6	111.2
Me_2PDI-2	108.9*	108.9*

*average C-N-C bond angle for all three Me-N-Me possibilities

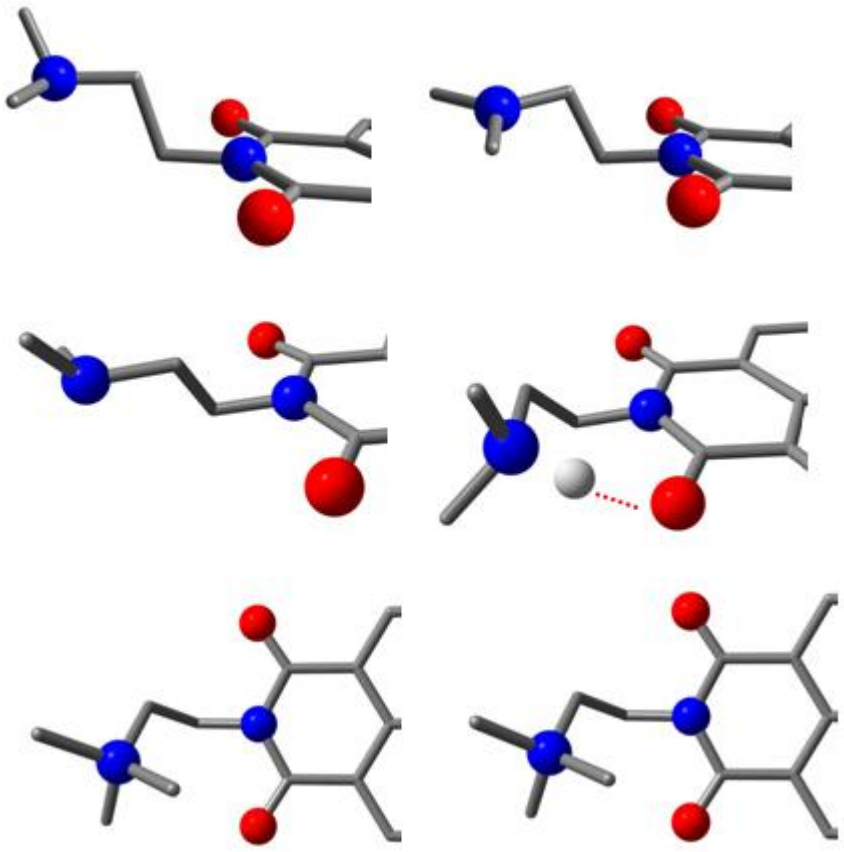

Figure S2. Changes in C–N–C bond geometry upon excitation from the GS (S_0) to the ESS (S_1) for the ethylene bridged compound, PDI-2, and its protonated and methylated derivatives, H_2PDI-2 and Me_2PDI-2, respectively.

CHAPTER 7 | SUMMARY OF NON-PUBLISHED PROJETCS

Chapter Summary

In this chapter, a brief summary is given of unpublished results. This is intended to highlight the background and context of the published work. This chapter is divided into four sections. Results and discussion are presented for work done within the Loewe SynChemBio and SFB 1083 networks and independent research into chemistry of the group 5 elements, niobium and tantalum, as well as work pertaining to the thiocatecholate-Pc project. A brief experimental section including noteworthy reactions related to the above projects is provided at the end.

7.1 Dithiolate and catecholate complexes

Two publications focused on the synthesis and properties of thiocatecholate–PcMg conjugates. As reported, 4,5-dithio-phthalonitrile was used as an analogous ligand with a small aromatic systems. Although only coordination to diphosphino metal ions ($[M(dppe)]^{2+}$) was reported, other combinations of ligands were explored.

To avoid the initially complicated coordination chemistry and assessment required for $K_8[(S_8Pc)Mg]$, with four thiocatecholate groups, the simple ligand 4,5-dithio-phthalonitrile (H_2dtpn) was first used as model system. In addition to dppe, the phosphine ligands, *bis*-(diphenylphosphin)methane (dppm), *bis*-(diphenyphosphine)ferrocene (dppf) and triphenylphosphine (PPh_3) in combination with Ni^{2+}, Pd^{2+} or Pt^{2+}, were first explored. Apart from PPh_3, all diphosphino-metal fragments could be successfully coordinated to $dtpn^{2-}$ in good yield. Complexation of these ligands to $[(S_8Pc)Mg]^{8-}$, however, afforded insoluble complexes that could not be analysed, even by absorption spectroscopy. This problem should be overcome by using more soluble diphosphine ligands. The use of neutral bidentate *N*-donor ligands that are known to act as good electron acceptor ligands in LLCT processes (e.g. bpy, phen) was also explored with Ni^{2+}, Pd^{2+} and Pt^{2+}. Addition of $dtpn^{2-}$ to $[MCl_2(N\text{-}N)]$ complexes always resulted in displacement of the neutral ligand to form salts of $[M(dtpn)_2]^{2-}$. Their coordination to $K_8[(S_8Pc)Mg]$ was therefore not explored.

Finally, a tetra-catecholate Pc ligand, $(HO)_8PcH_2$,[141] was synthesised and coordinated to $[Ni(dppe)]^{2+}$ to give the complex $[(dppeNi)_4(O_8PcH_2)]$. The optical properties of this complex are very similar to that of the corresponding thiocatecholate complex $[(dppeNi)_4(S_8PcMg)]$

(Figure **7.1**). The synthesis is also simpler (5 steps compared to 10 steps), and the intermediate tetra-catechol(ate) ligand is air stable. Time constraints prevented further research into this promising, potentially photoredox active system.

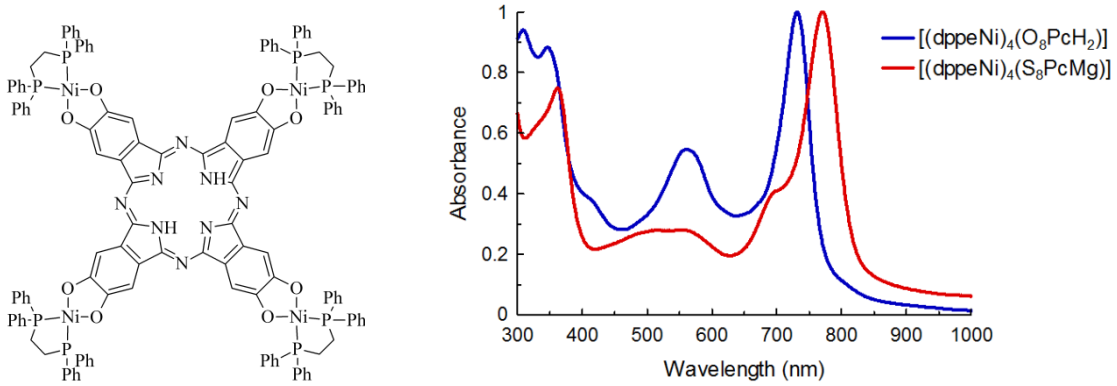

Figure 7.1: The structure (left) and UV–Vis absorption spectrum (right) for the tetranuclear complex [(dppeNi)$_4$(O$_8$PcH$_2$)] (black line) and [(dppeNi)$_4$(S$_8$PcMg)] (red line).

The tetra-catecholate and tetra-thiocatecholate complexes are intended for eventual use in (photo)redox processes. Cyclic voltammetry (CV) was therefore used to determine their basic redox properties. The corresponding mononuclear thiocatecholate complexes were also examined by CV for comparison. No reversible reduction or oxidation processes were seen for any of the Pc complexes. Mononuclear complexes, in contrast, showed two reversible reduction processes, although their oxidation was irreversible (Figure **7.2**). This irreversibility of the Pc complexes' redox processes was further explored by UV–Vis spectroscopy. The complex dissolved in DMF was mixed with $Na_2S_2O_4$ or CBr_4, to reduce or oxidise the complex, respectively. For both reagents, complete disappearance of all absorption bands above 400 nm was seen. This suggests complete decomposition of the Pc ligand upon both reduction and oxidation, perhaps due to the ring conjugation being broken and an associated instability. This could be solved by incorporating electron-donating or accepting groups on the Pc ligand to maintain the ring current.

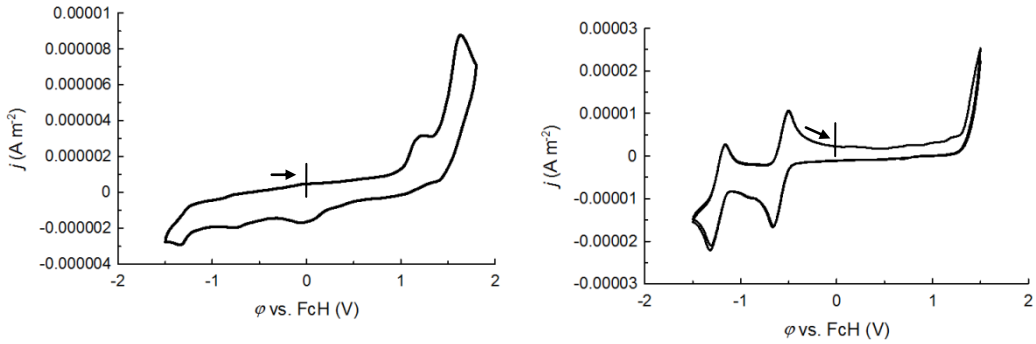

Figure 7.2: Cyclic voltammograms for [(dppeNi)$_4$(S_8PcMg)] (left: DMSO, GC electrode, scan rate 50 mV s^{-1}) and [Ni(dtpn)(dppe)] (right: DCM, GC electrode, scan rate 50 mV s^{-1}). The arrows indicate direction of scan and starting potential.

7.2 Work done within the Loewe SynChemBio network

Chemical syntheses play a central role in the life sciences in enabling the exploration of biological processes and for the production of medicines. Consequently, innovative synthetic chemistry is often found at the origin of the value-chain from initial discovery to medicine. Key to utilising the functionality of new chemicals is through specificity for biological targets. A combined approach to chemical function and selectivity for modulating biological processes was the goal of the Loewe SynChemBio network, which is outlined in the network description: “Innovative Synthetic Chemistry for the Selective Modulation of Biological Processes”. Within this network, the Sundermeyer, Göbel and Hartmann research groups were to collaborate on control of ribosomal protein synthesis through selective RNA targeting. This was to be done by coupling a chemical group to a miRNA strand. The conjugate would then selectively bind a target mRNA sequence and cause localised nucleotide strand cleavage. I therefore had the task of synthesising phthalocyanine complexes, which possessed high singlet oxygen quantum yields (Φ_Δ) for oxidative DNA cleavage. The Pc complexes also had to be modified with a functional group for coupling to a miRNA targeting sequence. G-quadruplex DNA was identified as an additional biological target during this project. Therefore, cationic water soluble Pc complexes became additional synthetic targets. The syntheses of the precursors and phthalocyanine complexes, as well as the results from our collaboration partners, will be discussed in the remainder of this section.

7.2.1 Pc-oligonucleotide conjugate

In designing the Pc-oligonucleotide conjugate, it was decided to couple to the Pc at the N-terminus of the oligonucleotide. This required functionalisation of the Pc ligand with a single carboxylic acid group, which could be linked to the free amine via the classic carbodiimide route (Scheme 1). Additionally, it was desirable that the Pc complex have good water solubility and a high singlet oxygen quantum yield. Although water solubility is typically easily achieved by the addition of charged groups, such as sulfonate or pyridinium, to the Pc ligand, this would have interfered with the selectivity of the targeting RNA sequence. Instead, the Pc ligand was extensively pegylated, as these groups are polar enough to promote water solubility, but at the same time neutral, and should not strongly interfere with RNA base pairing. High singlet oxygen quantum yields would be obtained by coordinating Zn with the Pc ligand and by substitution with thiolether groups at the β-positions. Scheme **7.1** shows the structure of the target A_3B asymmetric complex [($^{HOOC\text{^}S}$Pc)Zn] and its intended mode of action. In addition to the asymmetric Zn(Pc) complex, the A_4 symmetric octapegylated Zn(Pc) derivative, [(^{PegS8}Pc)Zn], [142] was also synthesised. Singlet oxygen quantum yields were determined for both to ensure that [($^{HOOC\text{^}S}$Pc)Zn] had sufficiently high activity for promoting DNA/RNA strand cleavage; the singlet oxygen quantum yield of [(^{PegS8}Pc)Zn] has already been reported in the literature.[142] Coupling experiments of the above described [($^{PegS/HOOC\text{^}S}$Pc)Zn] complex to mRNA were performed by the GÖBEL group (Goethe-Universität Frankfurt). Unfortunately, MS(ESI) analysis of the reaction solutions did not identify any coupling product between the Zn(Pc) derivative and the mRNA. It was however

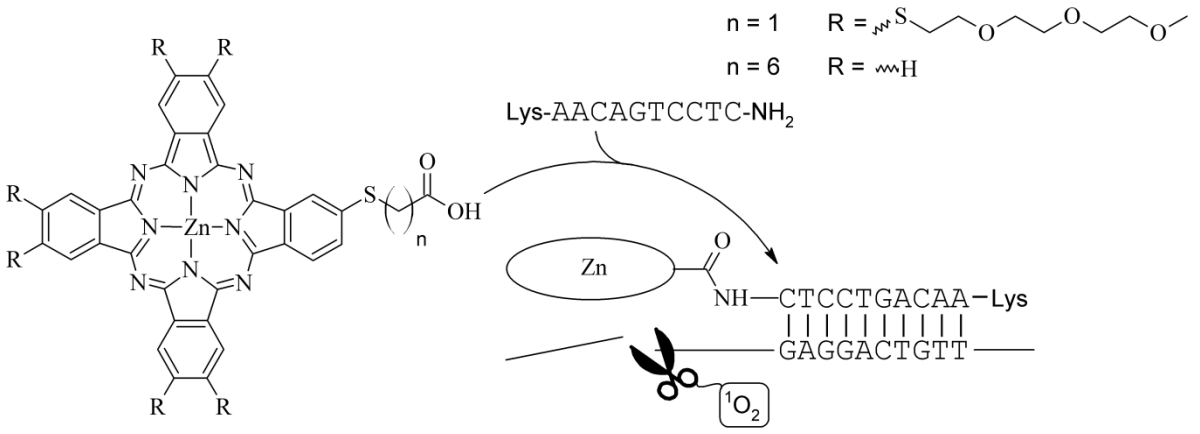

Scheme 7.1: Structure of the asymmetric Zn(Pc) complex [($^{PegS/HOOC\text{^}S}$Pc)Zn], and its intended coupling to an oligonucleotide *N*-terminus for selective RNA strand cleavage.

unclear if this was a problem of the coupling reaction or the analytic method, as fragmentation of the –$SCH_2COO(H)$– group induced during the ionisation step of MS analysis was observed for the pure asymmetric complex. A longer alkyl spacer between the thioether and carboxylic acid group should help to reduce this effect. Therefore, a new asymmetric complex ([(^{HOOCC6S}Pc)Zn]) was synthesised with a C_6H_{12} spacer in place of the CH_2 one. Also, this complex was not S-pegylated for convenience, as it was only intended for testing the Pc-RNA coupling reaction and subsequent analysis. Final purification of the desired complex was unfortunately not possible, as the required A_3B product could not be separated from the unsubstituted Zn(Pc). The low solubility of both species hindered chromatographic separation or selective extraction.

7.2.2 Cationic Pc complexes for G-quadruplex binding

Synthesis: Phthalocyanines have an innate affinity for G-quadruplex (G4) DNA, as already briefly discussed in section **1.3.2.1**. Within the SynChemBio network, we wanted to see if, not only binding, but also modification of the G4 DNA could be achieved using a Pc complex. To this end, a new octacationic Pc complex was synthesised. The precursor, 4,5-bis[(1-methyl-1H-imidazol-2-yl)sufanyl]benzene-1,2-dicarbonitrile, was synthesised from 4,5-dichlorophthalo-nitrile and 1-methyl-3-hydro-imidazole-2-thione, and was found to be very sparingly soluble. It was possible to synthesise the corresponding Mg(Pc) derivative in refluxing EtOH over several days. *N*-methylation afforded the octacationic complex, [(^{Me2}ITPc)Mg]I_8. Figure 7.**3** shows the synthesised octacationic PcMg, the structure of G4 DNA and their intended overlap with each other.

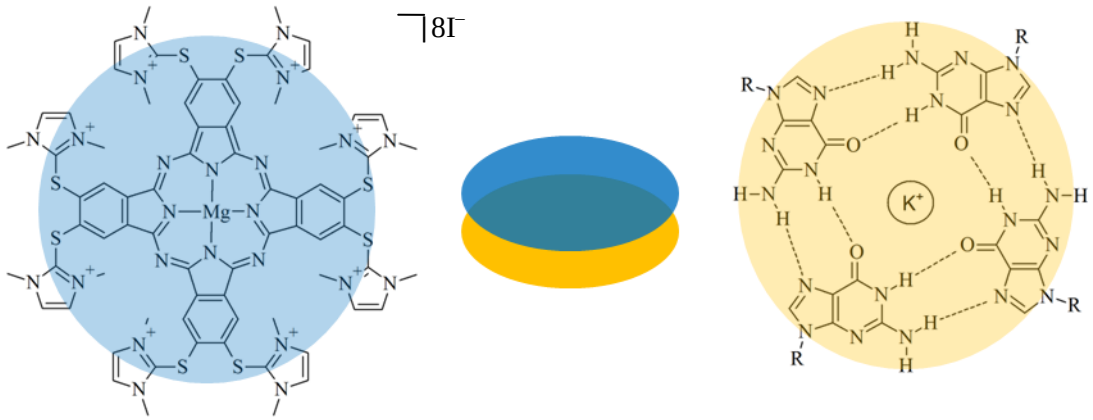

Figure 7.3: Structure of the octacationic complex [(^{Me2}ITPc)Mg]I_8 and its potential overlap with G4 DNA.

UV-Vis Spectroscopy: The neutral complex [(^{Me}ITPc)Mg] is not soluble in common organic solvents. However, when treated with acid, it is soluble in polar solvents, such as H_2O or MeOH. The UV-Vis spectra, however show that the complexes aggregate in solution; even when complete protonation of the complex using acetic acid or aqueous HCl (pH 1) is promoted (See Figure **7.4**).

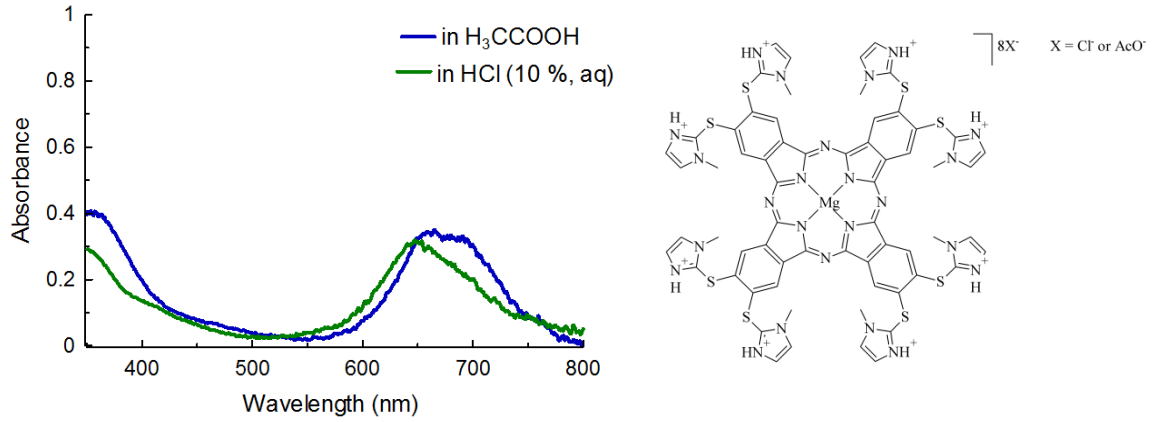

Figure 7.4: (left) UV-Vis spectra for [(^{Me}ITPc)Mg] when dissolved in AcOH (blue line) and HCl (10 %, aq) (green line). In both spectra, it is evident from the broad absorption in the Q-band region that only aggregated species are present. (right) Likely protonated structure of [(^{Me}ITPc)Mg]. Acidic conditions could also cause demetallation of the Pc ligand.

The solubility did improve upon quaternerization. The UV-Vis spectra below show the expect profile for a non-aggregated species (Fig. **7.5**). The molar attenuation coefficient for the complex was determined to be 70700 dm^3 mol^{-1} ml^{-1}. The complex does show surprisingly rapid decomposition when irradiated. This is suspected to be due, not to an inherent instability of the Mg(Pc) core, but rather through decomposition of the cationic side groups by hydroxyl radicals formed during irradiation. These insights helped later on to develop a new strategy for coupling thiocatecholate groups with a Pc ligand.

G4 DNA cleavage study: The singlet oxygen quantum yields (Φ_Δ) was first determined for [(^{Me2}ITPc)Mg]I_8. Although this complex demonstrates a low Φ_Δ value (0.07), it was considered sufficient to cause localised oxidative stress. In G4 DNA modification experiments, both [(^{Me2}ITPc)Mg]I_8 and the neutral octapegylation Zn complex, [(^{PegS8}Pc)Zn], were incubated

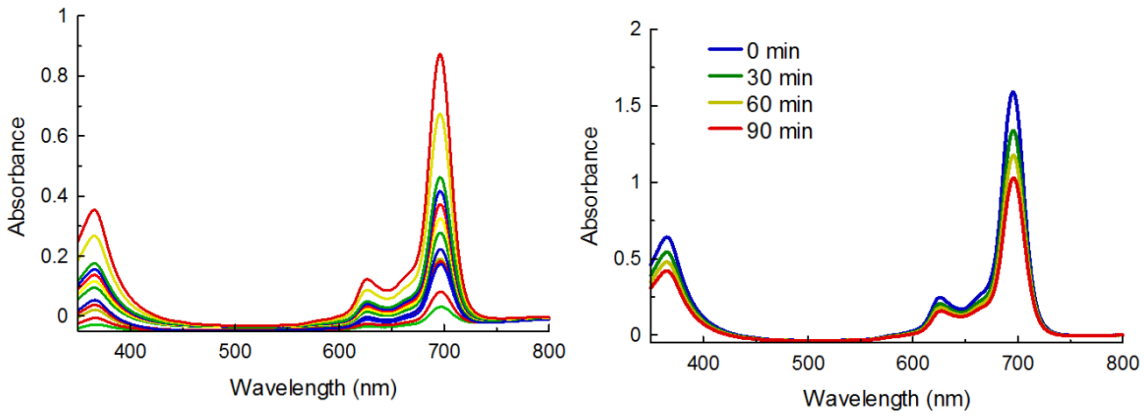

Figure 7.5: (Left) UV-Vis spectrum of [(^{Me2}ITPc)Mg]I_8 at different concentrations to determine its molar attenuation coefficient. (Right) Decomposition over time under irradiation (halogen; 300 W).

---

with G4 DNA. [(^{PegS8}Pc)Zn] was used included in this study to determine if non-regular strand cleavage would be caused by singlet oxygen production. After incubation, the samples were irradiated with light of wavelength >600 nm (lamp: halogen; 50 W). The molecular weight of the DNA samples after irradiation was determined by gel electrophoresis (Figure **7.6**). No strand cleavage was observed for either of the samples investigated, regardless of the irradiation time. These results support a study performed by CHERNONOSOV *et al.*[3], who reported that oligonucleotides exposed to singlet oxygen generated by Zn(Pc) derivatives were oxidised at specific nucleotide positions, but that no single or double strand breaks were induced.

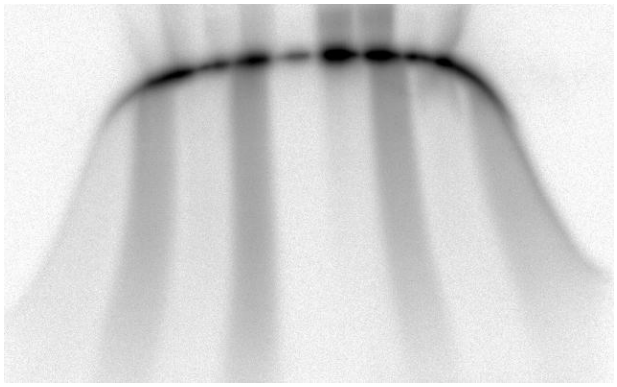

Figure 7.6: Gel electrophoresis image of G4 DNA incubated with and without [(^{Me2}ITPc)Mg]I_8. No evidence of strand breakage was seen in any of the samples.

7.3 Work done within the SFB 1083

The focus of the *Sonderforschungsbereich* (SFB) 1083 is the investigation of internal interfaces. The processes occurring at internal interfaces, or heterojunctions, between metals and semiconductors are the basis for many modern, high-tech devices, such as photovoltaic cells, organic light emitting diodes (OLEDs) and organic field effect transistors (OFETs).[144] The field of organic electronics, in particular, which uses π-conjugated small molecules and polymers, has seen active development in the past 25 years. Phthalocyanines generally show reversible oxidation and reduction behaviour, and are considered good electron donor molecules. In more physical terms, they can be considered as p-type semiconductors. Their use as TiO_2 photosensitising materials in organic solar cells reflects this property.

Within the SFB 1083, our goal was to study Pc monolayer formation on gold surfaces. The initial Zn(Pc) derivative synthesised and studied for the project was already discussed in Chapter 3, section 3.4. During this project, the A_3B-type $ZnPc^{SH}$ complex needed to be synthesised a total of six times to meet the demand for repeated measurements. Following this study, and concurrent to the work being done on thiolate protecting groups, we explored the use of 1,3-*N*-methylated-2-thio-benzimidazolium (dmbt) groups as thiolate protecting groups for thiol–gold SAM formation. Both the octasubstituted Mg(Pc) derivative and the disubstituted phthalonitrile derivative were deposited on amorphous gold substrates. X-ray phosphorescence spectra (XPS) were obtained for both samples to determine if –S–Au bonds had formed at the surface (Figure **7.6**). Almost complete thiolate formation, and therefore desired –S–Au bonding, was seen at the surface. This result shows that dmbt is a suitable group for masking the thiolate prior to monolayer formation. The Pc derivative showed only partial thiolate formation; the other sulfurs being oxidised to sulfide or sulfonate species. This is probably because no single molecular orientation is promoted in the octa-substituted Pc, so that not all sulfur atoms come into contact with the gold substrate. Figure **7.6** shows the XP spectra for the phthalonitrile and Pc containing films. Soon after these results were obtained, our research group pulled out of the SFB 1083 network, and no further work was done in this area.

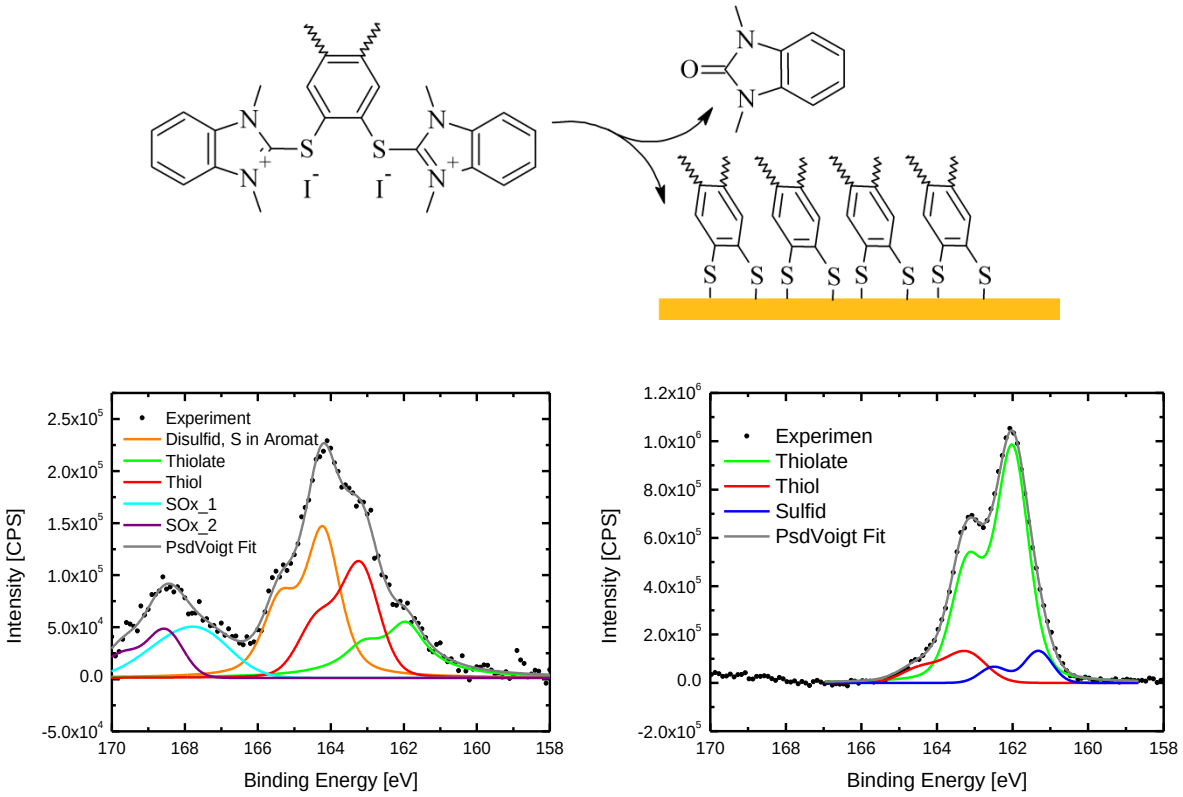

Figure 7.6: (top) Hydrolysis of the 2-thio-benzimidazolium groups at the Au surface yields a free thiocatechole. XP spectra for *octa*(dmbt)-Mg(Pc) (left) and *bis*(dmbt)-phthalonitrile (right) films deposited on amorphous gold (Au/SiO_2) using DMF/H_2O.

7.4 Coordination chemistry of Pc bound niobium and tantalum

In Section 3.X, the results of research into vanadium and chromium imido Pc chemistry are presented. However, the axial coordination of N-donor ligands was to PcNb and PcTa was also investigated. The results of this research are summarised in the following two sections.

7.4.1 Imido Nb and Imido Ta Pc complexes

Following the success of synthesising imido-vanadium Pc ([PcV(NR)]) complexes, we attempted to prepare the corresponding niobium(V) and tantalum(V) derivatives, [PcNb(NR)Cl] and [PcTa(NR)Cl], respectively. Attempts had been made previously in our group to synthesise these complexes, but were unsuccessful. Here, different methods were explored, some of which showed significant improvement over past attempts. While it was apparent that the target complexes could be synthesised this time, their final purity could not be guaranteed. The various synthetic approaches are briefly outlined below and depicted in Scheme **7.2**.

1) Template synthesis of Pc around a metal-imido trichloro complex

This was the first method explored by predecessors using $[M(NR)Cl_3(py)_2]$ (M = Nb, Ta) as the starting material. No Pc formation was evident in these reactions. Here, dme and thf adducts were synthesised instead of pyridine ones. Product formation was observed, as confirmed by MALDI-MS. There were, however, unassigned peaks in the ^1H NMR spectra for the complexes. Analytical chromatography suggested that there were multiple Pc species formed in these reactions.

2) Insertion of $[M(NR)Cl_3(thf)_2]$ into $[K_2Pc]$

Analogous to the preparation of [PcV(NR)] complexes, coordination of the metal imido complex by $[K_2Pc]$ was attempted. No indication that Nb or Ta had been coordinated by Pc was observed.

3) Metathesis reaction starting from $[PcMCl_3]$

Direct substation of two chlorido ligands of $[PcMCl_3]$ for an imido ligand was also attempted. Both tertiary amines in conjunction with primary amines and lithium amides were used to drive imido ligand formation. No replacement of the remaining chlorido ligands was observed.

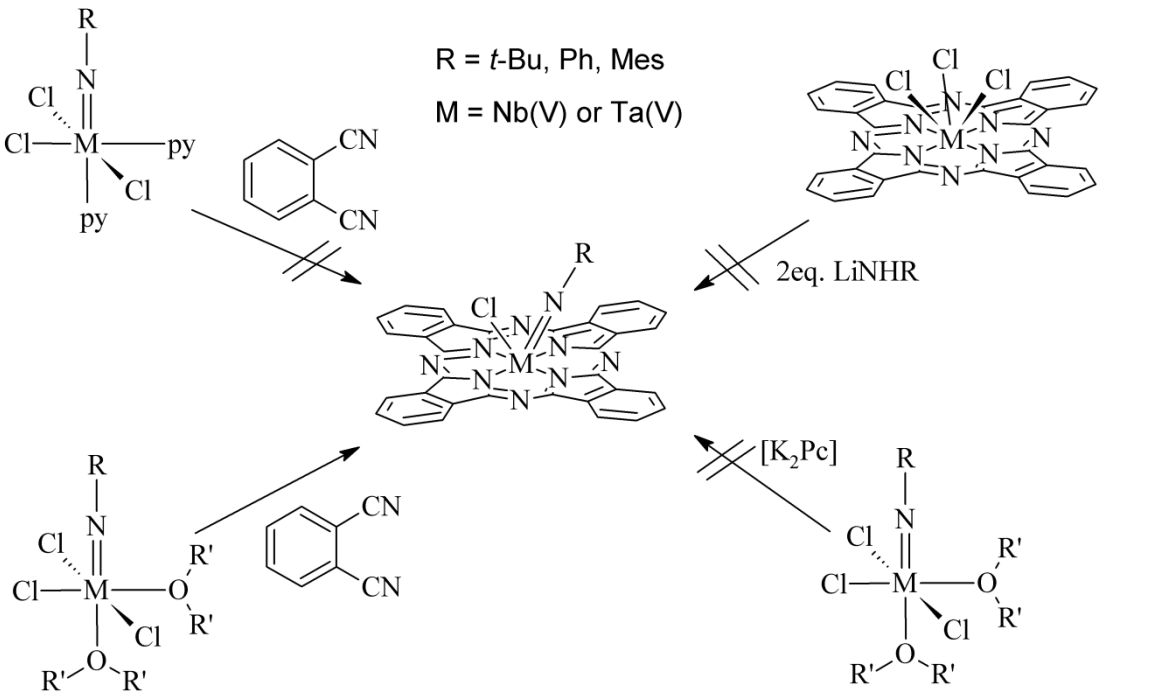

Scheme 7.2: Synthetic strategies for the synthesis of [PcM(NR)Cl] complexes.

In conclusion, it appears that template synthesis from a starting dme or thf adduct of $[M(NR)Cl_3]$ is a suitable method for the synthesis of [PcM(NR)Cl] complexes. Only improved methods for their purification need to be developed. The problem lies in their hydrolytic instability and low solubility, which render column chromatography unsuitable.

7.4.2 Axial coordination of a tripyrrolic ligand to $[PcNbCl_3]$ and $[PcTaCl_3]$

As seen in the previous section, the chlorido ligands of $[PcNbCl_3]$ and $[PcTaCl_3]$ were not easily removed. A tris-pyrrolic ligand, *meso*-pyrrolyl dipyrromethane,[145] was therefore synthesised that could bind Nb or Ta facially. Interest in this complex was further stimulated by TDDFT calculations, which predicted that the Pc, Nb and tris-pyrrole MOs would show unusual mixing, considering that the frontier MOs are typically associated with either the Pc or the axial ligand, but not both (Fig. **7.6**). Treatment of THF solutions of $[PcNbCl_3]$ or $[PcTaCl_3]$ with the lithium salt of pyr_3CH turned purple instantly. No further colour change was observed upon heating or stirring over several days. Initial MS analysis of the reaction mixtures detected an oxidised $[M+O]^+$ species of the target product, although this could be an artefact of the ionisation process. Work-up of the Nb containing solution always resulted in an irreversible colour change from purple to brown. Deliberate oxidation of the product caused the initial blue-green colour to return. This suggests that the target product is not stable, and that binding may not be through all three N-donor atoms of pyr_3CH. A blue-green coloured species is however isolated from reactions with $[PcTaCl_3]$. ^1H NMR spectra of the Ta species suggest that the target complex has been isolated. Its UV–Vis spectrum is also significantly different from that of the Nb species, showing two strong peaks in the Q-band

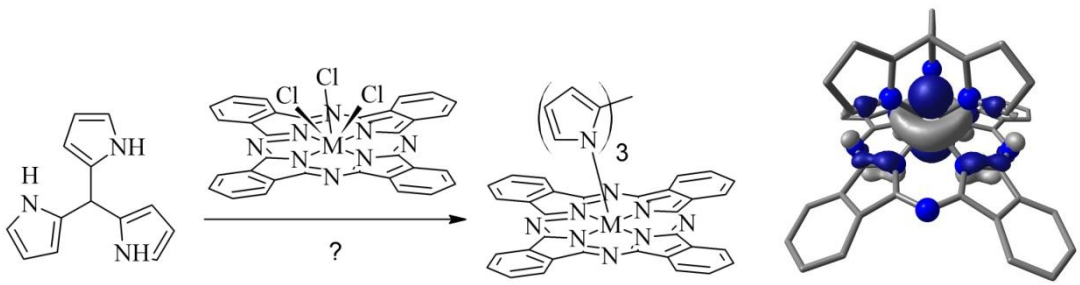

Figure 7.6: Potential coordination of tris(pyrrole)methan (pyr_3CH) to $[PcNbCl_3]$ and $[PcTaCl_3]$ (left), and the LUMO of $[PcNb(pyr_3CH)]$ as predicted by TDDFT calculations (right).

region, one of which is red-shifted beyond 700 nm. These differences in properties and reactivity appear to be solely metal-based. Further research is required to confirm this, and the true bonding situation in the Ta complex.

7.5 Experimental Section

General comments

Cyclic voltammetry (CV) was performed using an RHD Instruments microcell and temperature regulator. A Metrohm Autolab PGSTAT204 was used for the electrochemical interface and impedance measurements. Measurements were made under an N_2 atmosphere. A glassy carbon electrode was used as working electrode in conjugation with a Pt counter electrode and Ag/AgS reference electrode. Ferrocene was used as an internal standard for calibration of redox potentials. Dimethylsulfoxide (DMSO) and dichloromethane (DCM) were used as solvent for Pc and phthalonitrile complexes, respectively. Tetrabutyl ammonium hexafluorophosphate was used as electrolyte salt in all experiments. Phthalonitrile solutions were prepared at a concentration of 0.01 M, while saturated solutions were prepared for analysis of Pc complexes.

7.5.1 Syntheses of thiocatecholate and catecholate systems

$NiCl_2$(dppf) was synthesised according to.[146] 2,3,9,10,16,17,23,24-HO-PcH_2 was synthesised following the method of Ruf et al.[141], but using the dinitrile of Ivanov, *et al.*[147]

Synthesis of [bis-(diphenylphosphine)ferrocene](4,5-dithio-benzene-1,2-dicarbonitrile)-Nickel(II) (Ni(dtpn)(dppf))

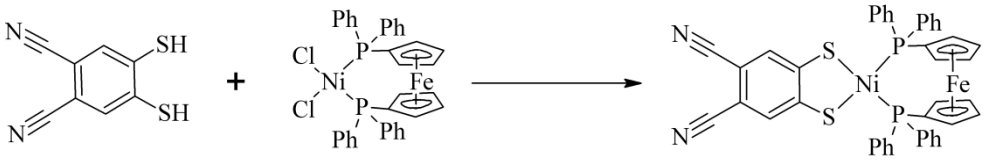

$NiCl_2$(dppf) (0.050 g; 0.074 mmol) was dissolved in $CHCl_3$ (10 ml) to give a green solution. H_2dtpn (0.014 g; 0.073 mmol) was then added to this solution, followed by NEt_3 (0.04 ml). This causes the solution colour to turn yellow-brown. The solution was sonicated for 15 min before being loaded onto a silica gel column. The product was eluted using $CHCl_3$ as the second coloured (tan) band. Solvent was evaporated to give the product as a red-brown solid.

^{1}H NMR ($CDCl_3$; 300 MHz; 298 K): δ (ppm) 4.24 (s, 4H, Fc); 4.42 (s, 4H, Fc); 7.37 (t, 8H, Ph); 7.46 (s, 2H, phthalonitrile); 7.50 (t, 4H, Ph); 7.80-7.85 (q, 8H, Ph)

^{13}C NMR ($CDCl_3$; 75 MHz; 298 K): δ (ppm) 105.77 (-*C*-CN); 117.17 (-*C*N); 128.15 (t); 130.98; 131.14; 134.75 (t); 156.78 (t); 162.50

^{31}P NMR (CDCl3; MHz; 298 K): δ (ppm) 27.60

MS(APCI+; DCM): Calc. for $C_{42}H_{30}N_2FeNiP_2S_2$ $[M+H]^+$: 803.1; Found: 803.1.

Synthesis of [tetra[bis(diphenylphosphino)ethane]nickel(II)](octa-β-hydroxolate-(phthalocyanine) ([(dppeNi)$_4$(O_8PcH_2)])

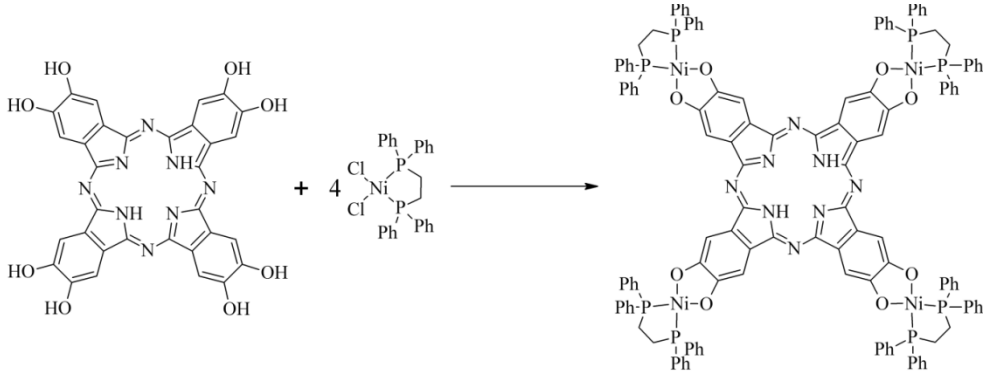

$(HO)_8PcH_2$ (0.10 g; 0.16 mmol) and $NiCl_2$(dppe) (0.33 g; mmol) were mixed together in MeOH/CH_2Cl_2 (1:5). NEt_3 (g; mmol) was added, causing the solution colour to change from green to blue. The solution was stirred for 4 h, during which time, the colour turns purple, and a purple solid precipitates. Solvent was evaporated and the solids were triturated with MeOH, Me_2CO and THF before being extracted with DCM. The extracts were combined and the solvent removed to leave a dark purple solid.

^{1}H NMR (DMSO-d6; 300 MHz; 298 K): δ (ppm) 1.25 (s, 8H, -C_2H_4-); 7.08 (m, 40H, Ph); 8.38 (s, 8H, Pc); 8.55 (m, 40H, Ph).

^{31}P NMR (DMSO-d6; 298 K): δ (ppm) 31.85.

UV–Vis (DMF): 731 (max), 561 (br), 405 (sh), 341, 305.

7.5.2 Syntheses for [(^{PegS8}Pc)Zn] and [($^{PegS6/HOOC\text{^}S}$Pc)Zn]

Synthesis of 2-[2-(2-methoxyethoxy)ethoxy]ethyl 4-methylbenzenesulfonate[148]

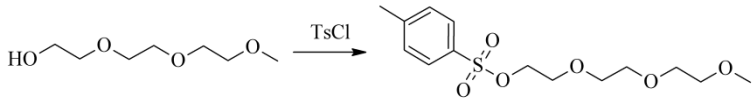

{2-[2-(2-methoxyethoxy)-ethoxy]-ethyl} (20.8 g; 126.5 mmol) and tosylchloride (24.1 g; mmol) were dissolved in THF (100 ml) and chilled on ice. KOH (27.9 g; mmol) was added to this solution slowly so as to maintain the temperature at 0 °C. The suspension was then stirred on ice for 1 h, before allowing it to gradually warm to room temperature over 4 h. Water (150 ml) was then added to the solution, and the organic phase was separated. The aqueous phase was then washed with water (2 x 50 ml). The organic portions were combined, dried over $MgSO_4$, filtered and the solvent was evaporated (rotavap) to leave a colourless oil.

Yield = 92 %.

^{1}H NMR ($CDCl_3$; 300 MHz; 298 K): δ (ppm) 2.43 (s, 3H, PhC*H*$_3$); 3.36 (s, 3H, OCH_3); 3.50-3.53 (m, 2H, CH_2); 3.58-3.60 (m, 6H, CH_2); 3.66-3.69 (m, 2H, CH_2); 4.13-4.16 (t, 2H, $PhS(O)_2O$-C*H*$_2$); 7.31-7.34 (m, 2H, Ph); 7.77-7.80 (m, 2H, Ph)

2-[2-(2-methoxyethoxy)-ethoxy]ethanthiol[149]

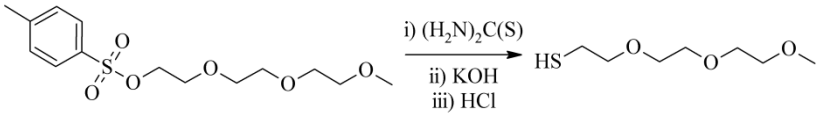

2-[2-(2-methoxyethoxy)ethoxy]ethyl 4-methyl-benzene-sulfonate (9.5 g; 34.7 mmol) was dissolved in EtOH (60 ml), and thiourea (3.0 g; 39.5 mmol) was added to this solution. The solution was then refluxed for 5 h. EtOH was then removed on a rotovap, and the residue was dissolved in a NaOH solution (21 % w/w; 60 ml). This solution was then refluxed for 4 h. It was then acidified with HCl (38 %, aq) to a pH of 2. The product was extracted with EtOAc (3 x 100 ml); the organic portions were combined, dried over Mg_2SO_4, filtered and the solvent was removed on a rotovap. The crude product was purified by distillation (50 °C at 10^{-3} mbar) to yield g of a clear pale-yellow liquid.

Yield = 60 %.

^{1}H NMR ($CDCl_3$; 300 MHz; 298 K): δ (ppm) 1.53-1.59 (t, 1H, SH); 2.63-2.70 (q, 2H, C*H*$_2$SH); 3.35 (s, 3H, -OCH_3); 3.51-3.64 (m, 10H, CH_2)

^{13}C NMR ($CDCl_3$; 75 MHz; 298 K): δ (ppm) 24.18, 58.95, 70.17, 70.49, 71.88, 72.83

4,5-bis({2-[2-(2-methoxyethoxy)ethoxy]ethyl}sulfanyl)benzene-1,2-dicarbonitrile[150]

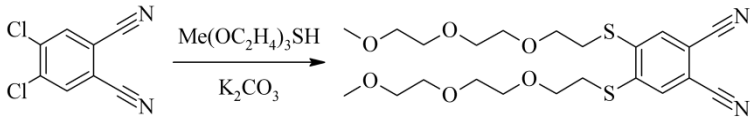

4,5-dichloro-phthalonitrile (1.16 g; 5.87 mmol) and finely powdered K_2CO_3 (8.40 g; 60.80 mmol) were mixed together before adding THF (40 ml). 2-[2-(2-methoxyethoxy)-ethoxy]ethanthiol (2.14; 11.80 mmol) was then added, and the suspension was stirred for 17 h at rt. H_2O (50 ml) was then added, and the two phases that formed were separated from each other. The aqueous phase was then extracted with THF (2 x 50 ml). The organic portions were combined, dried over Mg_2SO_4, filtered and the solvent was evaporated to leave a yellow oil. This was loaded onto silica and washed with Et_2O to elute the mono-substituted product as a yellow filtrate. Once the eluent was clear, THF was used to elute the desired product as a yellow-orange fraction. Solvent was removed to leave a dark orange-yellow oil.

Mass: 1.56 g

Yield = 55 %

^{1}H NMR ($CDCl_3$; 300 MHz; 298 K): δ (ppm) 2.49-2.54 (t, 2H, CH_2); 2.84-2.88 (t, 2H, CH_2); 3.00 (s, 6H, -CH_3); 3.16-3.43 (m, 20H, -CH_2-); 6.90 (s, 2H, Ar)

^{13}C NMR ($CDCl_3$; 75 MHz; 298 K): δ (ppm) 32.78, 59.02, 69.46, 70.65, 70.80, 71.95 (polyether); 111.56 (Ar); 115.50 (-CN); 129.54, 144.04 (Ar)

Synthesis of 6-[(3,4-dicyanophenyl)sulfanyl]acetic acid[151]

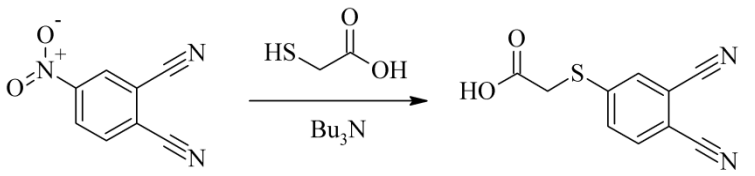

4-Nitrophthalonitrile (0.31 g; 1.77 mmol) and K_2CO_3 (1.30 g; 9.41 mmol) were mixed together in then dissolved in DMF (10 ml) to form a purple coloured solution. With vigorous stirring, HSAcOH (0.20 g; 2.15 mmol) was added, causing the solution colour to turn pale-yellow. Stirring was continued for 2 h, during which time, the suspension turns into a very thick slurry. Solids were dissolved by adding H_2O (50 ml). The solution was cooled to 0°C and then acidified to pH = 1 with HCl (37 %; aq). A beige precipitate forms that was filitered off and triturated with H_2O until the washing were neutral to litmus paper. Once dry, the solids were dissolved in THF and filtered through silica. Evaporation of the filtrate left a white solid.

Mass: 0.35 g

Yield = 92 %

^{1}H NMR (DMSO-d_6; 300 MHz; 298 K): δ (ppm) 4.06 (s, 2H, -SCH2-); 7.74-7.78 (dd, 1H, Ar); 8.00 (d, J_1 = 4.2 Hz, 1H, Ar); 8.06 (d, J_1 = 0.95 Hz, 1H, Ar)

^{13}C NMR (DMSO-d_6; 75 MHz; 298 K): δ (ppm) 33.37, 33.76, 114.88, 115.55, 130.35, 133.59, 146.06, 169.55

MS (APCI-; MeOH): *m/z* Calc. for $C_{10}H_5N_2O_2S$ $[M–H]^-$: 217.0077; Found: 217.0081.

Synthesis of 6-bromohexanoic acid[152]

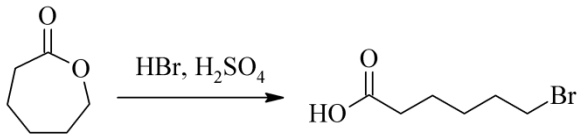

To ε-caprolactone (7.0 g) was added HBr (47 %, aq; 50 ml) and H_2SO_4 (98 %, 10 ml) dropwise. The solution was left to stand overnight (18 h) and then heated to reflux for 6 h. After cooling, the reaction solution was added to H_2O (200 ml) and extracted with Et_2O (3 x 150 ml). The organic portions were combined, dried over $MgSO_4$, filtered and the solvent was evaporated to leave a dark yellow oil. The oil eluted through a short silica column using Et_2O. The ether was then evaporated to afford the product as a clear oil.

^{1}H NMR ($CDCl_3$, 300 MHz, 298 K): δ (ppm) 1.44-1.54 (m, 2H, CH_2); 1.61-1.71 (m, 2H, CH_2); 1.82-1.93 (m, 2H, CH_2); 2.34-2.39 (t, 2H, CH_2COOH); 3.37-3.42 (t, 2H, CH_2Br)

^{13}C NMR ($CDCl_3$, MHz, 298 K): δ (ppm) 23.79, 27.56, 32.34, 33.27 (CH_2Br), 33.75 (CH_2COOH), 179.25 (COOH)

Synthesis of 6-mercaptohexanoic acid][153]

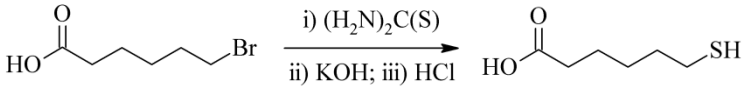

Method: 6-bromohexanoic acid and thiourea (4.50 g; 59.12 mmol) were dissolved in EtOH (50 ml). The solution was heated to reflux for 3 h. The EtOH was then evaporated and the residue was dissolved in H_2O. KOH (11.5 g; mmol) was added, and the solution was refluxed for a further 2 h to afford an orange solution. The solution was then acidifed while being cooled on an ice bath to pH 1 using HCl (37 %). The product was then extracted using EtOAc (3 x 100 ml). The organic portions were combined, dried over $MgSO_4$, filtered and the solvent was evaporated to leave a yellow oil. This was eluted through a short silica column using DCM. The product was obtained as a clear oil after evaporation of the DCM.

^{1}H NMR ($CDCl_3$, 300 MHz, 298 K): δ (ppm) 1.29-1.35 (t, 1H, -SH); 1.40-1.48 (m, 2H, CH_2); 1.57-1.68 (m, 4H, 2xCH_2); 2.32-2.37 (t, 2H, C*H*$_2$COOH); 2.47-2.55 (dt, 2H, C*H*$_2$SH); 11.48 (br, 1H, COOH)
^{13}C NMR ($CDCl_3$. 75 MHz, 298 K): δ (ppm) 24.03, 24.27, 27.66, 33.50 (CH_2SH), 33.85 (CH_2COOH), 180.00 (COOH)

Synthesis of 6-[(3,4-dicyanophenyl)sulfanyl]hexanoic acid (mCAHexSPN)

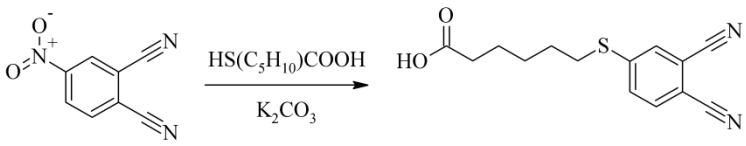

4-Nitrophthalonitrile (3.01 g; 17.33 mmol) was mixed with K_2CO_3 (7.5 g;), and then DMF (30 ml) was added to form a suspension with a purple supernatant. The suspension was cooled on ice while 6-mercaptohexanoic acid (2.8 g; mmol) was added dropwise with vigorous stirring. The purple colour instantly disappears as the supernatant becomes orange.

After addition of the thiol, stirring was continued for 15 h at rt. During this time, the entire suspension solidifies. It was then added to H_2O (150 ml) and acidified to pH 1 using HCl (37 %). A white solid forms that was collected by filtration and washed with H_2O until the washings were neutral. The solids were then dissolved in THF, dried over $MgSO_4$ and filtered. The solvent was evaporated to leave a yellow-orange solid. This was suspended in DCM and then loaded onto a short silica column. The column was then washed thoroughly with DCM, and then THF was used to elute the product. Evaporation of the solvent left a white solid.

Mass: 4.14 g

Yield = 87 %

^{1}H NMR (DMSO-*d6*, 300 MHz, 298 K): 1.35-1.67 (m, 6H, 3xCH_2); 2.18-2.22 (t, 2H, C*H*$_2$COOH); 3.11-3.16 (t, 2H, CH_2S); 7.72-7.76 (dd, 1H, Ar); 7.95 (s, 1H, Ar); 8.018-8.024 (d, 1H, Ar); 11.94 (br, 1H, COOH) (*contaminated with DMF)

^{13}C NMR (DMSO-*d6*, 75 MHz, 298 K): 23.93, 27.50, 27.63, 30.42, 33.49 (CH_2S), 109.56, 115.10, 115.61 (CN), 116.09 (CN), 130.30, 130.39, 133.62, 146.77, 174.29 (COOH)

MS (APCI+): Calc. for $C_{14}H_{13}N_2O_2S$ $[M+H]^+$: 273.0703; Found: 273.0706.

Synthesis of [(^{PEGS8}*Pc)Zn]*[142]

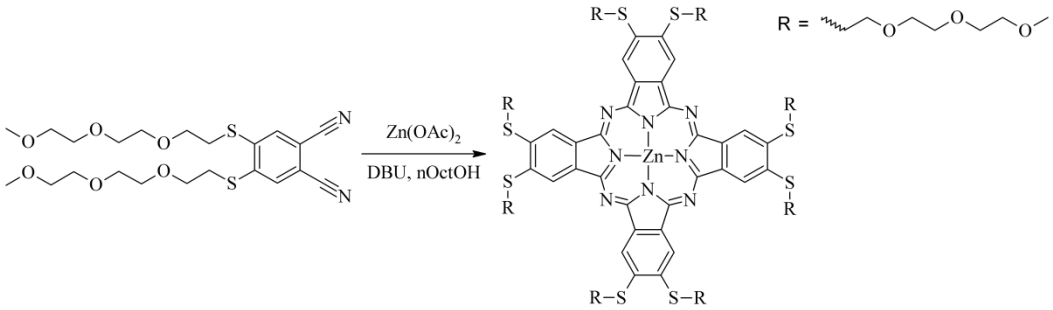

$Zn(OAc)_2$ (0.065 g; 0.3 mmol), E3SPN (0.24 g; 0.49 mmol) and DBU (0.12 g; 0.79 mmol) were dissolved in 1-hexanol (25 ml), and placed in a metal bath that had been preheated to 180 °C. The solution was refluxed for 1.5 h. The solution was then allowed to cool to room temperature before being diluted with Et_2O (40 ml). This solution was then washed twice with H_2O (25 ml) saturated with NaCl. The organic portion was then dried over $MgSO_4$ and evaporated to leave a dark green viscous solid. The product was purified by chromatography over silica (DCM:EtOH – 10:1).

Mass: 0.120 g

Yield = 49 %

^{1}H NMR (300 MHz; DMSO-d6; 298 K): 3.17 (s, 24H, -C*H*$_3$); 3.32-3.41 (m, 16H, CH_2); 3.53-3.56 (m, 16H, CH_2); 3.66-3.71 (m, 32H, -CH_2-); 3.77-3.81 (m, 16H, -CH_2-); 4.06-4.10 (t, 16H, -CH_2-); 8.73 (s, 8H, Pc)

^{13}C NMR (75 MHz; DMSO-d6; 298 K): 151.1, 138.0, 135.1, 130.0 (Ar), 71.2, 69.90, 69.87, 69.7, 57.9, 33.1 (Alk).

Synthesis of [(^{PEGS8}Pc)Mg]

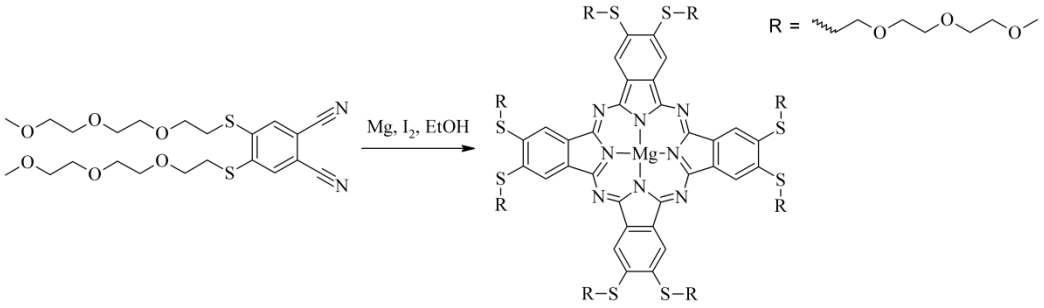

Magnesium powder (1.00 g: 43.5 mmol) and a crystal of iodine (catalyst) were suspended in EtOH (20ml), and the suspension was heated to reflux until all Mg powder had reacted to form magnesium ethoxide. The dinitrile (X) (1.26 g: 2.50 mmol) was added to this suspension, which was then refluxed for a further 20 h. The dark green solution was then cooled and filtered through filter aid. The filter aid was further washed with EtOH. All fractions were combined before adding petroleum ether, which caused an oily phase to separate out. This phase was extracted with Et_2O (3 x 100 ml). The extracts were combined and evaporated to leave a dark green viscous product, which analysis showed to be pure product.

Mass: 0.403 g

Yield = 32.8 %

^{1}H NMR (DMSO-d_6, 300 MHz, 298 K): δ (ppm) 3.15 (s, 24H, -CH_3); 3.36-3.39 (m, 16H, CH_2); 3.51-3.54 (m, 16H, CH_2); 3.63-3.77 (m, 48H, CH_2); 4.03 (t, 16H, -SCH_2-); 9.04 (s, 8H, Pc)

HRMS (APCI+): *m/z* Calc. for $[M+H]^+$: 1963.6759; Found: 1963.6745

Synthesis of [Zn(Pc(E3S)^{A3}(SCH$_2$COOH)^{B}]

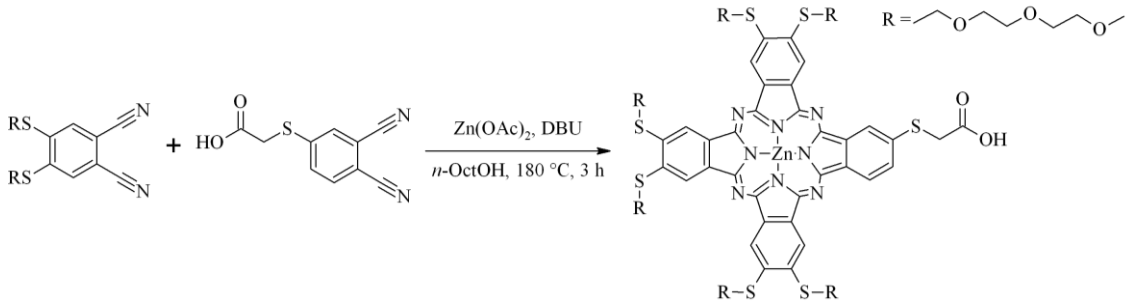

The dinitriles PN^{SPeg} (1.41 g; 2.90 mmol) and PN$^{S\text{^}COOH}$ (0.21 g; 0.96 mmol) and Zn(OAc)$_2$ (0.71 g; 3.87 mmol) were mixed together and dissolved in n-octanol (3 ml) and DBU (0.1 ml). The suspension was homogenised using an ultrasound bath and then heated to 190 °C for 3 h. The solids soon dissolved to give a dark green solution. After cooling to rt, the solution was diluted with hexane. The solids that separated were washed with hexane and extracted into THF. The THF extracts were filtered through silica before being evaporated to leave a sticky green residue. This was dissolved in EtOAc and loaded onto a silica gel column. The desired A$_3$B-type Pc was isolated as the second green band by elution with THF/EtOAc (10:2.5).

^{1}H NMR (300MHz; DMSO-*d6*; 298 K): δ (ppm) 3.2 – 3.8 (m, 93 H, -C*H*$_2$- & -C*H*$_3$); 7.79 (s, 9H, Pc)
MS(APCI+): *m/z* Calc. for [M–OH$_2$]$^+$: 1717.5; Found: 1717.3.

7.5.3 Syntheses for [(^{Me2}TIPc)Mg]I$_8$ and [(^{Me}TIPc)Mg]

Synthesis of 4,5-bis[(1-methyl-1H-imidazol-2-yl)sulfanyl]benzene-1,2-dicarbonitrile

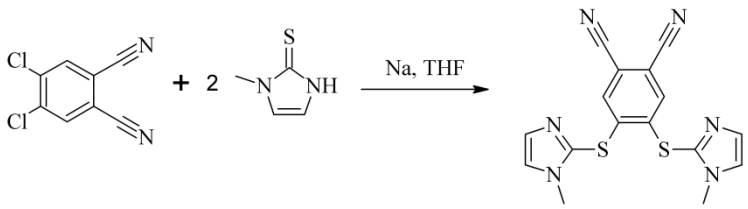

1-methyl-1*H*-imidazole-2-thiol (5.00 g; 43.8 mmol) was dissolved in THF (50 ml), and Na (1.00 g; 43.5 mmol) was added to this solution. The solution was stirred at rt until all Na had dissolved. 4,5-dichlorophthalonitrile (4.31 g; 21.9 mmol) was dissolved in THF (50 ml) and

chilled on ice. The sodium thiolate containing solution was added slowly to the other one with vigorous stirring (exothermic). A red colour develops instantly, but within 1 hour, a white coloured precipitate forms and the supernatant becomes yellow. The suspension was then diluted with MeOH (200 ml) and the precipitate was collected by filtration. This was washed with MeOH until the washings were colourless. The white solid thus obtained is of suitable purity for further reactions.

Mass: 4.08 g

Yield: 52.9 %

^{1}H NMR ($CDCl_3$, 300 MHz): δ (ppm) 7.61 (d, 2H, Im-ar), 7.23 (d, 2H, Im-ar), 7.14 (s, 2H, ar), 3.69 (s, 6H, N-C*H*$_3$)

MS: (APCI(+) HRMS): *m/z* 353.0637 ($M+H^+$), Calc. for $C_{16}H_{13}N_6S_2$: 353.0638

Synthesis of [(^{Me}ITPc)Mg]

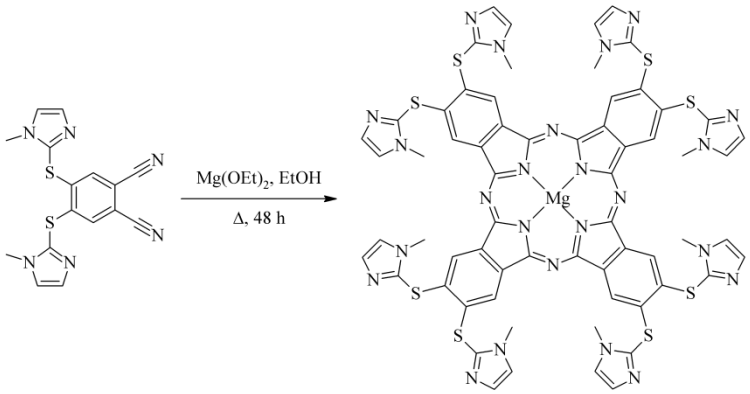

The dinitrile (2.99 g; 8.51 mmol) was mixed with $Mg(OEt)_2$ (1.54 g; 13.5 mmol). The mixture was suspended in TEG-MME (60 ml) and then placed in an oil bath preheated to 150 °C for h. During this time, all solids dissolve and the solution becomes blue. The solution was then cooled to rt, and H_2O (250 ml) was added slowly. This causes a green compound to precipitate. The precipitate was collected by filtration and washed thoroughly with H_2O until the washing were colourless. The solids were then suspended in EtOH with the aid of an ultrasound bath. Solvent was then evaporated to leave a dark green solid, which was washed using EtOH, Me_2CO, THF and Et_2O. The solid was insoluble in all solvents common organic laboratory solvents. It was sparingly soluble in acetic acid and dilute HCl (10%, aq), but not sufficiently so for NMR analysis.

Synthesis of [(^{Me2}ITPc)Mg]I_8

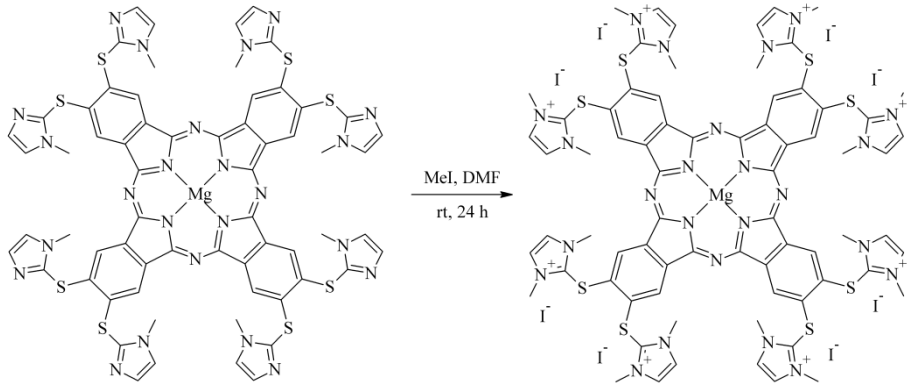

[(^{Me}ITPc)Mg] was dissolved in DMF (10 ml). MeI (3 ml) was added in excess, and the solution was warmed to 70 °C for 24 h. The solution was then poured into THF, and the precipitate that formed was collected and triturated with THF. The solids remaining were then dissolved in a minimal amount DMF and the resulting solution was added to THF to reprecipitate the product. This process was repeated until the obtained supernatant/filtrate was colourless.

^{1}H NMR (300 MHz, D_2O, 298 K): δ (ppm) 9.72 (8H, s, ar-Pc); 8.07 (16H, s, Im-N-CH_2CH_2-N); 4.17 (48 H, s, Im-CH_3)
UV-Vis (H_2O): 696, 658 (sh), 627, 366.

7.5.4 Notable syntheses involving niobium and tantalum

Comments
The synthesis of complexes [M(NR)Cl_3(dme)], where M is Nb or Ta, were performed according to the procedure described by KOROLEV *et al.*[154] [PcNbCl_3] and [PcTaCl_3] were synthesised according to the method of CELLUCCI *et al.*.[155] The tridentate ligand, pyr$_3$CH, was prepared following the method described by UMASEKHAR *et al.*[145].

General procedure for the synthesis of [PcM(NR)Cl_3] (M = Nb or Ta; R = tBu, Mes, Ph)
[M(N*t*Bu)Cl_3(dme)] (1 eq) and PN (5 eq) were dissolved in dichlorobenzene (7 ml) and heated to 170 °C for 22 h. The obtained blue-green solids were then triturated with pentane

(15 ml x 3) before extracting the remaining solids with DCM (4 x 50 ml). The extracts were combined and evaporated to leave a green solid.

[PcNb(NtBu)Cl]

Elemental analysis (%): Calc. (Found): C 60.73 (61.55), H 3.54 (4.71), N 17.71 (15.38)

^{1}H NMR (300 MHz; DMSO-*d6*; 298 K): δ (ppm) 7.82-7.95 (m, 8H, Pc); 8.13-8.16 (m, 8H, Pc); 1.66 (s, 14H, C*H*$_3$)

MS(MALDI+): Calc. for $C_{36}H_{26}N_9ClNb$ [M+H$^+$]: 711.01; Found: 711.91.

[PcTa(NtBu)Cl]

MS(MALDI+): Calc. for $C_{36}H_{26}N_9ClTa$ [M+H]$^+$: 799.14; Found: 799.06.

Attempted synthesis of [PcNb(pyr$_3$CH)]

(Pyr)$_3$CH (0.11 g; 0.52 mmol) was dissolved in THF (20 ml), and BuLi (2.75 M, 0.54 ml) was added to this solution at 0 °C. This solution was then added directly to solid [$PcNbCl_3$] (0.31 g; 0.43 mmol). The dark green suspension turns purple within minutes. It was sonicated for 10 min and then stirred at rt for 48 h and then heated to 70 °C for 7 h. Solvent was then removed *in vacuo* to leave a dark blue solid. This was dissolved in DCM and filtered. The filtrate was evaporated to leave a dark blue solid that turns dark brown within hours. Adding solvent to the brown solid does not cause the initial colour to be regained.

^{1}H NMR (300 MHz; THF-*d8*; 298K): δ (ppm) 5.60 (s, 1H, C*H*); 5.94 (s, 3H, Pyr); 6.08 (s, 3H, Pyr); 6.73 (s, 3H, Pyr); 7.08 – 8.63 (m, 8H, Pc); 9.91 (s, 3H, OH?).

MS(ESI+): Calc. for [M+O]$^+$: 829.14; Found: 830.13.

UV-Vis (THF): 687, 623 (sh), 518 (sh), 448 (sh), 352 (sh)

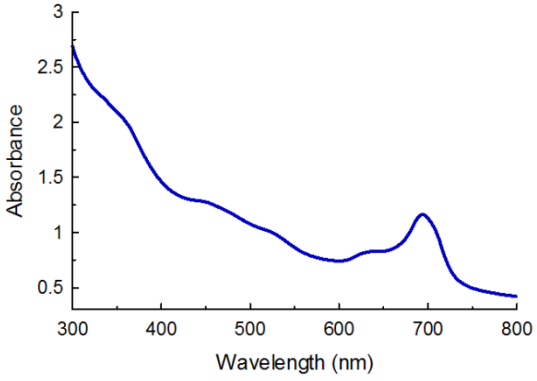

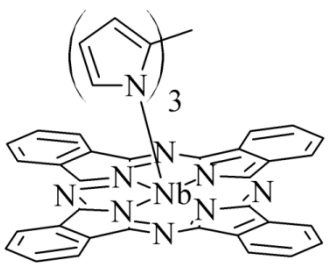

Attempted synthesis of [PcTa(pyr$_3$CH)]

(Pyr)$_3$CH (0.11 g; 0.52 mmol) was dissolved in THF (20 ml), and BuLi (2.75 M, 0.54 ml) was added to this solution at 0 °C. This solution was then added directly to solid [PcNbCl$_3$] (0.42 g; 0.52 mmol). The dark green suspension turns purple within minutes. It was sonicated for 15 min and then stirred at rt for 48 h and then heated to 70 °C for 8 h. Solvent was then removed *in vacuo* to leave a dark blue solid. This was dissolved in DCM and filtered. The filtrate was evaporated to leave a dark blue-green solid.

^{1}H NMR (THF-d8; 300 MHz; 298 K): δ (ppm) 5.45 (s, 1H, -C*H*); 5.96 (s, 3H, Pyr); 6.08 (s, 3H, Pyr); 6.59 (s, 3H, Pyr); 7.32-8.21 (m, 16H, Pc)

UV-Vis (THF): 708, 664, 634 (sh), 594 (sh), 525 (br), 468 (sh), 356 (sh)

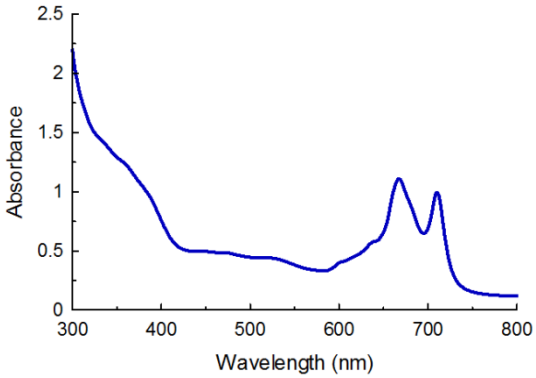

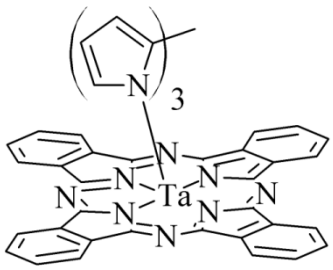

CHAPTER 8 | REFERENCES

[1] Theopompus, cited by Athenaeus (12:526), **200 B.C**.

[2] R. Brightman, *Nature*, **1956**, *177*, 815-821.

[3] A. von Baeyer, A. Emmerling, *Ber. Dtsch. Chem. Ges.,* **1870**, *3*, 514.

[4] A. Braun, J. Tcherniac, *Ber. Dtsch. Chem. Ges.,* **1907**, *40*, 2709–2714.

[5] D. Wöhrle, G. Schnurpfeil, S. Makarov, O. Suvora, *Chemie in unserer Zeit*, **2012**, *46*, 12–24.

[6] R.M. Christie and D.D. Deans, *J. Chem. Soc., Perkin Trans. 2*, **1989**, 193.

[7] I.- S. Tamgho, J. T. Engle, C. J. Ziegler, *J. Org. Chem.*, **2012**, *77(24)*, 11372-11376.

[8] T.J. Hurley, M.A. Robinson and S.I. Trotz, *Inorg. Chem.*, **1967**, *6*, 389-392.

[9] J.A. Elvidge and R.P. Linstead, *J. Chem. Soc.*, **1955**, 3536–3544.

[10] C.C. Leznoff and S. Greenberg, *Chem. Abstr.*, **1978**, *88*, 171797–171801.

[11] J.G. Young and W. Onyebuagu, *J. Org. Chem.,* **1990**, *55*, 2155–2159.

[12] C.C. Leznoff, S. Greenberg, B. Khouw and A.B.P. Lever, *Can. J. Chem.*, **1987**, *65*, 1705-1713.

[13] a) E. E. Reid, *Organic chemistry of bivalent sulfur. Vol. 3*, Chemical Publishing Co., New York. **1960**, Chap. 2; b) A. M. Islam, I. B. Hannout, A. M. El-Sharief, *Indian J. Chem., B: Org. Chem. Incl Med. Chem.*, **1977**, *15(1)*, 61-3.

[14] E.V. Kudrik, I.Y. Nikolaev and G.P. Shaposhnikov, *Russ. Chem. Bull., Int. Ed.*, **2000**, *49(12)*, 2027-2030.

[15] S.Y.S. Chow and D.K.P. Ng, *Org. Lett.*, **2016**, *18*, 3234-3237.

[16] C.C. Leznoff and T. W. Hall, *Tetrahedron Letters*, **1982**, *23*, 3023–3026.

[17] T.W. Hall, S. Greenberg and C.R. McArthur, Kh, *Nouv. J. Chim.,* **1982**, *6*, 653–658.

[18] N. Kobayashi, R. Kondo, S. Nakajima and T. Osa, *J. Am. Chem. Soc.*, **1990**, *112*, 9640–9641.

[19] A. Weitemeyer, H. Kliesch and D. Wöhrle, *J. Org. Chem.*, **1995**, *60*, 4900-4904.

[20] A. Sastre, B. Del Rey and T. Torres, *J. Org. Chem.*, **1996**, *61(24)*, 8591-8597.

[21] C.G. Claessens, D. Gonzalez-Rodriguez, B. del Rey, T. Torres, G. Mark, H.-P. Schuchmann, C. Von Sonntag, J.G. MacDonald and R.S. Nohr, *Eur. J. Org. Chem.,* **2003**, 2547-2551.

[22] E.H. Gacho, H. Imai, R. Tsunashima, T. Naito, T. Inabe, N. Kobayashi, *Inorg. Chem.*, **2006**, *45(10)*, 4170-4176

[23] M.J. Gouterman, *Chem. Phys.*, **1959**, *30*, 1139-1161.

[24] K. Ishii, H. Itoya, H. Miwa, M. Fujitsuka, O. Ito and N. Kobayashi, *J. Phys. Chem.*, **2005**, *109(26)*, 5781-5787.

[25] W.F. Kosonocky, S.E. Harrison and R. Stander, *J. Chem. Phys.*, **1965**, *43*, 831-833.

[26] M. Mac, A. Danel, K. Kizior, P. Nowak, A. Karocki and B. Tokarczyk, *Phys. Chem. Chem. Phys.*, **2002**, *5*, 988-997.

[27] T.-H. Huang, K.E. Rieckhoff and E.M. Voigt, *Chem. Phys.*, **1979**, *36*, 423-436.

[28] K. Kikuchi, M. Hoshi, T. Niwa, Y. Takahashi and T. Miyashi, *J. Phys. Chem.*, **1991**, *95*, 38–42.

[29] D. Wöhrle, M. Eskes, K. Shigehara and A. Yamada, *Synthesis*, **1992**, 194-196.

[30] T. Furuyama, K. Satoh, T. Kushiya and N. Kobabyashi, *J. Am. Chem. Soc.*, **2014**, *136*, 765-776.

[31] E.G. Gal'pern, E.A. Luk'yanets, M.G. Gal'pern, *Izvestiya Akademii Nauk SSSR, Seriya Khimicheskaya*, **1973**, *9*, 1976-80.

[32] N. Kobayashi, S.I. Nakajima, H. Ogata, T. Fukuda, *Chem. Eur. J.*, **2004**, *10(24)*, 6294-6312.

[33] R.P. Linstead, E.G. Noble and J.M. Wright, *J. Chem. Soc.*, **1937**, 911-921.

[34] T. Nyokong, *Coord. Chem. Rev.*, **2007**, *251*, 1707-1722.

[35] X.-F. Zhang, Q. Xi and J. Zhao, *J. Mater. Chem.*, **2010**, *20*, 6726-–6733.

[36] J.R. Darwent, P. Douglas, A. Harriman, G. Poter and M.C. Richoux, *Coord. Chem. Rev.*, **1982**, *44*, 83–126.

[37] D.S. Lawrence and D.G. Whitten, *Photochem. and Photobio*, **1996**, *64(6)*, 923–935.

[38] S. A. Mikhalenko, L. I. Solov'eva, E. A. Luk'yanets, *J. Gen. Chem. USSR* **1988**, *58*, 2618–2619.

[39] D. M. Roundhill, *Photochemistry and Photophysics of Metal Complexes*, Plenum Press, New York, **1994**, 10–11.

[40] P. Erk, H. Engelsberg (Ed.) *Phthalocyanines Dyes and Pigments*, Elsevier Science, San Diego, **2003**

[41] C.C. Leznoff and A. B.P. Lever, Eds., *Phthalocyanines, Properties and Applications*, Wiley-VCH: New York, **1989**.

[42] A. B. Sorokin, *Chemical Reviews*, **2013**, *113*, 8152–8191.

[43] F. Rollet, S. Morlat-Therias and J.-L. Gardette, *Polymer Degradation and Stability*, **2009**, *94*, 877-885.

[44] S.H. Kim, J.W. Namgoong, S.B. Yuk, J.Y. Kim, W. Lee, C. Yoon and J.P. Kim, *J. Incl. Phenom Macrocycl. Chem.*, **2015**, *82*, 195-202; b) J. Choi, S.H. Kim, W. Lee, C. Yoon, J.P. Kim, *New J. Chem.*, **2012**, *36*, 812.

[45] K.-Y. Law, *Chem. Rev.*,**1993**, *93*, 449–486

[46] a) I. López-Duarte, M. Wang, R. Humphry-Baker, M. Ince, M. V. Martínez-Díaz, M. K. Nazeeruddin, T. Torres, M. Grätzel, *Angew. Chem.*, **2012**, *124*, 1931–1934; b) J. Zaumseil, H. Sirringhaus, *Chemical Reviews*, **2007**, *107*, 1296–1323; c) E. Palomares, M. V. Martinez-Diaz, S. A. Haque, T. Torres, J. R. Durrant, *Chem. Commun.* **2004**, 2112–2113.

[47] G. de la Torre, P. Vazquez, F. Agullo-Lopez, T, Torres, *J. Mater. Chem.*, **1998**, *8*, 1671–1683.

[48] a) A.J. Pearson, T. Plint, S.T.E. Jones, B.H. Lessard, D. Credgington, T.P. Bender and N.C. Greenham, *J. Mater. Chem. C*, **2017**, *5*, 12688-12698; b) D. Zhao, W. Huang, Z. Qin, Z. Wang and J. Yu, *ACS Omega*, **2018**, *3*, 3348-3356; c) D. Hohnholz, S. Steinbrecher and M. Hanack, *J. Mol. Struct.*, **2000**, *521*, 231-237.

[49] X.D. Wang and O.S. Wolfbeis, *Chem. Soc. Rev.*, **2014**, 43, 3666-3761.

[50] a) X. Li, B.D. Zheng, X.H. Peng, S.-Z. Li, J.W. Ying, Y. Zhao, J.-D. Huang and J. Yoon, Phthalocyanines as medicinal photosensitizers: Developments in the last five years, *Coord. Chem. Rev.*, **2017**; b) N. Sekkat, H. Van den Bergh, T. Nyokong and N. Lange, *Molecules*, **2012**, *17*, 98-144.

[51] D. Dei, G. Chiti, M.P. De Filippis, L. Fanetti, F. Giuliani, F. Giutini, M. Soncin, G. Jori and G. Roncucci, *J. Porphyrins Phthalocyanines*, **2006**, *10*, 147–159.

[52] a) H. Yaku, T. Fujimoto, T. Murashima, D. Miyoshi and N. Sugimoto, *Chem. Commun*, **2012**, *48*, 6203-6216; b) H. Yaku, T. Murashima, D. Miyoshi and N. Sugimoto, *Molecules*, **2017**, *17*, 10586-10613.

[53] https://www.erneuerbare-energien.de/EE/Redaktion/DE/Dossier/eeg.html?cms_docId=73930

[54] *Bundesministerium für Wirtschaft und Energie*, www.erneubare-energien.de – Informationsportal Erneubare Energien.

[55] *BP Statistical Review of World Energy*, **2017**

[56] S. Elliot, *The Physics and Chemistry Solids*, John Wilely and Sons Ltd, Chichester, England, **1998**.

[57] a) D. M. Chapin, C. S. Fuller, G. L. Pearson, *J. Appl. Phys.*, **1954**, *25*, 676–677; b) S. Chhajed, M. F. Schubert, J. K. Kim, E. F. Schubert, *Appl. Phys. Lett.* **2008**, *93*, 251108-1–251108-3.

[58] M. Grätzel, *J. Photochem. Photobio. C: Photochem. Rev.*, **2003**, *4*, 145-153.

[59] M. Stuckelberger, R. Biron, N. Wyrsch, F.- J. Haug and C. Ballif, *Renew. Sus. Energy Rev.*, **2017**, *76*, 1497–1523.

[60] S. Moon, K. Kim, Y. Kim, J. Heo and J. Lee, *Scientific Reports*, **2016**, 1-6.

[61] M. Graetzel, *Nature*, **2001**, *414*, 338-344.

[62] A. Hagfeldt and M. Graetzel, *Acc. Chem. Rec.*, **2000**, *33*, 269-277.

[63] a) S. Arote, R. Ingle, V. Tabhane and H. Pathan, *J. Renewable Sustainable Energy*, **2014**, *6*, 013132; b) F. Lenzmann, J. Krueger, S. Burnside, K. Brooks, M. Grätzel, D. Gal, S. Rühle and D. Cahen, *J. Phys. Chem. B*, **2001**, *105(27)*, 6347-6352.

[64] S. Ardo and G.J. Meyer, *Chem. Soc. Rev.*, **2009**, *38*, 115-164.

[65] A. Hagfeldt, G. Boschloo, L. Sun, L. Kloo and H. Pettersson, *Chem. Rev.*, **2010**, *110*, 6595-6663.

[66] B.E. Hardin, H.J. Snaith and M.D. McGehee, *Nature Photonics*, **2002**, *6*, 162-169.

[67] J. Burschka, A. Dualeh, F. Kessler, E. Baranoff, N.L. Cevey-Ha, C. Yi, M. Nazeeruddin and M. Grätzel, *J. Am. Chem. Soc.*, **2011**, *133*, 18042‑18045.

[68] a) Y. Liu, H. Lin, J. Li and K. He, *Mater. Sci.Eng. B*, **2009**, *161*, 8–11; b) D. Qi and J. Jiang, *J. Phys. Chem. A*, **2011**,*115*, 13811–13820.

[69] a) E. A. Ermilov, J.-Y. Liu, R. Menting, Y.-S. Huang, B. Röder and D. K. P. Ng, *Phys. Chem. Chem. Phys.*, **2016**, *18*, 10964-10975; b) C. K. C. Bikram, N. K. Subbaiyan and F. D'Souza, *J. Phys. Chem. C*, **2012**, *116*, 11964-11972; c) A. K. Mandal, J. R. Diers, D. M. Niedzwiedzki, G. Hu, R. Liu, E. J. Alexy, J. S. Lindsey, D. F. Bocian and D. Holten, *J. Am. Chem. Soc.*, **2017**, *139*, 17547-17564; d) C. Aumaitre, C. Rodriguez-Seco, J. Jover, O. Bardagot, F. Caffy, Y. Kervella, N. Lopez, E. Palomares and R. Demadrille, *J. Mater. Chem. A*, **2018**, *6*, 10074-10084; e) T. Kawata, Y. Chino, N. Kobayashi and M. Kimura, *Langmuir*, DOI: 10.1021/acs.langmuir.8b01118; f) T. Jiang, N. F. Polizzi, J. Rawson and M. J. Therien, *J. Am. Chem. Soc.*, **2017**, *139*, 8415-8415.

[70] M.-E. Ragoussi, J.-H. Yum, A. K. Chandiran, M. Ince, G. de la Torre, M. Gratzel, M. K. Nazeeruddin and T. Torres, *ChemPhysChem*, **2014**, *15*, 1033.

[71] T. Ikeuchi, H. Nomoto, N. Masaki, M. J. Griffith, S. Mori and M. Kimura, *Chem. Commun.*, **2014**, *50*, 1941–1943.

[72] A. Yella, H. W. Lee, H. N. Tsao, C. Yi, A. K. Chandiran, M. K. Nazeeruddin, E. W. Diau, C. Y. Yeh, S. M. Zakeeruddin and M. Grätzel, *Science*, **2011**, *334*, 629-634.

[73] S.E. Koops, B.C. O'Regan, P.R.F. Barnes and J.R. Durrant, *J. Am. Chem. Soc.*, **2009**, *131*, 4808-4818.

[74] A. Mahmood, J.- Y. Hu, B. Xiao, A. Tang, X. Wang and E. Zhou, *J. Mater. Chem. A.*, **2018**, *6*, 16769–16797.

[75] H. Kang, G. Kim, J. Kim, S. Kwon, H. Kim and K. Lee, *Adv. Mater.*, **2016**, *28*, 7821-7861.

[76] G. de la Torre, G. Bottari and T. Torres, *Adv. Energy Mater.*, **2017**, *7*, 1601700.

[77] a) B. J. Campo, J. Duchateau, C. R. Ganivet, B. Ballesteros, J. Gilot, M. M. Wienk, W. D. Oosterbaan, L. Lutsen, T. J. Cleij, G. de la Torre, R. A. J. Janssen, D. Vanderzande, T. Torres, *Dalton. Trans.*, **2011**, *4*, 3979–3988; b) H. B. Gobeze, T. Tram, C. B. Kc, R. R. Cantu, P. A. Karr and F. D'Souza, *Chin. J. Chem.*, **2016**, *34*, 969-974.

[78] S. Honda, T. Nogami, H. Ohkita, H. Benten, S. Ito, *ACS Appl. Mater. Interfaces*, **2009**, *1*, 804–810.

[79] *Solar Fuels and Artificial Photosynthesis*, RSC, **2012,** www.rsc.org/solar-fuels

[80] A. Fujishima and K. Honda, *Nature*, **1972**, *238*, 37–38.

[81] a) X. Zhang, T. Peng and S. Song, *J. Mater. Chem. A*, **2016**, *4*, 2365-2402; b) N. Serpone, E. Pelizzetti and M. Grätzel, *Coord. Chem. Rev.*, **1985**, *64*, 225-245.

[82] C. Kutal, *Coord. Chem. Rev.*, **1985**, *64*, 191-206.

[83] Z. Han and R. Eisenberg, *Acc. Chem. Res.*, **2014**, *47*, 2537-2544.

[84] L. Gan, T. L. Groy, P. Tarakeshwar, S. K. S. Mazinani, J. Shearer, V. Mujica and A. K. Jones, *J. Am. Chem. Soc.*, **2015**, *137*, 1109-1115.

[85] B. H Solis, S. Hammes-Schiffer, *J. Am. Chem. Soc.*, **2012**, *134*, 15253-15256.

[86] Bo Zheng, Randy P. Sabatini, Wen-Fu Fu, Min-Sik Eum, William W. Brennessel, Lidong Wang, David W. McCamant and Richard Eisenberg, *PNAS*, **2015**, E3987-E3996.

[87] P. Du and R. Eisenberg, *Energy Environ. Sci.*, **2012**, *5*, 6012-6021.

[88] X. Hu, B. S. Brunschwig and J. C. Peters, *J. Am. Chem. Soc.*, **2007**, *129*, 8988–8998.

[89] J. L. Dempsey, B. S. Brunschwig, J. R. Winkler and H. B. Gray, *Acc. Chem. Res.*, **2009**, *42*, 1995–2004.

[90] A. Wegelius, N. Khanna, C. Esmieu, G. D. Barone, F. Pinto, P. Tamagnini, G. Berggren and P. Lindblad, *Energy Environ. Sci.*, **2018**, DOI: 10.1039/c8ee01975d

[91] M. P. McLaughlin, T. M. McCormick, R. Eisenberg and P. L. Holland, *Chem. Commun.*, **2011**, *47*, 7989–7991.

[92] a) G. N. Schrauzer and V. Mayweg, *J. Am. Chem. Soc.*, 1962, **84**, 3221–3221; b) A. Davison, N. Edelstein, R. H. Holm and A. H. Maki, *J. Am. Chem. Soc.*, 1963, **85**, 2029–2030; c) A. Davison, N. Edelstein, R. H. Holm and A. H. Maki, *Inorg. Chem.*, 1963, **2**, 1227–1232; d) H. B. Gray, R. Williams, I. Bernal and E. Billig, *J. Am. Chem. Soc.*, 1962, **84**, 3596–3597; e) E. Billig, R. Williams, I. Bernal, J. H. Waters and H. B. Gray, *Inorg. Chem.*, 1964, **3**, 663–666; f) J. A. McCleverty, *Prog. Inorg. Chem.*, 1968, **10**, 49–221.

[93] M. D. Ward and J. A. McCleverty, *J. Chem. Soc*., *Dalton Trans*., **2002**, 275–288; R. L. Cowan, D. B. Pourreau, A. L. Rheingold, S. J. Geib and W. C. Trogler, *Inorg. Chem.*, **1987**, *26*, 259-265

[94] a) S. D. Cummings and R. Eisenberg, *J. Am. Chem. Soc.*, **1996**, *118*, 1949-1960; b) D. Espa, L. Pilia, L. Marchio, F. Artizzu, A. Serpe, M. L. Mercuri, D. Simao, M. Almeida, M. Pizzotti, F. Tessore and P. DePlano, *Datlon Trams.*, **2012**, *41*, 3485-3493.

[95] W. Paw, S. D. Cummings, M. A. Mansour, W. B. Connick, D. K. Geiger and R. Eisenberg, *Coord. Chem. Rev.*, **1998**, *171*, 125-150.

[96] a) C. S. Velázquez, W. E**.** Broderick, M. Sabat, A. G. M. Barrett, and B. M. Hoffman, *J. Am. Chem. Soc.*, **1990**, *112*, 7408-7410; b) T. F. Baumann, J. W. Sibert, M. M. Olmstead, A. G. M. Barrett, and B. M. Hoffman, *J. Am. Chem. Soc.*, **1994**, *116*, 2639-2640; c) S. L. J. Michel, D. P. Goldberg, C. Stern, A. G. M. Barrett, and B. M. Hoffman, *J. Am. Chem. Soc.*, **2001**, *123*, 4741-4748; d) T. F. Baumann, M. S. Nasir, J. W. Sibert, A. J. P. White, M. M. Olmstead, D. J. Williams, A. G. M. Barrett, and B. M. Hoffman, *J. Am. Chem. Soc.*, **1996**, *118*, 10479-10486; e) J. W. Sibert, T. F. Baumann, D. J. Williams, A. J. P. White, A. G. M. Barrett, and B. M. Hoffman, , *J. Am. Chem. Soc.*, **1996**, *118*, 10487-10493; f) C. S. Velazquez, T. F. Baumann, M. M. Olmstead, H. Hope, A. G. M. Barrett, and B. M. Hoffman, *J. Am. Chem. Soc.*, **1993**, *115*, 9997-10003.

[97] T. Kimura, A. Yomogita, T. Matsutani, T. Suzuki, I. Tanaka, Y. Kawai, Y. Takaguchi, T. Wakahara, and T. Akasaka, *J. Org. Chem.*, **2004**, *69*, 4716-473.

[98] K. Berg, P.K. Selbo, A. Weyergang, A. Dietze, L. Prasmickaite, A. Bonsted, B.O. Engesaeter, E. Angellpetersen, T. Warloe, N. Frandsen A. Hogset, *J. Microsc.* **2005**, *218*, 133–147.

[99] a) H. Ali and J.E. van Lier, *Chem. Rev.*, **1999**, *99*, 2379-2450; b) K.C. Blanco, N.M. Inada, A.G. Salvio, J.D. Vollet-Filho, V.S. Bagnato, *J. of Tumor*, **2016**, *4(2)*, 386-392; c) C.A. Robertson, D. Hawkins and E.H. Abrahamse, *J. Photochem. Photobio. B: Biology*, **2009**, *96*, 1-8.

[100] U. Chilakamarthi andL. Giribabu, *Chem. Rec.*, **2017**, *17*, 775-802.

[101] Dennis E.J.G.J. Dolmans, Dai Fukumura and Rakesh K. Jain, *Nature Reviews | Cancer*, **2003**, *3*, 380-387.

[102] a) X. Li, B.-D. Zheng, X.-H. Peng, S.-Z. Li, J.W. Ying, Y. Zhao, J.-D. Huang and J. Yoon, *Coord. Chem. Rev.*, **2017**, http://dx.doi.org/10.1016/j.ccr.2017.08.003; (b) P. Mroz, A. Pawlak, M. Satti, H. Lee, T. Wharton, H. Gali, T. Sarna, and M. R. Hamblin, *Free Radicals Biol. Med.*, **2007**, *43*, 711–719.

[103] H. Ali, R. Langlois, J. R. Wagner, N. Brasseur, B. Paquette and J. E. van Lier, *Photochem. Photobiol.*, **1988**, *47*, 713–717.

[104] F. Dumoulin, M. Durmus, V. Ahsen and T. Nyokong, *Coord. Chem. Rev.*, **2010**, *254*, 2792-2847.

[105] E. R. Andreeva, O. O. Udartseva, I. N. Vozovikov, S. G. Kuzmin and E. M. Tararak, *Bull. Experimental Bio. Med.*, **2012**, *149(2)*, 262–264.

[106] J. Li, Y. Yang, P. Zhang, J.R. Sounik and M.E. Kenney, *Photochem. Photobiol. Sci.*, **2014**, *13*, 1690-1698.

[107] M. A. Hutnick, S. Ahsanuddin, L. Guan, M. Lam, E. D. Baron and J. K. Pokorski, *Biomacromolecules*, **2017**, *18*, 379–385.

[108] P.P.S. Lee, P.C. Lo, E.Y.M. Chan, W.P. Fong, W.H. Koc, D.K.P. Ng, *Tetrahedron Lett.*, **2005**, *46*, 1551–1554.

[109] S. Ye, N. Kang, M. Chen, C. Wang, T. Wang, Y. Wang, Y. Liu, D. Li and L. Ren, *Mol. Pharmaceutics*, **2015**, *12*, 2444-2458.

[110] L. Du, H. Qin, T. Ma, T. Zhang and D. Xing, *ACS Nano*, **2017**, *11*, 8930-8943.

[111] Q. Jia, J. Ge, W. Liu, X. Zheng, M. Wang, H. Zhang and P. Wang, *ACS Appl. Mater. Interfaces*, **2017**, *9*, 21124-21132.

[112] X. Li, X.-H. Peng, B.-D. Zheng, J. Tanq, Y. Zhao, B.-Y. Zheng, M.R. Ke and J.-D. Huang, *Chem. Sci.*, **2018**, *9*¸ 2098-2104.

[113] H. Yaku, T. Fujimoto, T. Murahima, D. Miyohi and N. Sugimoto, *Chem. Commun.*, **2012**, *48*, 6203-6216.

[114] J.A. Siddiqui, C.L. Grand, D.J. Bearss, L.H. Hurley, *Proc. Natl. Acad. Sci. U S A.*, **2002**, *99(18)*, 11593-11598.

[115] J. Alzeer, B. R. Vummidi, P. J. C. Roth, N. W. Luedtke, *Angew. Chem., Int. Ed.*, **2009**, *48*, 9362–9365.

[116] K. W. Hipps and U. Mazur, *Langmuir*, **2018**, *34*, 3-17.

[117] C. Vericat, M.E. Vela, G. Benitez, P. Carro and R.C. Salvarezza, *Chem. Soc. Rev.*, **2010**, *39*, 1805-1834.

[118] Thioalcohol: I. Chambrier, M.J. Cook and D.A. Russell, *Synthesis*, **1995**, 1283-1286. (thioether, alcohol, amine)

[119] Thioethers: a) F. Matemadombo, S. Griveau, F. Bedioui and T. Nyokong, *Electroanalysis*, **2008**, *20(17)*, 1863–1872; b) N. Nombona, K. Maduray, E. Antunes, A. Karsten and T. Nyokong, *J. Photochem. Photobio. B: Bio*., **2012**, *107*, 35–44; c) F. Matemadombo and T. Nyokong, *Electrochim. Acta*, **2007**, *52*, 6856–6864; d) F. Matemadombo, M. Durmuş, C. Togo, J. Limson and T. Nyokong, *Electrochim. Acta*, **2009**, *54*, 5557–5565; e) S. Moeno, E. Antunes and T. Nyokong, *J. Photochem. Photobio. A: Chem*., **2011**, *222*, 343–350; f) S. Nitahara, T. Akiyama, S. Inoue and S. Yamada, *J. Phys. Chem. B*, **2005**, *109*, 3944-3948

[120] Amine anchor: A. J. Jeevagan and S. A. John, *RSC Adv.*, **2013**, *3*, 2256-2264.

[121] Alkyl chain: K. Miyake, Y. Hori, T. Ikeda, M. Asakawa, T. Shimizu and S. Sasaki, *Langmuir*, **2008**, *24(9)*, 4708-4717.

[122] M. E. Wieder, D. C. Hone, M. J. Cook, M. M. Handsley, J. Gavrilovic and D. A. Russell, *Photochem. Photobiol. Sci.*, **2006**, *5*, 727-734.

[123] V. N. Nemykin, A. A. Purchel, A. D. Spaeth and M. V. Barybin, *Inorg. Chem.*, **2013**, *52* (19), 11004–11012

[124] J.-D. Huang, S. Wang, P.-C. Lo. W.-P. Fong, W.-H. Ko and D. K. P. Ng, *New J. Chem.*, **2004**, *28*, 348-354.

[125] (a) H.B. Gobeze, T. Tram, C.B. KC, R.R. Cantu. P.A. Karr, F. D'Souza, *Chin. J. Chem.*, **2016**, *34*, 969-974. (b) C.B. KC, F. D'Souza, *Coordination Chemistry Reviews*, **2016**, *322*, 104-141; (c) K.-C. Lin, L. Wang, T. Doane, A. Kovalsky, S. Pejic andC. Burda, *J. Phys. Chem. B*, **2014**, *118*, 14027-14036.

[126] A.B. Sorokin, *Chem. Rev.*, **2013**, *113* (10), 8152–8191.

[127] a) L. Fernandez, S. Thussing, A. Mänz, J. Sundermeyer, G. Witte and P. Jakob, *Phys. Chem. Chem. Phys.*, **2017**, *19*, 2495–2502; b) A. Lerch, L. Fernandez, M. Ilyn, M. Gastaldo, M. Paradinas, M. A. Valbuena, A. Mugarza, A. B. M. Ibrahim, J. Sundermeyer, U. Hofer and F. Schiller, *J. Phys. Chem. C.*, **2017**, *121*, 25353–25363.

[128] T. Niu, C. Zhou, J. Zhang, S. Zhong, H. Cheng, W. Chen, *J. Phys. Chem. C*, **2012**, *116*, 11565−11569.

[129] S. Kera, H. Yamane, H. Honda, H. Fukagawa, K. Okudaira, N. Ueno, *Surf. Sci*, **2004**, *566−568*, 571−578.

[130] (*a*) M. P. Coles and V. C. Gibson, *Polym. Bull.*, 1994, **33**, 529–533; (*b*) M. P. Coles, C. I. Dalby, V. C. Gibson, W. Clegg and M. R. J. Elsegood, *J. Chem. Soc., Chem. Commun.*, 1995, 1709–1711; (*c*) M. P. Coles, C. I. Dalby, V. C. Gibson, I. R. Little, E. L. Marshall, M. H. Ribeiro da Costa and S. Mastroianni, *J. Organomet. Chem.*, 1999, **591**, 78; (*d*) V. C. Gibson, *Eur. Pat. Appl. EP 641804 A2*BP Chemicals Ltd., UK, 1995; (*e*) U. Siemeling, L. Kölling, A. Stammler, H.-G. Stammler, E. Kaminski and G. Fink, *J. Chem. Soc., Chem. Commun.*, 2000, 1177–1178; (*f*) M. Schopf, J. Sundermeyer, J. Kipke, K. A. Rufanov, W. Heitz, U. Peucker, *EP1200453* (*B1*), Basell Polyolefine GmbH, 2003; (*g*) M. Schopf, J. Sundermeyer, J.Kipke,K.A.Rufanov,W. Heitz,U. Peucker, *WO 01/09148* (*A1*), Elenac GmbH, 2001; (*h*) V. R. Jensen and K. J. Børve, *Organometallics*, 2001, **20**, 616.

[131] W.-H. Leung, E.K. F. Chow, M.-C. Wu, P. W. Y. Kumand L.-L. Yeung, *Tetrahedron Lett.*, 1995, **36**, 107.

[132] W.-H. Leung, M.-T. Yu, M.-C. Wu and L.-L. Yeung, *Tetrahedron Lett.*, 1996, **37**, 891–892.

[133] D. Jan, F. Simal, A. Demonceau, A. F. Noels, K. A. Rufanov, N. A. Ustynyuk and D. N. Gourevitch, *Tetrahedron Lett.*, 1999, **40**, 5695–5699.

[134] J. L. Thorman, I. A. Guzei, V. G. Young, Jr. and L. K. Woo, *Inorg. Chem.*, **1999**, *38*, 3814–3824.

[135] L. M. Berreau, J. Chen and L. K. Woo, *Inorg. Chem.*, **2005**, *44*, 7304–7306.

[136] J.- L. Liang, J.- S. Huang, X.- Q. Yu, N. Zhu and C.- M. Che, *Chem. Eur. J.*, 2002, 8, 1563–1572.

[137] a) S.- M. Au, W.- H. Fung, M.- C. Cheng, C.- M. Che and S.- M. Peng, *Chemm Commun.*, **1997**, 1655–1656; b) S. K.- Y. Leung, W.- M. Tsui, J.- S. Huang, C.- M. Che, J.- L. Liang and N. Zhu, *J. Am. Chem. Soc.*, **2005**, *127*, 16629–16640.

[138] a) V. Lyaskovskyy, A. I. O. Suarez, H. Lu, H. Jiang, X. P. Zhang and B. de Bruin, *J. Am. Chem. Soc.*, **2011**, *133*, 12264–12273; b) B. Moubaraki, K. S. Murray, P. J. Nichols, S. Thomson and B. O. West, *Polyhedron*, **1994**, *13(3)*, 485–495.

[139] W. Darwish, E. Seikel, R. Käsmarker, K. Harms and J. Sundermeyer, *Dalton Trans.*, **2011**, *40*, 1787–1794.

[140] a) W. Darwish, E. Seikel, K. Harms, O. Burghaus and J. Sundermeyer, *Dalton Trans.*, **2011**, *40*, 1183–1188; b) E. Seikel, B. Oelkers, O. Burghaus and J. Sundermeyer, *Inorg. Chem.*, **2013**, *52*, 4451–4457.

[141] M. Ruf, A. M. Lawrence, B. C. Noll and C. G. Pierpont, *Inorg. Chem.*, **1998**, *37*, 1992–1999.

[142] D. Atilla, N. Saydan, M. Durmus, A. G. Gurek, T. Khan, A. Ruck, H. Walt, T. Nyokong and V. Ahsen, *J. Photochem. Photobio. A: Chem.*, **2007**, *186*, 298–307.

[143] A. A. Chernonosov, V. V. Koval, D. G. Knorre, A. A. Chernenko, V.M. Derkacheva, E. A. Lukyanets and O. S. Fedorova, *Bioinorganic Chemistry and Applications*, **2006**, 1-8.

[144] M. Gsänger, D. Bialas, L. Huang, M. Stolte and F. Würthner, *Adv. Mater.*, **2016**, *28*, 3615–3645.

[145] B. Umasekhar, E. Ganapathi, T. Chatterjee and M. Ravikanth, *Dalton Trans.*, **2015**, *44*, 16516–16527.

[146] C. Nataro and S. M. Fosbenner, *J. Chem. Ed.*, **2009**, *86(12)*, 1412–1415.

[147] A. V. Ivanov, P. A. Svinareva, L. G. Tomilova and N. S. Zefirov, *Russ. Chem. Bull., Int. Ed.*, **2001**, *50(5)*, 919–920.

[148] M. Ouchi, Y. Inoue, Y. Liu, S. Nagamune, S.Nakamura, K. Wada, T. Hakushi, *Bull. Chem. Soc. Japan*, **1990**, *63(4)*, 1260–1262.

[149] A. W. Snow, E. E. Foos, *Synthesis*, **2003**, *4*, 509–512.

[150] S. Dabak, V. Ahsen, F. Heinemann and P. Zugenmaier, *Mol. Cryst. Liq. Cryst.*, **2000**, *348*, 111–127.

[151] A. M. Sevim, C. Ilguen, A. Guel, *Dyes Pigments*, **2011**, *89(2)*, 162–168.

[152] D. Chaturvedi, A. K. Chaturvedi, N. Mishra, V. Mishra, *Org. Biomol. Chem.*, **2012**, *10(46)*, 9148–9151.

[153] M. S. Miftakhov, N. A. Danilova, Y. L. Vel'der, V. R. Sultanmuratova, A. A. Berg, G. A. Tolstikov, *Zhur. Org. Khimii*, **1988**, *24(9)*, 1864–1869.

[154] A. V. Korolev, A. L. Rheingold and D. S. Williams, *Inorg. Chem.*, **1997**, *36*, 2647–2665.

[155] L. Cellucci, C. Ercolani, P. J. Lukes, A. Chiesi-Villa and C. Rizzoli, *J. Porph. Phthalo.*, **1998**, *2*, 9–19.